Weak intermolecular interactions in organic systems: a concerted study involving x-ray and neutron diffraction and database analysis

Hoy, Vanessa J.

Weak Intermolecular Interactions in Organic Systems: A Concerted Study Involving X-ray and Neutron Diffraction and Database Analysis.

Vanessa J. Hoy

Thesis submitted in part fulfilment of the requirements for the degree of

Doctor of Philosophy

at the

University of Durham

Department of Chemistry

October 1996

Weak Intermolecular Interactions in Organic Systems: A concerted Study Involving X-ray and Neutron Diffraction and Database Analysis.

Submitted for the degree of Doctor of Philosophy, October 1996, by

Vanessa J. Hoy, University of Durham

ABSTRACT

This thesis can be divided broadly into two halves. The first half (Chapters 3 - 5) deals with crystallographic studies of compounds which contain weak intermolecular interactions or networks of these interactions. Whilst the later part (Chapters 7 - 9) describes the results of database surveys of three novel weak intermolecular interactions.

In Chapters 3 and 4 the neutron derived structures of 3,5-dinitrocinnamic acid, 2-ethynyladamantan-2-ol, 2- and 3-aminophenol are presented. All of the compounds contain complex networks of weak hydrogen bonds. The neuron diffraction data are used to determine accurate hydrogen atom poistions and thus characterise these hydrogen bonded networks. Some theoretical work is also described. In Chapter 5, X-ray diffraction studies of a series of iodobenzene derivatives are described. These compounds were synthesised in an attempt to engineer structures mediated by novel X...O_2N interactions. The structures of three iodo nitrobenzenes are presented wherein symmetrical bifurcated I...O_2N interactions mediate the primary ribbon motif. The structure of TCNQ derivative, in which I...N≡C play a structure determining role, is also described.

Chapters 7, 8 and 9 describe database studies of X...O_2N, C(ring)-H...O/N and C-F...H interactions. The frequencies and geometries of the interactions were determined and analysed. The data for X...O_2N interactions were used in conjunction with sophisticated IMPT calculations to determine prefered interaction geometries and interaction energies. Similar theoretical techniques were used to analyse the C(ring)-H...O/N and C-F..H interactions described in Chapters 8 and 9.

Background information and overviews of the general experimental procedures followed when performing the crystallographic and database studies are given in Chapters 2 and 6.

DECLARATION

The work described in this thesis was carried out in the Department of Chemistry at the University of Durham between October 1993 and September 1996, under the supervision of Prof. Judith A. K. Howard. All the work is my own, unless otherwise stated, and has not been submitted previously for a degree at this, or any other university.

Vanessa J. Hoy

ACKNOWLEDGEMENTS

First of all I would like to thank my supervisor, Prof. Judith Howard and the co-supervisors of the project, Dr. Frank Allen and Prof. Gautam Desiraju for the help, support and encouragement they have provided throughout the three years. I must also thank Prof. Desiraju and his students in Hyderabad for supplying all of the crystals used for the work described here.

The efforts of my local contacts at ISIS and the ILL, Dr. Chick Wilson and Dr. Garry McIntyre are very much appreciated and I would particularly like to thank Chick for the time he spent proof reading sections this thesis.

My colleagues, past and present, in Durham and at the CCDC have provided a vast amount of practical help and emotional support during the last three years. In particular I would like to thank: Dr. Roy Copley, Dr. Christian Lehmann, Dr. Jason Cole and Dr. Claire Wilson for teaching me what little I know about crystallography; Dr. Scott Rowland, Dr. Ian Bruno and Dr. Neil Stewart for providing the solutions to my problems with the CSDS and related software; and Mark Roden, Jacqui Cole, Pete Ford, Stephanie Hull, and Roy for taking me to the pub when things were bad and going to the pub with me when things were good.

Finally, I want to thank my friends outside of work for giving me the opportunity to take a breather now and again. In particular Dena Bellamy, Juliette Cook, Susie Dalton, Gill Thompson, Alison Sykes, Paula Rudkin, Monika Lauterbach, Irene Higler and all of the members of DUWHC past and present. Your support means a great deal.

TABLE OF CONTENTS

Appendix B - Seminars, Meetings, Courses and Conferences Attended

LIST OF FIGURES

LIST OF TABLES

Chapter 5 - X-ray Diffraction Studies of Compounds Engineered to Contain Nitro Oxygen...Iodine Interactions

Chapter 7 - Database and Theoretical Studies of Nitro Oxygen...Halogen Inteactions

Chapter 8 - Database Studies of the Hydrogen Bonding Properties of Three Membered Rings

LIST OF ABBREVIATIONS

Numerical definitions of the crystallographic abbreviations are given in Chapter 2.

BSSE	Basis Set Superposition Error
CSDS	Cambridge Structural Database System
esds	estimated standard deviations
eV	electron Volt
Goof	Goodness of fit
Hz	Hertz (s^{-1})
ICSD	Inorganic Chemical Structural Database
ILL	Institut Laue Langevin, Grenoble, France
IMPT	Intermolecular Pertubation Theory
MDF	Metals Data File
NIPMAT	Non-bonded Interaction Pattern Matrix
PDB	Protein Data Bank
PSD	Position Sensitive Detector
R1, wR2	Residual factors
SCF	Self Consistent Field
TCNQ	Tetracyanoquinodimethane
TDS	Thermal Diffuse Scattering

CHAPTER 1

Introduction

1.1 INTERMOLECULAR INTERACTIONS

Intermolecular interactions are the weak forces that bind molecules together. These forces govern the recognition, reaction, transport and regulation processes vital to life and determine many of the physical and chemical properties of molecular liquids and solids. The aim of supramolecular chemistry, the new science of intermolecular interactions (Lehn, 1995), is to predict and eventually to control the formation of intermolecular interactions by gaining a deeper understanding of their nature and their scope. The uses to which such knowledge could be put are many and span the whole scientific spectrum; from biochemistry and rational drug design, through crystal engineering and molecular devices to materials science and the mechanical properties of solids.

Crystallographers have been quick to realise that organic single crystals are perfect supermolecules (Dunitz, 1991; *Perspectives in Supramolecular Chemistry*, 1996) wherein *millions* of molecules are assembled through patterns of intermolecular interactions of startling complexity and precision. Moreover, they have recognised that the wealth of crystallographic data produced over the last sixty years by industrious crystallographers represents a vast and largely untapped source of the precise structural information needed to characterise these interactions. It is then unsurprising that crystallographic investigations remain at the forefront of supramolecular chemical research (*Crystallography of Supramolecular Compounds*, 1996).

1.2 CRYSTALLOGRAPHIC INVESTIGATIONS OF WEAK INTERMOLECULAR INTERACTIONS

Historically, crystallography has played a key role in the characterization of intermolecular interactions. The geometries of the O-H...O hydrogen bonds present in ice, first postulated by Latimer and Rodebush (1920), were determined experimentally using single crystal neutron diffraction (Peterson and Levy, 1957). Today this and several other crystallographic techniques are used to study an ever increasing range of intermolecular interactions.

1.2.1 Neutron Diffraction

Neutron diffraction is the only experimental method which provides accurate positional data for hydrogen atoms in molecular crystals and for this reason it is used widely to determine the geometries of hydrogen bonding interactions. Much recent interest has focused on the characterization of a new generation of weak hydrogen bonds. Weak hydrogen bonds, such as C-H...O, O-H...π, O-H...F, etc., have geometrical characteristics which are similar to those of more familiar O-H...O and N-H...O bonds but are believed to be less than half as strong (Desiraju, 1995). Individual studies, such as the recent investigations of O-H...π (Allen *et. al.*, 1996a) and N-H...π (Allen *et. al.*, 1996b) bonds, provide valuable insights into the nature of these unusual hydrogen bonding interactions. However, it is often more profitable to combine the data from several neutron diffraction experiments and to survey together. These studies can be used to determine the frequencies with which the various hydrogen bonding interactions occur, in addition to providing accurate *mean* hydrogen bond geometries. C-H...O bonding is one example of an interaction that has been studied extensively using this method (Kennard and Taylor, 1982; Steiner and Saenger, 1992 and 1993).

1.2.2 X-ray Diffraction

X-rays have several advantages over neutrons. They are easy to produce in large quantities using simple and relatively inexpensive equipment. As a result X-ray diffractometers can be purchased 'off-the-peg' and installed in virtually any laboratory. Neutrons, on the other hand, are very costly since they can only be produced in sufficient quantities at reactor or other large experimental installations and because the number of these installations is limited neutron beamtime is also extremely scarce. The other major advantage of X-rays over neutrons is flux. A typical reactor source generates a usable flux which is only about a hundredth of that of a standard laboratory X-ray tube. Consequently, neutron samples must be approximately 100 times larger than those required for X-ray diffraction experiments. Growing crystals of the required size for neutron diffraction often proves to be a major stumbling block.

For these reasons X-ray diffraction is the most commonly used technique for determining solid state molecular and intermolecular structure and although X-ray diffraction data cannot provide the highly accurate hydrogen atom positions attainable with neutrons it is used widely to characterize both hydrogen and non-hydrogen bonded intermolecular interactions. However, it is probably best suited to the study of non-hydrogen bonds where the problems associated with the poor resolution of hydrogen are not relevant. Interactions of this type investigated recently using X-ray diffraction include I...N≡C (Allen *et. al.*, 1994), Cl...N≡C (Reddy *et. al*, 1993), I...O_2N (Thalladi *et. al*, 1996), I...I, Br...Br, Cl...Cl (Pedireddi *et. al*, 1994), S...N, S...S, S...Cl (Suzuki *et. al*, 1992; Jorgensen *et. al*, 1994) and Au...Au (Pathaneni and Desiraju, 1993).

1.2.3 Database Analysis

The Cambridge Structural Database System (CSDS: Allen *et. al*, 1991) contains the crystal structures of over 160, 000 organic and organometallic compounds. This data is accessed using sophisticated CSDS search and retrieval software which is constantly

being developed and updated. One of the most recent improvements was the addition of a facility which allows users to perform interactive geometrical searches for both bonded and *non-bonded* fragments. This development in particular has lead to a dramatic increase in the use of the CSDS for investigating intermolecular interactions.

Database techniques are especially useful when studying weak intermolecular interactions. Weak interactions, like other stronger hydrogen bonds, have prefered interacting geometries. However, these geometries are often perturbed by 'interference' from other stronger interactions which are also present in the crystal lattice. The statistical averaging that takes place when database surveys involving hundreds or thousands of compounds are performed minimise the crystallographic 'noise' produced by this interference between incompatible sets of interactions thus generating more reliable mean geometrical data.

A large number of weak intermolecular interactions have been studied using the CSDS in recent years. These investigations typically involve analyses of contact frequencies, distances and angles in relevant fragments. Notable studies include an a comprehensive survey of interactions between halogens and nucleophiles (Lommerse *et. al.*, 1996), an analysis of C-F...H-C bonding in fluorohydrocarbons (Shimoni and Glusker, 1994) and a study linking C-H...O bond distances with carbon acidity (Desiraju and Pedireddi, 1992).

1.3 SCOPE OF THIS THESIS

This thesis can be divided broadly into two halves. The first half (Chapters 3 - 5) deals with crystallographic studies of compounds which contain weak intermolecular interactions or networks of these interactions. Whilst the later part (Chapters 7 - 9) describes the results of database surveys of three novel weak intermolecular interactions.

In Chapter 3 the neutron derived structures of 3,5-dinitrocinnamic acid and 2-ethynyladamantan-2-ol are presented. Both compounds contain complex networks of weak hydrogen bonds. The extensive C-H...O bond network present in 3,5-dinitrocinnamic acid is composed of 10 unique C-H...O interactions. The precise geometries of all of these interactions have been determined using the neutron diffraction data. Attempts to calculate the relative energies of C-H...O bonds present are also described. 2-Ethynyladamantan-2-ol contains a cooperative network (Jeffrey and Saenger, 1991) of O-H...O, C-H...O and unusual O-H...π hydrogen bonds. Once again, the geometries of all three interactions have been determined using the neutron diffraction data. This is the first time that an O-H...π bond has been characterised using neutron diffraction.

Chapter 4 describes the neutron diffraction analyses of 2- and 3-aminophenol. The exclusively O-H...N and N-H...O bonded networks predicted by others (Eling and Ermer, 1994) are not observed. Instead, both compounds contain cooperative networks of O-H...N, N-H...O, C-H...O and N-H...π bonds. The geometry of the unusual N-H...π bond is optimised because of extensive pyramidalisation of the aromatic amine group. Reasons for this pyramidalisation and for the unpredicted packing arrangement are discussed.

In Chapter 5 X-ray diffraction studies of a series of iodobenzene derivatives are described. These compounds were synthesised in an attempt to engineer structures mediated by novel X...O_2N interactions. The structures of three iodo nitrobenzenes are

presented wherein symmetrical bifurcated I...O_2N interactions mediate the primary ribbon motif. The structure of TCNQ derivative in which I...N≡C play a structure determining role is also described.

In Chapter 7 X...O_2N interactions are investigated using database techniques. The frequencies and geometries of all the interactions between NO_2 groups and the halogens Cl, Br and I present in compounds contained in the CSDS were retrieved. These data were used in conjunction with sophisticated IMPT calculations to determine the prefered geometries and energies of a range of different X...O_2N interactions. It has been shown that X...O_2N is both a common and an energetically favourable interaction and that its geometry is strongly dependent on the nature of the halogen 'donor' atom involved.

The results of a database survey of the hydrogen bond C-H donor and π acceptor properties of three membered rings are presented in Chapter 8. The frequencies and geometries of interactions between C-H groups attached to the three membered rings cyclopropane, cyclopropene, aziridine, oxirane and a variety of oxygen and nitrogen atom acceptors were obtained using the CSDS. These were compared with similar data for alkanic, alkenic and alkynic C-H groups. The results show that saturated three membered rings have hydrogen bond donating abilities which are comparable to those of alkenes and that cyclopropene is nearly as effective a C-H donor as acetylene. An analysis of the small number of O-H...π and N-H...π bonds in which three membered rings act as the π hydrogen bond acceptor is also presented.

Finally, Chapter 9 describes the database analysis of short C-F...H contacts involving mono-fluorinated C-F groups. Short contacts, of less than 2.35Å, between mono-fluorinated C-F groups and hydrogen atoms bound to carbon, oxygen and nitrogen atoms were located and parameterised using the CSDS. These data were divided up according to the inter- or intramolecular nature of the contact and the hybridization state of the carbon atom. Although the number of short C-F...H contacts is extremely small it is found that

$C(sp^3)$-F is a much better hydrogen bond acceptor than $C(sp^2)$-F. Theoretical calculations supporting this finding are also presented.

Background information and overviews of the general experimental procedures followed when performing the crystallographic and database studies are given in Chapters 2 and 6. Detailed introductions to all of the topics are provided at the beginning of the each chapter.

1.4 REFERENCES

Allen, F. H., Davies, J. E., Galloy, J. J., Johnson, O., Kennard, O., Macrae, C. F., Mitchell, E. M., Mitchell, G. F., Smith, J. M. and Watson, D. G. (1991) J. Chem. Inf. Comput. Sci., **31**, 187 - 204.

Allen, F. H., Goud, B. S., Hoy, V. J., Howard, J. A. K. and Desiraju, G. R. (1994) J. Chem. Soc., Chem. Commun., 2729 - 2730.

Allen, F. H., Howard, J. A. K., Hoy, V. J., Desiraju, G. R., Reddy, D. S. and Wilson, C. C (1996a) J. Am. Chem. Soc., **118**, 4081 - 4084.

Allen, F.H., Desiraju, G.R., Howard, J.A.K. Hoy, V. J. and Thalladi, V.R. (1996b) *Crystal Engineering and the Correspondence Between Molecular and Crystal Structures. Are 2- and 3- amino phenol anomalous?*, in preparation.

Crystallography of Supramolecular Compounds (1996) ed. Tsoucaris, G., Atwood, J.L. and Lipkowski, J., Kluwer Academic Publishers, the Netherlands.

Desiraju, G. R. (1995) Angew. Chem. (Int. Ed. Engl.), **34**, 2311 - 2327.

Desiraju, G., and Pedireddi, V. (1992) J. Chem. Soc., Chem. Commun., 988 - 990.

Dunitz, J.D. (1991) Pure Appl. Chem., **63**, 177.

Ermer, O. and Eling, A. (1994) J. Chem. Soc., Perkin Trans. 2, 925.

Jeffrey, G. A. and Saenger, W. (1991) *Hydrogen Bonding in Biological Structures*, Springer-Verlag, Berlin.

Jorgensen, T., Hansen, T. H. and Becher, J. (1994) Chem. Soc. Rev., **23**, 41.

Kennard, O. and Taylor, R. (1982) J. Am .Chem. Soc., **104**, 5063 - 5070.

Latimer and Rodebush (1920) J. Am. Chem. Soc., **42**, 1419 - 1433.

Lehn, J-M. (1995) *Supramolecular Chemistry: Concepts and Perspectives*, VCH, Weinheim.

Lommerse, J. P. M., Stone, A. J., Taylor, R. and Allen, F. H. (1996) J. Am. Chem. Soc, **118**, 3108 - 3116.

Pathaneni, S. S. and Desiraju, G. R. (1993) J. Chem. Soc., Dalton Trans., 2505.

Pedireddi, V. R., Reddy, D. S., Goud, B. S., Craig, D. C., Rae, A. D. and Desiraju, G. R. (1994) J. Chem. Soc., Perkin Trans. 2, 2353.

Perspectives in Supramolecular Chemsitry: The Crystal as a Supermolecular Entity. Vol. 2 (1996) ed. Desiraju, G.R., Wiley, Chichester.

Peterson, S. W. and Levy, H. A. (1957) Acta Crystallogr., **10**, 70.

Reddy, D. S., Panneerselvam, K., Pilati, T. and Desiraju, G. R. (1993) J. Chem. Soc., Chem. Commun., 661 - 662.

Shimoni, L. and Glusker, J. P. (1994) Struct. Chem., **5**, 383 - 397.

Steiner, T. and Saenger, W. (1992) J. Am. Chem. Soc., **114**, 10146 - 10154.

Steiner, T. and Saenger, W. (1993) J. Am. Chem. Soc., **115**, 4540 - 4547.

Suzuki, T., Fujii, H., Yamashita, Y., Kabuto, C., Tanaka, S., Harasawa, M., Mukai, T. and Miyashi, T. (1992) J. Am. Chem. Soc., **114**, 3034.

Thalladi, V. R., Goud, B. S., Hoy, V. J., Allen, F. H., Howard, J. A. K. and Desiraju, G. R. (1996) J. Chem. Soc, Chem. Commun., 401 - 402.

CHAPTER 2

Diffraction, X-rays, Neutrons and SXD

2.1 SINGLE CRYSTAL DIFFRACTION

2.1.1 Bragg's Law

The first X-ray diffraction pattern from a crystal was recorded in 1912 (Friedrich, Knipping and von Laue, 1912) and shortly afterwards an ionization spectrometer (Bragg and Bragg, 1913) was developed and used for the determination of crystal structures. During the course of these studies the Braggs discovered that the angular distribution of the X-radiation scattered by a single crystal was predictable. Their analyses were based on the assumption that the diffracted X-ray beam behaved as though it were reflected off crystal planes just like light off a mirror (***Figure 2.1.1***).

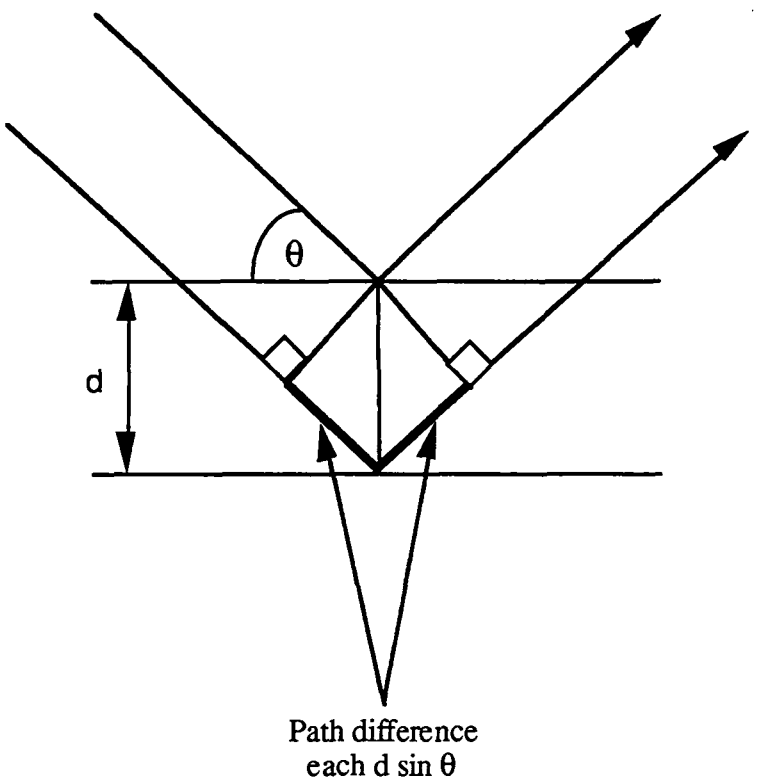

Figure 2.1.1 *- Illustration of the Bragg Equation.*

In these circumstances the X-rays diffracted by adjacent planes are only in phase with one another when the X-ray beam strikes the crystal planes at certain angles, θ. These angles

are given by the wavelength, λ, of the radiation and the distance, d, between adjacent planes according to the Bragg Equation -

$$n\lambda = 2d \sin \theta$$

2.1.2 X-rays as Atomic probes

Optical microscopes produce enlarged images of small objects by collecting and recombining the visible radiation scattered by the objects using a series of magnifying lenses. However, the resolution of these microscopes is limited to the wavelength of visible light (c. 6×10^{-7} m). In order to look at objects which are smaller than this it is necessary to used radiation which has a shorter wavelength. Therefore, high energy electrons are used in electron microscopes to view atoms and X-rays are used to determine the structures of the molecules that make up crystals (10^{-8} -10^{-10} m).

X-rays of the appropriate wavelength are produced by firing a beam of high energy electrons at a metal target. Two types of radiation are emitted; a continuous X-ray spectrum and sharp emission lines with wavelengths characteristic of the metal from which the target is made (***Figure 2.1.2***). It is the emission lines that are employed in X-ray diffraction experiments. They are produced because some of the electrons that strike the target have sufficient energy to eject electrons from the inner shells of the metal atoms. Electons from higher energy shells drop down into the inner shells to replace the ejected electrons. These electrons emit the energy difference between the outer and inner shells in the form of X-rays as they fall producing the sharp peaks in the X-ray specturm. The two most commonly used target materials are copper and molybdenum which produce sharp emission lines at 1.5418×10^{-10} m (Cu Kα) and 0.71069×10^{-10} m (Mo Kα).

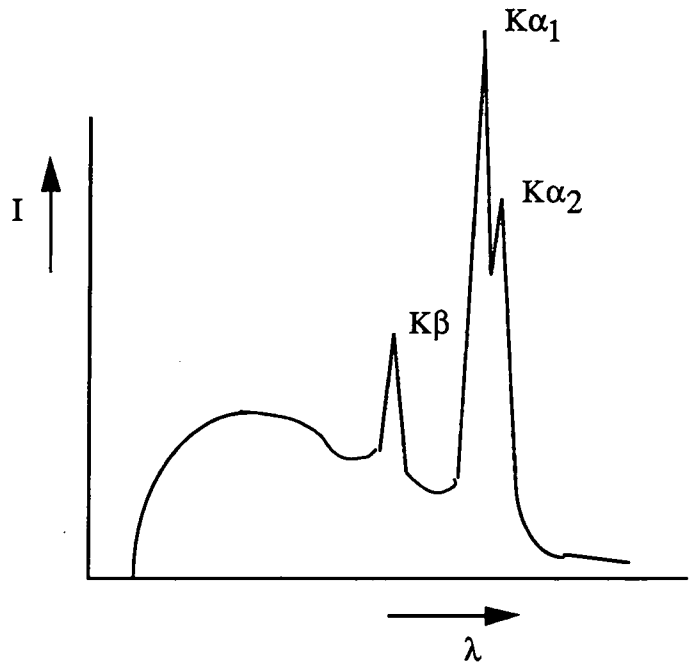

Figure 2.1.2 *- The spectrum of wavelengths produced by a typical X-ray tube.*

2.2 X-RAY DIFFRACTION EXPERIMENTS

The determination of molecular structures from single crystals using X-ray diffraction data is a complex process involving many steps. The following account describes, in general terms, each of those steps with particular reference to the instrumentation used to obtain the structural results described in this thesis. More comprehensive accounts can be found in any of the standard crystallography texts (see for example *Fundamentals of Crystallography*, Giacovazzo, 1992; *Crystal Structure Analysis: A Primer*, Glusker and Trueblood, 1985).

Two instruments were used to collect the X-ray data reported in this thesis; a Rigaku AFC6S four circle diffractometer (***Figure 2.2.1***) and a Siemens P4 four circle diffractometer. A schematic representation of a Eulerian four circle diffractometer is shown in ***Figure 2.2.2***. It consists of a radiation source, a computer controlled goniostat that consists of four concentric circles and a detector. Three of the circles (ϕ, χ and ω) are used to orientate the crystal in space. The fourth (2θ) is used to move the detector. All datasets were obtained using a Molybdenum Kα X-radiation source and low temperature data collections were performed using an Oxford Cryosystems nitrogen Cryostream device (Cosier and Glazer, 1986) attached to the diffractometer.

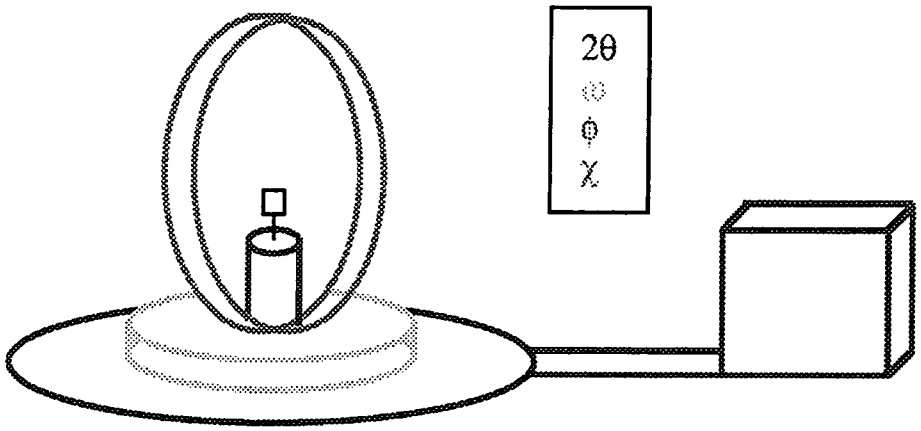

Figure 2.2.2 *- A schematic representation of a Eulerian four circle diffractometer.*

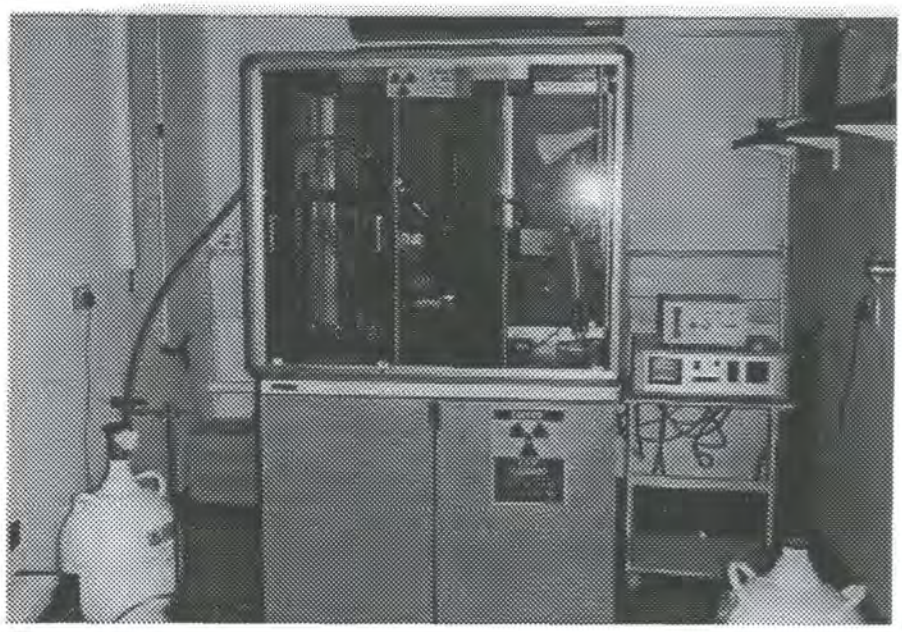

Figure 2.2.1 - The Rigaku AFC6S diffractometer.

2.2.1 Crystal Selection and Mounting

The first step in the experimental procedure was to examine the crystals under a polarising microscope. Crystals which were curved or otherwise deformed, which had large numbers of smaller crystals (or crystallites) attached to them, or which had re-entrant angles were rejected. The crystals were then examined using the polariser to ensure that they were single. Single crystals should extinguish sharply and completely when they are rotated in plane polarised light. Incomplete extinction usually means that the crystal is twinned. Ideal samples were, therefore, ones which extinguished completely, were clear, had well defined faces and, if possible, approximately equal dimensions (ie.were not needles or plates) in order to minimise differential absorption effects.

The overall sizes, as well as the relative dimensions, of the crystals were also important. The scattering power of a crystal depends on its volume as well as on its contents. However, as crystal size increases so does the amount of absorption and these two effects had to be balanced. In practise, an upper limit on crystal size is imposed by the diameter

of the homogenous X-ray beam produced by the instrument being used. Typically, samples had linear dimensions of between 0.1mm and 0.5mm.

The way in which the selected crystals were then mounted depended on their air and moisture sensitivity. Air stable compounds were simply glued to the end of a fine glass filament using small amounts of a fast setting epoxy resin. The filament was then inserted into a brass pip and secured with plasticine and more epoxy resin. The pip was fitted into a well in the top of a goniometer head and held in place using a grub screw. The goniometer head was then located on its mount on the ϕ circle of the diffractometer and screwed firmly into place.

Air sensitive crystals were handled using the oil drop method (Stalke and Kottke, 1993). This involved coating the crystals in a highly viscous perfluoropolyether oil whilst they were still under nitrogen. The oil formed a thin film around the crystals allowing them to be removed from the nitrogen atmosphere and attached to glass filaments as normal. The viscosity of the oil was such that no additional adhesive was required to do this. The mounted sample was then put onto the diffractometer and rapidly cooled causing the oil to harden and form a rigid, impenetrable barrier around the crystal.

Finally, the mounted crystal was optically centred in the X-ray beam. A crystal which is correctly centred does not precess when the ϕ and χ axes of the diffractometer are rotated.

2.2.2 Indexing

A blind peak search was performed to locate reflections for preliminary orientation matrix determination. The type of search employed depended on the instrument being used.

The Siemens P4 locates a single reflection then scans through a hemisphere of reciprocal space which is centered on that reflection and has a radius determined by the anticipated minimum cell length. When 4 reflections have been found an orientation matrix is

determined. Subsequent reflections are indexed using this matrix. If indexing fails the updated reflection list is used to redetermine the orientation matrix. The search stops when 10 reflections have been successfully indexed using the same matrix.

The Rigaku AFC6S diffractometer systematically zig-zags through reciprocal space until 20 suitable peaks have been found. These 20 are then indexed together or, if initial indexing fails, in smaller groups.

Both instruments used the same strategy for indexing the reflections located during the peak search. The procedure, known as the 'real space method' or 'auto-indexing' (Sparks, 1976 and 1982; Clegg, 1984), involves selecting three non-coplanar reciprocal lattice vectors (reflections) from the list and arbitarily assigning them indices 100, 010 and 001. An orientation matrix and unit cell are then generated from the three 'indexed' reflections. Although this cell, **a' b' c'**, is not the correct cell, it must be a subcell of the real lattice and so all vectors between points in the real lattice are also vectors in the lattice described by the subcell. However, the reverse is not generally true.

The auto-indexing program generates real space vectors, **t**, where -

$$\mathbf{t} = u\mathbf{a}' + v\mathbf{b}' + w\mathbf{c}' \ (u, v, w \text{ integral})$$

Each one is then tested against all the observed reciprocal lattice vectors to ascertain whether it is a possible real lattice vector. This is done by determining the dot product **t.x**, where **x** are the coordinates of the reciprocal lattice vectors. If **t** is a real lattice vector **t.x** will be integral. Vectors **t** are generated up to a maximum value for each integer or for their sum and those satisfying the **t.x** criterion are stored. The lengths of these vectors and the angles between pairs of them are calculated and three are then selected to form the required cell.

The hemispherical search used by the Siemens P4 yielded cell parameters quickly but was always combined with a search for reflections at fractional indices to ensure that the cell determination was reliable. The searching regime used by the other machine, whilst slower, involved surveys of larger volumes of reciprocal space and generally led to more reliable cell parameters at the first attempt.

2.2.3 Data Collection

Most modern diffractometers are supplied with data collection software which selects data collection parameters on the basis of the positions, intensities and profiles of the reflections located during the initial peak search and then conducts the data collection automatically. These programs ensure that single crystal diffraction data are collected quickly and with little user intervention. However, since data collection is the most important and time consuming part of any single crystal diffraction experiment it is vital to check that the computer generated data collection parameters are appropriate and to reset parameters manually where necessary.

The first of these parameters is the scan type used to collect the data. Most of the X-ray diffraction experiments described in this thesis employed $\omega/2\theta$ scans which involve the coupled movement of both the crystal and the detector. However, ω scans, in which only the crystal is rotated, were sometimes used. The latter were selected when peak profiles were broad or when one or more of the cell axes were particularly long since peaks are often close in θ in such circumstances. The widths of these scans were determined by the widths of the peaks located during the initial peak search. The scans had to be wide enough to encompass the whole of each peak and some background intensity on either side. However, excessively wide scans were avoided since these waste diffractometer time and can lead to overestimates of background. Both fixed and variable width scans were used. The Rigaku AFC6S and the Siemens P4 use the same two component function to determine the widths of variable width scans; width ($^\circ\omega$) = A + Btanθ. The form of this function is such that the scans broaden as 2θ increases compensating for

increases in peak width due to wavelength dispersion at higher 2θ. The constant A was derived experimentally from higher angle data in each case. B is characteristic of the wavelength of the radiation used.

Several factors were considered when deciding how much data to collect. Generally, it is only necessary to collect one unique set of data in order to adequately solve and refine a crystal structure. However, collecting extra symmetry equivalent reflections is usually advantageous and can be vital. Merging equivalent reflections reduces the systematic errors within a dataset, improves the precision and provides an indication of the internal consistency of the data. Furthermore, comparison of equivalent reflections is necessary to determine the absolute configurations of chiral compounds. Accordingly, some equivalents were measured during each of the X-ray diffraction experiments described in this thesis.

The upper 2θ limit selected also affected the amount of data collected. The X-ray scattering power of all crystals falls off sharply as 2θ increases because of the finite extent of the electronic cloud which diffracts the incoming beam, with respect to the incident X-ray wavelengths. This makes it difficult to resolve the peaks from the background at high 2θ angles. By imposing a 2θ cut-off the time spent collecting these very weak data is limited. The appropriate 2θ limit is determined by the diffracting power of the crystal and the wavelength of the radiation used. Limits of up to 65° were used for the X-ray diffraction experiments described later.

The precision with which a reflection is measured is proportional to the square root of the time spent making the measurement. It is therefore possible to improve the precision of measurements by scanning reflections more slowly or repeatedly. During X-ray diffraction experiments it is normal to vary the length of time spent scanning reflections in order to ensure that both the strong and the weak data are measured to the same relative precision. This can be achieved in several different ways. The Rigaku AFC6S software requires the user to select a target value for the precision of each measurement.

Reflections are then scanned and re-scanned until this target value is reached or the maximum number of re-scans specified by the user have been performed. The scan speed remains constant throughout the experiment. The Siemens P4 also requires the user to specify a target value for the precision of each measurement. However, re-scans are not used. Instead, each reflection is quickly prescanned and this information is used to determine the scan speed required to obtain the desired precision. A second scan is then performed at this speed. As a result, the scan speed varies, within user defined limits, throughout the experiment. Details of the precision of the measurements made and the scan speeds used during each X-ray diffraction experiment described in this thesis are given in the relevant experimental sections.

The final decision to be made prior to data collection concerns the choice of the check or standard reflections. This small group of reflections are re-measured at regular intervals during the data collection in order to monitor the extent of any radiation damage or other decay of the crystal. The standards chosen for the X-ray diffraction experiments described later had moderate intensities, intermediate 2θ values and came from different regions of reciprocal space.

2.2.4 Data Reduction

Data reduction is the process of converting the intensity data that were measured during a diffraction experiment into the structure factors which are required to solve and refine crystal structures. The intensity of a reflection (I_{hkl}) is related to its structure factor amplitude (F_{hkl}) thus -

$$I_{hkl} = \left(\frac{\lambda^3 \, r_o^2 V}{V_c^2} \right) \frac{1}{w} LPAE \, |F_{hkl}|^2$$

Where λ is the wavelength of the radiation used, V is the crystal volume, V_c is the unit cell volume, r_o is the electron radius and w is the angular scanning velocity. *L*, *P*, *A* and *E* are correction factors. The process also converts the esds of the intensites into

corresponding esds for the structure factors and merges duplicate or symmetry equivalent reflections to yield a unique set of scaled data. The corrections mentioned are routinely applied to the data at this stage and are described below.

2.2.4.1 The Lorentz Correction

The Lorentz correction is a geometric correction and is applied to compensate for the fact that Bragg peaks at different 2θ angles pass through their diffracting positions at different speeds. The correction takes the form $L = 1/\sin 2\theta$ for Eulerian four circle diffractometers.

2.2.4.2 The Polarisation Correction

The polarisation correction is also a geometric correction. It is applied because the X-ray beam is partially polarised when diffraction occurs. The degree of this polarisation depends on the 2θ angle and is given by $P = (1 + \cos^2 2\theta)/2$. A correction must also be made for the partial polarisation of the incident X-ray beam by the monochromator crystal. The form and magnitude of this correction depends on the orientation of the monochromator relative to the equatorial plane of the diffractometer and the physical characteristics of the crystal. Monochromator polarisation factors are usually measured experimentally.

2.2.4.3 The Absorption Correction

The absorption correction compensates for attenuation of the X-ray beam as it passes through the crystal. The amount by which the intensity of a reflection is reduced by absorption depends on the volume of the crystal (V), its linear absorption coefficient (μ) and the path length (t) of the X-ray beam through the crystal for that reflection. The correction factor (A) is the reciprocal of this value and is given by -

$$A = \frac{1}{V}\int e^{-\mu t} dV$$

This integral can be solved directly only for simple solids such as spheres and cylinders. Absorption corrections are applied to crystals with more complex shapes using either numerical (Busing and Levy, 1957; Wells, 1960) or empirical methods (Furnas, 1957; North, Phillips and Mathews, 1968). Numerical corrections involve determining the Miller indices of the bounding faces of the crystal and their precise dimensions. This information is used to construct a mathematical model of the crystal which is then divided up into a Gaussian grid. The contributions made by each of the grid points to the total absorption are evaluated and summed to approximate the integral above.

Empirical absorption corrections are also widely used. The most common type of empirical correction involves ψ scans. Reflections that have χ values close to 90° are scanned as the crystal is rotated about the diffraction vector, ψ. For reflections with χ values close to 90° this is achieved almost exclusively by rotating the ϕ axis of the diffractometer. Since the path length of the X-ray beam through the crystal varies with ψ the measured intensity of the reflection at different ψ angles will be different due to absorption and some extinction and double reflection effects. An absorption curve relating absorption to ϕ can be derived empirically from these data since most of the angular variation described is in ϕ.

Both numerical and empirical ψ scan absorption corrections have been applied to the datasets described in this thesis. Details of the method used and the magnitude of the correction applied in each case are given in the relevant experimental sections.

2.2.4.4 The Decay Correction

The decay correction compensates for variations in the intensities of reflections over time caused by radiation damage or other deterioration of the crystal. The correction is based on changes in the intensities of the standard reflections which are re-measured at regular intervals throughout the data collection. Simple decay corrections use straight line functions to describe this variation. More complex corrections involve polynominal and exponential functions.

2.2.4.5 The Extinction Correction

Extinction reduces the intensity of strong reflections at low 2θ angles and is especially pronounced in crystals with low mosaic spreads. There are two types of extinction. Primary extinction occurs when a portion of the diffracted beam is diffracted a second time by the same set of Miller planes. The phase lag introduced by this 'double' diffraction causes destructive interference and lowers the intensity of the diffracted beam (see ***Figure 2.2.3a***). Secondary extinction occurs when separate mosaic blocks within a crystal are aligned indentically with respect to the incident X-ray beam. A portion of the incident beam is diffracted by the mosaic blocks close to the surface of the crystal. The remainder penetrates deeper into the crystal and is diffracted by other identically aligned mosaic blocks (see ***Figure 2.2.3b***). However, the blocks deep within the crystal contribute less diffracted intensity because those above them 'shield' them from the incident intensity which has already been diffracted.

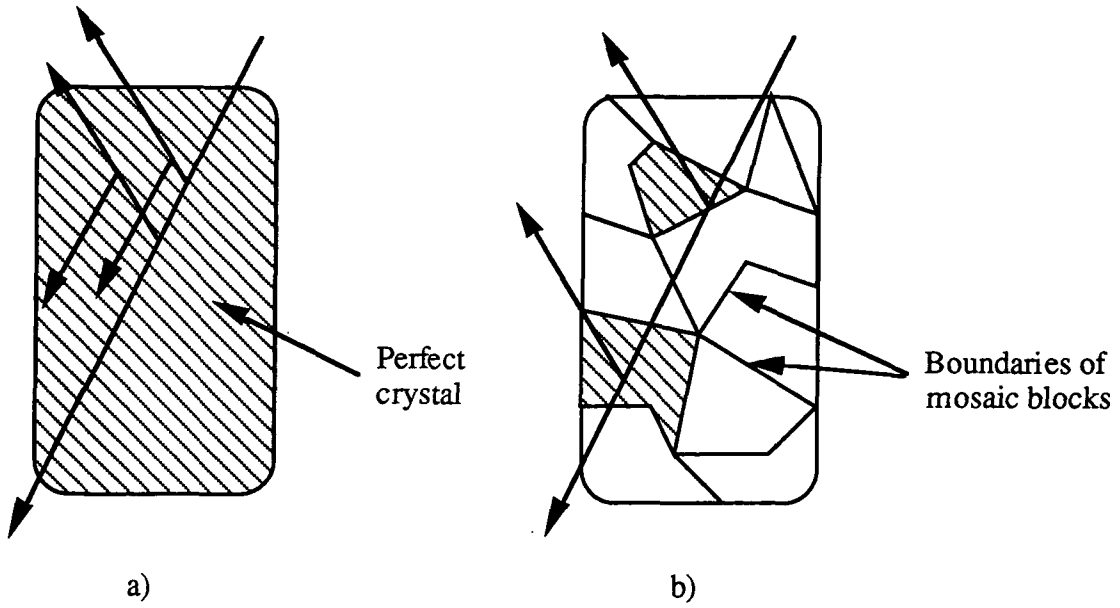

Figure 2.2.3 *- Schematic representations of a) primary and b) secondary extinction effects.*

The quantities that dictate the magnitude of extinction effects, the mosaic spread and the domain radius, are usually unknown and empirical extinction corrections are often applied during structure refinement. The empirical extinction corrections applied to the X-ray data described in this thesis were made during structure refinement using SHELXL-93 (Sheldrick, 1993). An EXTI parameter was refined and used to generate a multiplication factor of the form -

$$k\left[\frac{1}{\sqrt[4]{1 + 0.001 \times EXTI \times F_c^2 \times \lambda^3 / \sin 2\theta}}\right]$$

Both the Lorentz and polarisation corrections are instrument specific and were applied by the data collection software during the early stages of the data reduction procedure. Absorption and decay corrections were applied after the raw intensites have been converted into structure factor amplitudes. Other systematic effects including thermal diffuse scattering (TDS), anomalous dispersion and multiple reflection should be small and were ignored.

The data reduction programs used to process the datasets described in this thesis were the Molecular Structure package TEXSAN (Molecular Structure Corporation, 1989) and the Siemens package XSCANS (Siemens, 1994).

2.2.5 Space Group Determination

The next step was to determine the space group symmetry of the crystal. Criteria, including the Laue symmetry, the Bravais lattice type, the cell parameters and the systematic absences are used by computer programs to determine space groups.

To differentiate between centrosymmetric and non-centrosymmetric space groups normalised structure factors were calculated (Wilson, 1942 and 1949). These are structure factors that are corrected for the effects of atomic shape which cause diffracted intensities to decrease as $\sin\theta/\lambda$ increases. They are derived thus -

$$|E_{hkl}| = \frac{|F_{hkl}|}{\sqrt{|F|_{\theta_{hkl}}{}^2}}$$

Where $|F|_{\theta_{hkl}}{}^2$ is the mean value of all structure factors that have a scattering angle of θ_{hkl}. Since $|E_{hkl}|$ values are independent of scattering angle the underlying intensity distributions present within datasets become apparent when they are analysed. The theoretical probability distributions of $|F_{hkl}|$ and $|E_{hkl}|$ vary depending on whether a structure is centric or acentric. Comparison of the mean of the $|E_{hkl}|$ values for a structure with theoretical values for centric and acentric structures therefore suggests whether an inversion centre is present. The function used by many space group determination programs for this purpose is $|E_{hkl}|^2 - 1$. Typically, for a centric distribution the mean value of this function calculated using all data is 0.97 while for an acentric distribution the value is 0.74 (Karle, Dragonette and Brenner, 1965).

All the space group determinations described in this thesis were carried out using the XPREP program within SHELXTL (Sheldrick, 1995).

2.2.6 Structure Solution

For structure solution, the structure factor amplitudes derived from the intensity measurements made during the diffraction experiment must be converted into an electron density distribution using a Fourier Transform. However, these Fourier Transforms can only be solved if the magnitudes *and* the phases of the structure factor amplitudes are known. The phases of the structure factor amplitudes cannot be derived from the experimental data and other methods must be used to overcome the so called 'phase problem'.

Historically, Patterson methods were used to determine the phases of the structure factor amplitudes. A Patterson function is the Fourier Transform of the square of the modulus of the structure factors. Patterson functions can be calculated without any phase information. However, the peaks in a Patterson map do not correspond directly to atomic positions. Instead, they represent inter-atomic vectors. The height of each Patterson peak corresponds to the product of the atomic numbers of the atoms linked by the vector. Patterson methods are therefore particularly effective when just a few heavy atoms are present. In these situations the heavy atoms usually dominate the scattering and the Patterson peaks which represent the vectors between them are the most prominent features in the Patterson map. Once the peaks representing the vectors between the heavy atoms have been identified it is possible to determine the positions of the heavy atoms. This information is used to derive a set of 'heavy atom' phases which are combined with the structure amplitudes and converted into an electron density distribution. These electron density maps are then used to determine the positions of other atoms within the crystallographic unit cell. The process can be repeated until all the non-hydrogen atoms are located.

Unfortunately, Patterson methods cannot normally be used to solve 'light atom only' structures because there is very little texture in the Patterson maps derived from such compounds. At first heavy atom substitution was the only way to overcome these difficulties and relatively few small organic crystal structures were solved. However, direct phasing methods which do not rely on the presence of heavy atoms now provide an alternative.

Direct methods (Sayre, 1952) of structure solution use the statistical relationships between the phases and the magnitudes of structure factor amplitudes to derive the approximate phases mathematically from the measured intensities. Sets of trial phases are generated for the strongest reflections in the dataset. The phases of the remaining reflections are predicted on the basis of the trial phases with a reliability for each reflection based on its intensity. The phase assignment with the best figure of merit is then used to generate an electron density map from which the atom positions can be derived.

Both Patterson and direct methods were used to solve the structures described in this thesis. The program SHELXS-86 (Sheldrick, 1990) was used in all cases.

The starting models obtained by Patterson or direct methods were usually incomplete and the 'missing' atoms often had to be located using difference Fourier synthesis. This procedure involves subtracting the calculated electron density of the incomplete model from the observed electron density -

$$\Delta\rho(\mathbf{r}) = \rho_{obs}(\mathbf{r}) - \rho_{calc}(\mathbf{r}) = \frac{1}{V}\sum [F(\mathbf{h})_{obs} - F(\mathbf{h})_{calc}]\, e^{-2\pi i \mathbf{h}.\mathbf{r}}$$

Since the true phases of the observed structure factors are unknown the calcluated phases of the incomplete model are used to approximate them. These calculations generated maps in which the missing atoms showed up as positive peaks of observed density which were not matched by peaks in the model.

The difference Fourier maps used to locate the missing atoms in the structures described in this thesis were produced during the early stages of structure refinement using the packages SHELXTL (Sheldrick, 1995) and SHELXL-93 (Sheldrick, 1993).

2.2.7 Structure Refinement

Structure solutions are based on approximate phases and as a result they only yield approximate atomic positions. In order to improve the quality of the structural model it was necessary to include a parameter, K, that scaled the data and parameters that described the thermal motion of the atoms and their site occupancies in addition to their positions. The values of these parameters were then adjusted to obtain the closest possible match between the experimentally observed data and that derived from the model. This structure refinement was carried out using least squares methods. In least squares the values of the parameters are adjusted so as to minimise the weighted sum of the squares of the deviations between the observed and the calculated structure factors or their squares, Q -

$$Q = \sum w(|F_{hkl}|_{obs} - G|F_{hkl}|_{calc})^2$$

$$Q = \sum w(|F_{hkl}|_{obs}^2 - G|F_{hkl}|_{calc}^2)^2$$

Where the summation is over all independent reflections, hkl , w is the weight for each term and G is the reciprocal of the overall scale factor, K.

In order to assess the quality of the overall fit two types of residual factor were calculated: the Goodness-of-fit (Goof) and the R-factor (R1, wR2). The mathematical forms of these residual factors are -

$$\text{Goof} = S = \sqrt{\frac{\sum w(F_{obs}^2 - F_{calc}^2)^2}{N - P}}$$

$$wR2 = \sqrt{\frac{\sum w(F_{obs}^2 - F_{calc}^2)^2}{\sum w(F_{obs}^2)^2}}$$

$$R1 = \frac{\sum ||F_{obs}| - |F_{calc}||}{\sum |F_{obs}|}$$

Where N is the number of reflections used and P is the number of parameters refined. When the model matches the experiment perfectly Goof will equal 1.0 and wR2 will have a value equal to Rσ which is the sum of the errors associated with the reflections divided by the sum of the observed structure factors.

The weighting, *w*, of each reflection estimates the precision of its measurement. Simple weighting schemes such as $1/\sigma^2(|F_{hkl}|_{obs})$ are sometimes used to ensure that measurements which are considered to be unreliable have a small influence on the refinement. However, it is not always possible to obtain accurate estimates of the errors in measurements, and weighting schemes which modify these during the refinement are often used. Such weighting schemes are usually based on an analysis of the variance of the weighted residual across regions of data separated in 2θ and in intensity. A good weighting scheme will tend to increase the consistency of this variance across all regions of data. The weighting scheme used by the refinement program SHELXL-93 (Sheldrick, 1993) is of this latter type and has the form -

$$w = \frac{1}{[\sigma^2(F_{obs}^2) + (a \times P)^2 + (b \times P)]}$$

Where P is $(F_{obs}^2 + 2F_{calc}^2)/3$ and a and b are refined parameters.

All the structure refinements described in this thesis were carried out using either SHELXTL (Sheldrick, 1995) or SHELXL-93 (Sheldrick, 1993).

2.3 NEUTRON DIFFRACTION

2.3.1 Neutrons as Atomic Probes

Elsasser (1936) first suggested that the motion of neutrons was determined by wave mechanics and that therefore they would be diffracted by crystalline materials just like X-rays. Neutron diffraction was observed experimentally by several workers shortly afterwards (Halban and Preiswerk, 1936; Mitchell and Powers, 1936). These experiments were performed using radium-beryllium neutron sources which produce polychromatic beams. Although these were sufficient to demonstrate that diffraction did occur it was not possible to obtain quantitative data from these experiments. It was not until the emergence of nuclear reactors in the 1940s that crystallographers were provided with plentiful sources of neutrons. These reactors generated neutrons in large enough quantities to allow collimated and monochromated beams to be produced with intensities that were sufficient for diffraction experiments. The first neutron diffractometer was built at the Argonne National Laboratory in the USA in 1945 (Zinn, 1947) and since that time numerous instruments have been built at reactor sources. More recently time-of-flight techniques and alternative methods for generating neutrons have been used to perform neutron diffraction studies.

All the neutrons used to probe solid state structures must have wavelengths which are comparable to inter-atomic distances, just like X-rays. The wavelength of a neutron is determined by its velocity -

$$\lambda = \frac{h}{mv}$$

Where h is Planck's constant and m is the mass of the neutron. Neutrons in thermal equilibrium with their surroundings have root mean square velocities, v, which depend on temperature -

$$\frac{1}{2}mv^2 = \frac{3}{2}kT$$

Where k is Boltzmann's constant. By combining these two equations it is possible to relate the wavelength of a neutron in thermal equilibrium to its temperature -

$$\lambda^2 = \frac{h^2}{3mkT}$$

From this it can be shown that the wavelengths of neutrons in equilibrium at temperatures of 0°C and 100°C are 1.55Å and 1.33Å respectively. Luckily, these thermal and epithermal neutrons are easily obtained from reactor and other sources using moderating materials such as graphite or heavy water. The neutrons are slowed down and brought into thermal equilibrium in the moderator by repeated collisions with atomic nuclei. The energies of the neutrons emerging from the moderator have a Maxwellian distribution with a maximum corresponding to the moderator temperature.

Generally, neutron diffraction experiments are carried out using similar instrumentation and procedures to the X-ray experiments described in Section 2.2. The important components are the neutron source, the crystal orienter (typically a standard four circle Eulerian cradle) and the detector.

2.3.1.1 Neutron Sources

The majority of single crystal neutron diffraction experiments are still carried out using continuous monochromatic neutron beams produced by reactor sources. Such beams are entirely analogous to the beams produced by X-ray tubes.

The neutrons are produced in a self sustaining fission reaction in the reactor core. These fast neutrons pass through a moderator where they are slowed down to thermal and epithermal energies. This white beam is monochromated using a single crystal of beryllium, graphite or similar which is orientated such that a given crystal plane will

diffract radiation of the desired wavelength. The monochromatic beam is then collimated to produce a narrow unidirectional neutron beam (***Figure 2.3.1***). The intensity of this beam is only around 1% of that of the white beam which emerges from the reactor because most of the neutrons are lost when the beam is monochromated. Despite this apparent inefficiency, high flux reactor sources produce sufficient intensities, particularly at low neutron energies, to conduct accurate single crystal structural studies on samples of modest size.

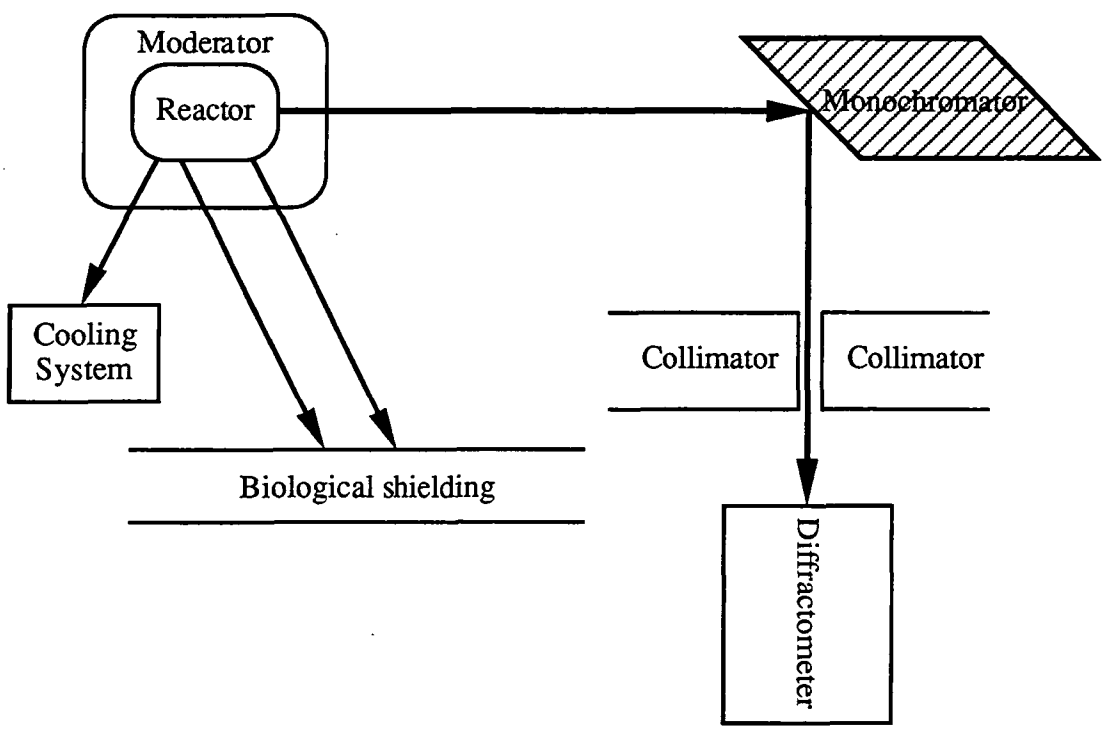

Figure 2.3.1 *- A schematic representation of a generic reactor source.*

At pulsed sources neutrons are generated in discrete pulses either by firing bunches of high velocity exciting particles at a heavy metal target or in a reactor. A pulse of high energy, fast, neutrons is produced which then passes through a moderator where the neutrons are slowed down by repeated collisions with atomic nuclei. The pulses emerge from the moderator and pass straight into the instrument (***Figure 2.3.2***). There is no need to monochromate the beam because it is pulsed and so the time at which each neutron pulse begins its journey from the target to the instrument's detector is known. By measuring the time at which each neutron arrives at the detector its time-of-flight, t, can be

determined. Since the distance between the target and the instrument's detector, L, is fixed, the velocity, v, and thus the wavelength, λ, of each neutron can be determined using de Broglie's equation (***Equation 2.3.1***). This technique is known as time-of-flight neutron diffraction.

$$\lambda = \frac{ht}{mL} \qquad \textit{Equation 2.3.1}$$

Three different neutron producing reactions have been used successfully in pulsed sources. These are photo-neutron production by electrons, spallation by protons and fission.

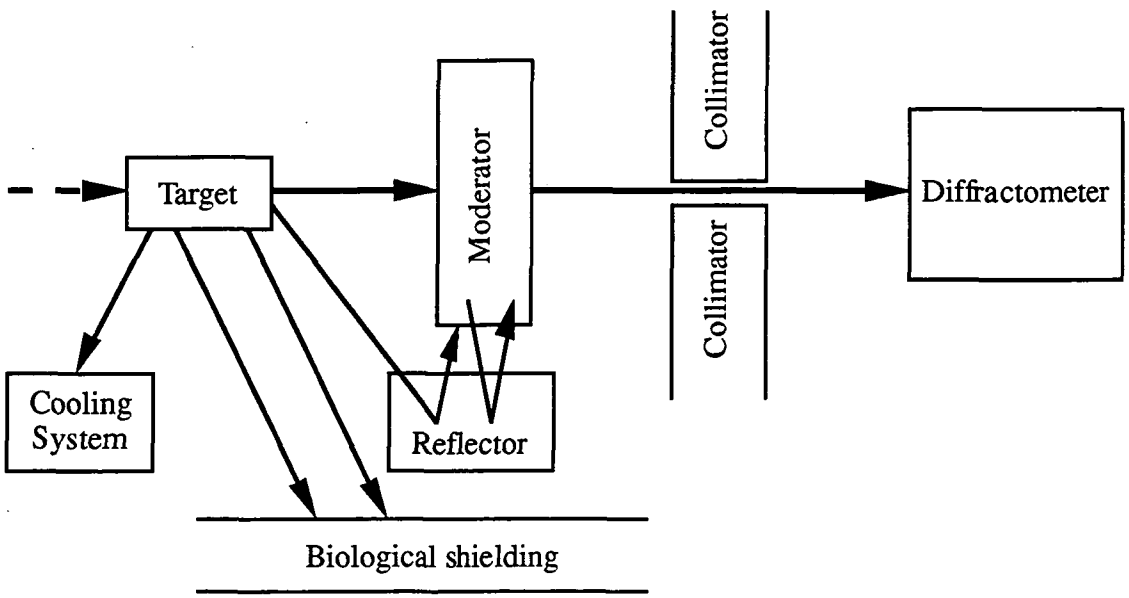

Figure 2.3.2 *- A schematic representation of a generic pulsed neutron source.*

Electrons produce neutrons in a two stage process. First the electrons are accelerated and fired at a heavy metal target. Here the electron charges interact strongly with the electromagnetic fields of the target nuclei causing the electrons to decelerate rapidly. This deceleration produces bremsstrahlung or "braking radiation" and heat. The γ rays produced then excite some of the target nuclei, which subsequently decay with the

emission of a neutron. This process is extremely inefficient, with only a few percent of the incident electrons giving rise to a neutron. However, electrons are easy to produce and accelerate and this method was used extensively to produce pulsed neutron beams when the technique was in its infancy.

Proton spallation involves firing extremely high energy protons at a heavy metal target. The protons hit the target with such force that they 'chip' neutrons off the metal nuclei. Because the protons have such high energies they penetrate deep into the target metal and interact with many nuclei, generating around 30 neutrons per proton. Clearly, the process is much more efficient than those involving electrons but the high cost of proton accelerators make proton spallation a more expensive technique.

Nuclear fission, the same process that occurs in the steady reactors and is used to produce continuous neutron beams, can also be used as the basis of pulsed neutron sources. The pulses can be created mechanically by cycling the fissile material to create a pulsed reactor. Alternatively, the pulses can be produced by a fast neutron source such as the target of an electron accelerator which is surrounded by fissile material. The fissile material acts as a 'neutron-multiplier' producing between 5 and 100 times more neutrons than were present in the fast pulse. The precise amount of multiplication that occurs can be adjusted using control rods. These sources are called neutron 'boosters' and can produce pulses faster than mechanical systems. However, background levels can be high. The background is reduced by combining a neutron 'booster' with a mechanical device that cycles the fissile material in time with the fast neutron pulse. These 'dynamic' or 'super boosters' have low backgrounds but the frequency with which pulses can be produced is limited by the mechanical cycling device.

2.3.1.2 Neutron Detectors

Like X-rays, neutrons are electrically neutral so in order to be detected they must be absorbed and modified by the detecting material. Perhaps the simplest type of neutron

detector is the proportional counter. Proportional counters contain a pressurised absorbing gas such as ^3He or BF_3. Neutrons passing through this gas are captured by the gas molecules. These absorption reactions produce charged secondary particles -

$$^3He + n \longrightarrow H^+ + {}^3H^-$$

$$^{10}B + n \longrightarrow {}^7Li + {}^4He^+ + \gamma$$

The charged particles collide with other molecules and ionise them. The electrons produced by this ionisation go on to ionise further gas molecules. This cascade of electrons is detected by an anode wire. The signal obtained is proportional to the number of primary particles.

Another common type of neutron detector is the scintillation counter. These detectors contain a fluorescent material such as ZnS doped with B_2O_3 and Ag. Incoming neutrons are captured by the doping material producing high velocity decay products. These excite the electrons in the fluorophor from the valence band into the conduction band. When the excited ions return to the ground state they emit light. The light is collected by reflectors and transmitted to a photomultiplier which converts it into an electrical signal.

2.3.2 Advantages and Disadvantages of Neutrons

Despite the high cost, complexity and the need for large samples neutron diffraction experiments continue to be performed because neutrons have many unique properties which make them more useful than X-rays in some circumstances.

Unlike X-rays, which are scattered by electrons, neutrons are scattered by atomic nuclei. Consequently, the neutron scattering power of an atom is not strongly related to its atomic number (***Figure 2.3.3***). This has several advantages: it is possible to locate light atoms, such as hydrogen, precisely in the presence of heavier ones, it is possible to distinguish

between light elements adjacent to one another in the periodic table and finally, since isotopes of the same element can also have substantially different neutron scattering cross-sections (eg. ^{1}H and ^{2}H: ***Figure 2.3.3***), neutron diffraction is ideal for structural investigations of isotopically labelled species.

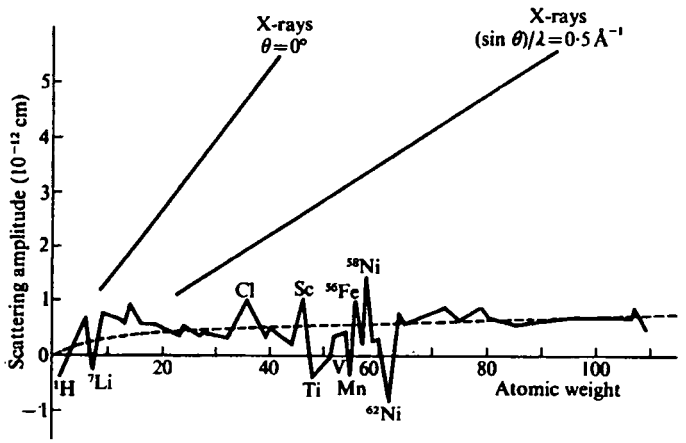

Figure 2.3.3 *- Variation in neutron scattering length with atomic mass.*

Neutrons are non-destructive and can be used to study even the most delicate biological materials without causing radiation damage. They are also electrically neutral and therefore highly penetrating. As a result neutrons can probe bulk materials non-destructively. When used in conjuction with cryostats, furnaces high pressure cells or other speciallised sample environments they can provide measurements of bulk processes under realistic conditions.

Lastly, neutrons possess a magentic moment. This magentic moment couples directly with spatial variations in the magentisation of materials on an atomic scale and makes it possible to study magnetic structure and dymanics using neutron diffraction.

2.4 SXD AT ISIS

Three of the four neutron experiments descibed in this thesis were conducted using the single crystal time-of-flight Laue diffractometer, SXD (Wilson, 1990), at the ISIS proton spallation source (the fourth was conducted on D19 at the Institut Laue Langevin (ILL), Grenoble, France). Both the layout and operation of SXD are very different from those of the typical four circle diffractometer and therefore these aspects are described fully in the sections that follow.

2.4.1 The ISIS Proton Spallation Source

The pulsed source ISIS is a proton spallation source. A proton beam is produced by accelerating a stream of H^- through a linear accelerator (linac). The beam of H^- then passes through a stripper foil which removes the electrons. The bare protons thus generated are accelerated further in a synchrotron, where they are bunched into two groups. When they reach the desired energy (800 MeV at ISIS) both bunches are ejected almost simultaneously by a magnetic 'kicker'. The protons are guided by magnets along the extracted proton beam line and hit a tantalum or uranium target. When the high energy protons hit the target they liberate neutrons by a variety of nuclear processes. The fast neutrons produced then pass through a series of hydrogenous moderators where they are slowed down to thermal and epithermal energies. SXD is situated on the ambient temperature (316K) water moderator. The pulses emerging from the moderator are somewhat broader than they were when they entered it because all of the neutrons that make up the pulse spend slightly different lengths of time in the moderator colliding with the water molecules. However the broadening is not significant because the moderators are small in order to retain pulse resolution and allow time-of-flight methods to be used on the full white beam. The whole process, which is shown schematically in ***Figure 2.4.1***, is repeated 50 times each second to produce the pulsed beam.

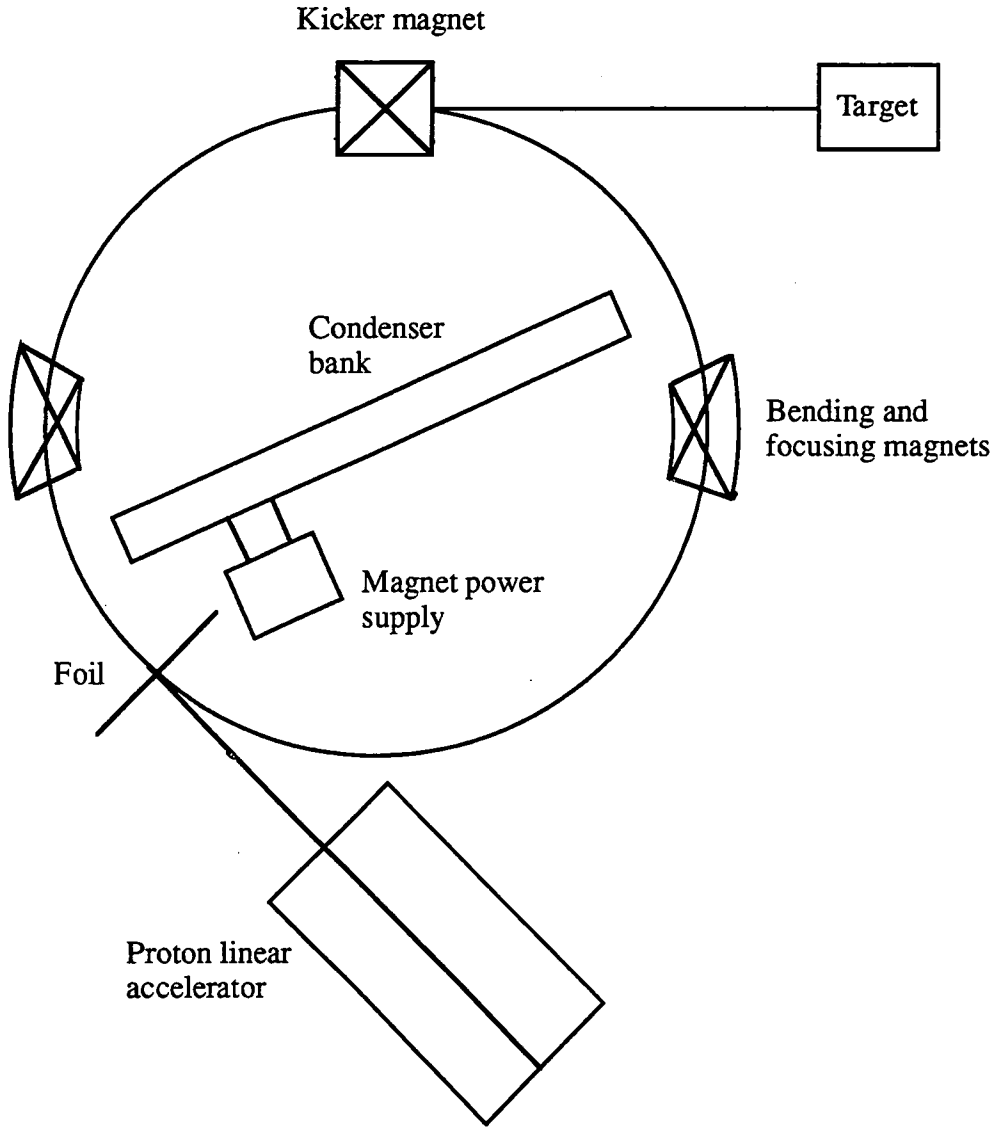

Figure 2.4.1 *- A schematic representation of a proton spallation neutron source.*

2.4.2 SXD

SXD is a time-of-flight single crystal Laue diffractometer. Laue diffraction is the term used to decribe what happens when a stationary single crystal is bathed in a beam of X-rays or neutrons with a continous spectrum of wavelengths instead of one of a single wavelength. Since the beam is composed of radiation of all wavelengths Braggs' Law (Section 2.1.1) is satisfied for many sets of crystal planes simultaneously and complex diffraction patterns are observed. Although Laue diffraction patterns are complex, time-of-flight techniques simplify their interpretation and enable all of the three dimensional

data that they contain to be extracted. SXD has been designed to take full advantage of this. It combines the time sorted white neutron beam available at ISIS with two large position sensitive (PSD) 'area' detectors thus enabling large volumes of reciprocal space to be surveyed in a single measurement or frame. ***Figure 2.4.2*** shows a typical three dimensional frame of SXD data containing around 400 Bragg peaks.

Figure 2.4.3 shows the layout of SXD. It consists of a collimator made of 'crispy-mix' (powdered B_4C in resin), which allows the diameter of the incoming beam to be reduced to any one of series of values between 8 and 15mm; for the measurements described here a 10mm diameter beam was used, a sample stage mounted on a crystal orientator comprised of two perpendicular circles, ϕ and χ, and two large PSDs each made up of a 64 by 64 array of fibre-optic encoded ZnS scintillation counters (***Figure 2.4.4***). The whole instrument is surrounded by sheets of 5cm thick borated polyethene shielding to reduce background scattering (***Figure 2.4.4***) and sits in a small blockhouse constructed of steel reinforced concrete and borated wax. In addition to the helium Displex closed cycle refrigerator (CCR, 12- 300K) used for all the experiments described in Chapters 3 and 4, SXD can also accommodate a liquid helium 50mm bore 'Orange' cryostat or a vanadium element furnace unit allowing data collections to be conducted over the temperature range 1.5 - 1200K. The data collection temperature is monitored using a Rh-Fe thermocouple. The Instrument is controlled and data is collected using a VAX Workstation 3600 located in a cabin above the blockhouse.

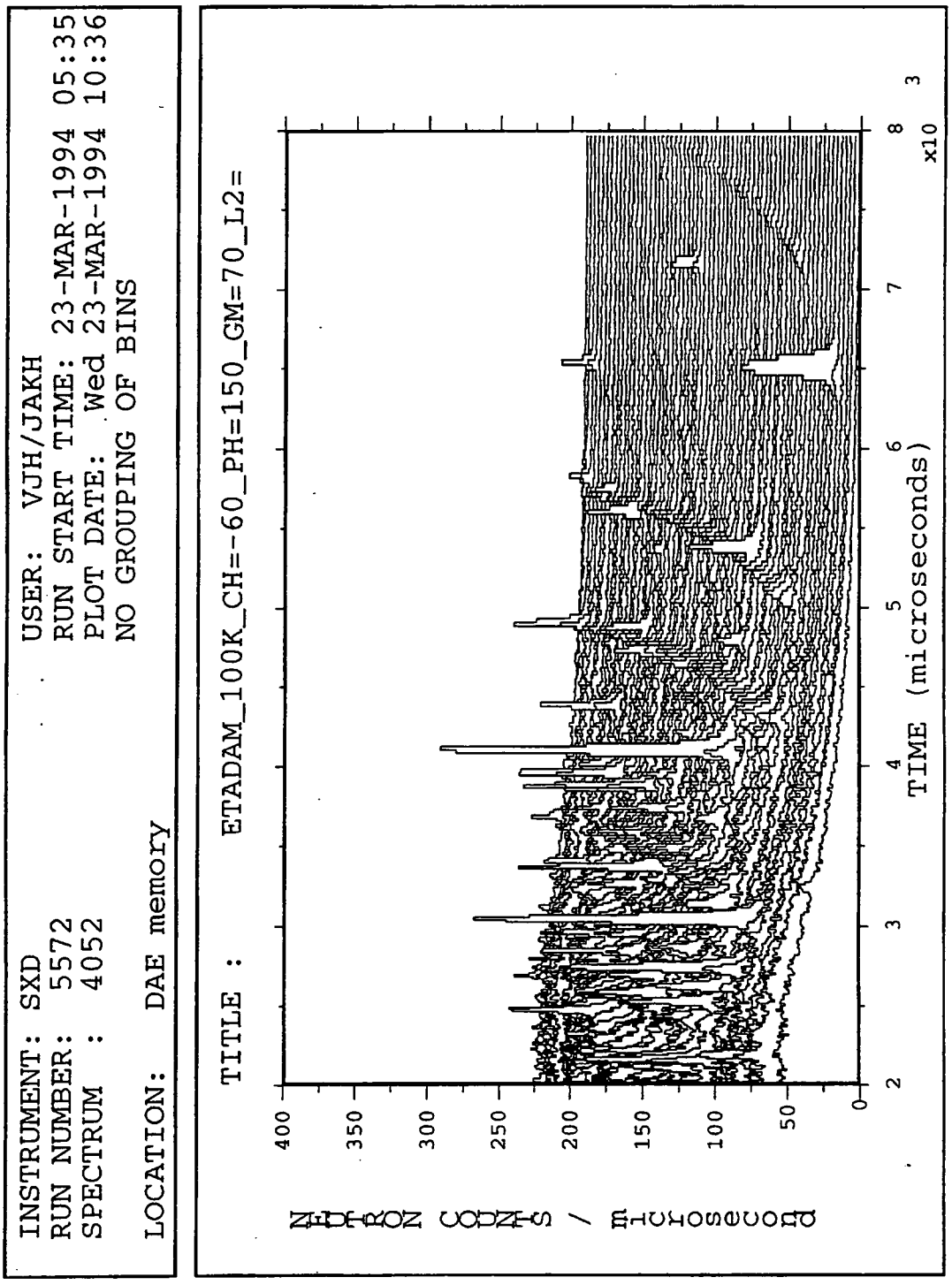

Figure 2.4.2 *- A typical frame of data from SXD.*

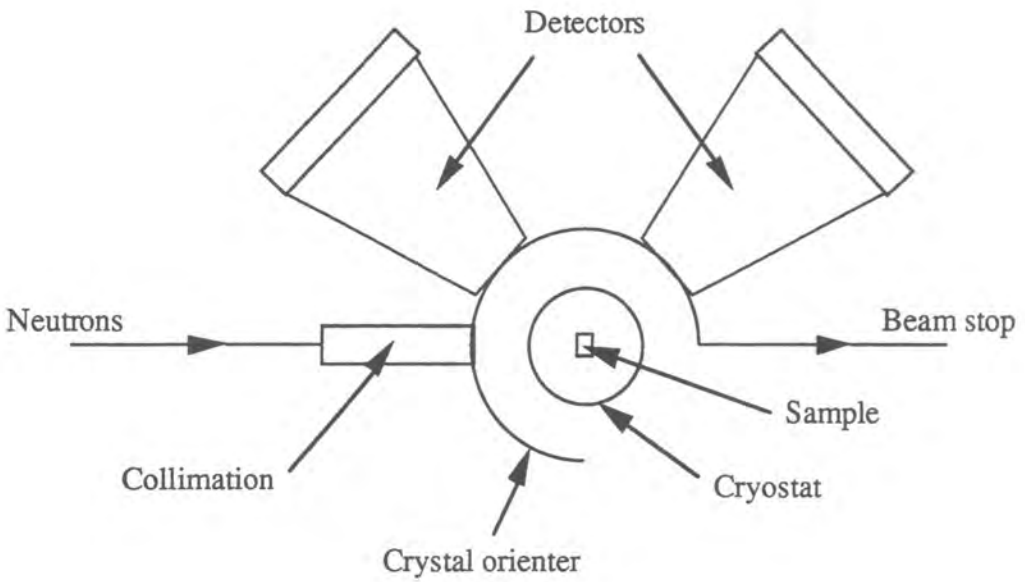

Figure 2.4.3 *- The layout of SXD.*

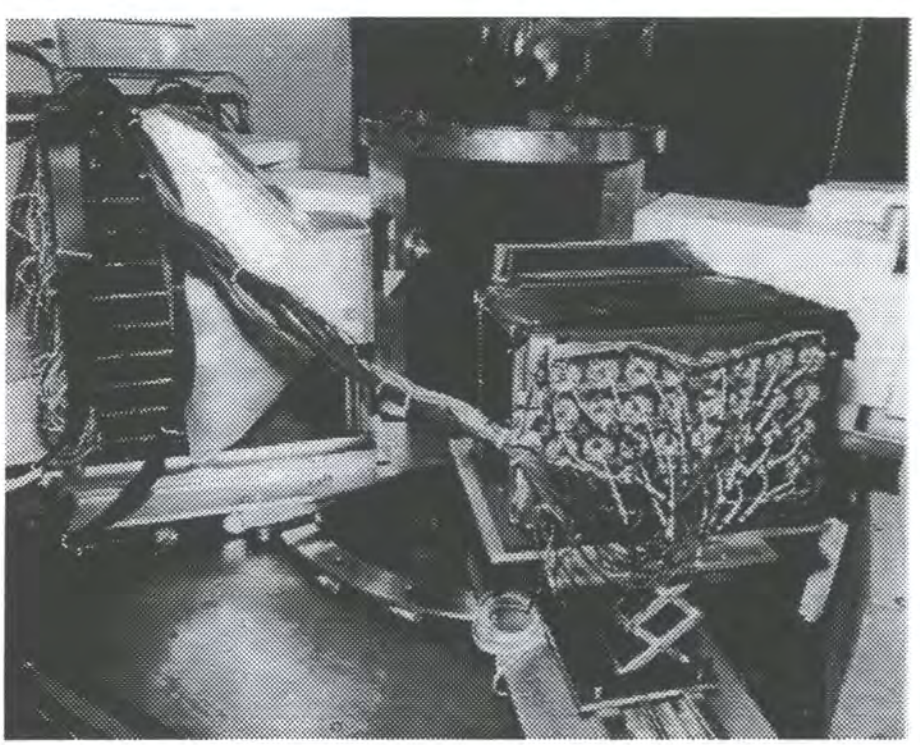

Figure 2.4.4 *- A view of SXD showing the PSDs and the borated polyethene shielding.*

2.4.3 An Overview of SXD Experimental Procedure

2.4.3.1 Crystal Selection and Mounting

Since the neutron flux at ISIS is in the region of 100 times lower than the X-ray flux of a standard laboratory tube, the crystals used for neutron diffraction must have volumes which are correspondingly larger than those used for X-ray diffraction experiments. In practise this means that neutron crystals of between 1 and 100mm^3 (depending of the nature of the sample) are required in order to obtain sufficiently high diffracted intensity.

The samples used for low temperature data collections involving the helium Displex are mounted on short (20 - 40mm) tapered (6 - 1mm) aluminium pins using a fast setting epoxy resin. These samples are sometimes wrapped in this aluminum foil to ensure that the sample remains firmly adhered to the aluminium pin when it is cooled whilst hanging upside down on the SXD sample stage. Excess glue is masked using cadmium to reduce hydrogen scattering. The mounted sample is inserted into a copper block at the tip of the CCR head and held in place using a 1.5mm hex head grub screw. The position of the pin is adjusted such that the distance from the centre of the sample to the recessed underside of the top flange on the CCR head is 276mm. This ensures that the centre of the sample coincides with the beam centre when the CCR head is inserted into the sample tank. Since the diameter of the neutron beam is large compared with the sample, additional crystal centering is not normally required.

2.4.3.2 Data Collection Methodology and Initial Indexing

During the three years over which the experiments described in Chapters 3 and 4 were conducted the data collection methodology used on SXD evolved considerably. Early structural studies employed a single PSD at only one 2θ angle. Later, data were collected with the detector at two different 2θ angles. This modification increased the intesities of some of the weakest reflections in each frame giving rise to higher numbers of observable

reflections in the whole dataset. Finally, in 1995, a second detector was introduced allowing data to be collected at two 2θ angles simultaneously thus reducing data collection times and simplying experimental procedures.

Section 2.4.2 describes how large volumes of reciprocal space can be surveyed in a single measurement using SXD. This makes it possible to collect complete sets of diffraction data from crystals in just a few different orientations. Typical data collection strategies involve collecting between 15 and 46 frames from each detector, at a series of χ and ϕ angles selected to ensure good coverage of reciprocal space. Since the angles subtended by each detector are large it is possible to move both χ and ϕ in steps of up 30° and still guarantee good overlap between the frames. Each frame is typically exposed for between 1 and 6 hours, depending on the nature of the sample and the size of the unit cell.

Since there are several hundred Bragg peaks in each frame of data it is possible to index a crystal lattice using just one frame. Peak positions are determined and used to derive an orientation matrix (see Section 2.2.2). This matrix is refined and used to index the peaks located in subsequent frames.

2.4.3.3 Data Reduction

The reflections in the frames are located in one of two ways: either by a simple peak searching routine or by using the previously determined orientation matrix to predict the positions of the peaks. The former method is used more frequently at present.

Structure factor information is extracted from the raw intensities measured by SXD in a multi-stage process (Wilson, 1996). The peaks are integrated using a profile fitting approach based on the known analytical shape of the reflections in the time-of-flight direction, well understood from the characteristics of the ISIS source and moderator. The function used is a Gaussian convoluted with a decaying exponential function, which is found to reproduce the peak shape well. The variable parameters in this fit are the

Gaussian height and width and the time constant of the exponential, all of which vary with time-of-flight. This method is found to be both sensitive and reliable in the integration of both strong and weak peaks. It should be noted that reflections for which this profile fitting procedure fails after four attempts on different integration windows are excluded from the data set, thus resulting in a somewhat reduced occurrence of very weak or "unobserved" peaks in the final data set.

The reflection intensities are then normalised to the incident beam profile using the incoherent scattering from a polycrystalline vanadium sample. Semi-empirical absorption corrections are also applied at this stage, using the vanadium and sample scattering. The resulting intensities are then reduced to structure factors. These data are used in the CCSL (Brown and Matthewman, 1993) least squares refinement program SFLSQ, to apply a variable wavelength extinction correction based on the Becker-Coppens formalism (Becker and Coppens, 1974) using a Gaussian model with one variable parameter, the mosaic spread.

2.5 REFERNECES

Becker, P., Coppens, P.(1974) Acta Cryst. A**30**, 129 and 148.

Bragg, W. H. and Bragg, W. L. (1913) Proc. R. Soc. A, **88**, 428.

Brown, P.J. and Matthewman, J.C. (1993) *Rutherford Appleton Laboratory Report*, RAL-93-009.

Busing, W. R. and Levy, H. (1957) Acta Crystallogr., **10**, 180

Clegg, W. (1984) J. Appl. Cryst., **17**, 334.

Cosier, J. and Glazer, A. M. (1986) J. Appl. Cryst., **19**, 105.

Elsasser, W. M. (1936) C.r. hebd. Séanc. Acad. Sci. Paris, **202**, 1029.

Friedrich, W., Knipping, P. and von Laue, M. (1912) Proc. Bavarian Acad. Sci., 303.

Furnas, T. C. (1957) *Single Crystal Orienter Instruction Manual*, General Electric X-ray Corp., Milwaukee.

Giacovazzo, C. (1992) *Fundmentals of Crystallography*, Oxford University Press,

Glusker, J. and Trueblood, K. N. (1985) *Crystal Structure Analysis: A Primer 2nd Edn.*, Oxford University Press, New York.

Halban, H. and Preiswerk, P. (1936) C.r. hebd. Séanc. Acad. Sci. Paris, **203**, 73.

Karle, I. L., Dragonette, K. S. and Brenner, S. A. (1965) Acta Crystallogr., **19**, 713.

Mitchell, D. P. and Powers, P. N. (1936) Phys. Rev., **50**, 486.

Molecular Structure Corporation, (1989) TEXSAN, Version 5.0, TEXRAY Structure Analysis Package. MSC, 3200 Research Forest Drive, The Woodlands, TX77381, U.S.A.

North, A. C. T., Phillips, D. C. & Matthews, F. S., (1968) Acta Crystallogr., A**24**, 351-359.

Sayre, D. (1952) Acta Crystallogr., **5**, 60.

Sheldrick, G. M., (1990) Acta. Crystallogr., A**46**, 467-473.

Sheldrick, G. M., (1995) SHELXTL, Version 5.03/VMS, Siemens Analytical X-ray Instruments Inc., Madison, Wisconsin, U.S.A.

Sheldrick, G., M. (1993) SHELXL-93: *Program for the refinement of crystal structures using single crystal diffraction data*, University of Gottingen, Germany.

Siemens (1994) *XSCANS: X-ray Single Crystals Analysis System*, Version 2.1, Siemens Analytical X-ray Instruments Inc., Madison, Wisconsin, USA.

Sparks, R. A. (1976) *Crystallographic Computing Techniques*, ed. Ahmed, F. R., Munskgaard, Copenhagen, pp. 452 - 467.

Sparks, R. A. (1982) *Crystallographic Computing*, ed. Sayre, D., Clarendon Press, Oxford, pp. 1 - 18.

Stalke, D. S. and Kottke, T. (1993) J. Appl. Cryst., **26**, 615 - 619.

Wells, M. (1960) Acta Crystallogr., **13**, 722.

Wilson, A. J. C. (1942) Nature, **150**, 152.

Wilson, A. J. C. (1949) Acta Crystallogr., **2**, 318.

Wilson, C. C. (1990) *Neutron Scattering Data Analysis 1990*, ed. Johnson, M. W., IOP Conference Series Vol. 107, Adam Higler, Bristol, p 145 - 163.

Wilson, C. C. (1996) J. Mol. Struct., in press.

Zinn, W. H.(1945) Phys. Rev., **71**, 752.

CHAPTER 3

Neutron Diffraction Studies of 3,5-Dinitrocinnamic Acid and 2-Ethynyladamantan-2-ol

3.1 INTRODUCTION

3.1.1 3,5-Dinitrocinnamic Acid

The X-ray derived crystal structure of 3,5-dinitrocinnamic acid (**I**) was first reported in 1991 (Desiraju and Sharma, 1991). The study revealed that **I** crystallises as a carboxylic acid type O-H...O dimer in which the two hydrogen bonded molecules are related by two fold rotational symmetry. Since carboxylic acid dimers typically pack about inversion centres (Desiraju, 1989), the structure of **I** is somewhat unusual. An analysis of the packing indicated that there is an extensive C-H...O bonded network present in the crystal lattice involving up to 7 unique C-H...O bonds with C...O separations of less than 3.75Å but because the hydrogen atom positions were not well resolved by the X-ray analysis, precise hydrogen bond geometries could not be determined.

It could be argued that since 3,5-dinitrocinnamic acid is particularly well suited to the formation of C-H...O bonds, because it possesses acidic, alkenic and aromatic protons as well as numerous oxygen atom acceptors, it is not surprising that such a complex C-H...O bond network is formed. However, the crystal structure of the related compound 2,4-dinitrocinnamic acid (**II**), which possesses the same structural features as **I**, is known to contain far fewer C-H...O bonds (Desiraju and Sharma 1991) and interestingly it crystallises as an inversion centre dimer. This difference was attributed, by Desiraju and Sharma, to differences in the conformational flexibilities of the two molecules. In **II** the 2-NO_2 group is sterically hindered by the acid side chain and cannot participate effectively in C-H...O bonding. However, in **I** both NO_2 groups are sterically unhindered and all four nitro oxygen atoms form C-H...O bonds.

Desiraju and Sharma went on to conclude that it is the presence of the additional C-H...O bonds in the crystal structure of **I** which is responsible for the unusual two fold symmetry adopted by the carboxylic acid dimers. This conclusion was reached based on the differences between the structures of **I** and **II**, the results of computer modelling of **I**

which showed that the directional requirements of the C-H...O bonded network are not compatible with the inversion centre dimer found in **II** and simple molecular orbital calculations which indicated that the energy difference between the inversion centre and the two fold dimer structures is as low as 0.55kcal mol^{-1}, considerably less than the energy of a single C-H...O bond (1.0 - 3.2 kcal mol^{-1}: Rovira *et. al.*, 1995).

This conclusion was significant because prior to the publication of these results it had been assumed that C-H...O bonds were too weak to compete with O-H...O and other strong hydrogen bonds in determining crystal packings. However, since accurate hydrogen bond geometries could not be determined from the X-ray data, more detailed investigations of the energies of the C-H...O bonds and their role in determining the structure of **I** could not be conducted. Therefore a low temperature neutron diffraction study of 3,5-dinitrocinnamic acid was undertaken. The aim was to obtain the precise positions of the hydrogen atoms in the molecule, confirm the existence of the C-H...O bond network and determine accurate C-H...O hydrogen bond geometries. It was hoped that these lengths and angles could be used to calculate approximate energies for the unique C-H...O bonds present in the crystal lattice and so assess the importance of each bond and of the network as a whole in determining the crystal structure of **I**.

3.1.2 2-Ethynyladamantan-2-ol

The original X-ray analysis of 2-ethynyladamantan-2-ol (**III**) was conducted in 1982 by Lin *et. al.* (1982). They found that **III** crystallises in the monoclinic space group $P2_1/c$ and has two independent molecules, **A** and **B**, in the asymmetric unit. **A** and **B** are held together by a strong O-H...O hydrogen bond between the hydroxyl groups. In addition an intramolecular O-H...π bond between the hydroxyl and alkynic portions of molecule **A** was described. No other "unusually short intermolecular distances" were reported.

However, a more recent study involving infra-red analysis (Steinwender *et. al.*, 1993) has called into question the accuracy of this description of the structure of **III**. The

authors of the study measured both the solution and solid state infra-red spectra of **III** and compared the bending and stretching modes assigned to the O-H and C≡C-H groups in each. They found that the stretching modes of both O-H groups shift to lower frequency and are broader and more intense in the solid state. Whereas, the O-H bending modes shift to higher frequency relative to their positions in the solution spectrum. All of these observations are consistent with the formation of hydrogen bonds. Variations in the extent of the red shift of the stretching modes of the two O-H groups and the fact that the crystal structure of **III** was already known enabled Steinwender and co-workers to assign the shifts to the formation of two different O-H...X hydrogen bonds. The first is the O-H...O bond between crystallographically independent molecules in the same asymmetric unit as described previously (Lin *et. al.*, 1982) and the second is an unusual intermolecular O-H...π bond between the hydroxyl group of molecule **A** and the alkynic portion of a crystallographically equivalent molecule in an adjacent asymmetric unit. No evidence of an intramolecular O-H...π bond was found.

Only a small number of these O-H...π bonds have been described before (Hardy and MacNicol, 1976; Nakatsu *et al.*, 1978; Ueji *et al.*, 1982; Rzepa *et al.*, 1991; Al-Juaid *et. al.*, 1992) and recent database surveys (Viswamitra *et al.*, 1993; Rzepa, Smith and Webb, 1994) show that these interactions are very rare. Rzepa, Smith and Webb (1994) located only 13 structures* containing O-H...π bonds "significantly shorter than the van der Waals' contact distance".

A similar comparison of the stretching and bending modes of the C≡C-H groups in **III** in solution and in the solid state (Steinwender *et. al.*, 1993) revealed that one is involved in hydrogen bonding but that the other is not. The shifts observed for the former C≡C-H were attributed to a C-H...O bond between the alkynic C-H group of molecule **A** and the hydroxyl group of molecule **B** which was overlooked by the authors of the original X-ray study.

---

* 2-ethynyladamantan-2-ol was one of these.

The authors used the available X-ray crystallographic data to obtain approximate geometries for the hydrogen bonds which they had proposed. Both the C-H...O bond (H...O, 2.26Å; C-H...O, 171°) and the O-H...π (H...π, 2.22Å; O-H...π, 169° where π is the C≡C bond mid-point) bond have almost ideal hydrogen bond geometries which, if accurate, make 2-ethynyladamantan-2-ol an excellent model system for both types of weak interaction. Therefore, a low temperature neutron diffraction study of **III** was undertaken in order to confirm the hydrogen bonding scheme proposed by Steinwender and co-workers (1993) and to characterize accurately the C-H...O and unusual O-H...π bonds thought to be present.

3.2 EXPERIMENTAL DETAILS

Both of the neutron diffraction experiments described in this chapter were conducted at the pulsed neutron source, ISIS, on the Laue time-of-flight diffractometer, SXD (Wilson, 1990). The proton spallation neutron source at ISIS and the layout of SXD are described in Section 2.3. These sections focus on the details specific to each experiment with reference to the appropriate parts of Section 2.3 where necessary. Both experiments were conducted using similar procedures and under the same conditions and are therefore described together in the following sections.

3.2.1 Preliminary Studies

3.2.1.1 Low Temperature Stability

It is desirable to conduct neutron diffraction experiments at low temperatures in order to reduce thermal motion and increase the signal to noise ratio. However, since the original X-ray analyses of both 3,5-dinitrocinnamic acid (Desiraju and Sharma, 1991) and 2-ethynyladamnatan-2-ol (Lin *et. al.*, 1982) were conducted at room temperature the stability of these compounds at low temperature could not be guaranteed. In order to overcome this problem small crystalline samples of each compound were cooled and examined carefully using X-rays prior to the start of each neutron experiment.

In both cases a small crystal, taken from the same batch as the larger neutron crystals, was mounted on a glass fibre with epoxy resin and placed on the Rigaku AFC6S diffractometer. Orientation matrix and cell information were obtained, using standard auto-indexing procedures, from 20 reflections and in both cases the parameters calculated were in good agreement with those reported in the original structure determinations. Once the cell parameters had been determined, one of the sharpest and most intense Bragg peaks located during the indexing procedure was selected and repeatedly scanned while the crystal was cooled to 80K.

The cooling device used was an Oxford Cryosystems nitrogen Cryostream (Cosier and Glazer, 1986) which maintains stable temperatures over the range 77.4 - 323K. The crystals were cooled at a rate of 120K an hour and in steps of 10K in order to minimise thermal shock. Prior to cooling and after each 10K drop in temperature the monitor reflection was scanned. A gradual shift in the position of the peak is to be expected when the sample is cooled since the thermal motion is frozen out and the crystal lattice contracts. (It was therefore necessary to re-centre the monitor reflection approximately every 50K). However, any sudden change in peak position or in the shape of peak profile, such as splitting or a dramatic change in intensity, indicates that the sample has undergone a phase transition or has deformed in some other way. Luckily, no such changes were observed in either sample at temperatures above 80K and it was therefore concluded that both 3,5-dinitrocinnamic acid and 2-ethynyladamantan-2-ol are stable down to 80K.

3.2.1.2 Crystal Quality

In order to assess the quality of the large crystals grown for neutron diffraction they were examined optically with a polarising microscope and investigated using X-rays prior to each neutron experiment.

Large samples (10 - 100mm^3) which passed initial screening using the polarising microscope, were mounted using plasticine in specially made cups, adapted from large Lindemann tubes, (***Figure 3.2.1***) and placed on the Rigaku AFC6S diffractometer (3,5-dinitrocinnamic acid) or on the Siemens P4 diffractometer (2-ethynyladamantan-2-ol). Although these samples were far too large to fit in the homogenous X-ray beam of either instrument it was still possible to index them successfully using standard auto-indexing procedures. The X-ray tube was operated at low power in order to avoid saturating the detector. Several crystals of each compound were investigated in this way and each one that yielded the correct cell parameters after

auto-indexing was considered to be single and suitable for neutron diffraction. All these indexing investigations were carried out at room temperature.

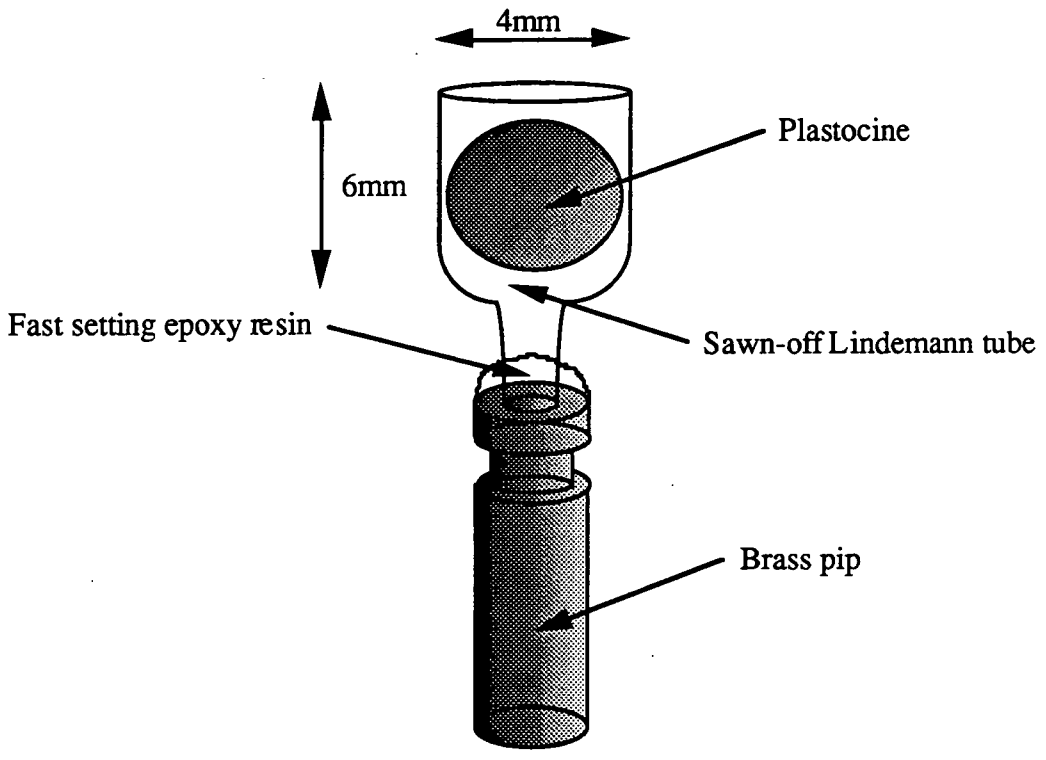

Figure 3.2.1 *- Cup used to mount neutron crystals on laboratory X-ray diffractometer.*

3.2.2 Crystal Selection and Mounting

The 3,5-dinitrocinnamic acid crystal chosen for the neutron diffraction experiment was an amber coloured square plate with approximate dimensions 5 x 5 x 3mm which had been indexed successfully using X-radiation. Before it was mounted, the crystal was wrapped in a very thin aluminium foil. The purpose of the foil is to ensure that the sample remains firmly adhered to the aluminium pin on which it is mounted when it is cooled, whilst hanging upside down in the SXD sample canister. The wrapped sample was glued to a tapered aluminium pin using a fast setting epoxy resin and a small crystallite growing on one of the rectangular faces was shielded from the incoming neutron beam using a piece of cadmium shielding attatched to the end of the pin (***Figure 3.2.2***).

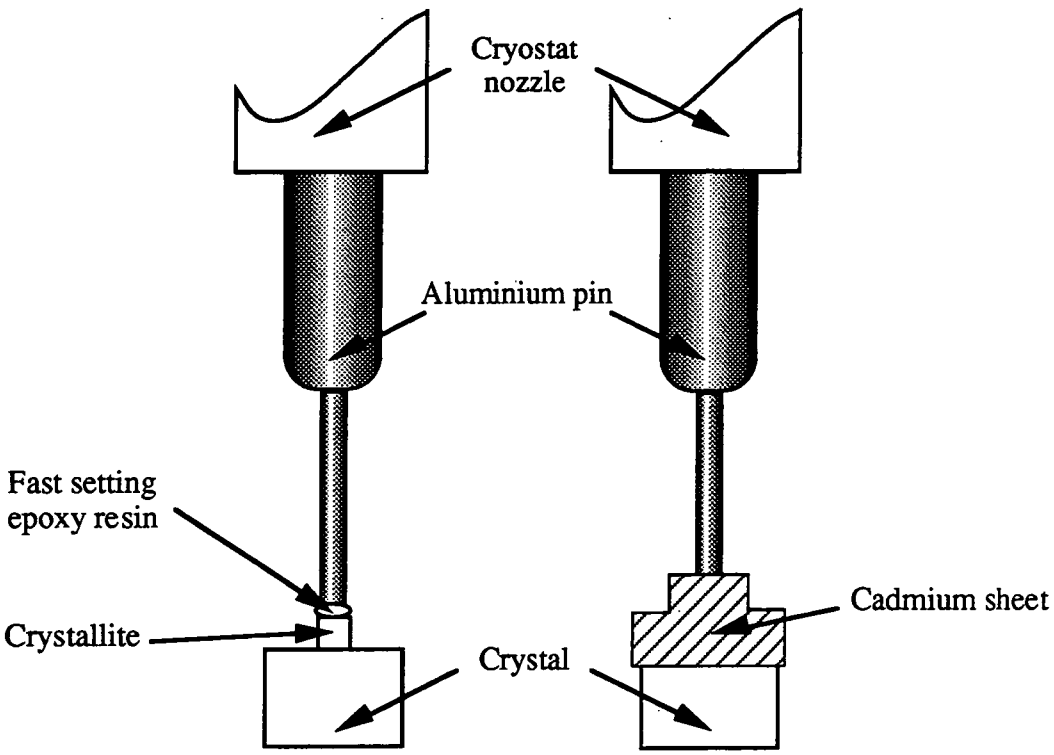

Figure 3.2.2 *- Schematic representation of the way in which the 3,5-dinitrocinnamic acid sample was mounted for the neutron diffraction experiment.*

The mounted crystal was fitted to the end of the cryostat nozzle and an aluminium foil "sample catcher" was placed around it. The cryostat was then inserted into the sample canister and bolted into place (see Section 2.4.2). The air was evacuated from the sample canister and the crystal was cooled to 100K.

The 2-ethynyladamantan-2-ol sample which was used for the neutron diffraction experiment was a clear, previously indexed crystal with approximate dimensions 3 x 2 x 1.5mm. Once again the sample was wrapped in thin aluminium foil prior to mounting and attached to an aluminium pin using fast setting epoxy resin. However, since there were no crystallites or other flaws in the sample no additional cadmium shielding was required in this case. The mounted sample was attached to the end of the cryostat and surrounded by a foil sample catcher in exactly the same way as the 3,5-dinitrocinnamic acid crystal. The

The cryostat was then bolted into the sample canister, the air was evacuated and the sample was cooled to 100K.

3.2.3 Data Collection and Indexing

Both of the experiments described in this chapter were conducted prior to the introduction of the second detector on SXD (see Section 2.3.3.2). The first structure determination (3,5-dinitrocinnamic acid) took place in November 1993 and was performed with a single detector at just one 2θ angle. The second experiment (2-ethynyladamantan-2-ol) was conducted in March 1994 by which time data were routinely collected at two 2θ angles.

3.2.3.1 Indexing and Data Collection for 3,5-Dinitrocinnamic Acid

The data collection regime employed for this experiment involved rotating ϕ from 0° to 180° in steps of 30° at χ angles of 0°, 30°, 60° and 90°. Frames of data were collected at each of these 28 different crystal orientations and initally each frame was 'exposed' for 900 μA. Since the neutron beam at ISIS operated at approximately 180 μA an hour it was anticipated that it would take roughly 5 hours to collect each frame. Data from the first of these frames were used to index the cell (see ***Table 3.2.1***).

After three or four frames had been collected in this way it became apparent that a fault had developed on the detector. The first eight rows had stopped registering any neutron counts and this had created a blank region at the bottom of each frame. In order to compensate for this the data collection regime was amended. A second set of frames were collected, at lower counting statistics, which were offset from the first set by 15° in ϕ. Thus, the first frame in this new set was collected at $\phi = 15°$ and $\chi = 0°$, the second at $\phi = 45°$ and $\chi = 0°$ and so on for all four χ angles. The result was to bring reflections close to the edge of the detector in the first set of frames close to the centre of the detector in the second set. Increasing the overlap between the frames in this way ensured that no

reflections were lost in the blind region on the detector. However, the total data collection time for the experiment was increased considerably as a result.

Table 3.2.1 *- Details of the data collections and structure refinements for 3,5-dinitrocinnamic acid and 2-ethynyladamantan-2-ol.*

Compound	3,5-Dinitrocinnamic acid	2-Ethynyladamantan-2-ol
Formula	$C_9H_6N_2O_6$	$C_{12}H_{16}O$
Molecular Weight	238.0	176.0
ρcalc (gcm^{-1})	1.625	1.212
a (Å)	15.728(5)	6.779(3)
b (Å)	7.745(5)	22.491(10)
c (Å)	16.050(5)	12.649(6)
α (°)	90	90
β (°)	95.53(3)	93.88(3)
γ (°)	90	90
Volume ($Å^3$)	1946(2)	1930(2)
Crystal System	Monoclinic	Monoclinic
Space Group	C2/c	$P2_1/c$
Z	8	8
Morphology	Square plate	Rectangular prism
Colour	Amber	Colourless
Size (mm)	5 x 5 x 3	3 x 2 x 1.5
No. of Measured Data	7300	12628
No. of Unique Data	2054	3503
No. of Observed Data	2054	3503
σ(I) Cut Off	$I > -4\sigma(I)$	$I > -4\sigma(I)$
R_{merg}	0.053	0.056
No. Parameters Refined	208	523
R	0.061 (F)	0.083 (F)
wR	0.132 (F^2)	0.182 (F^2)
GooF	1.065	1.134
Weighting Scheme	$1/\sigma^2$	$1/\sigma^2$
Δρ min ($Å^{-3}$)	-1.367	-1.663
Δρ max ($Å^{-3}$)	1.602	2.056

Problems with the neutron source during the later part of the experiment made it necessary to reduce the counting statistics from 900 μA to 700 μA for the original set of frames and from 450 μA to 350 μA for the overlapping frames in order to complete the data collection within the eight days available.

3.2.3.2 Data Collection and Indexing for 2-Ethynyladamantan-2-ol

The data collection procedure used for 2-ethynyladamantan-2-ol was identical to the one used for 3,5-dinitrocinnamic acid. The first data set was collected with the detector centred at $2\theta = 55°$ and comprised of a series of 28 frames measured at ϕ angles of 0°, 30°, 60°, 90°, 120°, 150° and 180° and at χ angles of 0°, 30°, 60° and 90°. Each frame was collected for 900 μA. Data from the first of these frames were used to determine an orientation matrix and cell parameters (see ***Table 3.2.1***). The detector was then moved to a position centred at $2\theta = 125°$ and an identical set of 28 frames were measured. Once again each frame was collected for 900 μA.

3.2.4 Data Processing and Refinement.

Structure factor information was extracted from the raw data obtained during these experiments using the procedures described in Section 2.3.3.4. Both data sets were corrected for absorption and extinction and merged prior to structure refinement. The refinement package used was SHELXL-93 (Sheldrick, 1993). Coherent neutron scattering lengths for C, N, O and H were taken from International Tables (Sears, 1992). The heavy atom positions from the original X-ray structure determinations were used as the starting models for both refinements. Hydrogen atoms were located in subsequent difference maps.

3.2.4.1 Data Processing and Structure Refinement for 3,5-Dinitrocinnamic acid

Of the 52 frames measured during the experiment only the 28 collected with higher counting statistics were used to obtain structure factor information. A total of 7300 reflections were extracted from the 28 frames. These data were merged yielding 2054 unique observed reflections with an R_{merg} of 0.054.

The structure of 3,5-dinitrocinnamic acid was refined, using these 2054 data, by full matrix least squares methods on F^2. All atoms were modelled anisotopically and a $1/\sigma$ weighting scheme was applied to the data. The refinement converged with a conventional R of 0.061 and a GooF of 1.065. ***Table 3.2.1*** gives further details of the data collection and refinement.

3.2.4.2 Data Processing and Refinement for 2-Ethynyladamantan-2-ol

Structure factor information was extracted from 47 of the 56 frames collected during the experiment. Peak searching located 12628 reflections in these 47 frames which, when merged, yielded 3503 unique observed reflections with an R_{merg} of 0.056.

The structure of 2-ethynyladamantan-2-ol was refined using block matrix least squares methods on F^2. Once again all atoms were modelled anisotropically and a $1/\sigma$ weighting scheme was applied to the data. The refinement converged with a conventional R of 0.083 and a GooF of 1.134. ***Table 3.2.1*** gives more details.

3.3 STRUCTURE OF 3,5-DINITROCINNAMIC ACID

3.3.1 Structural Details

Figure 3.3.1 shows the 50% probability thermal ellipsoid plot of the neutron derived structure of 3,5-dinitrocinnamic acid. ***Tables 3.3.1.*** and ***3.3.2*** contain bond lengths and selected interbond angles.

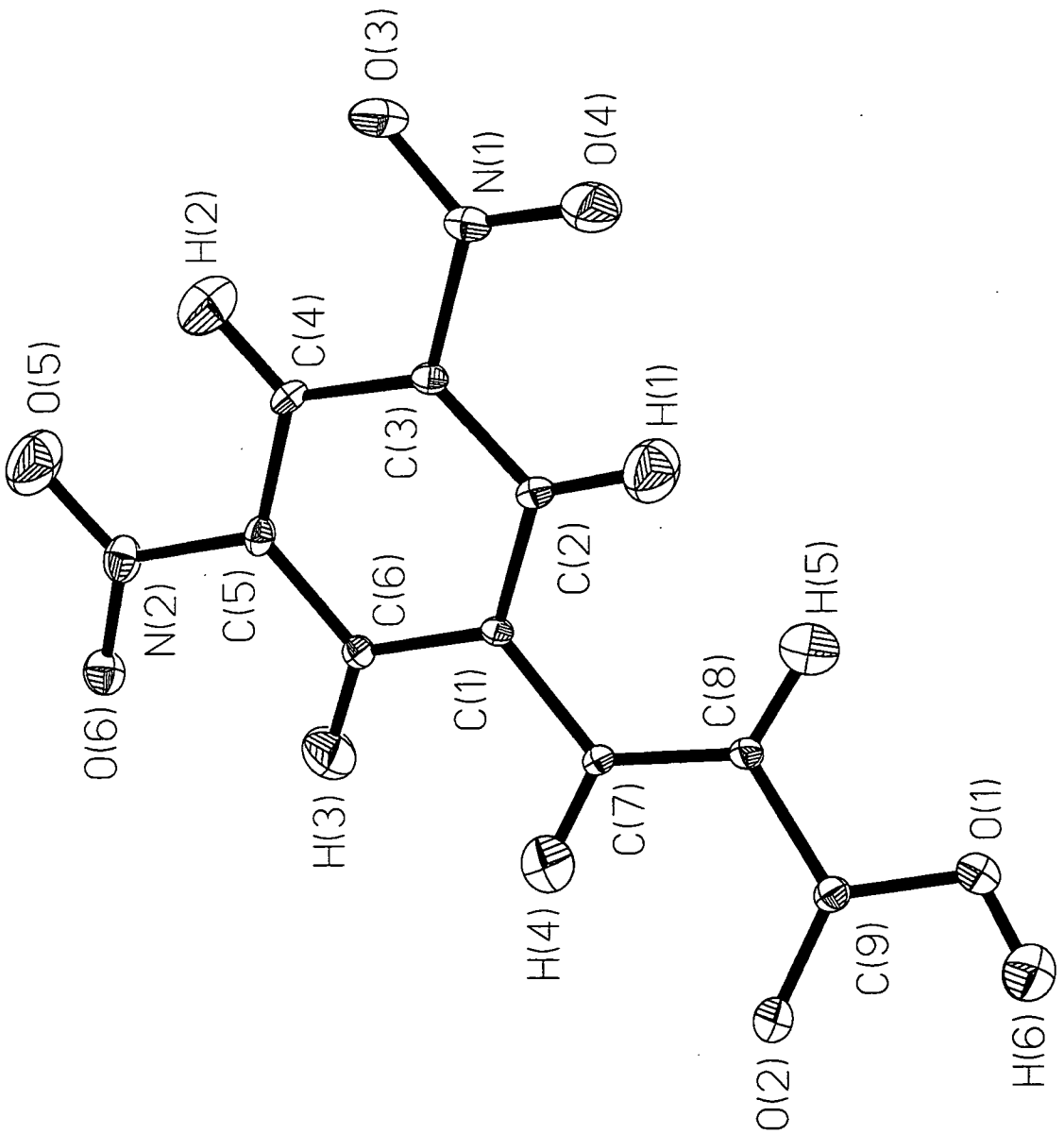

Figure 3.3.1 *- 50% probability thermal ellipsoid plot of 3,5-dinitrocinnamic acid.*

Table 3.3.1 *- Bond lengths in 3,5-dinitrocinnamic acid.*

	Length (Å)		Length (Å)
C(1) - C(6)	1.397(3)	C(7) - C(8)	1.342(3)
C(1) - C(2)	1.399(3)	C(7) - H(4)	1.057(6)
C(1) - C(7)	1.474(3)	C(8) - C(9)	1.470(3)
C(2) - C(3)	1.376(3)	C(8) - H(5)	1.081(6)
C(2) - H(1)	1.114(5)	C(9) - O(2)	1.226(3)
C(3) - C(4)	1.388(3)	C(9) - O(1)	1.322(3)
C(3) - N(1)	1.463(2)	N(1) - O(4)	1.205(3)
C(4) - C(5)	1.386(3)	N(1) - O(3)	1.215(3)
C(4) - H(2)	1.095(6)	N(2) - O(5)	1.210(4)
C(5) - C(6)	1.397(3)	N(2) - O(6)	1.215(3)
C(5) - N(2)	1.467(2)	O(1) - H(6)	0.986(7)
C(6) - H(3)	1.081(5)		

Table 3.3.2 *- Selected interbond angles in 3,5-dinitrocinnamic acid.*

	Angle(°)		Angle(°)
C(6) - C(1) - C(2)	119.9(2)	C(7) - C(8) - C(9)	118.9(2)
C(6) - C(1) - C(7)	117.4(2)	O(2) - C(9) - O(1)	123.5(2)
C(2) - C(3) - C(4)	123.8(2)	O(4) - N(1) - O(3)	123.6(2)
C(4) - C(5) - C(6)	123.2(2)	O(5) - N(2) - O(6)	123.9(2)
C(8) - C(7) - C(1)	125.4(2)	C(9) - O(1) - H(6)	109.6(4)

3.3.2 The C-H...O Bonded Network

In order to locate all of the close contacts present in the neutron derived crystal structure of 3,5-dinitrocinnamic acid a systematic search was performed using Non-bonded Interaction Pattern Matrix (NIPMAT) analysis (Rowland, 1995). NIPMAT analysis uses a shaded distance matrix to display nearest neighbour contacts between all atoms in the crystallographic asymmetric unit. To account for differences in atomic size, the absolute contact distance is normalised by subtracting the sum of the van der Waals' radii of the two relevant atoms. The results are plotted as a shaded matrix in which the darkest squares represent the closest contacts.

NIPMAT analysis has several advantages over other methods of locating intermolecular contacts such as packing diagrams or programs which search crystal structures for hydrogen bonds such as PLATON (Spek, 1990). It is a truly systematic method which does not involve the use of any *a priori* information about what kinds of interactions are attractive. This means that it can be used to locate unconventional interactions, for instance C-H...O, O-H...C or X...O_2N, without adaptation. Another advantage is that quantitative results are presented in a simple graphical form allowing complex interaction patterns to be analysed quickly and easily. NIPMAT makes comparison of hydrogen bonded networks in isostructural compounds particularly straightforward.

Figure 3.3.2 is the NIPMAT for the neutron derived structure of 3,5-dinitrocinnamic acid. Predictably, the carboxylic acid O-H...O hydrogen bond gives rise to the darkest square in the matrix indicating that it is the 'strongest' intermolecular interaction present. However, the large number of shaded squares in the matrix indicate that numerous other interactions are present in the network. In particular there are 13 close O...H contacts* in the C-H...O hydrogen bonding region of the matrix. Of these 13, 7 have already been decribed (Desiraju and Sharma, 1991) but the remaining 6 interactions are new. The precise geometries of all 13 of these contacts were determined from the neutron derived atomic coordinates using PLATON (Spek, 1990) and are shown in ***Table 3.3.3***

* Any contact that appears as a shaded square in the NIPMAT is shorter than the sum of the van der Waals radii of the two atoms involved plus a tolerance of 1.0Å. Thus *all* the C-H...O contacts located are shorter than 3.37Å.

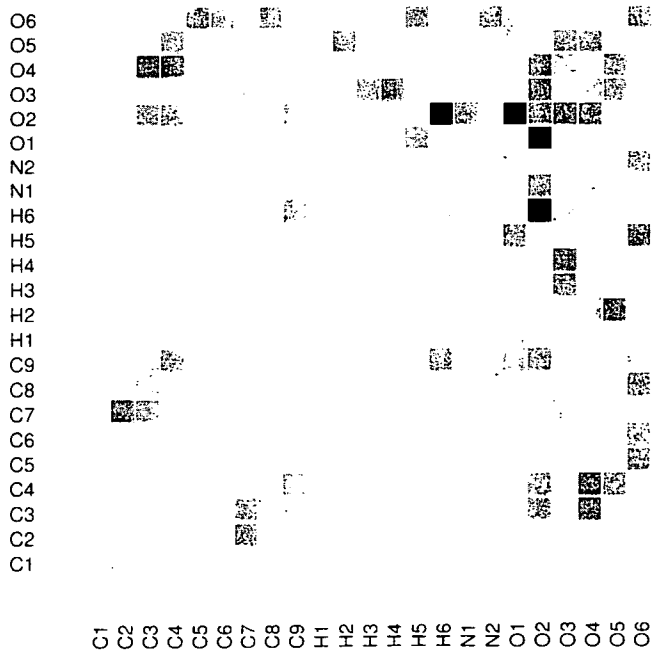

***Figure 3.3.2** - NIPMAT of the neutron derived stucture for 3,5-dinitrocinnamic acid.*

***Table 3.3.3** - Geometries of the 13 C-H...O close contacts present in the neutron derived structure of 3,5-dinitrocinnamic acid and located using NIPMAT.*

Identifier	Contact	H...O Distance (Å)	C-H...O Angle (°)
1	H(1)...O(1)[a]	2.858(8)	126.0(11)
2	H(1)...O(5)[b]	3.029(9)	159.9(12)
3	H(1)...O(6)[b]	3.167(9)	152.3(12)
A	H(2)...O(2)[c]	3.300(9)	> 100°
B	H(2)...O(4)[d]	3.045(9)	> 100°
4	H(2)...O(5)[e]	2.421(8)	145.5(12)
5	H(3)...O(3)[f]	2.576(8)	147.6(12)
6	H(3)...O(5)[g]	3.075(9)	118.9(11)
C	H(3)...O(6)[g]	3.258(9)	> 100°
7	H(4)...O(3)[f]	2.446(8)	153.0(13)
8	H(4)...O(4)[f]	3.051(9)	137.7(11)
9	H(5)...O(1)[a]	2.642(8)	157.3(12)
10	H(5)...O(6)[b]	2.456(8)	122.4(11)

Symmetry operators used to generate equivalent atoms - a -x, 1-y, -z; b 0.5 +x, -0.5+y, z; c -0.5-x, 0.5-y, -z; d -0.5-x, 0.5+y, -0.5-z; e -1-x, y, -0.5-z; f x, 1-y, 0.5+z, g -1-x, 1-y, -z.

Of the 13 contacts located using NIPMAT, 3 fail to satisfy accepted angular criteria for intermolecular C-H...O bonding i.e. they have C-H...O angles of less than 100°. The remaining 10 interactions organise the O-H...O dimers into corrugated sheets (see ***Figure 3.3.3***) which stack on top of one another along [010] (***Figure 3.3.4***).

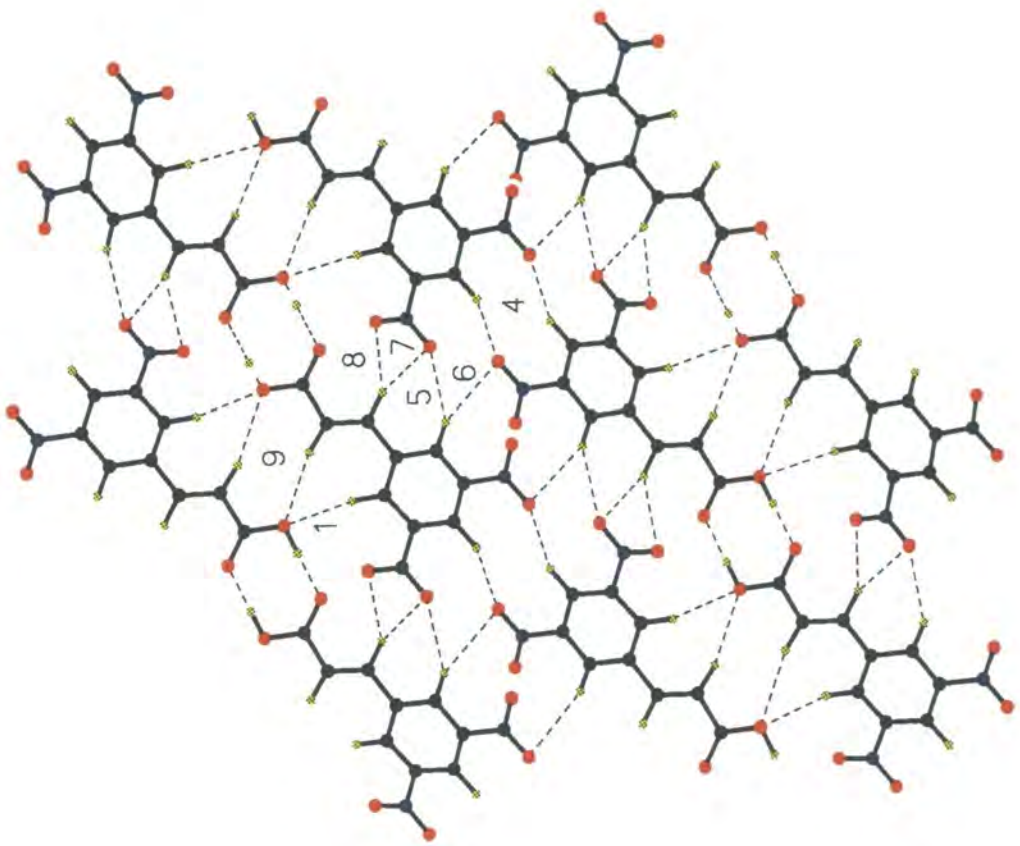

Figure 3.3.3 - *Packing of 3,5-dinitrocinnamic acid viewed along [100], showing the intra-sheet interactions* ***1***, ***4***, ***5***, ***6***, ***7***, ***8*** *and* ***9***.

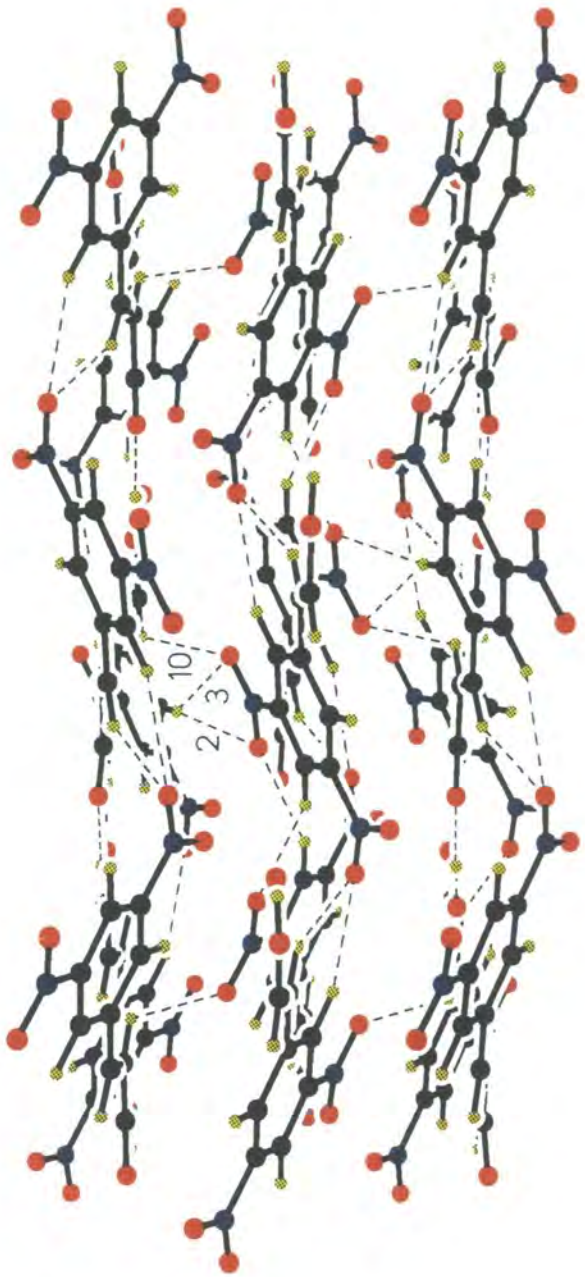

Figure 3.3.4 *- Packing of 3,5-dinitrocinnamic acid viewed along [010], showing the inter-sheet interactions* ***2***, ***3*** *and* ***10***.

3.3.3 Theoretical Calculations*

Inspection of ***Table 3.3.3*** reveals that there are two distinct groups of C-H...O contacts present in 3,5-dinitrocinnamic acid. There is a group of 5 interactions which have H...O separations of around 2.5Å (**4**, 2.421(8)Å; **5**, 2.576(8)Å; **7**, 2.446(8)Å; **9**, 2.642(8)Å and **10**, 2.456(8)Å) and a second group of 4 contacts with H...O separations of approximately 3.1Å (**2**, 3.039(9)Å; **3**, 3.167(9)Å; **6**, 3.075(9)Å and **8**, 3.051(9)Å). Only 1 interaction out of the 10 is of intermediate length (**1**, 2.858(8)Å). Compared with the sums of the van der Waals radii of oxygen and hydrogen (2.72Å: Bondi, 1964; 2.62Å: Rowland and Taylor, 1996) this second group of contacts are exceedingly long and would normally be disregarded as insignificant. However, these contacts are near linear with a mean C-H...O angle of 142.1° and distance criteria by themselves are not a good way of assessing the strength or importance of essentially electrostatic interactions. To better determine the significance of each of the C-H...O contacts present in 3,5-dinitrocinnamic acid and to explore the length-strength relationship of these interactions simple theoretical calculations were performed which, it was hoped, would yield the approximate electrostatic contributions to the relative energies of the C-H...O bonds in the network.

Accurate theoretical characterizations of weak intermolecular interactions such as C-H...O hydrogen bonds are difficult because errors caused by basis set superposition (BSSE) (Liu and McLean, 1973) and electron correlation can be significant and must be reduced or eliminated by using adequate basis sets, correcting the BSSE (Boys and Bernardi, 1970) and employing correlated theoretical methods such as second order Moller-Plesset pertubation theory (Moller and Plesset, 1934) or the Coupled Electron Pair Approximation (Meyer, 1971; Meyer, 1973). Despite these problems numerous high level *ab initio* studies have been performed on simple model C-H...O bonded systems (see for example Rovira *et. al.*, 1995; van Mourik, 1994 and references cited therein). However,

---

* Performed in collaboration with B. Bracke, Department of Chemistry, University of Wales, Cardiff, CF1 3TB.

such analyses have not been extended to larger model systems or real crystal structures because of the high computational costs involved. Our aim was to circumvent these difficulties by taking a more simplistic approach.

The neutron derived geometry of 3,5-dinitrocinnamic acid was used as the starting point. Mulliken atomic point charges were determined for an isolated molecule of **I** with this geometry using a 6-31G* basis set. These point charges were then arranged around a central 3,5-dinitrocinnamic acid molecule according to the C_2/c space group symmetry of the crystal to generate a simulated crystal lattice comprised of 139 neighbouring molecules in a sphere of radius 15Å. The Mulliken atomic point charges on the central molecule under the influence of this crystal field were redetermined and used to replace the point charges on the surrounding molecules. This iterative optimisation procedure was repeated until a self consistent set of Mulliken atomic point charges was obtained. ***Table 3.3.4*** lists the Mulliken point charges for each atom in the isolated molecule and in the molecule in the self consistent crystal field.

These self consistent atomic point charges can be used, in combination with the bond lengths given in ***Table 3.3.3***, to evaluate an approximate electrostatic contribution to the energy of each C-H...O bond using Coulombs Law. The electrostatic energy of each interaction is equal to the work done in overcoming the Coulombic force between two atomic point charges in order to bring them from infinity to a distance, r , from one another. It is given by the integral of Coulomb's Law with respect to r (***Equation 3.3.1***). If the two atomic point charges are of opposite sign then clearly this energy will be negative. ***Table 3.3.5*** shows these energies for each of the 10 C-H...O bonds described in Section 3.3.2.

$$U_{12} = \frac{1}{4\pi\varepsilon_0} \frac{q_1 q_2}{r} \qquad \textit{Equation 3.3.1}$$

Table 3.3.4 *- Mulliken point charges for each atom in an isolated molecule of 3,5-dinitrocinnamic acid and in a molecule in the self consistent crystal field.*

Atom	Point Charge - Isolated (eV)	Point Charge - Crystal (eV)
C(1)	-0.262	-0.310
C(2)	0.186	0.199
C(3)	0.122	0.128
C(4)	0.212	0.268
C(5)	0.103	0.099
C(6)	0.170	0.187
C(7)	0.113	0.035
C(8)	-0.154	-0.153
C(9)	0.675	0.680
N(1)	0.192	0.217
N(2)	0.192	0.212
O(1)	-0.505	-0.525
O(2)	-0.528	-0.587
O(3)	-0.368	-0.422
O(4)	-0.370	-0.396
O(5)	-0.364	-0.386
O(6)	-0.374	-0.434
H(1)	0.158	0.195
H(2)	0.177	0.177
H(3)	0.133	0.168
H(4)	0.107	0.151
H(5)	0.115	0.164
H(6)	0.280	0.332

Table 3.3.5 *- Lengths and electrostatic energies of the 10 C-H...O bonds present in the neutron derived structure of 3,5-dinitrocinnamic acid.*

Indentifier	H...O Distance (Å)	Energy (kcal mol^{-1})
1	2.858	11.89
2	3.029	8.25
3	3.167	8.87
4	2.421	9.37
5	2.576	9.14
6	3.075	7.00
7	2.446	8.65
8	3.051	6.51
9	2.642	10.82
10	2.456	9.62

The absolute values of the energies given in ***Table 3.3.5*** are far higher than the values for the total energies of typical C-H...O bonds derived by more sophisticated *ab initio* methods (1.0 - 3.2 kcal mol^{-1}: Rovira et. al., 1995). However, this is not surprising when you consider that only an approximate attractive electrostatic contribution to the C-H...O bond energies has been determined. The repulsive exchange repulsion energy term has not been included. Inaccuracies in the absolute values of the electrostatic contributions to the C-H...O bond energies also result from the use of Mulliken population analysis to derive the atomic point charges. Mulliken partitioning assumes that bonded atoms share the bond electron density equally. In the case of symmetrical bonds (for example the C≡C in actylene) this assumption is valid. However, the majority of chemical bonds are not symmetical and have polarity (for example carbonyl C=O bonds or the C=C bond in asymmetrical alkenes like fluoroethene). Clearly, the electron density in these bonds will not be shared equally by the two atoms and the use of Mulliken population analysis in such case will introduce errors. Despite these limitations we believe that the *relative* electrostatic contributions to the C-H...O bond energies derived here have some meaning.

Figure 3.3.5 is a plot of C-H...O bond distance versus electrostatic energy for each of the 10 bonds described in Section 3.3.2. The two groups of C-H...O bonds are clearly identifable as two clusters of points at around 2.5Å and 3.1Å. As one might expect the longer contacts are generally of lower energy than the shorter ones. The mean energy of the 5 short contacts identified above is 9.52 kcal mol^{-1} compared with a mean energy of 7.66 kcal mol^{-1} for the 4 long contacts. However, the spread in energy within both groups is large and the long contacts of highest energy are as strong as the short contacts of low energy (**7**, 2.446Å and 8.65 kcal mol^{-1}; **5**, 2.776Å and 9.14 kcal mol^{-1} cf. **2**, 3.029Å and 8.25 kcal mol^{-1}; **3**, 3.167Å and 8.87 kcal mol^{-1}). Furthermore, the shortest C-H...O bonds are not the strongest. The two contacts with the highest electrostatic energies, **1** (2.858Å) and **9** (2.642Å), are both somewhat longer than the shortest bonds in the network, **4** (2.421Å) and **7** (2.446Å). Such observations illustrate that electrostatic interactions operate over long ranges and that consequently even the longest C-H...O bonds present in 3,5-dinitrocinnamic acid may have significant energies.

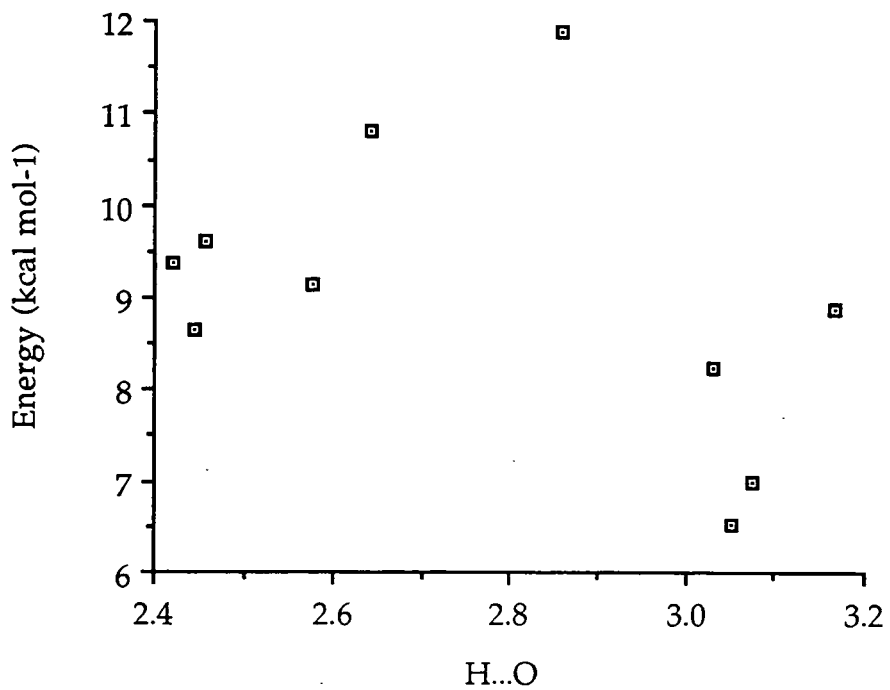

***Figure 3.3.5** - Plot of C-H...O bond distance versus bond energy for the 10 shortest C-H...O bonds in 3,5-dinitrocinnamic acid.*

3.4 STRUCTURE OF 2-ETHYNYLADAMANTAN-2-OL

3.4.1 Structural Details

Figure 3.4.1 shows the 50% probability thermal ellipsoid plot of the neutron derived structure of 2-ethynyladamantan-2-ol. ***Tables 3.4.1*** and ***3.4.2*** contain bond lengths and selected interbond angles.

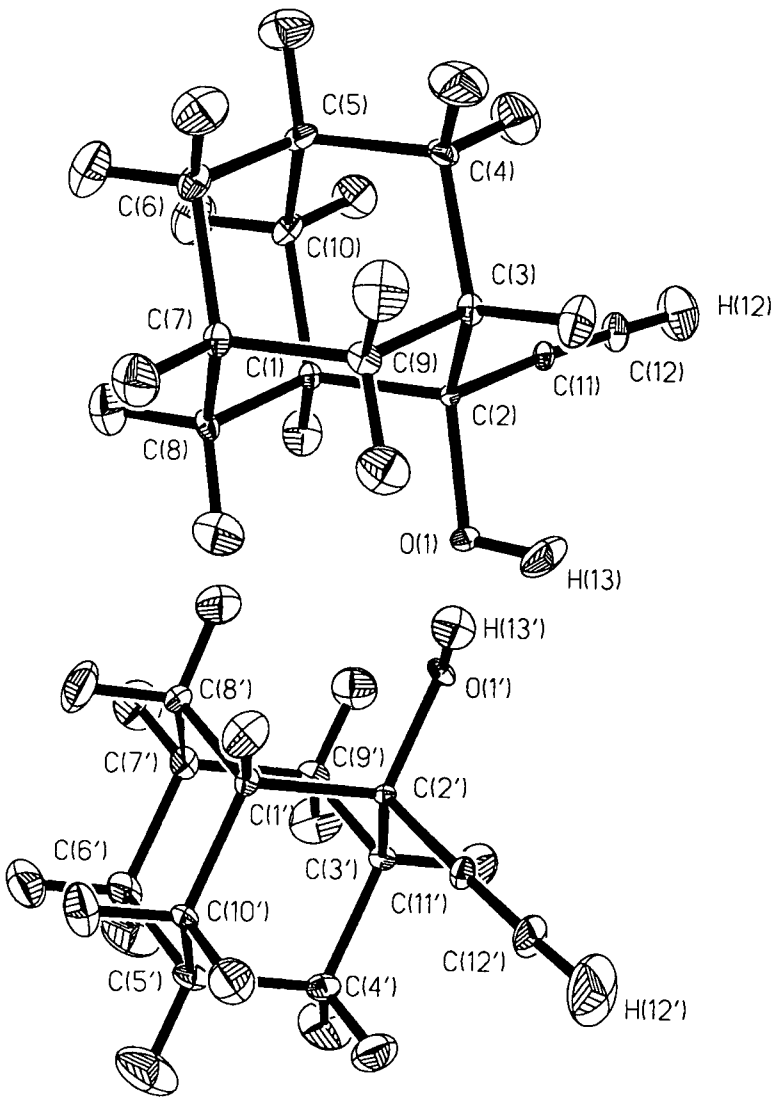

Figure 3.4.1 *- 50% probability thermal ellipsoid plot of 2-ethynyladamantan-2-ol.*

Table 3.4.1 *- Bond lengths in 2-ethynyladamantan-2-ol.*

	Length (Å)		Length (Å)
C(1)-C(2)	1.550(5)	C(1)'-C(2)'	1.570(5)
C(1)-C(8)	1.532(5)	C(1)'-C(8)'	1.563(6)
C(1)-C(10)	1.527(5)	C(1)'-C(10)'	1.533(6)
C(1)-H(1)	1.099(8)	C(1)'-H(1)'	1.086(9)
C(2)-O(1)	1.443(6)	C(2)'-O(1)'	1.423(6)
C(2)-C(3)	1.555(5)	C(2)'-C(3)'	1.552(5)
C(2)-C(1)1	1.489(4)	C(2)'-C(1)1'	1.491(5)
C(3)-C(4)	1.551(6)	C(3)'-C(4)'	1.523(6)
C(3)-C(9)	1.541(5)	C(3)'-C(9)'	1.539(6)
C(3)-H(3)	1.088(9)	C(3)'-H(3)'	1.091(9)
C(4)-C(5)	1.550(6)	C(4)'-C(5)'	1.539(6)
C(4)-H(4)	1.069(10)	C(4)'-H(4)'	1.103(12)
C(4)-H(41)	1.076(10)	C(4)'-H(42)	1.096(11)
C(5)-C(6)	1.536(5)	C(5)'-C(6)'	1.563(7)
C(5)-C(10)	1.554(6)	C(5)'-C(10)'	1.545(6)
C(5)-H(5)	1.064(11)	C(5)'-H(5)'	1.063(13)
C(6)-C(7)	1.537(6)	C(6)'-C(7)'	1.542(6)
C(6)-H(6)	1.095(10)	C(6)'-H(6)'	1.106(11)
C(6)-H(61)	1.088(10)	C(6)'-H(62)	1.059(13)
C(7)-C(8)	1.559(5)	C(7)'-C(8)'	1.546(6)
C(7)-C(9)	1.551(5)	C(7)'-C(9)'	1.537(6)
C(7)-H(7)	1.085(8)	C(7)'-H(7)'	1.094(11)
C(8)-H(8)	1.081(10)	C(8)'-H(8)'	1.065(12)
C(8)-H(81)	1.052(12)	C(8)'-H(82)	1.074(10)
C(9)-H(9)	1.091(9)	C(9)'-H(9)'	1.078(12)
C(9)-H(91)	1.075(11)	C(9)'-H(92)	1.106(10)
C(10)-H(10)	1.067(10)	C(10)'-H(10)'	1.095(9)
C(10)-H(101)	1.113(8)	C(10)'-H(102)	1.099(11)
C(11)-C(12)	1.210(4)	C(11)'-C(12)'	1.210(6)
C(12)-H(12)	1.057(8)	C(12)'-H(12)'	1.041(14)
O(1)-H(13)	0.944(10)	O(1)'-H(13)'	0.953(11)

Table 3.4.2 - Selected interbond angles in 2-ethynyladamantan-2-ol.

	Angle(°)		Angle(°)
C(1)-C(2)-C(3)	109.27(25)	C(1)'-C(2)'-C(3)'	108.03(39)
C(1)-C(10)-C(5)	109.53(31)	C(1)'-C(10)'-C(5)'	110.22(32)
C(1)-C(8)-C(7)	109.94(30)	C(1)'-C(8)'-C(7)'	109.17(34)
C(2)-C(3)-C(4)	109.11(28)	C(2)'-C(3)'-C(4)'	110.59(29)
C(2)-C(3)-C(9)	109.47(28)	C(2)'-C(3)'-C(9)'	109.61(32)
C(2)-O(1)-H(13)	110.30(62)	C(2)'-O(1)'-H(13)'	110.63(60)
C(2)-C(11)-C(12)	176.64(39)	C(2)'-C(11)'-C(12)'	178.09(46)
O(1)-C(2)-C(11)	107.98(28)	O(1)'-C(2)'-C(11)'	108.18(35)
C(11)-C(12)-H(12)	179.45(67)	C(11)'-C(12)'-H(12)'	176.01(82)
C(4)-C(5)-C(6)	109.52(33)	C(4)'-C(5)'-C(6)'	108.72(34)
C(4)-C(5)-C(10)	108.91(30)	C(4)'-C(5)'-C(10)'	109.05(35)
C(6)-C(7)-C(8)	109.61(31)	C(6)'-C(7)'-C(8)'	110.53(33)
C(6)-C(5)-C(10)	109.69(32)	C(6)'-C(5)'-C(10)'	109.94(37)
C(10)-C(1)-C(8)	110.24(28)	C(10)'-C(1)'-C(8)'	109.61(34)

3.4.2 The Hydrogen Bonded Network

Inspection of the packing of the neutron derived structure of 2-ethynyladamantan-2-ol reveals that all three of the hydrogen bonds predicted on the basis of the infra red spectroscopic evidence (Steinwender *et. al.*, 1993) are present. A comparison of the X-ray and neutron derived geometries of these contacts is given in ***Table 3.4.3***. The primary structural motif is a tetrameric loop (**IV**) which comprises of O-H...O and C-H...O bonds between alternating **A** and **B** molecules (see ***Figure 3.4.2***). These tetrameric loops are in turn held together by O-H...π bonds between **A** molecules, generating stacks of loops along [100] (see ***Figure 3.4.3***).

Figure 3.4.2 *- Packing of 2-ethynyladamantan-2-ol viewed along [100], showing the tetrameric loop sython , **IV**.*

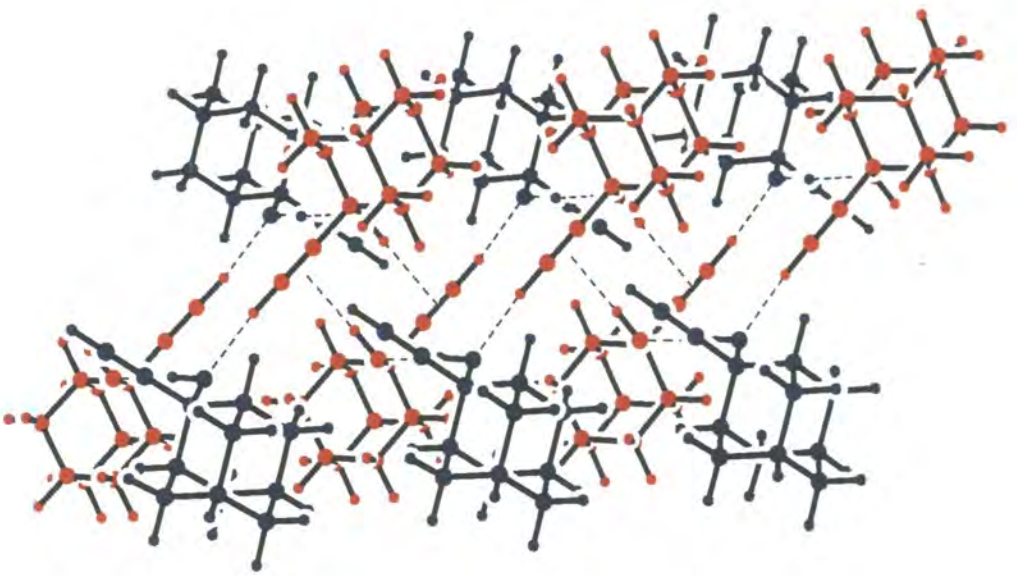

Figure 3.4.3 *- Packing of 2-ethynyladamantan-2-ol viewed along [010], showing the stacking of tetrameric loops along [100] which is mediated by O-H...π bonds.*

Table 3.4.3 *- Comparison of X-ray and neutron derived geometries of the hydrogen bonds present in 2-ethynyladamantan-2-ol.*

		X-ray	Neutron
O(1)'-H(13)'...O(1)	O...O	2.84Å	2.813(5)Å
	H...O	2.06Å	1.845(8)Å
	O-H..:O	143°	175.9(6)°
C(12)-H(12)...O(1)'	C...O	3.18Å	3.135(5)Å
	H...O	2.23Å	2.070(8)Å
	C-H...O	171°	173.3(6)°
O(1)-H(13)...π	O...C(11)	3.35Å	3.326(5)Å
	H...C(11)	2.35Å	2.384(8)Å
	O-H...C(11)	163°	166.5(6)°
	O...C(12)	3.25Å	3.227(5)Å
	H...C(12)	2.25Å	2.294(9)Å
	O-H...C(12)	163°	163.6(5)°
	O...π	3.25Å	3.221(4)Å
	H...π	2.22Å	2.258(8)Å
	O-H...π	169°	179.0(4)°

The O-H...π bond present in the crystal structure of 2-ethynyladamantan-2-ol is the first to be characterized by neutron diffraction. An examination of the geometry of this rare type of bond reveals that it is short and linear with the O-H group clearly directed towards the mid-point of the alkynic triple bond (2.258(8)Å, 179.0(5)°) rather than towards either of the alkyne carbon atoms (2.384(8)Å, 166.5(6)°; 2.294(9)Å, 163.6(5)°). This preference is unequivocally demonstrated only by the neutron analysis (see ***Table 3.4.3***).

The C-H...O bond between the alkynic portion of molecule **A** and the hydroxyl portion of molecule **B** in 2-ethynyladamantan-2-ol is also unusual. An analysis of its geometry indicates that it is among the shortest and most linear C-H...O bonds known (2.070(8)Å, 173.3 (6)°). A CSDS (Allen *et. al.*, 1991) search for short C-H...O contacts in neutron derived structures located just one C-H...O bond which is shorter than the bond in

2-ethynyladamantan-2-ol and that contact, in methylthymine, is less linear (2.045Å, 170.9°).

Although the alkynic proton present in 2-ethynyladamantan-2-ol is acidic and therefore makes a good C-H hydrogen bond donor the reason for the formation of such a short C-H...O bond in 2-ethynyladamantan-2-ol was not clear. In an effort to resolve this problem all neutron derived structures containing C-H...O contacts of less than 2.25Å were compared with each other and with 2-ethynyladamantan-2-ol. The aim was to identify structural features common to some or all of the compounds which could explain why short C-H...O bonds are formed. A total of 17 compounds were located using these criteria and an inspection of their structures revealed that they all possess one or more of the following: i) a highly acidic C-H group ii) an oxygen atom present as an anion iii) a cooperative network of hydrogen bonds (Jeffrey and Saenger, 1991) in which the C-H...O bond is involved. In the case of 2-ethynyladamantan-2-ol i) and iii) are present. The cooperativity between the C-H...O and O-H...O bonds in 2-ethynyladamantan-2-ol (***Figure 3.4.2***) results in a short C-H...O bond and a correspondingly long O-H...O bond (1.845(8)Å, 175.9(6)°). O-H...O bonds of this type are typically around 1.75Å.

Another indication of the exceptional nature of the C-H...O bond present in 2-ethynyladamantan-2-ol is the lengthening of the alkynic C-H bond in molecule **A** (1.070(8)Å) compared with the same bond in molecule **B** (1.045(12)Å), which is not involved in C-H...O bonding.

3.5 CONCLUSIONS

The neutron study of 3,5-dinitrocinnamic acid confirms that there is an extensive C-H...O bond network present in the structure. A total of 10 unique C-H...O bonds were located which range in length from 2.421Å to 3.167Å. These interactions organise the O-H...O bonded dimers into stacks of corrugated sheets.

Simple theoretical calculations indicate that even the longest C-H...O bonds in the network may have significant electrostatic energies and thus play a role in determining the crystal structure of **I**. Such observations demonstrate that distance criteria should be used cautiously when determining the importance of C-H...O contacts in crystal structures.

The neutron study of 2-ethynyladamantan-2-ol provides clear evidence that there is an intermolecular O-H...π hydrogen bond present in the structure (H...π = 2.258(8)Å, O-H...π = 179.0(5)°). It is the first time that such an O-H...π bond has been characterized by neutron diffraction.

Additionally, the study reveals that there is an exceptionally short and linear C-H...O bond present in **III** (H...O = 2.070(8)Å, C-H...O = 173.3(6)°) which was overlooked in the original X-ray structure determination. A survey of the CSDS indicates that it is amongst the shortest C-H...O bonds known. Its unusual geometry appears to be the result of cooperativity between the alternating C-H...O and O-H...O bonds which make up the primary tetrameric loop motif present in the structure.

3.6 REFERENCES

Al-Juaid, S. S., Al-Nasr, A. K. A., Eaborn, C. and Hitchcock, P. B. (1992) J. Organomet. Chem., **429**, C(9).

Allen, F. H., Davies, J. E., Galloy, J. J., Johnson, O., Kennard, O., Macrae, C. F., Mitchell, E. M., Mitchell, G. F., Smith, J. M. and Watson, D. G. (1991) J. Chem. Inf. Comput. Sci., **31**, 187 - 204.

Bondi, A. (1964) J. Chem. Phys., **68**, 441 - 451.

Boys, S. F. and Bernardi, F. (1970) Mol. Phys., **19**, 553.

Coiser, J. and Glazer, A. M. (1986) J. Appl. Cryst., **19**, 105.

Desiraju, G. R. (1989) *Crystal Engineering: The Design of Organic Solids*, Elsevier, Amsterdam, pp. 130.

Desiraju, G. R. and Sharma, C. V. K. M. (1991) J. Chem. Soc., Chem. Commun., 1239 - 1241.

Hardy, A. D. U.and MacNicol, D. D. (1976), J. Chem. Soc., Perkin Trans. 2, 1140.

Jeffrey, G. A. and Saenger, W. (1991) *Hydrogen Bonding in Biological Structures*, Springer-Verlag, Berlin.

Lin, S. Y., Okaya, Y., Chiou, D. M. and le Noble, W. J. (1982) Acta Crystallogr. B**38**, 1669 - 1671.

Liu, B. and McLean, A. D.(1973) J. Chem. Phys., **84**, 457.

Meyer, W. (1971) Int. J. Quant. Chem. Symp., **5**, 341.

Meyer, W. (1973) J. Chem. Phys., 58, 1017.

Moller, C. and Plesset, M. S. (1934) Phys. Rev., **46**, 618.

Nakatsu, K., Yoshioka, H., Kunimoto, K., Kinugasa, T. and Ueji, S. (1978) Acta Crystallogr., B**34**, 2357 - 2359.

Rovira, M. C., Novoa, J. J., Whangbo, M-H. and Williams, J. M. (1995) Chem. Phys., **200**, 319 - 335.

Rowland, R. S. (1995) Am. Cryst. Assoc. Abstr., **23**, 63 (Abstract 2a.5.B, Montreal Meeting.)

Rowland, R. S. and Taylor, R. (1996) J. Chem. Phys., **100**, 7384 - 7391.

Rzepa, H. S., Smith, M. H. and Webb, M. L. (1994) J. Chem. Soc., Perkin Trans. 2, 703 - 707.

Rzepa, H. S., Webb, M. L., Slawin, A. M. Z. and Williams, J. (1991), J. Chem. Soc., Chem. Commun., 765.

Sears, V. F. (1992) *Scattering Lengths for Neutrons: International Tables for Crystallography, Volume C*, ed. Wilson, A.J.C., Kluwer Academic Publishers, the Netherlands, pp. 383 - 391.

Sheldrick, G., M. (1993) SHELXL-93: *Program for the refinement of crystal structures using single crystal diffraction data*, University of Göttingen, Germany.

Spek, A. L. (1990) Acta Crystallogr. A**46**, C34.

Steinwender, E., Lutz, E. T. G., van der Maas, J. H. and Kanters, J. A. (1993) Vib. Spec., **4**, 217 - 229.

Ueji, S., Nakatsu, K., Yoshioka, H., Kunimoto, K., and Kinoshita, K. (1982) Tetrahedron Lett., **23**, 1173.

van Mourik, T. (1994) *Correlated ab initio Calculations on Weakly Bonded Systems*, Ph.D. thesis, University of Utrecht, pp. 93 - 114.

Viswamitra, M., Radhakrishnan, R., Bandekar, J. and Desiraju, G. R. (1993) J. Am. Chem. Soc., **115**, 4868 - 4869.

Wilson, C. C. (1990) *Neutron Scattering Data Analysis 1990*, ed. Johnson, M. W., IOP Conference Series Vol. 107, Adam Higler, Bristol, pp. 145 - 163.

CHAPTER 4

Neutron Diffraction Studies of 2- and 3-Aminophenol

4.1 INTRODUCTION

4.1.1 Alcohol-Amine Recognition

The goal of crystal engineering is to design and build stable crystals with specific structural features such as ribbons, sheets, cavities or channels based solely on intermolecular interactions (Desiraju, 1989). In order to achieve this it is necessary to identify robust substructural motifs or patterns of intermolcular interactions which are transferable from one crystal structure to another (Desiraju, 1995). Motifs involving weak interactions such as C-H...O (Sharma *et. al.*, 1991; Biradha *et. al.*, 1993; Pedireddi *et. al.*, 1996) and I...O_2N (Allen *et. al.*, 1994; Thalladi *et. al.*, 1996) have been described. However most motifs are based on strong O-H...O, N-H...O, etc. hydrogen bonds since they are generally regarded as crystal structure determining interactions. Typically, these motifs involve O-H or N-H donors and C=O acceptors (Aakeroy and Seddon, 1993; Fan *et. al.*, 1994; MacDonald and Whitesides, 1994) but recent studies have shown that predictable crystal structures can also be obtained using compounds containing only alcohol and amine groups (Ermer and Eling, 1994; Hanessian *et. al.*, 1994 and 1995). The use of these alcohol-amine mutual recognition patterns as 'building blocks' in crystal engineering has also been discussed (Borman, 1995).

Alcohols and amines are complementary with respect to hydrogen bonding. The hydroxyl group possesses two lone pair acceptors but only one hydrogen atom donor. Whereas, the amino group has two hydrogen atom donors and only one lone pair acceptor. Clearly, neither group can fulfill its potential hydrogen bonding valency, of 3, by itself. However, if the two groups are combined they can satisfy each others hydrogen bonding requirements simultaneously, forming one O-H...N and two N-H...O hydrogen bonds. Ermer and Eling (1994) have suggested that this stoichiometric complementarity favours the formation of alcohol-amine complexes wherein the molecules form tetrahedral networks mediated by strong hydrogen bonds. Two possible hydrogen bonded

architectures, based on the structures of diamond and wurtzite (see ***Figure 4.1.1***), were proposed.

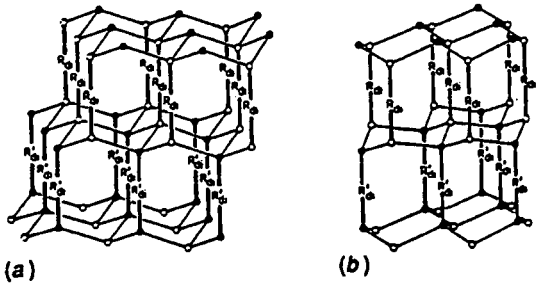

Figure 4.1.1 *- Tetrahedral a) super-diamond and b) super-wurtzite alcohol-amine mutual recognition motifs.*

Ermer and Eling (1994) tested their ideas about supramolecular assembly via alcohol-amine mutual recognition by determining the crystal structures of a variety of diphenol-aromatic diamine complexes and two linear aminophenols. They found that the diphenol-diamine complexes have tetrahedral structures like that of diamond whereas 4-aminophenol and 4,4'-hydroxyaminobiphenyl have super-wurtzite structures. Both types of structure are mediated exclusively by networks of O-H...N and N-H...O bonds. Each oxygen and nitrogen atom within these networks participates in 3 hydrogen bonds, as predicted.

More recently, Hanessian *et. al.* (1994 and 1995) have used alcohol-amine mutual recognition patterns to form supramolecular assemblies of chiral diols and diamines. They have found that the 1:1 complexes of enantiomerically pure trans-1,2-diaminocyclohexanes and (1S, 2S)-trans-1,2-cyclohexanediol form triple stranded helicate structures whose helicity is controlled by the chirality of the diamine. The cyclohexane rings of both the diol and the diamine are stacked in four vertical columns about a central staircase-like core formed by eight-membered, square planer O-H...N and N-H...O hydrogen bonded units which involve one functional group from each molecule (see ***Figure 4.1.2***). The remaining functional groups participate in two

symmetrical sets of N-H...O hydrogen bonds which flank the central core (***Figure 4.1.2***). The oxygen and nitrogen atoms in the staircase are four coordinate, however those involved in the flanking N-H...O hydrogen bonds are three coordinate. The unshared N-H on these flanking amino groups points inward towards the central core (***Figure 4.1.2***).

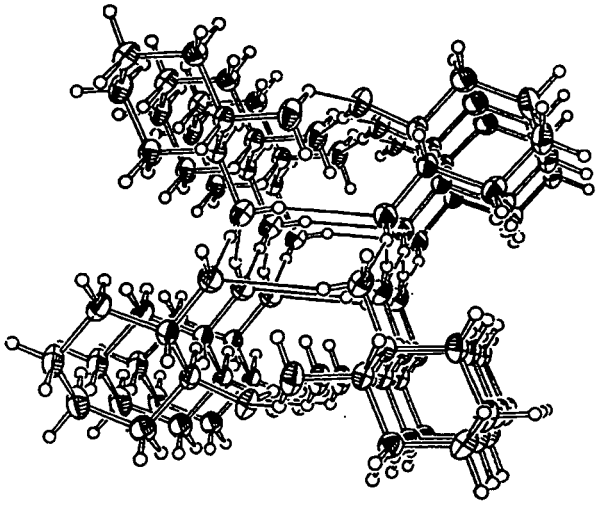

Figure 4.1.2 *- Packing of 1:1 complex trans-1,2-diaminocyclohexanes and (1S, 2S)-trans-1,2-cyclohexanediol.*

Both studies show that alcohol-amine mutual recognition can be used effectively to mediate supramolecular assemblies. Ermer and Eling (1994) have been successful in obtaining predictable crystal structures based on tetrahedral alcohol-amine mutual recognition patterns using simple linear difunctional aromatic molecules. However, Hanessian's work demonstrates that these tetrahedral motifs are not transferable to simple aliphatic systems and that many other patterns of O-H...N and N-H...O bonds are possible. Clearly, further investigations are necessary in order to understand alcohol-amine mutual recognition patterns and use them effectively as 'building blocks' in crystal engineering. A good starting point for these investigations would be to determine the crystal structures of some non-linear amino alcohols using neutron diffraction. The compounds 2- (I) and 3-aminophenol (II) have many structural features in common with those studied by Ermer and Eling (1994). However, because they are asymmetrical they

have the potential to form more complex hydrogen bonded networks than their linear analogue. They would therefore provide a fair but rigorous test of the transferability of tetrahedral alcohol-amine mutual recognition motifs.

4.1.2 Aromatic Amine Pyramidalization

Aryl amino groups are known to activate aromatic rings towards electrophilic substitution at the *ortho* and *para* positions. Most organic text books (see for example Morrison and Boyd, 1987; Fessenden and Fessenden, 1990) attribute this to resonance effects. It is argued that the amino nitrogen atom donates its lone pair electron density to the ring generating the canonical forms shown in ***Figure 4.1.3***. This resonance description implicitly assumes that the amino nitrogen atom is planar (sp^2 hybridised) so as to maximize π donation to the ring (see **3**, **4** and **5** in ***Figure 4.1.3***).

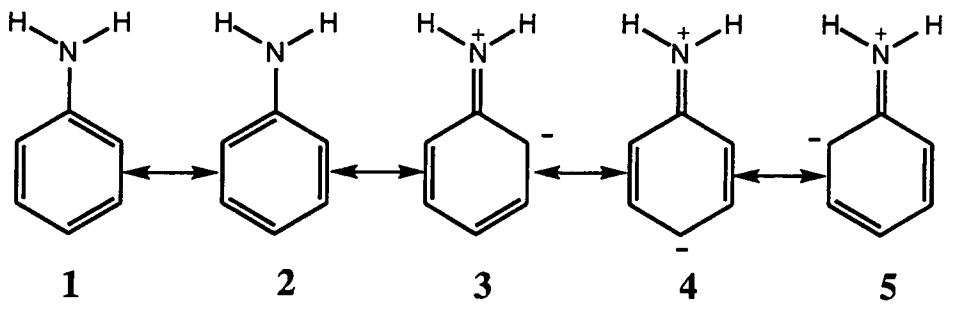

Figure 4.1.3 *- Resonance description of the of the delocalisation of the amino lone pair in aniline.*

The results of a survey of the geometries of aromatic amines appear to confirm this hypothesis. ***Figure 4.1.4*** is a histogram of the pyramidality parameter, Σ, which is the sum of the angles about the amino nitrogen atom for each of the 300 or more aromatic amines contained in the CSDS (Allen *et. al.*, 1991). Planar sp^2 hybridized nitrogen atoms have $\Sigma = 360.0°$ and perfectly tetrahedral sp^3 hybridized nitrogen atoms have $\Sigma = 328.4°$ (assuming a tetrahedral angle of 109.47°). The histogram appears to show that the vast majority of the aromatic NH_2 groups in the dataset are perfectly planar and that there are relatively few examples of pyramidal (sp^3 hybridized) NH_2 groups. A more

comprehensive survey of the geometries of R_1=C-NR_2R_3 fragments (where R_1 = $C(sp^2)$ and R_2, R_3 = $C(sp^3)$ or H: Allen *et. al.*, 1995) indicated a similar preference for planar, $N(sp^2)$, groups. However, the study also showed that NR_2R_3 groups acting as hydrogen bond acceptors in short N...H-O and N...H-N interactions tend to have distorted, pyramidal, geometries.

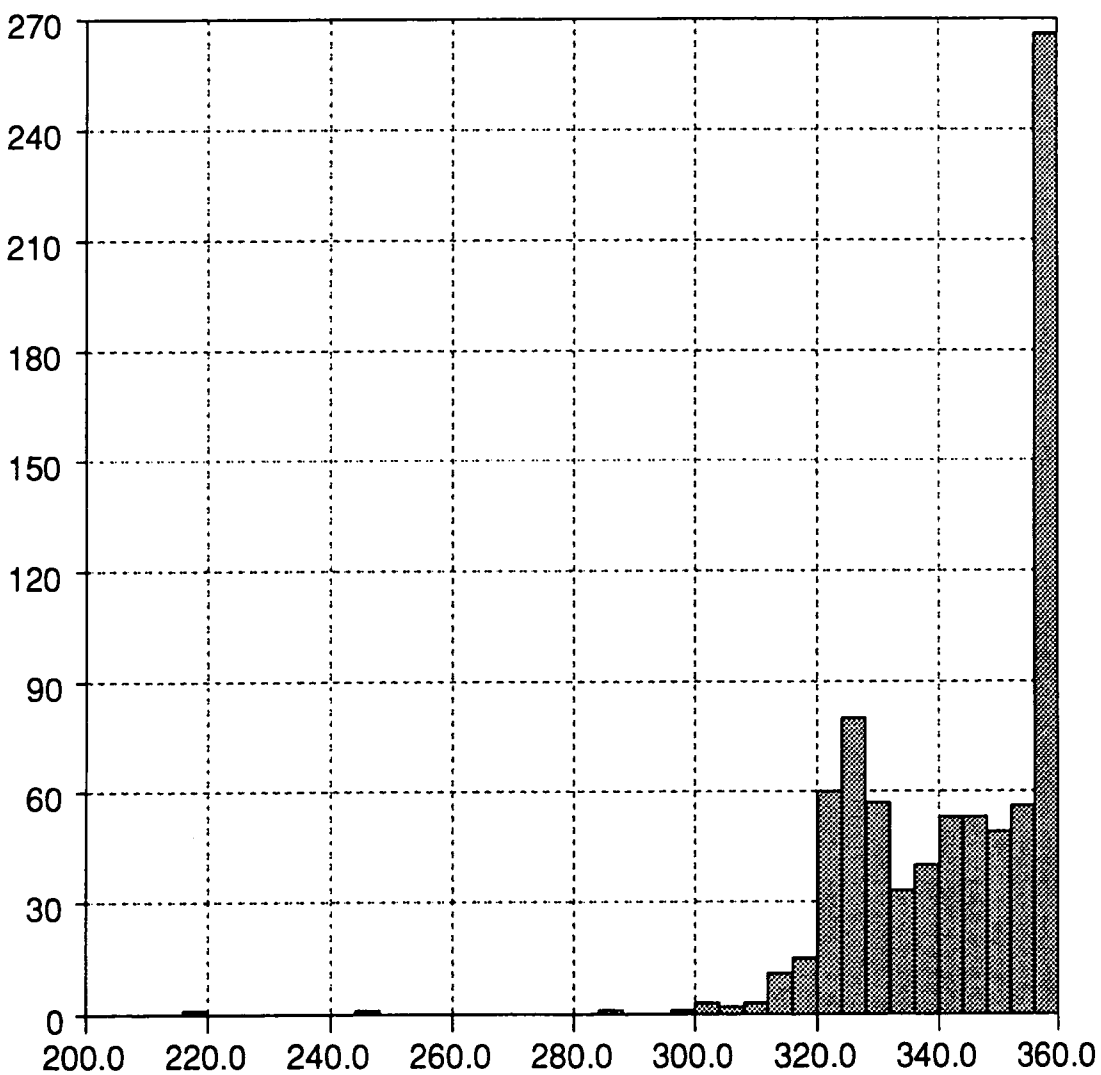

Figure 4.1.4 *- Histogram of the pyramidality parameter, Σ, for all aromatic amine groups located in the CSDS.*

Theoretical and experimental studies also indicate that neutral aryl amino groups are not always planar. Adams (1993) conducted a series of *ab initio* molecular orbital calculations on aniline, aminopyridine and the protonated analogues of these molecules. All of the non-protonated species studied were calculated to be pyramidal with Σ values of 339.3°, 344.2°, 338.5° and 344.8° for aniline and the *ortho*, *meta* and *para* derivitives of aminopyridine respectively. These optimised geometries are in good agreement with those obtained experimentally for other aromatic amines using neutron diffraction (Stalhandske, 1976; O'Connell and Maslen, 1967).

The extent of π electron donation by the amino groups in these systems was also investigated. As expected, Adams (1993) found that NH_2 is a π donor in all cases and that the extent of π donation increases when the amino group and the aromatic ring are constrained to be co-planar although the increase is very small (0.03eV for aniline). The extent of π donation also increases as the electron demand from the ring increases so that the amino groups in 2- and 4-aminopyridine donate more π density to the ring than those in 3-aminopyridine and aniline (0.12eV cf. 0.09eV). This is reflected in a 5° flattening of the NH_2 pyramids in the former of the two compounds (see above). However, overall the amino groups are σ electron withdrawing and have negative charges (-0.171eV, -0.146eV, -0.166eV and -0.157ev for aniline and the *ortho*, *meta* and *para* derivatives of aminopyridine respectively). The σ electron withdrawing effect is enhanced when the amino nitrogen atom is sp^2 hybridized. This increases the overall negative charge on NH_2 (from -0.171eV to -0.205eV for aniline) and makes the planar form less stable. Such results could indicate that the apparent predominance of planar NH_2 groups in the CSDS is an artefact and that the widespread use of idealised hydrogen atom positions when refining X-ray data has masked a real preference for pyramidal, $N(sp^3)$, geometries in these systems.

X-ray structural analyses of **I** and **II** indicate that the amino groups in both molecules are pyramidal, as expected (**I**: Aven *et. al.*, 1981; **II**: Brunie *et. al.*, 1974). The hydroxyl group, like the amino group, is π electron donating so electron demand from both rings is

low, favouring the pyramidal geometry. However, the *meta* derivative is better able to stabilize the amino π density (see ***Figure 4.1.5***) and ought therefore to have a flatter NH_2 group. Unfortunately, it is not possible to compare the geometries of the amino groups in **I** and **II** because the amino hydrogen atoms are poorly resolved by the X-ray analysis. Neutron diffraction data would yield precise hydrogen atom positions and allow the comparison to be made.

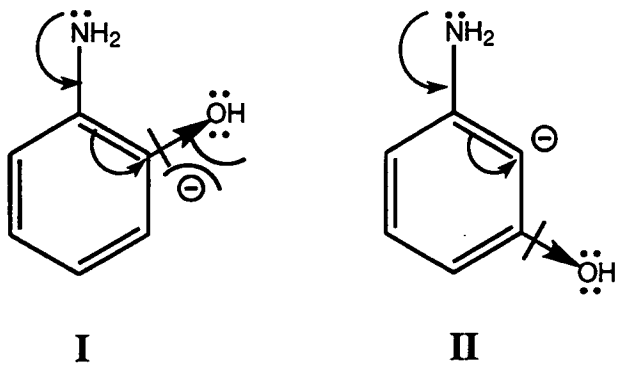

I **II**

***Figure 4.1.5** - II is better able to stabilise the amino π density than I because there are no adverse steric effects and the inductive effect of the OH group is favourable.*

4.1.3 Aims

Low temperature single crystal neutron diffraction studies of 2- and 3-aminophenol were undertaken in order to determine whether the tetrahedral alcohol-amine mutual recognition patterns described by Ermer and Eling (1994) are transferable to non-linear aminophenols. Additionally, the accurate hydrogen atom positions obtained were used to determine whether *meta* aminophenol, **II**, has a flatter NH_2 geometry than the *ortho* compound, **I**, as predicted.

4.2 EXPERIMENTAL DETAILS

The neutron structure determination of 2-aminophenol was conducted at the pulsed neutron source, ISIS, on the Laue time-of-flight diffractometer, SXD (Wilson, 1990). The proton spallation neutron source at ISIS and the layout and operation of SXD are described in Section 2.3. The sections pertaining to this experiment therefore focus on specific experimental details with reference to Section 2.3 where necessary.

The neutron diffraction study of 3-aminophenol was carried out at the Institut Laue Langevin (ILL) reactor source in Grenoble, France on the four circle diffractometer, D19. D19 is a single crystal diffractometer which is equiped with a large (64° x 4°) multiwire PSD. The layout of the instrument in shown schematically in ***Figure 4.2.1***.

The monochromator deflects neutrons of a single wavelength along guides and into the instrument. Any one of three different monochromator crystals (graphite [002], germanium [11n], [335] or copper [220]) can be rotated into a diffracting position allowing wavelengths of between 1Å and 2.4Å to be accessed. The incoming beam is collimated to maximum diameter of 10mm before it strikes the sample which is mounted on a Huber four circle crystal orientator. The ϕ axis of the crystal orientator is offset so that a compact 2 stage helium Displex CCR (12 - 300K) can be attached to the instrument.

The diffracted beam is detected by a 'banana shaped' PSD (see ***Figure 4.2.2***). The detector is placed symmetrically about the equatorial plane such that the sample is at the centre of the vertical curvature. It is mounted on a γ arm ($\gamma = 2\theta$ in the equatorial plane) which rotates on air cushions. The detector is comprised of 16 vertical cathode arcs which are crisscrossed by 512 short anode wires. At the standard sample to detector distance of 1.15 m the detector has a resolution of 0.25° x 0.125°. Further details about the experimental procedures used in conjuction with D19 are given in Section 4.2.3.

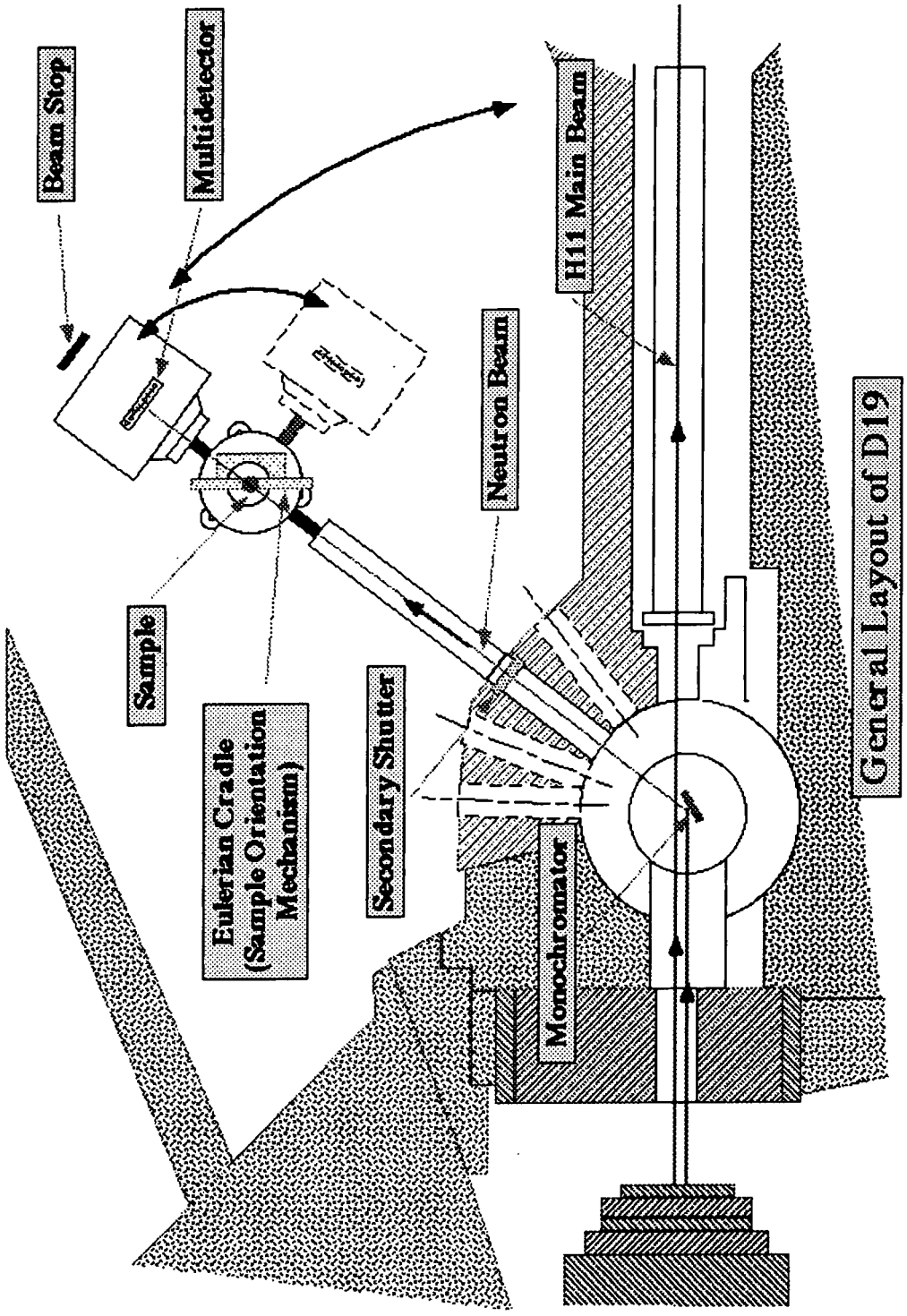

Figure 4.2.1 *- The layout of D19.*

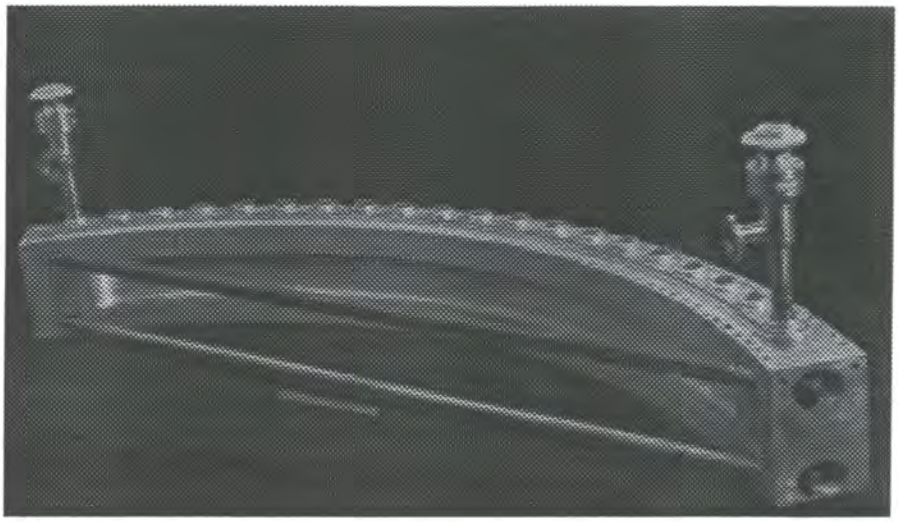

Figure 4.2.2 *- The 'banana shaped' multiwire PSD on D19.*

4.2.1 Preliminary Studies

The low temperature stability of the samples was assessed by indexing small single crystals of both compounds, then slowly cooling them whilst repeatedly scanning an intense Bragg peak located during the indexing procedure. The experimental procedures used were entirely analogous to those employed to assess the low temperature stabilities of the compounds described in Chapter 3 and are detailed fully in Section 3.2.1.1. These experiments showed that both **I** and **II** are stable at temperatures above 80K.

The quality of the large crystals of **I** and **II** grown for neutron diffraction analysis was tested optically using a polarising microscope and experimentally with X-rays prior the the start of the neutron diffraction experiments. Section 3.2.1.2 contains details of the procedures used. Only crystals which passed these tests were considered to be single and suitable for neutron diffraction.

4.2.2 2-Aminophenol

Numerous large 2-aminophenol crystals suitable for neutron diffraction analysis were identified. All of them had the same external morphology (see ***Figure 4.2.3***) and similar

dimensions (4.1 x 4.1 x 3.3 mm). The largest of these was selected for the neutron diffraction experiment. The crystal was mounted in exactly the same way as the samples described in Chapter 3 (see Section 3.2.2 for details) and was then cooled to 100K using a helium CCR.

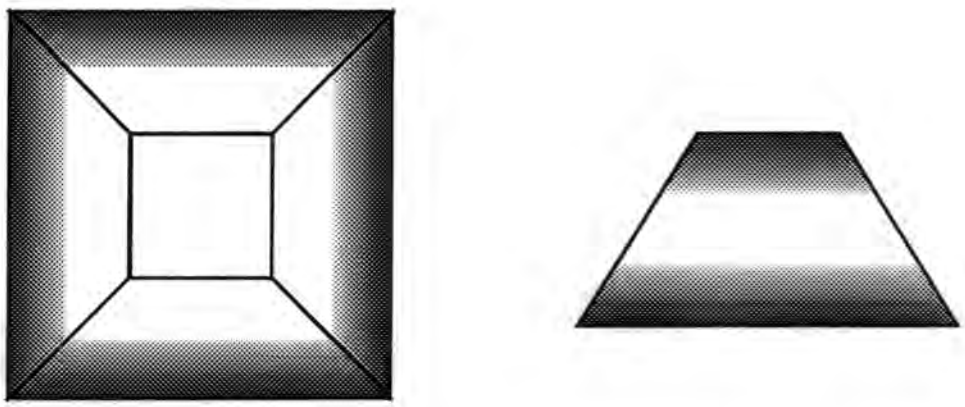

Plan Elevation

Figure 4.2.3 *- Morphology of the 2-aminophenol crystals.*

This experiment was carried out in January 1995 after the introduction of the second PSD on SXD (see Section 2.3.3.2). The two detectors were centred at 2θ angles of 57° and 125°. Data were collected by both detectors simultaneously at 28 different crystal orientations yielding 56 unique frames. Each frame was 'exposed' for 900 μA. Data from the first high angle frame were used to obtain an orientation matrix and cell parameters (see ***Table 4.2.1***)

Structure factor information was extracted from the frames using the procedures described in Section 2.3.3.4. A total of 8112 reflections were measured in the 56 frames . These data were corrected for absorption and extinction before being merged to yield 2046 unique reflections with an R_{merg} of 0.06. The structure refinement was carried out using SHELXL-93 (Sheldrick, 1993). Coherent neutron scattering lengths for C, N, O and H were taken from Internataional Tables (Sears, 1992) and the heavy atom positions from the original X-ray structure determination (Aven *et. al.*, 1981) were used as the starting model. Hydrogen atoms were located in subsequent difference maps. The fully

anisotropic refinement converged with a conventional R of 0.0634 and a GooF of 1.243. Further details are given in ***Table 4.2.1***.

Table 4.2.1 *- Details of the data collections and structure refinements for 2- and 3-aminophenol.*

Compound	2-aminophenol (I)	3-aminophenol (II)
Formula	C_6H_7NO	C_6H_7NO
Molecular Weight	109.0	109.0
ρcalc (gcm^{-1})	1.325	1.276
a (Å)	19.655(2)	11.226(2)
b (Å)	7.157(2)	6.101(2)
c (Å)	7.770(2)	8.282(2)
α (°)	90	90
β (°)	90	90
γ (°)	90	90
Volume ($Å^3$)	1093.0(4)	567.2(3)
Crystal System	Orthorhombic	Orthorhombic
Space Group	Pbca	$Pca2_1$
Z	8	4
Morphology	Trapezoidal	Flattend needle
Colour	Brown	Grey/Brown
Size (mm)	4.1 x 4.1 x 3.3	5.3 x 1.7 x 0.65
No. of Measured Data	8112	2532
No. of Observed Data	8112	2037
No. of Unique Data	2046	1227
σ(I) Cut Off	$I > -4\sigma(I)$	$I > -4\sigma(I)$
R_{merg}	0.06	0.048
No. Parameters Refined	136	136
R	0.0634 (F)	0.0681 (F)
wR	0.1439 (F^2)	0.0654 (F^2)
GooF	1.243	1.477
Weighting Scheme	1/σ	1/σ
Δρ min ($Å^{-3}$)	-2.362	-0.959
Δρ max ($Å^{-3}$)	4.326	0.937

4.2.3 3-Aminophenol

The 3-aminophenol crystal selected for the neutron diffraction experiment was a flattened needle with pointed ends which had dimensions of 5.3 x 1.7 x 0.65 mm. The crystal was wrapped in thin aluminium foil and then glued to a flat headed aluminium pin using 'KwikFill', a two stage epoxy cement. It was mounted on the flatter of its two smallest faces such that its longest dimension was parallel with the pin (see ***Figure 4.2.4***). The mounted crystal was then attatched to the ϕ circle of the crystal orientator.

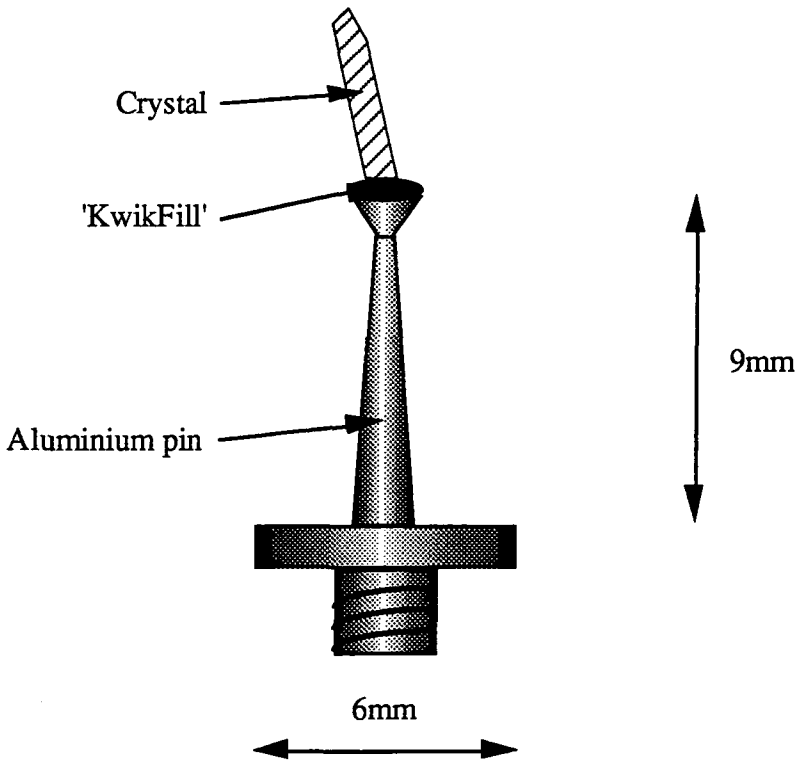

Figure 4.2.4 *- Schematic representation of the way in which the 3-aminophenol sample was mounted for the neutron diffraction experiment.*

The 1 1 7 reflection from the vertically focussing Ge monochromater crystal was used to produce a monochromatic neutron beam with a wavelength of 0.95452Å (no filter was required to remove $\lambda/2$ because the 2 2 14 reflection is absent). A rough orientation matrix, based on the X-ray cell, was obtained from three peaks prior to cooling. The crystal was then cooled to 100K and the rough orientation matrix was gradually improved using reflections scanned during the data collection (see ***Table 4.2.1***). The majority of

the data were collected in normal-beam Weissenberg geometry. The small number of unique reflections that were missed by the normal-beam scan were collected separatly in equitorial-plane geometry. A complete unique set of data and some equivalents were collected out to $\sin\theta/\lambda = 0.745°$. A number of higher angle data were also measured.

Integrated intensities were obtained from the raw data using the $\sigma(I)/I$ method (Wilkinson *et. al.*, 1988) with the program PEAKINT. A Gaussian integration absorption correction was applied to the data using the program D19ABS. Corrections for absorption by the walls of the cylindrical cryostat shields were also applied. In all, 2532 reflections were measured of which 2037 were observed. When merged these yielded 1277 unique reflections ($R_{merg} = 0.048$). The structure refinement was carried out, using the merged data, with SHELXL-93 (Sheldrick, 1993). Coherent neutron scattering lengths for C, N, O and H were taken from International Tables (Sears, 1992) and the heavy atom positions from the original X-ray structure determination (Brunie *et. al.*, 1974) were used as the starting model. Hydrogen atoms were located in subsequent difference maps. The fully anisotropic refinement converged with a conventional R of 0.0681 and a GooF of 1.477. Further details are given in ***Table 4.2.1***.

4.3 NEUTRON STRUCTURES OF 2- AND 3-AMINOPHENOL

4.3.1 Structural Details

Figure 4.3.1 shows the 50% probability thermal ellipsoid plot of the neutron derived structure of 2-aminophenol. ***Tables 4.3.1*** and ***4.3.2*** contain bond lengths and selected interbond angles. ***Figure 4.3.2*** and ***Tables 4.3.3*** and ***4.3.4*** contain the equivalent information for 3-aminophenol.

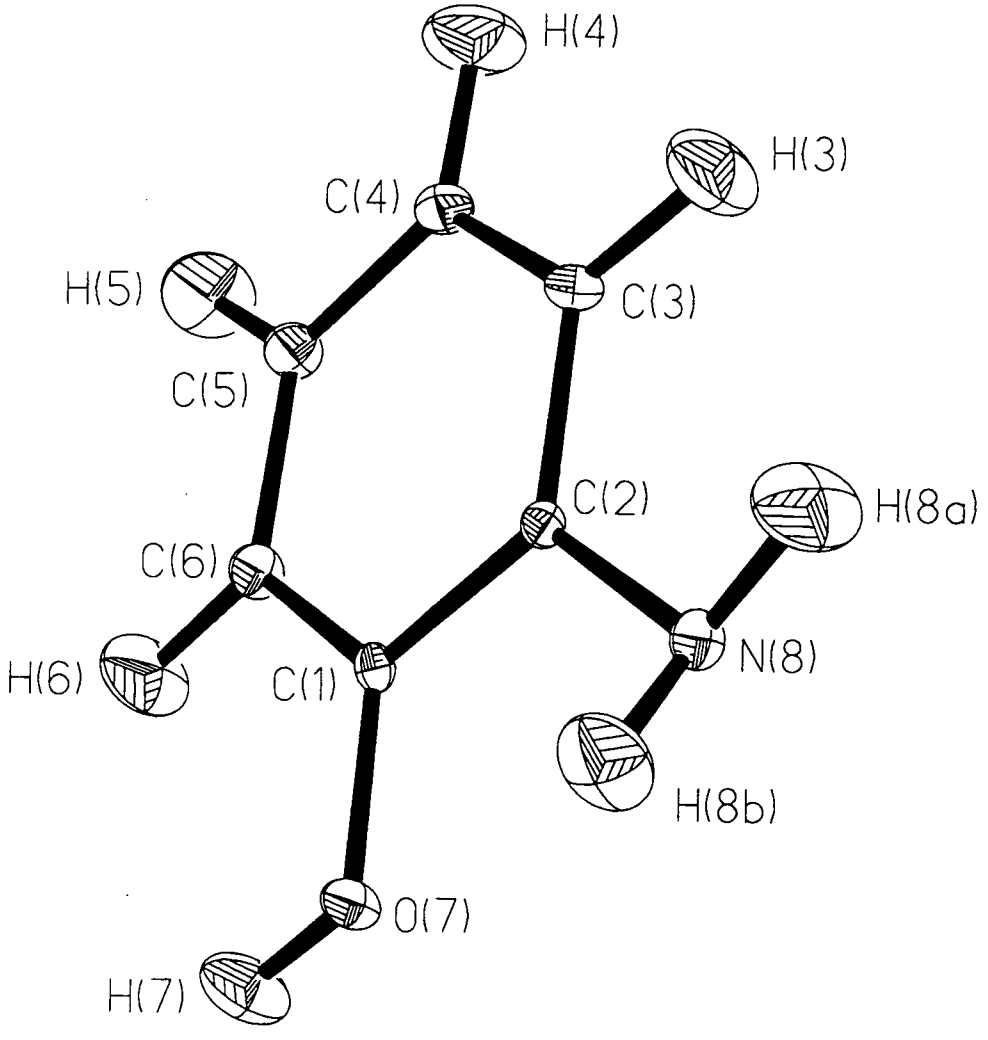

Figure 4.3.1 *- 50% probability thermal ellipsoid plot of 2-aminophenol.*

Table 4.3.1 *- Bond lengths in 2-aminophenol.*

	Length(Å)		Length(Å)
C(2) - C(3)	1.397(2)	C(5) - H(5)	1.079(3)
C(2) - C(1)	1.410(2)	C(4) - C(3)	1.398(2)
C(2) - N(8)	1.4126(14)	C(4) - H(4)	1.088(4)
C(1) - O(7)	1.366(2)	C(3) - H(3)	1.084(4)
C(1) - C(6)	1.389(2)	O(7) - H(7)	1.001(3)
C(6) - C(5)	1.400(2)	N(8) - H(8a)	1.021(3)
C(6) - H(6)	1.076(4)	N(8) - H(8b)	1.021(3)
C(5) - C(4)	1.397(2)		

Table 4.3.2 *- Selected interbond angles in 2-aminophenol.*

	Angle(°)		Angle(°)
C(6) - C(1) - C(2)	119.59(11)	C(1) - O(7) - H(7)	111.6(2)
C(2) - C(3) - C(4)	120.76(12)	C(2) - N(8) - H(8a)	112.4(2)
C(4) - C(5) - C(6)	119.98(12)	C(2) - N(8) - H(8b)	113.7(2)
C(1) - C(2) - N(8)	118.11(10)	H(8b)-N(8)-H(8a)	109.1(3)
C(2) - C(1) - O(7)	116.89(11)		

Table 4.3.3 *- Bond lengths in 3-aminophenol.*

	Length(Å)		Length(Å)
C(2) - C(3)	1.406(3)	C(6) - H(6)	1.088(6)
C(2) - C(1)	1.411(3)	C(5) - C(4)	1.409(4)
C(2) - H(2)	1.090(5)	C(5) - H(5)	1.097(6)
C(1) - O(7)	1.366(3)	C(4) - H(4)	1.095(5)
C(1) - C(6)	1.405(3)	N(8) - H(8a)	1.025(6)
C(3) - C(4)	1.397(3)	N(8) - H(8b)	1.027(6)
C(3) - N(8)	1.424(3)	O(7) - H(7)	1.009(6)
C(6) - C(5)	1.406(3)		

Table 4.3.4 *- Selected interbond angles in 3-aminophenol.*

	Angle(°)		Angle(°)
C(6) - C(1) - C(2)	120.4(2)	C(1) - O(7) - H(7)	111.7(4)
C(2) - C(3) - C(4)	119.8(2)	C(3) - N(8) - H(8a)	112.0(4)
C(4) - C(5) - C(6)	120.6(2)	C(3) - N(8) - H(8b)	112.2(3)
C(2) - C(1) - O(7)	121.4(2)	H(8b)-N(8)-H(8a)	107.3(5)
C(2) - C(3) - N(8)	119.7(2)		

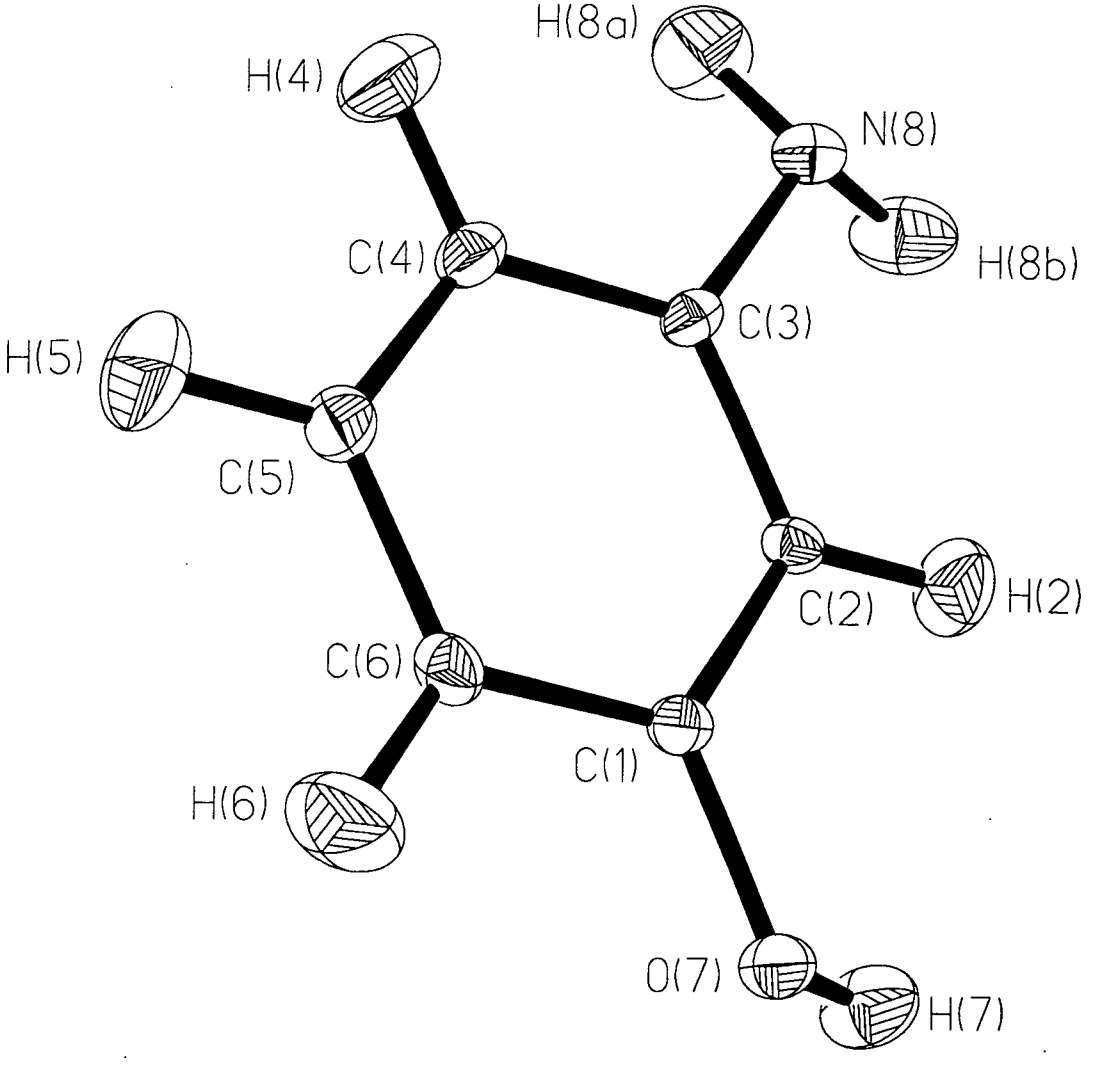

Figure 4.3.2 *- 50% probability thermal ellipsoid plot of 3-aminophenol.*

The Figures and ***Tables 4.3.2*** and ***4.3.4*** clearly show that the amino groups in **I** and **II** are pyramidal. The pyramidalization is pronounced in both compounds with the amino nitrogen atoms lying 0.331Å and 0.358Å above the basal planes of the pyramids in **I** and **II**. The sums of angles around the amino nitrogen atoms, Σ, are 335.2° and 331.5° for **I** and **II** respectively. These are close to the tetrahedral value of 328.7° suggesting that both amino nitrogen atoms are sp^3 hybridized. The sp^3 hybridization of the amino nitrogen atoms is confirmed by inspection of the C-N bond lengths in the two compounds. These are 1.4127(14)Å and 1.424(3)Å for **I** and **II** respectively. These values are typical of *single* sp^2 carbon atom to nitrogen atom bond lengths (C-N = 1.416Å; C=N = 1.316Å: Allen *et. al.*, 1987).

The amino groups in both aminophenols are more pyramidal than the NH_2 groups in the energy optimised aniline and aminopyridine molecules (Adams, 1993). This confirms that the presence of a π electron donating hydroxyl substituent lowers electron demand by the aromatic ring disfavouring amino π donation and leading to pyramidal amino group geometry. However, the prediction that **II** would be less pyramidal than **I** because it is better able to stabilize the amino π density (see ***Figure 4.1.6***) is not shown by the experiment. The amino group in 3-aminophenol is, in fact, more pyramidal than that of 2-aminophenol (331.5° cf. 335.2°) suggesting that the inductive and steric effects described in Section 4.1.2 are negligible when electron demand and the extent of amino π donation are low.

4.3.2 Hydrogen Bonded Networks

Careful inspection of the neutron derived structures of **I** and **II** reveals that the simple stoichiometric alcohol-amine mutual recognition patterns observed by others (Ermer and Eling, 1994; Hanessian *et. al.*, 1994 and 1995) are not present in these non-linear compounds (see ***Figures 4.3.3*** and ***4.3.4***). The hydroxyl and amino groups in both molecules participate in just two strong hydrogen bonds, one O-H...N and one N-H...O (A and B in ***Figure 4.3.3a***). The remaining coordination site on the hydroxyl oxygen

atom is occupied by an aromatic C-H...O hydrogen bond (C) and the second amino N-H is involved in an unusual N-H...π bond (D). The formation of N-H...π hydrogen bonds is favoured in these systems because the aromatic ring is particularly electron rich (see Section 4.1.2). The pyramidal geometry of the amino group also foreshortens the N-H...π contact. The geometries of all the hydrogen bonds in the networks are given in ***Table 4.3.5***.

Table 4.3.5 *- Comparison of the geometries of the 4 unique hydrogen bonds present in both* ***I*** *and* ***II***.

	I		**II**	
Interaction	H...X(Å)	Y-H...X(°)	H...X(Å)	Y-H...X(°)
O-H...N	1.776	172.7	1.757	168.1
N-H...O	2.121	156.7	2.025	165.6
C-H...O	2.551	160.7	2.524	129.0
N-H...π	2.309	145.0	2.409	148.7

The formation of weak C-H...O and N-H...π hydrogen bonds at the expense of a second strong N-H...O bond, in both **I** and **II**, suggests that another pattern of intermolecular interactions is dictating crystal packing. ***Figures 4.3.5*** are packing diagrams of a) **I** and b) **II**. They show that the aromatic rings in both compounds are arranged such that adjacent rings are mutually perpendicular giving rise to a herringbone pattern. 4-Aminophenol (Ermer and Eling, 1994) also adopts this packing arrangement (see ***Figure 4.3.6***). The herringbone motif is observed in many other aromatic compounds, including benzene and has been identified as a supramolecular synthon (Desiraju, 1995).

In 4-aminophenol the establishment of the herringbone motif does not interfere with the tetrahedral motif described by Ermer and Eling (1994). The two motifs are 'insulated' from one another and as a result both are observed in the crystal structure. However, in the non-linear aminophenols **I**, **II** it is not possible for the herringbone motif and the tetrahedral hydrogen bonded motif to co-exist.

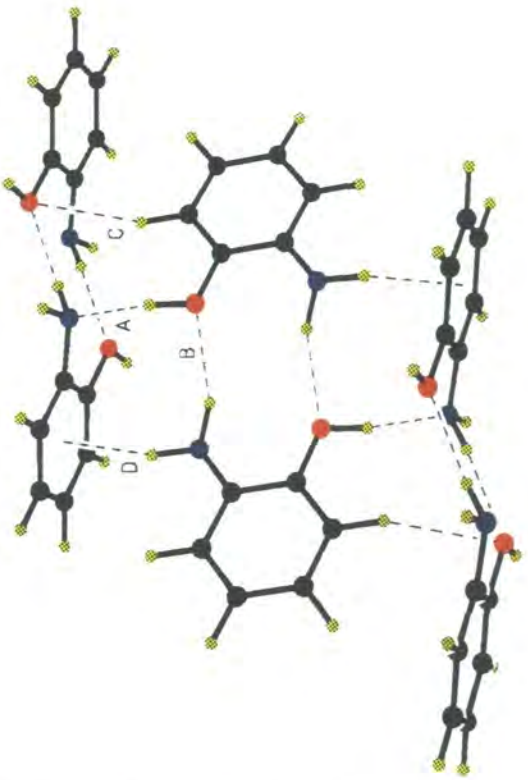

Figure 4.3.3 - *Packing of 2-aminophenol.*

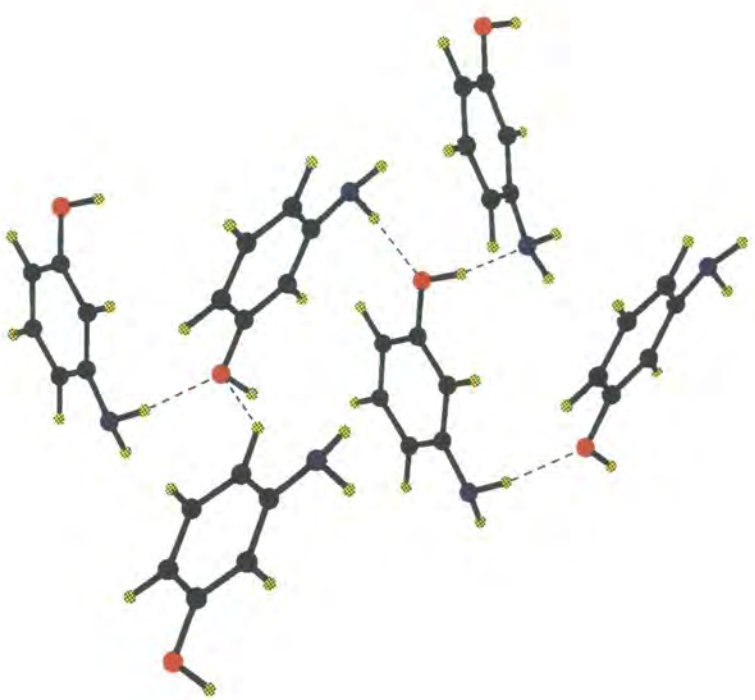

Figure 4.3.4 - *Packing of 3-aminophenol.*

Figures 4.3.5 *- Herringbone packing of a) 2-aminophenol and b) 3-aminophenol.*

Figure 4.3.6 *- Herringbone packing of 4-aminophenol*

The results of the neutron diffraction analysis show that in **I** and **II** the herringbone motif dominates the crystal packing and the tetrahedral network of strong hydrogen bonds is not observed. Instead, a network of both strong (O-H..O and N-H...O) and weak (C-H...O and N-H...π) hydrogen bonds is formed. This network retains two of the key features of the tetrahedral motif described by Ermer and Eling (1994). Each hydroxyl and amino group participates in the maximum attainable 3 hydrogen bonds and tetrahedral environments are maintained about both heteroatoms. This confirms that the structures of simple aminophenols are mediated by tetrahedral networks of hydrogen bonds in which each functional group fulfills it potential hydrogen bonding valency, as Ermer and Eling (1994) predicted. However, these networks are not always composed exclusively of strong hydrogen bonds (despite the complementarity of the hydroxyl and amino groups in this respect) and they are not always structure determining.

Such observations illustrate that straightforward correspondances between molecular and crystal structures are not always obtained. Such correspondances exist only when the different sets of significant intermolecular interaction present in a crystal structure are 'insulated' from one another. In the absence of such 'insulation' i.e. when sets of significant interactions interfere then unpredictable crystal structures often arise.

4.4 CONCLUSIONS

The results of the neutron studies of 2- and 3-aminophenol show unequivocally that the amino groups in both compounds are pyramidal. Surprisingly, the amino group in 3-aminophenol is more pyramidal than that in 2-aminophenol. Presumably, because the steric and inductive effects which make the meta derivative better able to stablize the lone pair density donated by the amino group (see ***Figure 4.1.6***) are negligible when electron demand from the ring and therefore the extent of amino π donation are low.

These studies also show that the tetrahedral networks comprised exclusively of O-H...N and N-H...O bonds which mediate the structures of many linear aminophenols (Ermer and Eling, 1994) are not present in these non-linear compounds. Instead, tetrahedral networks involving both strong (O-H...N and N-H...O) and weak (C-H...O and N-H...π) bonds are observed. The formation of unusual N-H...π bonds is favoured in these systems because the aromatic rings are electron rich. The pyramidal geometry of the amino group also foreshortens the N-H...π contact.

The hydrogen bonding pattern predicted by Ermer and Eling is perturbed to allow the molecules to pack herringbone fashion. These herringbone motifs are common in aromatic compounds and appear to be structure determining in 2- and 3-aminophenol.

4.5 REFERENCES

Aakeroy, C. B.and Seddon, K. R.(1993) Chem. Soc. Rev., 397.

Adams, D. B. (1993) J. Chem. Soc., Perkin Trans. 2, 567 - 571.

Allen, F. H., Bird, C. M., Rowland, R. S., Harris, S. E. and Schwalbe, C. H. (1995) Acta Crystallogr. B**51**, 1068 - 1081.

Allen, F. H., Davies, J. E., Galloy, J. J., Johnson, O., Kennard, O., Macrae, C. F., Mitchell, E. M., Mitchell, G. F., Smith, J. M. and Watson, D. G. (1991) J. Chem. Inf. Comput. Sci., **31**, 187 - 204.

Allen, F. H., Goud, B. S., Hoy, V. J., Howard, J. A. K. and Desiraju, G. R. (1994) J. Chem. Soc., Chem. Commun., 2729 - 2730.

Allen, F., Brammer, L., Kennard, O., Taylor, R. and Watson, D. (1987), J. Chem. Soc., Perkin Trans. 2, S1 - S19.

Aven, L., Bernal,. I., Korp, J. D.and Mills, J. L. (1981) J. Cryst. Mol. Struc., **11**, 117.

Biradha, K., Sharma, C. V. K., Panneerselveam, K., Shimoni, L., Carell, H. L., Zacharias, D. E. and Desiraju, G. R. (1993) J. Chem. Soc., Chem. Commun., 1473.

Borman, S. (1995) Chemical & Engineering News, December 11 issue, 33.

Brunie, G., Declerq, J. P., Germain, G., de Rango, C. and Tsoucaris, G. (1974) Cryst. Struc. Commun., **3**, 485.

Desiraju, G. R. (1989) *Crystal Engineering: The Design of Organic Solids*, Elsevier, Amsterdam.

Desiraju, G. R. (1995) Angew. Chem. (Int. Ed. Engl.), **34**, 2311 - 2327.

Ermer, O. and Eling, A. (1994) J. Chem. Soc., Perkin Trans. 2, 925.

Fan, E., Vincent, C., Geib, S. J. and Hamilton, A. D.(1994) Chem. Mater , **6**, 1113.

Fessenden, R. J. and Fessenden, J. S. (1990) *Organic Chemistry, 4th Edn.*, Brooks-Cole, California.

Hannessian, S., Gomtsyan, A., Simard, M. and Roelens, S. (1994) J. Am. Chem. Soc., **116**, 4495.

Hannessian, S., Simard, M. and Roelens, S. (1995) J. Am. Chem. Soc., **117**, 7630.

MacDonald, J. C. and Whitesides, G. M. (1994) Chem. Rev., **94**, 2383.

Morrison, R. T. and Boyd, R. N. (1987) *Organic Chemistry, 5th Edn.*, John Wiley, New York.

O'Connell, A. M. and Maslen, E. N. (1967) Acta Crystallogr., **22**, 134.

Pedireddi, V. R., Jones, W., Chorlton, A.P. and Docherty, R. (1996) J. Chem. Soc., Chem. Commun., 997 - 998.

Sears, V. F. (1992) *Scattering Lengths for Neutrons: International Tables for Crystallography, Volume C*, ed. Wilson, A.J.C., Kluwer Academic Publishers, the Netherlands, pp. 383 - 391.

Sharma, C. V. K., Panneerselveam, K., Pilati, T. and Desiraju, G. R. (1991) J. Chem. Soc., Chem. Commun., 832.

Sheldrick, G., M. (1993) SHELXL-93: *Program for the refinement of crystal structures using single crystal diffraction data*, University of Göttingen, Germany.

Stalhandske, C. (1976) Acta Crystallogr. B**32**, 2806.

Thalladi, V. R., Goud, B. S., Hoy, V. J., Allen, F. H., Howard, J. A. K. and Desiraju, G. R. (1996) J. Chem. Soc, Chem. Commun., 401 - 402.

Wilkinson, C., Khamis, H. W., Stansfield, R. F. D. and McIntyre, G. J. (1988) J. Appl. Cryst., **21**, 471 - 478.

CHAPTER 5

X-ray Diffraction Studies of Compounds Engineered to Contain Nitro Oxygen...Iodo Interactions

5.1 INTRODUCTION

Interactions between nitro oxygen and iodine atoms were first described by Desiraju *et. al.* (1993). They proposed a structural model for 4-iodo-β-nitrostyrene (**I**) which involved the symmetrical I...O_2N interaction depicted in ***Figure 5.1.1a***. This model of the structure of **I** was based on analysis of the crystal structures of 4-chloro- and 4-bromo-β-nitrostyrene (Desiraju and Pedireddi 1989; Pedireddi, Sarma and Desiraju, 1992). Its accuracy could not be confirmed experimentally since it was impossible to grow crystals of sufficient quality for X-ray diffraction. However, subsequent database analyses of Cl...O_2N, Br...O_2N and I...O_2N interactions (Desiraju et. al., 1993; Chapter 7) have shown that, although systems possessing both I and NO_2 are quite rare, more than half of them do contain close I...O_2N contacts. The corresponding percentages for Cl...O_2N and Br...O_2N are somewhat lower. Furthermore, the majority of the I...O_2N contacts are of the symmetrical bifurcated type shown in ***Figure 5.1.1a***.

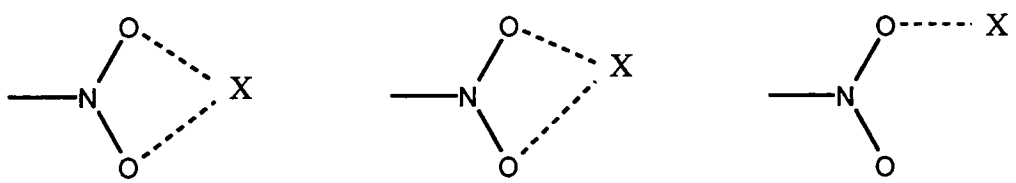

Figure 5.1.1 *- The a) symmetrical bifurcated, b) asymmetrical bifurcated and c) mono-coordinate X...O_2N bonding motifs.*

The high frequency with which the symmetrical I...O_2N interaction occurs in relevant systems suggests that it is an ideal supramolecular synthon. The term synthon was first used by Corey (1967) to describe the structural units within molecules which can be made by known synthetic routes. This definition was adapted recently by Desiraju (1995) who used the term supramolecular sython to describe the structural units within supermolecules which can be assembled by the formation of known patterns of intermolecular interactions.

Desiraju describes a good supramolecular synthon as possessing "...generality and predictability". Database analysis indicates that the symmetrical I...O_2N motif has both. However, as Desiraju points out, supramolecular synthons must also be, "...robust enough to be exchanged from one network structure to another...". Since there are only a limited number of published crystal structures containing both I and NO_2 it is difficult to assess the robustness of the I...O_2N interaction using database techniques. The obvious alternative is to design and determine the structures of crystals which contain both iodine and a nitro group in environments which favour the formation of I...O_2N interactions and then to introduce functional groups which can form alternative intermolecular interactions. This chapter describes the results of diffraction analyses of three such compounds.

The first two compounds to be investigated were the 1:1 co-crystal of 1,4-diiodobenzene and 1,4-dinitrobenzene (**II**) and the one component system 4-iodonitrobenzene (**III**). These systems were selected because they only contain the functional groups I and NO_2 and therefore have very few options other than to participate in I...O_2N interactions. The third compound selected for study was the 1:2 co-crystal of 1,4-dinitrobenzene and 4-iodocinnamic acid (**IV**). This system provides a more rigorous test of the robustness of the I...O_2N synthon since carboxylic acid groups, which are capable of forming strong O-H...O hydrogen bonds, are also present.

Finally, the structures of **II**, **III** and **IV** were compared with that of the 1:1 co-crystal of 1,4-diiodobenzene and TCNQ (**V**). Interactions between halogens and cyano groups have been described by several authors (see for example Desiraju and Harlow, 1989) and have been shown to mediate crystal structures (Reddy *et. al.* 1993). Since X...O_2N and X...N≡C are both polarisation induced halogen...nucleophile type interactions it was of interest to compare the geometries of any I...O_2N interactions found with that of a related I...N≡C interaction.

Unlike the structural studies described in the preceeding chapters, these investigations were carried out using X-ray diffraction analysis. X-ray diffraction is more suitable in this case because hydrogen is not involved in the intermolecular interaction being studied. This means that it is not vital to accurately locate hydrogen atoms and so the problems associated with the poor scattering of X-rays by hydrogen can be ignored. The advantages of using X-rays instead of neutrons are outlined in Section 1.2.2.

5.2 EXPERIMENTAL DETAILS

Data for **II**, **IV** and **V** were collected using a Rigaku AFC6S four circle diffractometer. Data for **III** were collected on a Siemens P4 four circle diffractometer. All four experiments were conducted at 150K using an Oxford Cryosystems nitrogen Cryostream cooling device (Cosier and Glazer, 1986). Chapter 2 contains details about the instrumentation and experimental procedures used. ***Table 5.2.1*** contains crystal sample, data collection and structure refinement details.

Structure factors were obtained from the raw intensity data for **II**, **IV** and **V** using the TEXSAN (Molecular Structure Corporation., 1989) program PROCESS. The data from **III** were reduced to structure factors using Seimens' XSCANS software (Siemens, 1994). Emprical absorption corrections were applied to the data for **II** and **IV** based on azimuthal, ψ, scans of the three reflections. A numerical absorption correction, based on the indices of the crystal faces and on crystal size, was applied to the data for **III**. No correction was applied to the data from **V**.

The four structures were solved either by direct (**II** and **IV**) or Patterson (**III** and **V**) methods using the SHELXS-86 package (Sheldrick, 1990). The subsequent refinement of structure **V** was performed using SHELXTL (Sheldrick, 1995). **II**, **III** and **IV** were refined, on F^2, using SHELXL-93 (Sheldrick, 1993). In all cases positional parameters and anisotropic thermal parameters were refined for all non-hydrogen atoms, whilst hydrogen atoms were located in difference maps and their positional and isotropic thermal parameters were refined.

Table 5.2.1 *- Details of crystal samples, data collections and structure refinement for* ***II, III, IV*** *and* ***V****.*

Compound	II	III	IV	V
Formula	$C_{12}H_6I_2N_2O_4$	$C_6H_4INO_2$	$C_{15}H_{11}N_2O_6I$	$C_{18}H_8N_4I_2$
Molecular Weight	498.0	249.0	358.1	267.0
Dcalc (g cm^{-1})	2.332	2.332	1.923	1.993
a (Å)	9.662(2)	7.545(2)	7.719(2)	7.658(2)
b (Å)	9.780(2)	7.802(2)	9.246(2)	7.782(1)
c (Å)	7.550(2)	6.5990(10)	9.988(2)	7.833(1)
α (°)	90	91.43(3)	111.43(3)	75.65(1)
β (°)	93.43(3)	92.03(3)	107.76(3)	96.47(2)
γ (°)	90	66.00(3)	94.03(3)	99.38(1)
Volume ($Å^3$)	712.2(2)	354.63(14)	618.5(2)	444.9(1)
Crystal System	Monoclinic	Triclinic	Triclinic	Triclinic
Space Group	C2/m	P-1	P-1	P-1
Z	2	2	2	1
Morphology	Cube	Needle	Needle	Square prism
Colour	Yellow	Colourless	Yellow	Red
Size (mm)	.4 x .4 x .4	.2 x .2 x .6	.1 x .1 x .9	.3 x .3 x .1
Absorption (mm^{-1})	4.429	4.448	2.594	3.540
2θ Range (°)	5 - 50	5 - 65°	5 - 50°	5 - 50
Scan Speed(°ϖmin^{-1})	2 - 16	Variable	2 - 16	2 - 16
No. Measured Data	1411	2725	2313	1694
No. Unique Data	665	2560	2165	1568
No. Observed Data	664	2560	2165	1485
σ (I) Cut Off	I > -4 σ (I)	I > -4 σ (I)	I > -4 σ (I)	I > 4 σ (I)
Rmerge	0.0356	0.0076	0.0423	0.015
Parameters Refined	61	108	196	121
Final R	0.0164 (F)	0.0254	0.0479	0.0152
Final Rw	0.0445 (F^2)	0.0469	0.0673	0.0216
Goof	1.250	1.127	1.066	1.09
Weighting Scheme	0.0112, 0.96	0.0225, 0.15	0.028	0.0002
Δρ min (e $Å^{-3}$)	-0.575	-0.899	-0.49	-0.40
Δρ max (e $Å^{-3}$)	0.622	0.921	0.35	0.32

5.3 STRUCTURAL RESULTS

5.3.1 1:1 Co-crystal of 1,4-Diiodobenzene and 1,4-Dinitrobenzene (II)

Figure 5.3.1 shows the 50% probability thermal ellipsoid plot of the X-ray derived structure of **II**. ***Tables 5.3.1*** and ***5.3.2*** contain bond lengths and selected interbond angles.

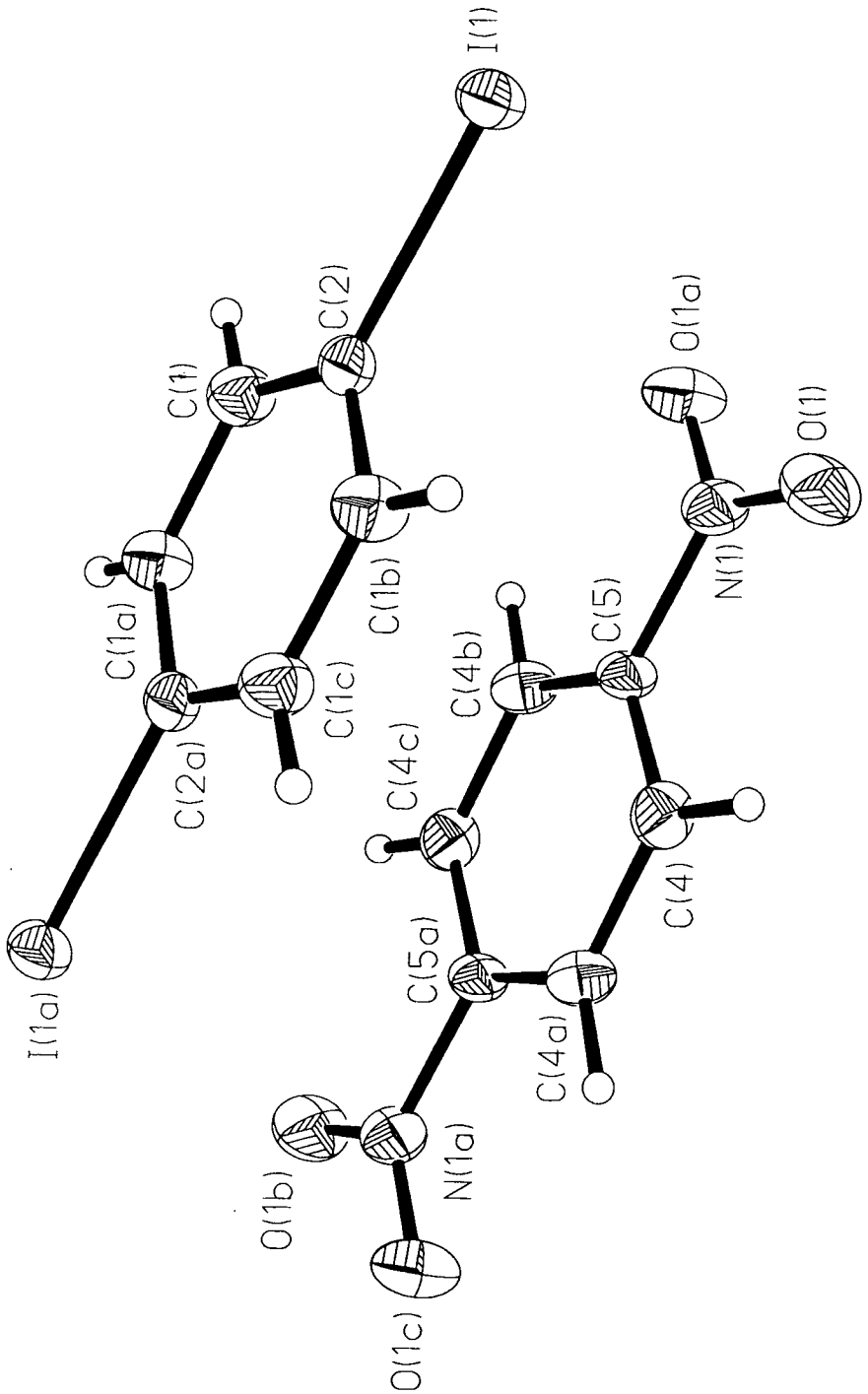

Figure 5.3.1 *- 50% probability thermal ellipsoid plot of* ***II****.*

Table 5.3.1 - Selected bond lengths in complex II.

	Length(Å)		Length(Å)
I(1) - C(2)	2.113(5)	N(1) - C(5)	1.484(6)
C(2) - C(1)	1.328(4)	C(5) - C(4)	1.379(4)
C(1) - C(1a)	1.398(7)	C(4) - C(4a)	1.404(6)
O(1) - N(1)	1.221(4)		

Table 5.3.2 - Selected interbond angles in complex II.

	Angle(°)		Angle(°)
I(1) - C(2) - C(1)	119.2(2)	O(1) - N(1) - C(5)	117.9(2)
C(1) - C(2) - C(1b)	121.5(4)	N(1) - C(5) - C(4)	118.0(2)
C(2) - C(1) - C(1a)	119.2(2)	C(4) - C(5) - C(4b)	123.9(4)
O(1) - N(1) - O(1a)	124.3(4)	C(5) - C(4) - C(4a)	118.0(2)

The crystal structure of **II**, viewed along [001], is shown in ***Figure 5.3.2***. The Figure reveals that there is a complex pattern of intermolecular interactions present in the structure. The primary structural motif is a symmetrical bifurcated I...O_2N interaction (**A** in ***Figure 5.3.2*** which links 1,4-diiodobenzene and 1,4-dinitrobenzene molecules to form linear ribbons, as predicted. These interactions are constrained by the crystallographic symmetry to be perfectly symmetrical and flat (2/m) with I(1)...O(1) = 3.45Å and C(2)-I(1)...O(1) = 161.3°.

In addition the ribbons are connected laterally by two unique types of C-H..O interaction; a 10-membered ring self recognition motif between adjacent 1,4-dinitrobenzene molecules with C(4)...O(1) = 3.31Å and C(4)-H(4)...O(1) = 122° and a mutual recognition interaction between the dinitrobenzene and the diiodobenzene with C(1)...O(1) = 3.44Å and C(1)-H(1)...O(1) = 145° (**B** and **C** respectively in ***Figure 5.3.2***). There are also two C-H...I interactions present, one connecting dinitro and diiodo benzenes (**D** in ***Figure 5.3.2***, C(4)...I(1) = 4.31Å and C(4)-H(4)...I(1) = 149°) and another between diiodobenzenes (**E** in ***Figure 5.3.2***, C(1)...I(1) = 4.14Å and C(1)-H(1)...I(1) = 135°).

These four interactions bind the I...O_2N mediated ribbons together, forming corrugated molecular sheets which π stack (π...π = 3.78Å) such that dissimilar molecules overlap (***Figure 5.3.3***) to produce the three dimensional structure.

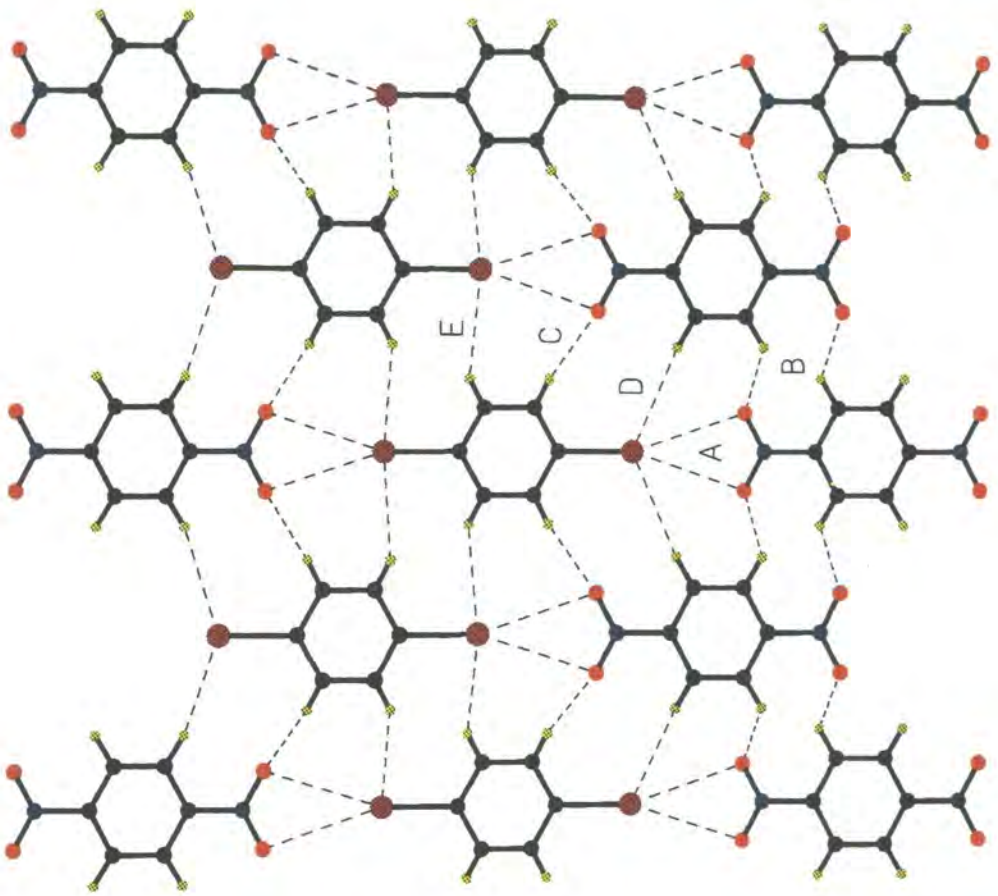

Figure 5.3.2 - *Packing of* ***II*** *viewed along [001].*

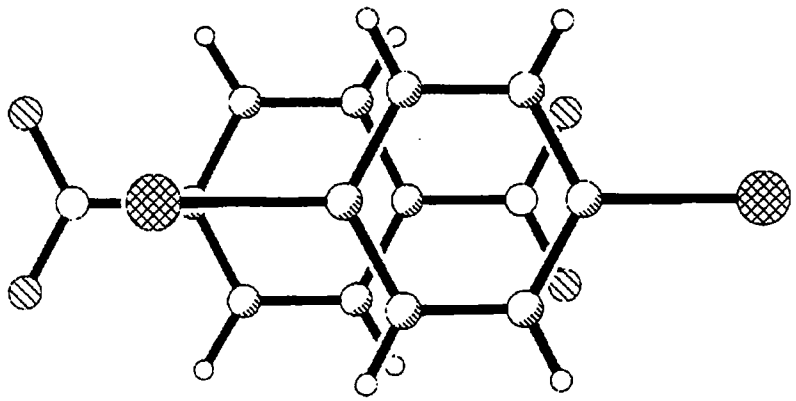

Figure 5.3.3 - π stacking of II.

5.3.2 4-Iodonitrobenzene (III)

Figure 5.3.4 shows the 50% probability thermal ellipsoid plot of the X-ray derived structure of **III**. *Tables 5.3.3* and *5.3.4* contain bond lengths and selected interbond angles.

Table 5.3.3 - Bond lengths in complex III.

	Length(Å)		Length(Å)
I(1) - C(4)	2.098(2)	N(1) - C(1)	1.472(3)
O(1) - N(1)	1.232(2)	C(1) - C(2)	1.382(3)
O(2) - N(1)	1.222(2)	C(1) - C(6)	1.385(3)
C(4) - C(5)	1.390(3)	C(6) - C(5)	1.397(3)
C(4) - C(3)	1.396(3)	C(2) - C(3)	1.397(3)

Table 5.3.4 - Selected interbond angles in complex III.

	Angle(°)		Angle(°)
C(5) - C(4) - C(3)	121.4(2)	O(1) - N(1) - C(1)	118.2(2)
C(5) - C(4) - I(1)	119.16(14)	C(2) - C(1) - N(1)	118.5(2)
C(3) - C(4) - I(1)	119.44(14)	C(1) - C(6) - C(5)	118.3(2)
O(2) - N(1) - O(1)	123.3(2)	C(1) - C(2) - C(3)	118.5(2)

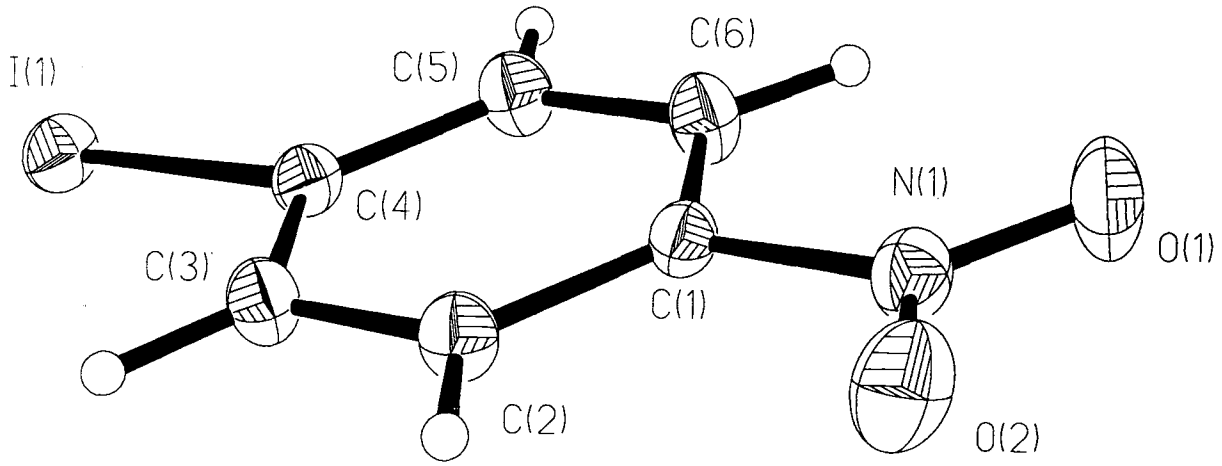

Figure 5.3.4 *- 50% probablilty thermal ellipsoid plot of* ***III****.*

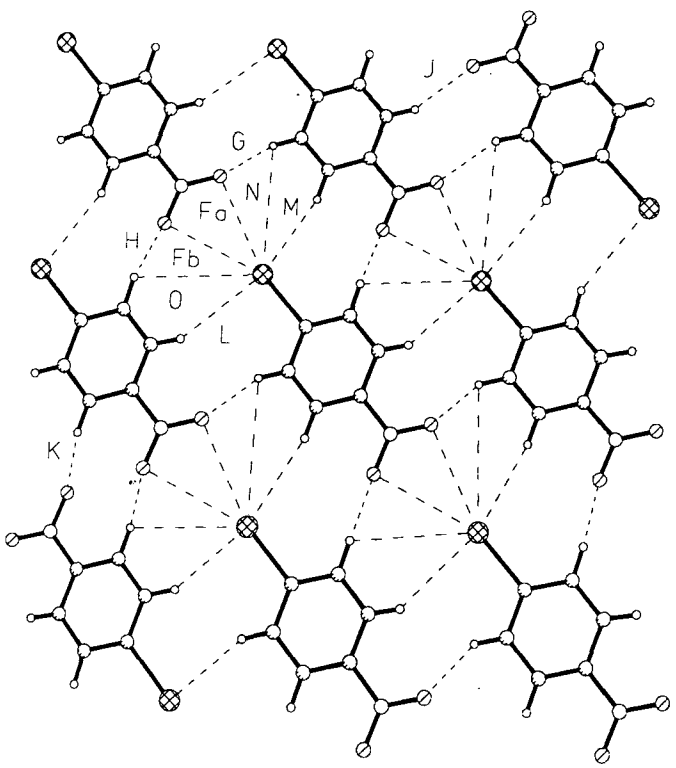

Figure 5.3.5 *- Packing of* ***III*** *viewed along [100].*

A view along [100] of the crystal structure of **III** (***Figure 5.3.5***) reveals that **III** packs much like **II**. As in **II**, symmetrical bifurcated I...O_2N interactions (**F** in ***Figure 5.3.5***) are present, linking 4-iodonitrobenzene molecules together to form extended ribbons. However, in this case there are no crystallographic contraints on the symmetry of the I...O_2N interactions and they are slightly asymmetric (**Fa**, I(1)...O(2) = 3.466Å and C(1)-I(1)...O(2) = 157.9°; **Fb**, I(1)...O(1) = 3.327Å and C(1)-I(1)...O(1) = 163.8°). Once again the I...O_2N mediated ribbons are connected by lateral C-H...O and C-H...I interactions (**G**, C(5)...O(2) = 3.288Å, C(5)-H(5)...O(2) = 114.9°; **H**, C(3)...O(1) = 3.438Å, C(3)-H(3)...O(1) = 135.2°; **J**, C(2)...O(2) = 3.438Å and C(2)-H(2)...O(2) = 150.4°, **K**, C(6)...O(1) = 3.377Å and C(6)-H(6)...O(1) = 128.4°; **L** C(2)...I(1) = 4.142Å, C(2)-H(2)...I(1) = 121.5°; **M**, C(6)...I(1) = 4.104Å, C(6)-H(6)...I(1) = 150.1°; **N**, C(5)...I(1) = 4.268Å and C(5)-H(5)...I(1) = 148.4°; **O**, C(3)...I(1) = 4.165Å and C(3)=H(3)...I(1) = 140.9° in ***Figure 5.3.5***.

5.3.3 1:2 Co-crystal of 1,4-Dinitrobenzene and 4-Iodocinnamic Acid (IV)

Figure 5.3.6 shows the 50% probability thermal ellipsoid plot of the X-ray derived structure of **IV**. ***Tables 5.3.5*** and ***5.3.6*** contain bond lengths and selected interbond angles.

In contrast to **II** and **III** above, the primary structural motif in **IV** (shown, viewed in the plane of the aromatic ring, in ***Figure 5.3.7***) is the O-H..O mediated inversion centre dimer between pairs of cinnamic acid molecules (**P**, O(3)...O(4) = 2.649Å and O-H...O = 167.8°). However, the I...O_2N interaction demonstrates its robustness in the presence of these strong hydrogen bonds by once again mediating the extended ribbon structure of **IV**. In this case the carboxylic acid dimers are 'glued' together by 1,4-dinitrobenzene molecules which form asymmetrical bifurcated I...O_2N interactions with the iodine atoms para to the cinnamic acid groups (**Qa**, I(1)...O(1) = 3.306 and C(1)-I(1)...O(1) = 169.9°; **Qb**, I(1)...O(2) = 3.655Å and C(1)-I(1)...O(2) = 154.7°).

Table 5.3.5 - Bond lengths in complex IV.

	Length (Å)		Length (Å)
I(1) - C(1)	2.095(4)	C(2) - C(3)	1.385(6)
N(1) - O(1)	1.213(5)	C(11) - C(10)	1.374(6)
N(1) - O(2)	1.218(5)	C(11) - C(12)	1.379(6)
N(1) - C(10)	1.472(5)	C(4) - C(3)	1.377(6)
O(3) - C(9)	1.269(5)	C(5) - C(4)	1.386(6)
O(4) - C(9)	1.263(5)	C(4) - C(7)	1.473(6)
C(1) - C(6)	1.382(6)	C(12) - C(10a)	1.378(6)
C(1) - C(2)	1.384(6)	C(9) - C(8)	1.476(6)
C(6) - C(5)	1.390(6)	C(8) - C(7)	1.331(6)

Table 5.3.6 - Selected interbond angles in complex IV.

	Angle(°)		Angle(°)
O(1)-N(1)-O(2)	123.7(4)	C(11)-C(10)-N(1)	118.4(4)
O(1)-N(1)-C(10)	119.0(4)	O(4)-C(9)-O(3)	123.5(4)
O(2)-N(1)-C(10)	117.3(4)	O(4)-C(9)-C(8)	117.8(4)
C(6)-C(1)-C(2)	119.9(4)	O(3)-C(9)-C(8)	118.8(4)
C(6)-C(1)-I(1)	120.2(3)	C(7)-C(8)-C(9)	122.1(4)
C(10)-C(11)-C(12)	118.8(4)	C(4)-C(5)-C(6)	121.1(4)
C(3)-C(4)-C(7)	119.2(4)	C(4)-C(3)-C(2)	121.6(4)
C(10a)-C(12)-C(11)	118.9(4)	C(8)-C(7)-C(4)	127.1(4)
C(11)-C(10)-C(12a)	122.3(4)		

Symmetry transformations used to generate equivalent atoms: a 1-x, 2-y, 1-z

The ribbons in **IV** are joined laterally by a complex network of C-H...O bonds. There are four distinct C-H...O mutual recognition interactions between the 1,4-dinitrobenzene and 4-iodocinnamic acid molecules, involving both nitro and carboxylic acid oxygen atoms (**R**, C(7)...O(2) = 3.647Å and C(7)-H(7)...O(2) = 141.5°; **S**, C(2)...O(1) = 3.417Å and C(2)-H(2)...O(1) = 137.0°; **T**, C(11)...O(3) = 3.363Å and C(11)-H(11)...O(3) = 126°; **U**, C(12)...O(4) = 3.347Å and C(12)-H(12)...O(4) = 126.0° in Figure 5.3.3.2). Addtionally there are three C-H...O self recongnition interactions, two between cinnamic acid molecules (**V**, C(5)...O(4) = 3.688Å and C(5)-H(5)...O(4) = 159.8°; **W**, C(6)..O(3)

= 3.590Å and C(6)-H(6)...O(3) = 121.1°) and one between dinitrobenzene molecules (**X**, C(11)...O(2) = 3.476Å and C(11)-H(11)...O(2) = 141.4°). There is also evidence of C-H...I bonding. Once again π...π interactions (π...π = 3.714Å) complete the three dimensional structure.

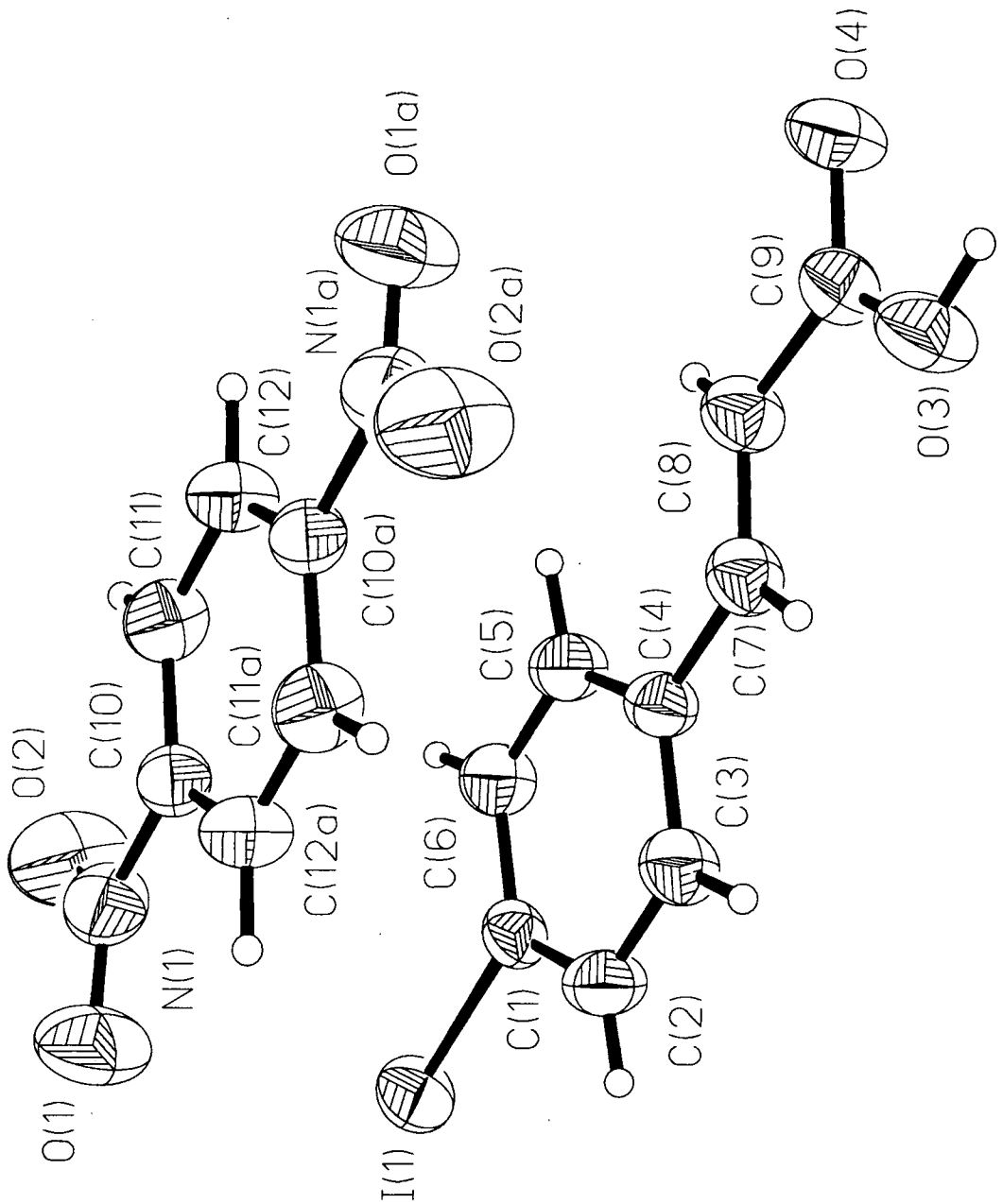

Figure 5.3.6 *- 50% probability thermal ellipsoid plot of* ***IV****.*

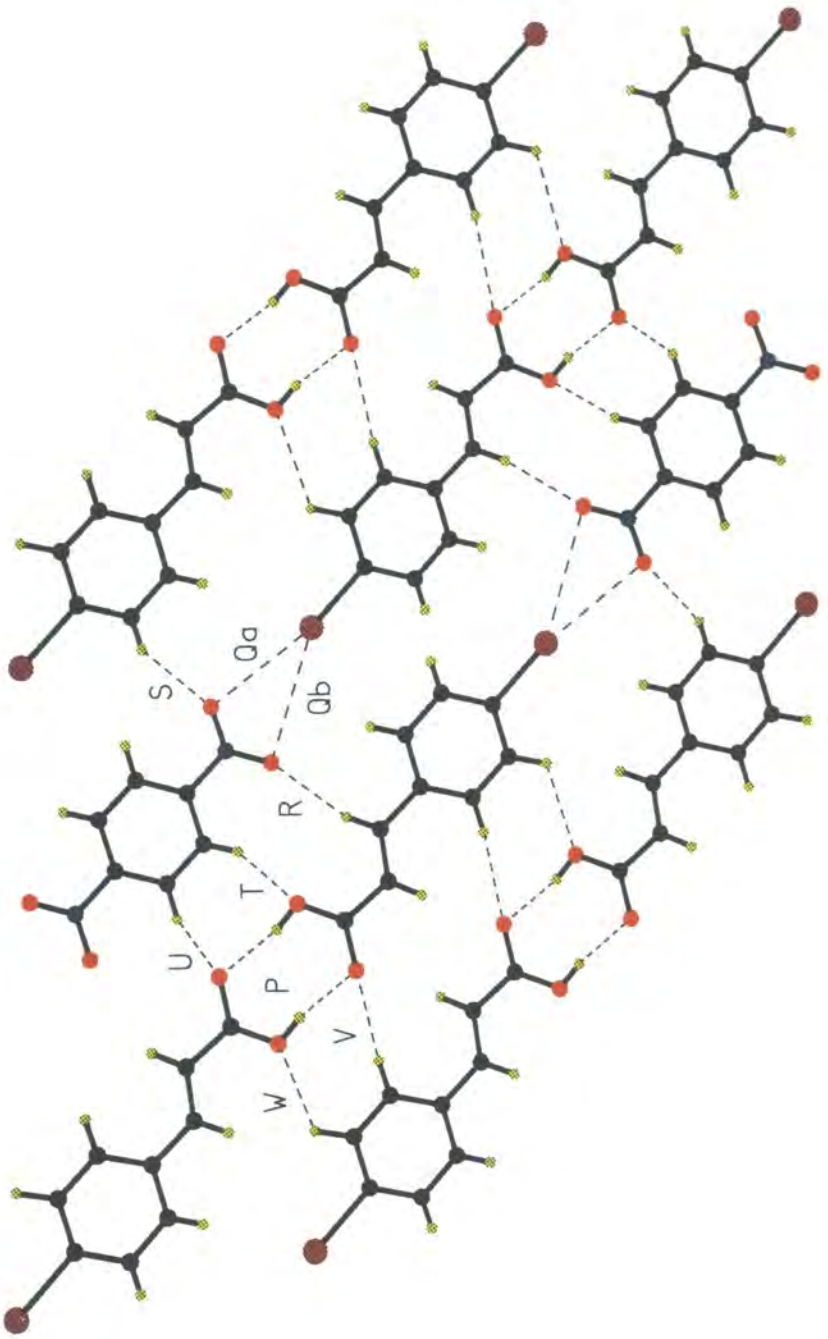

Figure 5.3.7 *- Packing of* ***IV*** *viewed in the aromatic ring plane.*

5.3.4 1:1 Co-crystal of 1,4-Diiodobenzene and TCNQ (V)

Figure 5.3.8 shows the 50% probability thermal ellipsoid plot of the X-ray derived structure of **V**. ***Tables 5.3.7*** and ***5.3.8*** contain selected bond lengths and interbond angles.

Table 5.3.7 *- Selected bond lengths in complex V.*

	Length(Å)		Length(Å)
N(1) - C(1)	1.148(4)	C(4) - C(6)	1.445(4)
N(2) - C(2)	1.144(4)	C(6) - C(5a)	1.334(3)
C(2) - C(3)	1.444(4)	I(7) - C(7)	2.101(2)
C(1) - C(3)	1.441(4)	C(7) - C(8)	1.394(4)
C(3) - C(4)	1.383(3)	C(7) - C(9)	1.383(4)
C(4) - C(5)	1.446(3)	C(9) - C(8a)	1.397(3)

Table 5.3.8 *- Selected interbond angles in complex V.*

	Angle(°)		Angle(°)
N(1) - C(1) - C(3)	178.5(3)	C(4) - C(5) - C(6a)	120.8(2)
N(2) - C(2) - C(3)	179.3(3)	C(4) - C(6) - C(5a)	120.9(2)
C(1) - C(3) - C(2)	116.0(2)	I(7) - C(7) - C(8)	118.6(2)
C(1) - C(3) - C(4)	121.2(2)	I(7) - C(7) - C(9)	119.8(2)
C(2) - C(3) - C(4)	122.7(2)	C(8) - C(7) - C(9)	112.6(2)
C(3) - C(4) - C(5)	120.7(2)	C(7) - C(8) - C(9a)	118.8(2)
C(3) - C(4) - C(6)	121.1(2)	C(7) - C(9) - C(8a)	119.6(2)

Figure 5.3.9 shows the structure of complex **V**. Here, in contrast to **II**, **III** and **IV** the principal I...N≡C interaction (**Y** in the Figure) involves only one cyano group from each geminal pair giving rise to a zig-zag molecular ribbon structure (I(7)...N(1) = 3.37Å and C(7)-I(7)...N(1) = 178°). This asymmetrical interaction arises because the separation of the two nitrogen termini in TCNQ is too wide to allow iodine to bridge, as it does in **II**, **III** and **IV**. The non-coordinating I...N distance is 4.29Å, too long to be significant, thus

the I...N≡C interaction is best described as analogous to the mono-coordinate bonding motif described in Chapter 7.

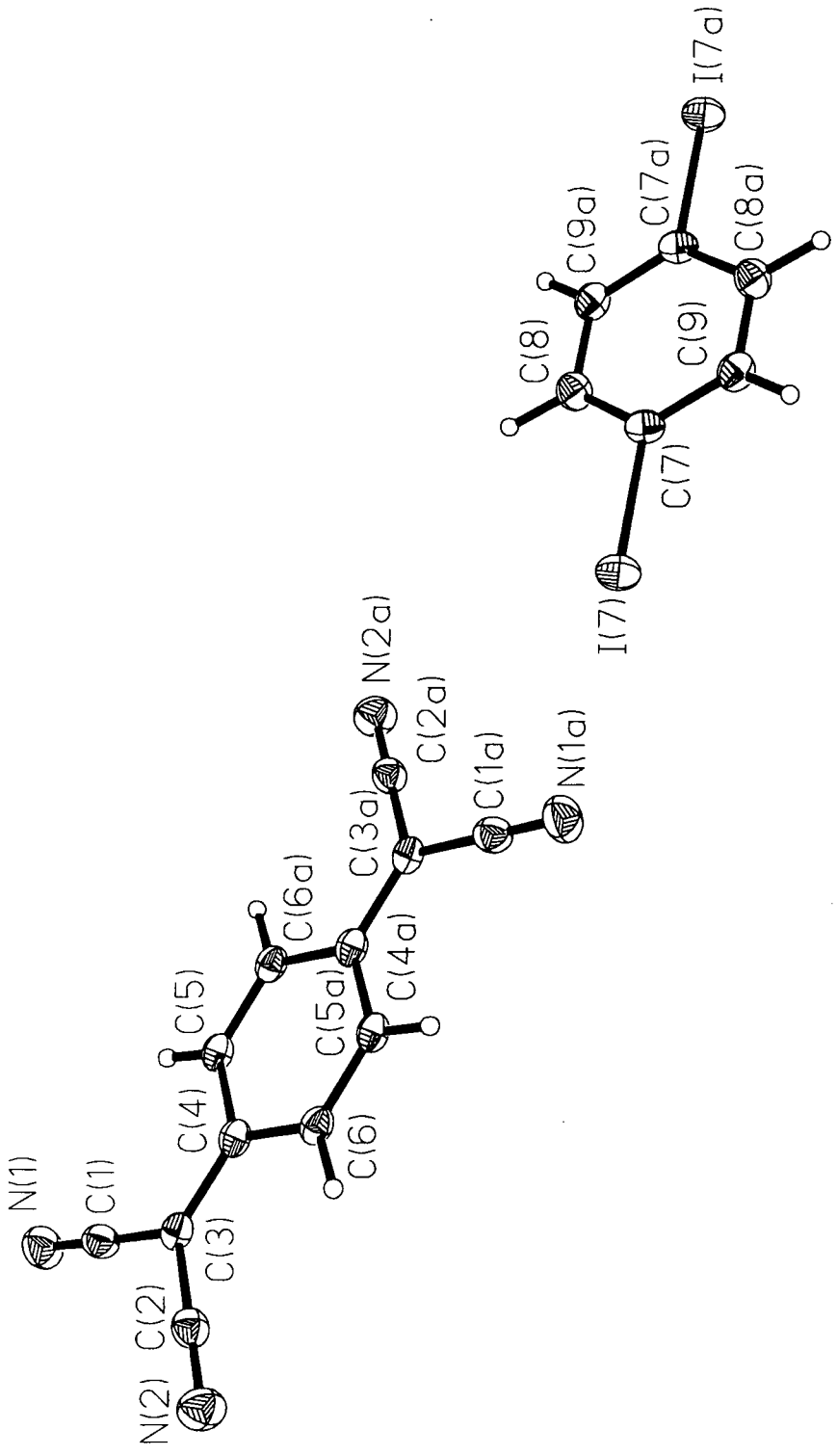

Figure 5.3.8 *- 50% probability thermal ellipsoid plot of* ***V****.*

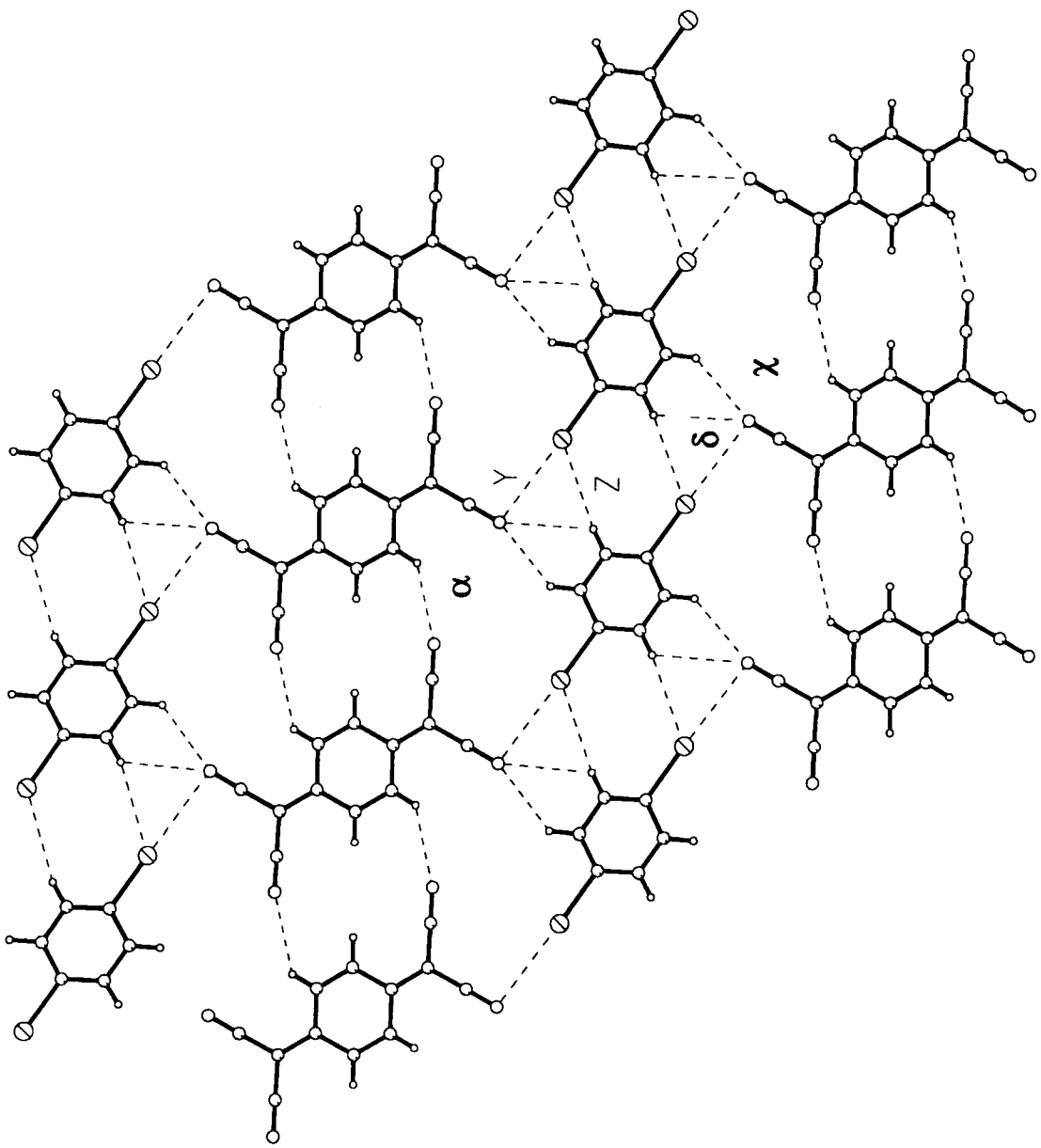

Figure 5.3.9 - *Packing of V viewed in the aromatic ring plane.*

This structure too contains numerous additional weak hydrogen bonding interactions which organise the zig-zag ribbons into corrugated sheets. There is a C-H...I self recognition motif between diiodobenzenes (**Z** in ***Figure 5.3.9***) with C(9)...I(7) = 4.04Å and C(9)-H(9)...I(7) = 153°. Self recognition of TCNQ molecules occurs via the formation of two C-H...N mediated dimers (interactions α and β in ***Figure 5.3.9***). α has C(5)...N(2) = 3.42Å and C(5)-H(5)...N(2) = 134° and β has C(5)...N(1) = 3.21Å and C(5)-H(5)...N(1) = 99°. Two C-H...N mutual recognition motifs are also present. Both involve the coordinating N atom on TCNQ (interactions χ and δ in ***Figure 5.3.9***) and have C(8)...N(1) = 3.47 Å, C(9)...N(1) = 3.64 Å and C(8)-H(8)...N(1) = 128°, C(9)-H(9)...N(1) = 117° for χ and δ respectively.

5.4 CONCLUSIONS

The results described in this chapter show that bifurcated I...O_2N interactions occur generally and predictably in suitable systems and often play a structure determining role. I...O separations are typically within the sums of the van der Waal's radii of the two atoms (I = 1.98Å and O = 1.52Å: Bondi, 1964).and C-I...O angles tend towards linearity, despite the geometrical restrictions imposed by the bifurcated nature of the interaction. The presence of linear I...O_2N mediated ribbons in the structure of **IV** demonstrates that the bifurcated I...O_2N motif retains its integrity even in the presence of strong O-H...O hydrogen bonds. This, and the other structural results, indicates that the motif is sufficiently robust to be exchanged between network systems and therefore satisfies all of the criteria for a good supramolecular synthon.

The I...N≡C interaction present in **V** has geometrical characteristics comparable to those of the I...O_2N interactions in structures **II**, **III** and **IV**. The I...N contact is shorter than the sum of the van der Waals' radii of iodine and nitrogen (I = 1.98Å and N = 1.55Å: Bondi, 1964) and the C-I...N angle is close to 180°. However, the mono-coordinate nature of the interaction, which results from the large separation between the terminal nitrogen atoms in TCNQ, gives rise to zig-zag ribbons in **V** contrasting with the linear ribbons present in **II**, **III** and **IV**.

5.5 REFERENCES

Bondi, A. (1964) J. Chem. Phys., **68**, 441 - 451.

Corey, E. J. (1967) Pure Appl. Chem., **14**, 19.

Cosier, J. and Glazer, A. M. (1986) J. Appl. Cryst., **19**, 105.

Desiraju, G. R. (1995) Angew. Chem. (Int. Ed. Engl.), **34**, 2311 - 2327.

Desiraju, G. R. and Harlow, R. L. (1989) J. Am. Chem. Soc., **111**, 6757.

Desiraju, G. R. and Pedireddi, V. R. (1989) J. Chem. Soc., Chem. Commun., 1112.

Desiraju, G. R., Pedireddi, V. R., Sarma, J. A. R. P. and Zacharias, D. E. (1993) Acta Chim. Hung., **130** (3-4), 451 - 465.

Molecular Structure Corporation (1989) TEXSAN, *Version 5.0, TEXRAY Structure Analysis Package*. MSC, 3200 Research Forest Drive, The Woodlands, TX77381, U.S.A.

Pedireddi, V. R., Sarma, J. A. R. P.and Desiraju, G. R. (1992) J . Chem. Soc., Perkin Trans. 2, 311.

Reddy, D.S., Panneerselvam, K., Pilati, T. and Desiraju, G.R. (1993) J. Chem. Soc., Chem. Commun., 661 - 662.

Sheldrick, G. M., (1990) Acta. Crystallogr. A**46**, 467-473.

Sheldrick, G. M., (1995) SHELXTL, Version 5.03/VMS, Siemens Analytical X-ray Instruments Inc., Madison, Wisconsin, U.S.A.

Sheldrick, G., M. (1993) SHELXL-93: *Program for the refinement of crystal structures using single crystal diffraction data*, Uinversity of Göttingen, Germany.

Siemens (1994) XSCANS, *X-ray Single Crystals Analysis System*, Version 2.1, Siemens Analytical X-ray Instruments Inc., Madison, Wisconsin, USA.

CHAPTER 6

The Cambridge Structural Database

6.1 INTRODUCTION

6.1.1 An Historical Perspective

During its early years, crystallography was a time consuming science. Laborious manual methods were used to collect, solve and refine X-ray diffraction data and it often took several years to complete a single structure. Consequently, only a few new crystal structures were published annually. This made it possible for individual researchers to survey the whole of the primary crystallographic literature and perform systematic analyses of related structures by hand. Many such studies were conducted during the 1950s and 60s dealing with topics such as bond lengths, molecular conformations (Sutton, 1958 and 1965) and hydrogen bonding (Pimental and McClellan, 1960; Sutor, 1963).

The number of crystal structure determinations being performed increased steadily during the 1960s as improvements in diffractometer design and manufacture and increasing levels of automation enabled more researchers to collect data in less time. It became impossible for individuals to conduct comprehensive searches of the primary literature and secondary publications, such as *Wycoff's Crystal Structures* and *Structure Reports*, came into their own.

The advent of affordable computer technology, in the mid 1960s, brought further change. Fully automated data collections could be conducted around the clock using computer controlled diffractometers, the repetitive mathematical procedures associated with structure solution and refinement were performed by computers in a fraction of the time possible previously and new direct phasing methods (Sayre, 1952) for solving crystal structures were developed, enabling crystallographers to determine the structures of a much larger range of compounds, in particular simple organic species.

These improvements led to an explosion in the number of crystal structures being reported annually (from 224 in 1960 to 1258 in 1970). Systematic analyses of the crystallographic data became unfeasible and the wealth of chemical information contained therein was in danger of going largely unexploited. In order to avoid this, structural data began to be complied into computerised databases which could be searched systematically using software developed specifically for the purpose.

6.1.2 The Cambridge Structural Database System

The Cambridge Structural Database System (CSDS: Allen *et. al.*, 1991) is the largest of the four fully retrospective computerised crystallographic databases in use today. It was set up in 1965 and at present it contains the crystal structures of over 150, 000 organic and metallo-organic compounds. The other databases store information about inorganic compounds (Inorganic Chemical Structural Database, ICSD), proteins (Protein Data Bank, PDB) and metals (Metals Data File, MDF).

CSDS definitions of organic and metallo-organic compounds are broad* and as a result the Database contains structural information on a huge range of different molecules, from large transition metal complexes to simple aliphatics. This data is accessed using sophisticated CSDS search and retrieval software which is constantly being developed and updated. New options include interactive geometrical searches and on-line statistical analysis. Such improvements have led to a considerable increase in the use of the CSDS for research purposes in recent years.

Figure 6.1.1 is a histogram showing the number of publications which have used the CSDS as a data source each year for the last 20 years†. The Figure shows that there was a steady increase in the use of the Database throughout the 1970s and early 80s. By 1985 around 20 papers involving Database analysis were being published each year. Database

---

* Compounds are included in the CSDS if they contain at least one C-C or C-H bond.

† ***Figure 6.1.1*** was compiled using the Database of Database use.

use remained static during the late 1980s but began to increase dramatically in the 1990s. The resurgence of interest in the Database can be attributed in part to improvements to the software but also to growing research interest in topics such as supramolecular assembly, crystal engineering and crystal structure prediction since, as Desiraju (1995) recently pointed out, crystallographic database analysis is to these subjects what "retrosynthetic analysis is to organic chemistry."

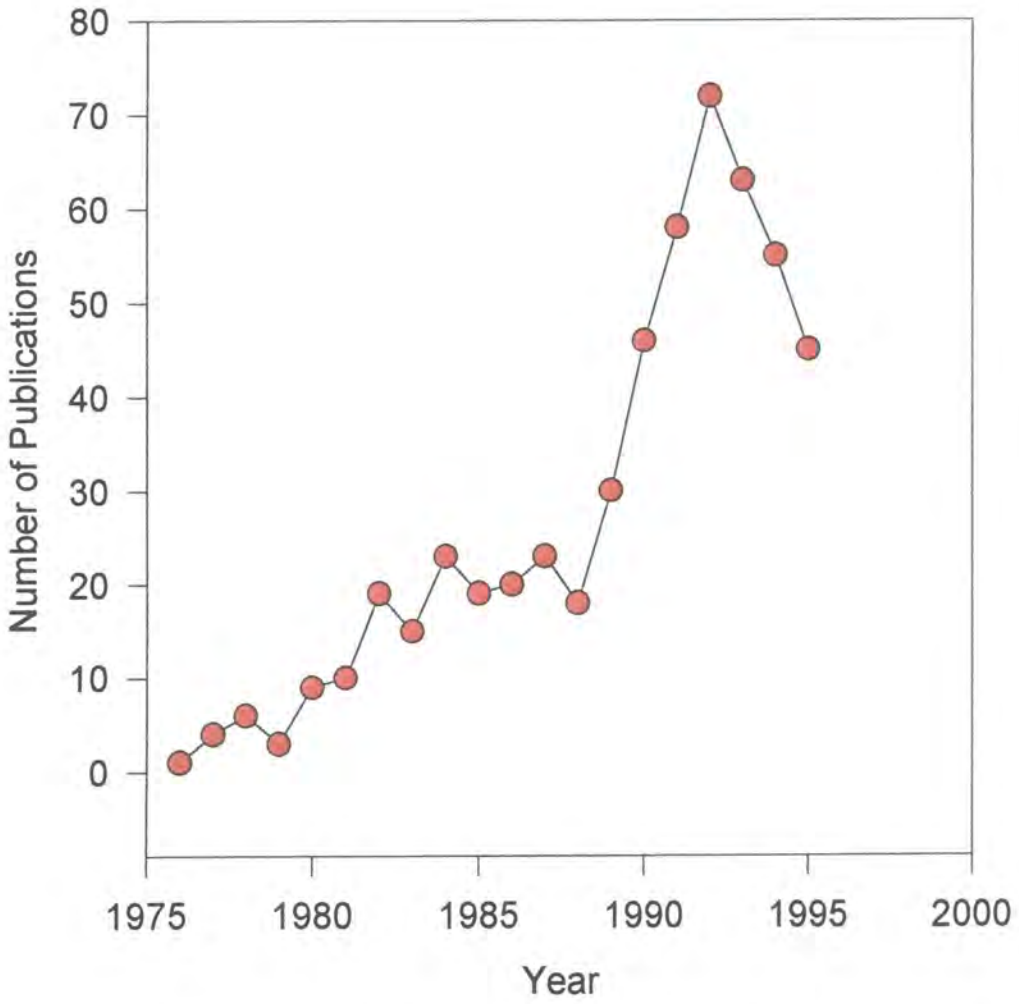

Figure 6.1.1 *- Histogram showing the number of studies published in the last 20 years which used the CSDS as a primary data source.*

6.2 COMPONENTS OF THE CSDS

6.2.1 Structural Data

Structural data are recorded in the CSDS in three different ways. The three are most conveniently described in terms of their 'dimensionality' and are represented schematically in ***Figure 6.2.1***.

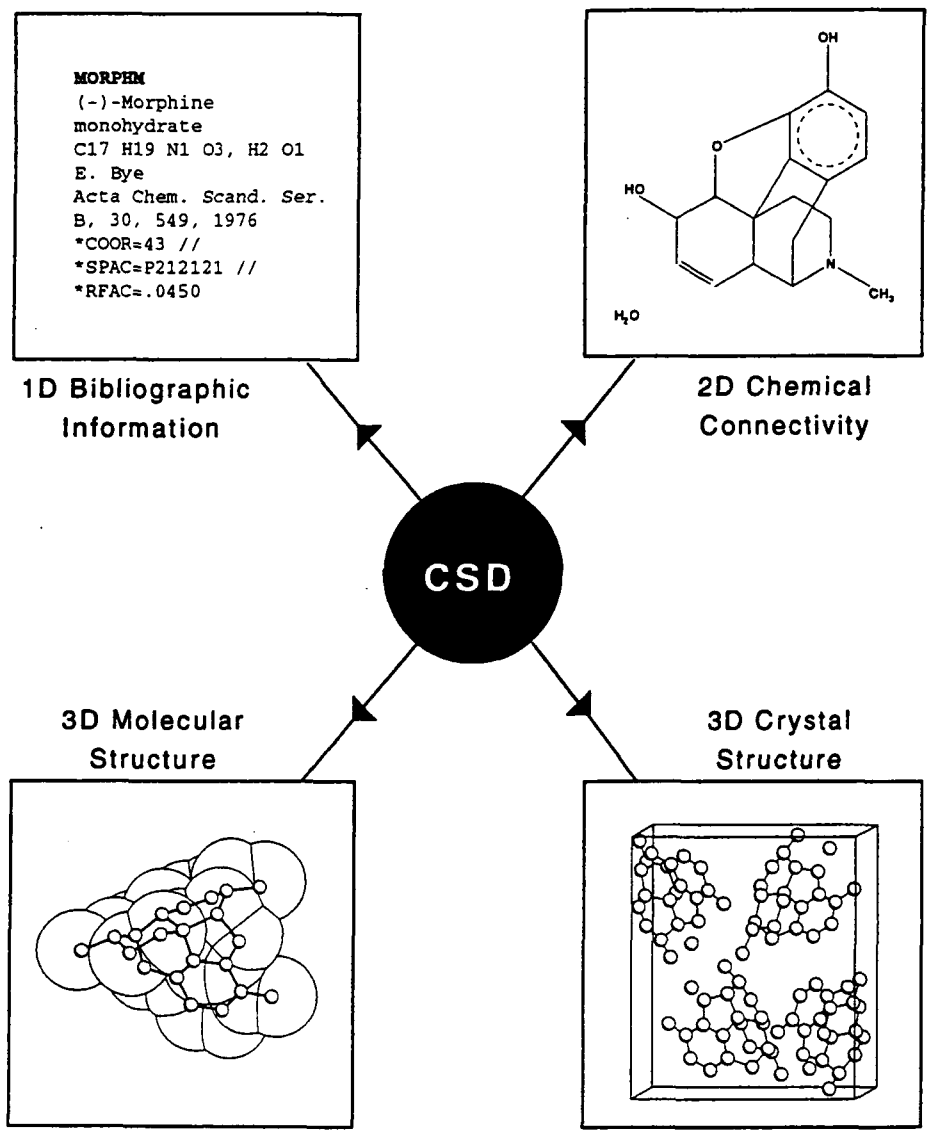

Figure 6.2.1 *- Summary of the different types of structural information stored in the CSDS.*

The 'one dimensional' data is text and simple numerical information pertaining to each entry. Information such as compound name, molecular formula, biblographical details, cell parameters and data collection temperature fall into this catagory. The 'two dimensional' data are the chemical structure of each entry. This information is encoded in the form of two connectivity tables. The first of these tables stores atom properties and the second stores bond properties. Examples of these tables are shown in ***Figure 6.2.2*** for a simple organic fragment.

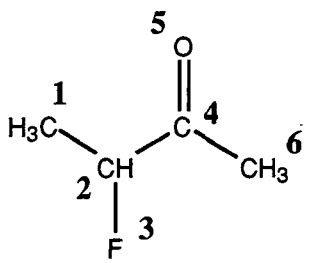

Atom Properties						
Atom Number	1	2	3	4	5	6
Element Number	C	C	F	C	O	C
No. Connected Non-hydrogen Atoms	1	3	1	3	1	1
No. Terminal Hydrogen Atoms	3	1	0	4	0	3
Net Charge	0	0	0	0	0	0

Bond Properties					
Atom 1 of Bond	2	2	2	4	4
Atom 2 of Bond	1	3	4	5	6
Bond Type	1	1	1	2	1

Figure 6.2.2 - *'Two dimensional' chemical connectivity data for a simple organic fragment.*

The final catagory is the 'three dimensional' data which consists of the fractional coordinates, space group and symmetry operators for each entry. This information is used to establish a crystallographic connectivity using standard covalent radii. The chemical and crystallographic connectivities are then mapped onto one another so that atom and bond properties can be matched to the three dimensional structure.

All of this 'one, two and three dimensional' data is extracted from the primary literature. Over 500 journals are represented in the CSDS. Every entry is subjected to a series of computerised checks to ensure that the information contained in the Database is consistent and accurate.

6.2.2 Software

The CSDS is supplied with a suite of fully interactive graphical software which allows users to search the structural information, retrieve data, perform complex statistical analyses and display entries graphically. A summary of the software packages available is given in ***Figure 6.2.3***.

QUEST3D (CSDS User Manual, 1994a) is the major data search and retrieval program. It is used to define and execute text, numeric and two and three dimensional chemical fragment searches. Composite searches are performed by linking these definitions, or 'tests', together using the Boolean logical operators AND, OR and NOT. Entries which satisfy the input search criteria are displayed on-screen in either a one, two, three or a two and three dimensional format. The user can rotate, translate and magnify the three dimensional structural diagrams before deciding to save or reject the entries. Information about the saved entries is written to several files which can be read by other CSDS programs. Some of these files are generated every time a search is performed but others are only produced if the user requests them or if the search includes geometrical parameters. The information content of these different files is described in the CSDS User Manual (1994c).

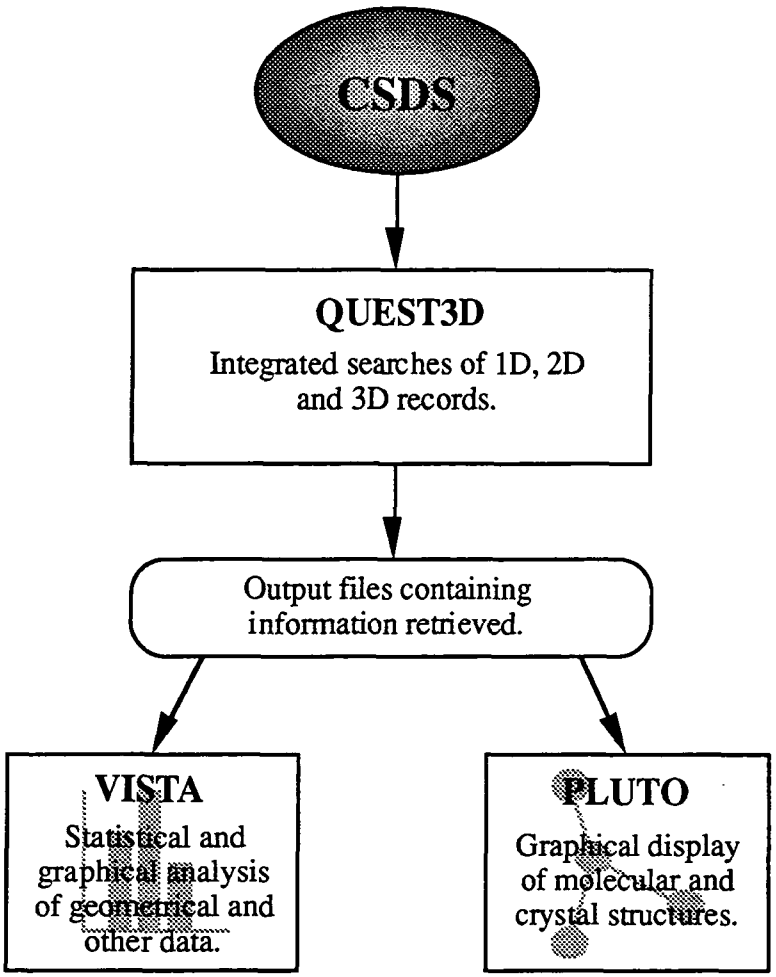

Figure 6.2.3 *- Summary of the CSDS software.*

VISTA (CSDS User Manual, 1995) is a statistical analysis program. It allows users to apply simple mathematical transformations and numerical tests to data derived from structural searches. Histograms, scattergrams and polar plots can also be produced. The data points in these plots can be selected allowing users to identify and examine the structures to which they correspond. More complex multivariate statistical procedures such as principal component analysis (PCA: Chatfield and Collins, 1980) can also be performed using VISTA.

PLUTO (CSDS User Manual, 1994a) is a crystallographic graphics program that can be used to visualise saved entries in several ways. Molecular structures can be rotated, translated and magnified to obtain the desired view. Ball and stick, space filling, stereo

and packing plots can then be generated and saved as PostScript files. PLUTO can also be used to explore non-bonded interaction networks.

6.3 RESEARCH APPLICATIONS OF THE CSDS

The CSDS is used widely by both academics and industrialists and it is currently supplied to several hundred academic institutions and industrial concerns all over the world. Many chemists and crystallographers use it routinely to perform simple searches for bibliographic information or to compare the cell parameters of an unknown material with those of compounds which have already been crystallographically characterized. However, the CSDS has many other applications.

6.3.1 Crystallographic Studies

A small number of researchers have used the CSDS to study crystallographic systematics. Kennard and Taylor (1986) used data abstracted from the CSDS in an attempt to determine the reliability of the estimates of precision (esds) used by crystallographers. Others have used the CSDS to compile space group frequency tables (Mighell, Himes and Rodgers, 1983) and attempted to rationalise the results (Wilson, 1988, 1990, 1991 and 1993; Brock and Dunitz, 1994).

6.3.2 Mean Molecular Dimensions

Numerous studies have employed the CSDS to determine the mean lengths of a large number of different types of chemical bonds. Recently, tables of these mean bond lengths have been produced for both organic (Allen *et. al.*, 1987) and organometallic (Orpen *et. al.*, 1989) compounds. A study of interbond angles and conformation in peptides has also been performed (Ashida *et al.*, 1987).

6.3.3 Conformational Analysis

The CSDS has been used extensively to analyse molecular conformation. The conformations of five, six, seven and eight membered carbocycles have been thoroughly

investigated (Allen, Doyle and Taylor, 1991a,b and c; Allen, Doyle and Auf der Heyde, 1991; Allen, Howard and Pitchford, 1993; Allen, Howard, Pitchford and Vinter, 1994; Allen, Garner, Howard and Pitchford, 1994). Other studies have examined the conformations of certain bioorganic (Murray-Rust and Motherwell, 1978a and b, Murray-Rust and Bland, 1978) and organometallic fragments

6.3.4 Reaction Pathways

By combining information about conformation and non-bonded interactions it is possible to analyse reaction pathways using the CSDS. The method was pioneered by Bürgi and Dunitz who used the CSDS to analyse changes in the geometries of the C=O groups in six natural products as the intramolecular non-bonded N...C=O distances decreased (Bürgi, Dunitz and Shefter, 1973a and b). The technique has since been used to study reaction pathways in many other systems including metal complexes.

6.3.5 Non-bonded Interactions

A large number of non-bonded interactions have been studied using the CSDS. These investigations typically involve analyses of non-bonded contact frequencies, distances and angles in relevant fragments. Notable studies include an investigation of C-H...O hydrogen bonding using neutron derived structural data (Taylor and Kennard, 1982) and a comprehensive survey of interactions between halogens and nucleophiles (Lommerse *et. al.*, 1996). Database studies of C-H...O, X...O_2N and C-F...H interactions are described in Chapters 7, 8 and 9 of this thesis.

6.4 GENERAL NON-BONDED SEARCH METHODOLOGY

This section describes, in general terms, the procedures used to conduct the studies described in Chapters 7, 8 and 9 of this thesis. The chemical fragments and non-bonded contact definitions used in each case are described in the relevent chapters. All searches were performed using Versions 5.08 - 5.10 of the CSDS (the October 1994, April 1995 and October 1995 releases containing 126,353, 140,236 and 146,272 entries respectively). Searches for bonded substructures and inter- or intramolecular non-bonded contacts were carried out using the QUEST3D program. Subsequent statistical analyses of the data were performed using the VISTA program

6.4.1 Preliminary Searches

Before searches for non-bonded contacts were conducted, preliminary surveys of the CSDS were performed. The aim of these searches was to indentify all entries containing the substructural fragments relevant to the study in question which also satisfied a series of stringent secondary search criteria. The purpose of these secondary search criteria was to ensure that only relevant, complete and precise structural data were included in the final statistical analyses. The secondary constraints were applied in the form of CSDS Bit Screens (CSDS User Manual, 1994b). These Bit Screens were used to ensure that entries were selected for further analyses only if they:

- were organic according to CSDS definitions (Bit Screen 57)
- were error free (Bit Screen 32)
- exhibited no crystallographic disorder (Bit Screen 35)
- had crystallographic R-factors < 0.075 (Bit Screen 89)
- contained complete two and three dimensional data records (Bit Screens 85 and 153)

The entries located during these preliminary searches were used to construct database sub-sets upon which all subsequent non-bonded contact searches were performed. Since these

database subsets were tiny (hundreds of entries) compared with the full Database (more than a hundred thousand entries) this procedure ensured that the computationally expensive non-bonded contact searches were conducted quickly and efficiently.

6.4.2 Non-bonded Contact Searches

All non-bonded contacts were defined using the CONTACT and PARAMETER functions in QUEST3D. Secondary contact distances and angles were also defined using the PARAMETER function. Geometrical constraints were applied to these parameters using the SELECT function. The positions of all the hydrogen atoms involved in non-bonded contacts were 'normalised' or repositioned along their X-ray determined H-Y bond vectors at a distance equal to the appropriate neutron derived mean H-Y bond length (Allen *et. al.*, 1987) using the HNORM function.

HNORM compensates for the large systematic errors in X-ray derived H-Y bond lengths introduced because X-rays are scattered by electrons and not atomic nuclei. In hydrogen The 1s electron on a hydrogen atom participating in a H-Y bond in 'pulled' towards the other bonded atom. This produces an aspherical 1s electron cloud and tends to foreshorten X-ray derived H-Y bond lengths. On average X-ray derived H-Y bond lengths are 0.1 - 0.2Å shorter than the equivilent bond lengths determined by neutron diffraction.

6.5 REFERENCES

Allen, F. H., Davies, J. E., Galloy, J. J., Johnson, O., Kennard, O., Macrae, C. F., Mitchell, E. M., Mitchell, G. F., Smith, J. M. and Watson, D. G. (1991) J. Chem. Inf. Comput. Sci., **31**, 187 - 204.

Allen, F. H., Garner, S. E., Howard, J. A. K. and Pitchford, N. A. (1994) Acta Crystallogr. B**49**, 395 - 404.

Allen, F. H., Howard, J. A. K. and Pitchford, N. A. (1993) Acta Crystallogr. B**49**, 910 - 928.

Allen, F. H., Howard, J. A. K., Pitchford, N. A. and Vinter, J. G. (1994) Acta Crystallogr. B**50**, 382 - 395.

Allen, F., Brammer, L., Kennard, O., Taylor, R. and Watson, D. (1987), J. Chem. Soc., Perkin Trans. 2, S1 - S19.

Allen. F. H., Doyle, M. J. and Auf der Heyde, T. P. E. (1991) Acta Crystallogr. B**47**, 412 - 424.

Allen. F. H., Doyle, M. J. and Taylor, R. (1991a), Acta Crystallogr. B**47**, 29 - 40.

Allen. F. H., Doyle, M. J. and Taylor, R. (1991b), Acta Crystallogr. B**47**, 41 - 49.

Allen. F. H., Doyle, M. J. and Taylor, R. (1991c), Acta Crystallogr. B**47**, 50 - 61.

Ashida, T., Tsunogae, Y., Tanaka, I and Yamane, T. (1987) Acta Crystallogr. B**43**, 212.

Brock, C. P. and Dunitz, J. D. (1994) Chem. Mater., **6**, 1118.

Bürgi, H. B., Dunitz, J. D. and Shefter, E. (1973a) Cryst. Struct. Commun., **3**, 667.

Bürgi, H. B., Dunitz, J. D. and Shefter, E. (1973b) J. Am. Chem. Soc., **95**, 5065 - 5067.

Cambridge Structural Database System Users Manuals (1994a), *Getting Started with the CSD System*, Cambridge Crystallographic Data Centre, 12 Union Road, Cambridge, U.K.

Cambridge Structural Database System Users Manuals (1994b), *Volume III*, Appendix 1, Cambridge Crystallographic Data Centre, 12 Union Road, Cambridge, U.K.

Cambridge Structural Database System Users Manuals (1994c), *Volume III*, Appendix 15, Cambridge Crystallographic Data Centre, 12 Union Road, Cambridge, U.K.

Cambridge Structural Database System Users Manuals (1995), *VISTA 2.0 Users Guide*, Cambridge Crystallographic Data Centre, 12 Union Road, Cambridge, U.K.

Chatfield, C. and Collins, A. J. (1980) *Introduction to Multivariate Analysis*, Chapman and Hall, London.

Desiraju, G. R. (1995) Angew. Chem. (Int. Ed. Engl.), **34**, 2311 - 2327.

Kennard, O. and Taylor, R.(1986) Acta Crystallogr. B**42**, 112.

Lommerse, J. P. M., Stone, A. J., Taylor, R. and Allen, F. H. (1996) J. Am. Chem. Soc, **118**, 3108 - 3116.

Mighell, A. D., Himes, V. L.and Rodgers, J. D. (1983) Acta Crystallogr. A**39**, 737.

Murry-Rust, P and Motherwell, W. D. S. (1978a) Acta Crystallogr. B**34**, 2518 - 2526.

Murry-Rust, P and Motherwell, W. D. S. (1978b) Acta Crystallogr. B**34**, 2534 - 2546.

Murry-Rust, P. and Bland, R. (1978) Acta Crytstallogr. B**34**, 2527 - 2533.

Orpen, A. G., Brammer, L., Allen, F. H., Kennard, O., Watson, D. G. and Taylor, R.(1989) J. Chem. Soc., Dalton Trans., S1.

Pimentel, G. C. and McClellan, A. L. (1960) *The Hydrogen Bond*, Freeman, San Francisco.

Sayre, D. (1952) Acta Crystallogr., **5**, 60.

Sutor, D. J. (1963) J. Chem. Soc, 1105 - 1113.

Taylor, R. and Kennard, O. (1982) J. Am. Chem. Soc., **104**, 5061 - 5070.

Wilson, A. J. C. (1988) Acta Crystallogr. A**44**, 715.

Wilson, A. J. C. (1990) Acta Crystallogr. A**46**, 742.

Wilson, A. J. C. (1991) Z. Krystallogr., **197**, 85.

Wilson, A. J. C. (1993) Acta Crystallogr. A**49**, 795.

CHAPTER 7

Database and Theoretical Studies of Nitro Oxygen...Halogen Interactions

7.1 INTRODUCTION

7.1.1 Nitro Oxygen...Halogen Interactions as Supramolecular Synthons

Interest in X...O_2N interactions as building blocks in crystal engineering arose from the observation that 4-chloro- (**I**) and 4-bromo-β-nitrostyrene (**II**) adopt very different crystal packings (Desiraju and Pedireddi 1989; Pedireddi, Sarma and Desiraju, 1992). The structure of **I** is characterized by C-H...O_2N and C-H...Cl interactions (***Figure 7.1.1***) whilst in **II**, the bromine atom is directed towards and almost equidistant from the both of oxygen atoms of the NO_2 group. The linear ribbons mediated by these Br...O_2N interactions are held together by lateral C-H...O bonds, as in **I**, to form sheets (***Figure 7.1.2***). In a later study (Desiraju *et. al.*, 1993) a model for the structure of the 4-iodo analogue of **I** and **II** (**III**) was proposed which was based on the symmetrical X...O_2N interactions observed in **II**. However, **III** proved difficult to crystallise making it impossible to confirm the accuracy of the model experimentally.

In the same study (Desiraju *et. al.*, 1993) the results of a simple database survey of X...O_2N interactions were described. Organic compunds containing at least one NO_2 group and either Cl, Br or I were retrieved. The distances D_1 and D_2 from the halogen to each of the nitro oxygen atoms were determined for all of the fragments located in which the halogen lies within 30° of the nitro group plane. By plotting D_1 against D_2 for each of the halogen sub-sets the authors were able to identify three unique X...O_2N bonding modes: the symmetrical motif, (**P**, $D_1 \approx D_2$), observed in 4-bromo-β-nitrostyrene, an asymmetric bifurcated motif, (**Q**, $D_1 < D_2$) and a motif (**R**, $D_1 << D_2$) in which the halogen interacts with only one of the nitro oxygen atoms (***Figure 7.1.3***).

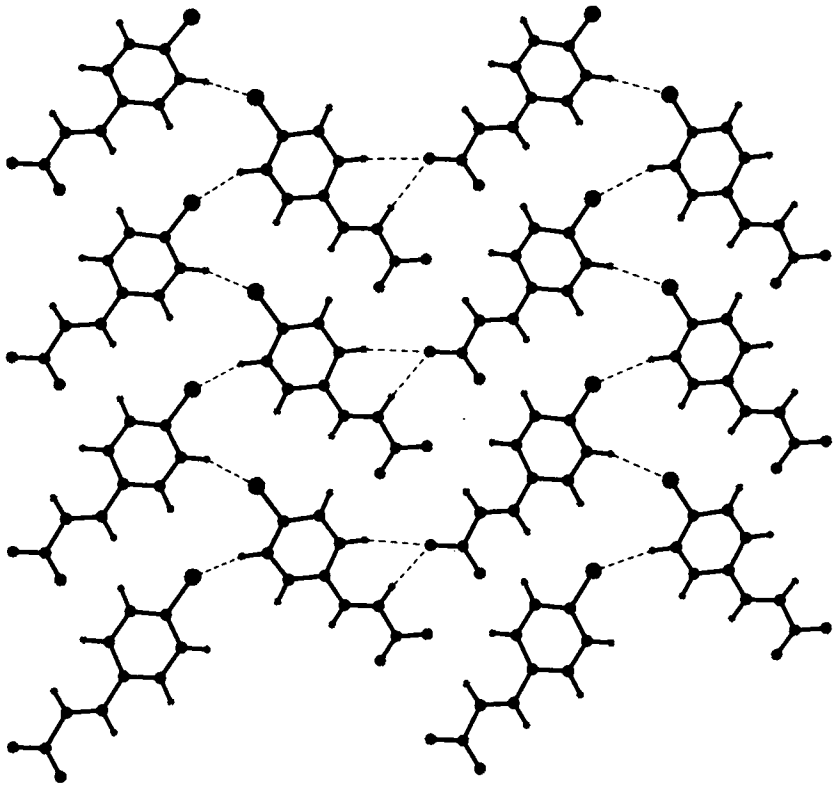

Figure 7.1.1 *- Packing of 4-chloro-β-nitrostyrene.*

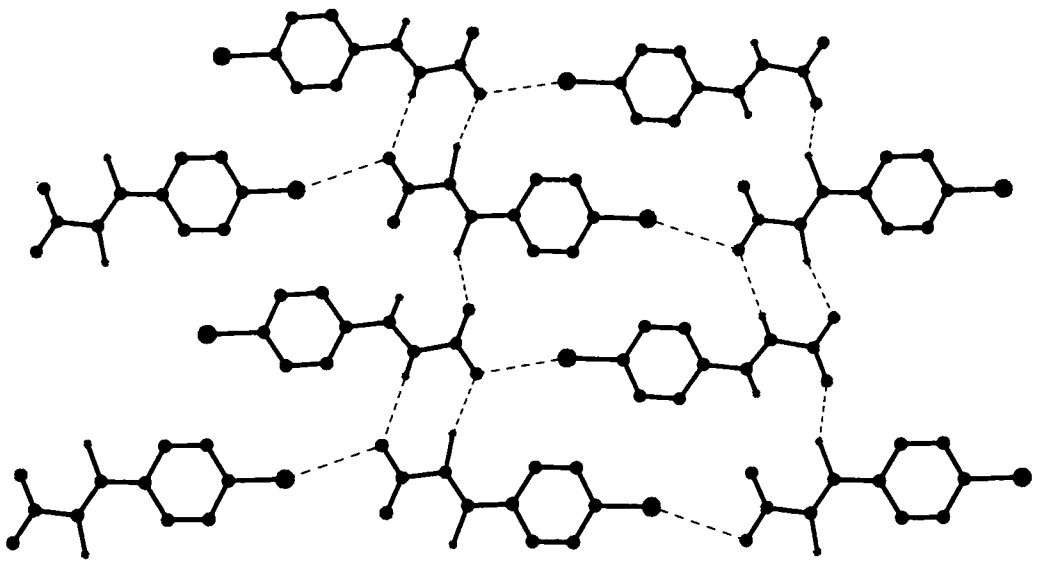

Figure 7.1.2 *- Packing of 4-bromo-β-nitrostyrene.*

More recently the crystal structures of the 1:1 complex of 1,4-diiodobenzene and 1,4-dinitrobenzene (**IV**) , 4-iodo-nitrobenzene (**V**) and the 2:1 complex of 4-iodocinnamic acid and 1,4-dinitrobenzene (**VI**) have been determined (**IV**: Allen *et. al.*, 1994; **V** and **VI**: Thalladi *et. al.*, 1996)*. All three compounds contain perfectly symmetric or near symmetric **P** type I...O_2N interactions. The presence of I...O_2N mediated ribbons in all three structures and particularly in **VI**, indicates that these interactions are able to dictate crystal packing, even in the presence of stronger O-H...O bonds.

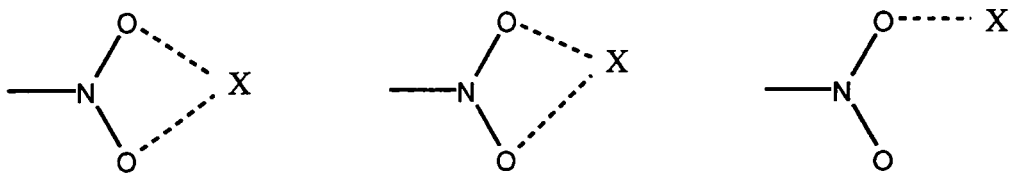

P **Q** **R**

Figure 7.1.3 *- The three X...O_2N bonding motifs **P**, **Q** and **R**.*

These results show that X...O_2N interactions can be effective supramolecular synthons (Desiraju, 1995). However, because of the limited scope of the earlier database study (Desiraju *et. al.*, 1993) relatively little is known about the preferred geometries of these interactions and in particular, how the preferred geometries change when different halogens are involved. Since such information is of interest if X...O_2N interactions are to be used effectively as supramolecular synthons, a comprehensive database survey of the interactions between the carbon bound halogen atoms Cl, Br, I and the oxygen atoms of nitro groups was undertaken, in order to determine their relative frequencies and preferred geometries.

* These crystal structure determinations are also described in Chapter 5 of this thesis.

7.1.2 The Energies of Nitro Oxygen...Halogen Interactions

Another topic of interest when considering X...O_2N interactions as supramolecular synthons is the strength of the X...O_2N bond. If this strength is known it can be compared with the strengths of other possible interactions in order to determine whether the X...O_2N bond, or another interaction, is likely to dominate crystal packing. However, whilst qualitative energy relationships can sometimes be inferred, it is impossible to obtain reliable interaction energies from crystal data. Quantitative estimates of X...O_2N interaction energies must be derived by theoretical methods.

The difficulties with performing theoretical calculations on systems involving weak intermolecular interactions were described in Chapter 3 (Section 3.3.3). However, the development of correlated theoretical methods and BSSE corrections now make it possible to perform such calulations reliably for simple model systems. Intermolecular Pertubation Theory (IMPT: Hayes and Stone, 1984) is one of these correlated methods. It is particularly well suited for calculations involving intermolecular interactions because the total interaction energies obtained are summations of several separate energy terms. Thus, making it possible to determine the nature of the interaction, as well as its total energy.

First order IMPT energies are composed of an electrostatic term, E_{es}, and an exchange-repulsion term, E_{er}. The electrostatic term describes the Coulombic interaction between the charge distributions of the two molecules. The exchange-repulsion term is the sum of the attractive exchange of electrons with parallel spins and the repulsive force which prevents electrons with parallel spins occupying the same region in space. E_{es} can be attractive or repulsive but E_{er} is always repulsive for self consistant field (SCF) dimers.

The second order IMPT energies incorporate several additional energy terms. The polarisation or induction energy term, E_{pol}, describes the changes induced in the wavefunction of one molecule by the presence of the second. It is an intramolecular term. Whereas, the charge transfer energy, E_{ct}, is due to the transfer of electrons from one

molecule to the other and thus describes changes in the wavefunctions of both molecules. Finally, a dispersion energy term, E_{disp}, is calculated. The polarization and charge transfer terms calculated uisng IMPT are free from BSSE. However, the partition of these two energy terms is not entirely basis set independent (Stone, 1993).

By combining the database survey already outlined with this type of high level *ab initio* calculation on appropriate model systems, a more complete picture of the X...O_2N interaction and its suitability for crystal engineering applications would be obtained. Such combined studies have already been conducted successfully for strong hydrogen bonds (see for example Jeffery and Saenger, 1991 and references cited therein) and weaker intermolecular interactions (see for example Lommerse *et. al.*, 1996). Therefore, a series of theoretical calculations were performed on a model Cl...O_2N system, with various interaction geometries, using IMPT. The aims were to calculate approximate energies for the various Cl...O_2N interactions and to determine the ideal Cl...O_2N bond geometry which could be compared with the geometries observed experimentally.

7.2 METHODOLOGY

7.2.1 Nitro Oxygen...Halogen Interaction: Database Searches

Version 5.10 of the CSDS (October 1995 containing 146,272 entries) was used for this study and the general search procedure outlined in Chapter 6 was followed unless otherwise stated.

Preliminary searches were carried out to locate all the CSDS entries that contain both the C-NO_2 fragment and either a C-Cl, C-Br or C-I fragment. In these initial searches no restriction was placed on the hybridization state of the carbon to which the nitro group is attached. However, the results (denoted as P in ***Table 7.3.1***) were subsequently sub-divided into two groups according to the nature of the nitro carbon atom. The first group contained only C(sp^3)-NO_2 fragments and the second only C(aromatic)-NO_2 fragments.

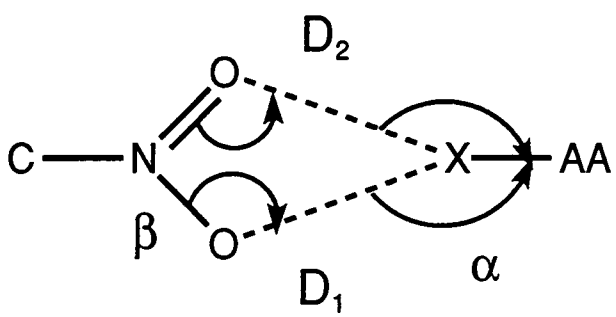

X = Cl, Br or I

Figure 7.2.1 *- The search fragment used to locate X...O_2N interactions.*

Searches for intermolecular interactions between halogens and nitro oxygen atoms were conducted on the database sub-sets derived from the preliminary searches. For each interaction located the X...O distances (D_1 and D_2) and the angles C-X...O(1) and X...O(1)-N (α and β) were determined (***Figure 7.2.1***). The values of the spherical polar angles χ and ϕ, which describe the elevation (χ) and rotation (ϕ) of the interaction vector, [X...O], with respect to the plane of the nitro group, were also calcluated for each

interaction (***Figure 7.2.2***). Additionally, in the case of the C(aromatic)-NO_2 sub-sets, the torsion angle (τ) that describes the conformation of the NO_2 group with respect to the aromatic ring were recorded. Finally, two indirect parameters were derived for each interaction: Asymm = D_2 - D_1 and R = D_1/Σ_{vdw}.

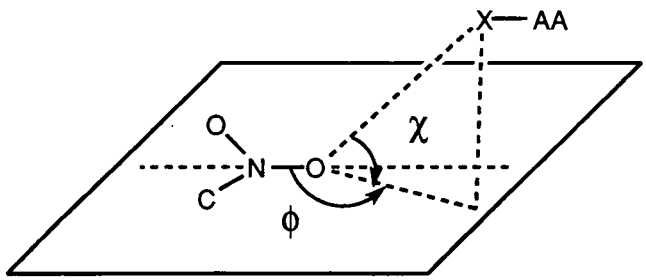

Figure 7.2.2 *- Definitions of the spherical polar angles χ and ϕ.*

Two sets of geometical criteria were used to define the X...O_2N interactions. The first set of criteria, denoted as **A**, required that D_1 be less than or equal to the sums of the van der Waal's radii of O and X plus a tolerance of 0.2Å. The second set, **B**, restricted the search to interactions where D_1 is less than or equal to the sums of the van der Waal's radii of O and X without any tolerance. Clearly, both D_1 and D_2 will satisfy these distance criteria in symmetrical **P** type interactions and so two hits will be recorded. In order to ensure that subsequent analyses were performed on sets of unique X...O_2N interactions these duplicate hits were removed from the datasets manually. In all cases D_1 was chosen such that it was the shorter of the two X...O distances.

7.2.2 Nitro Oxygen...Halogen Interaction: Theoretical Calculations*

IMPT calculations (Hayes and Stone, 1984) were used to determine the energies of Cl...O_2N interactions in a simple model system. The calculations were performed with the package CADPAC 4.2 (Amos, 1994) on a Silicon Graphics Indigo 2 workstation.

---

* Performed in collaboration with J.P.M Lommerse, CCDC, 12, Union Rd., Cambridge, CB2 1EZ.

7.2.2.1 Choice of Model System

When choosing a model for the IMPT calculations on the X...O_2N interactions several factors had to be considered. It was important to avoid large (many electron) systems in order to keep the computational time down. However, it was also necessary to select a system which accurately represented the kinds of environments in which X...O_2N interactions are known to occur.

The simplest model system that could be chosen to is the nitromethane-halomethane dimer. However, a previous IMPT study of Cl...O=C interactions (Lommers *et. al.*, 1996) revealed that chloromethane gave unsatisfactory results when it was used as the model Cl 'donor'. This is because the majority of the Cl atoms involved in Cl...O=C interactions are bound to aromatic or sp^2 hybridized carbon atoms which are poorly modelled by CH_3Cl. Analysis of the 96 criteria **B** Cl...O_2N contacts that were located in the CSDS (***Table 7.3.1***) showed that 70 (73%) involve C(aromatic)-Cl or C(sp^2)-Cl but only 26 (27%) involve C(sp^3)-Cl. Clearly, chloromethane is also an unrepresentative Cl 'donor' in this case. A better choice would be halobenzene but switching from halomethane to halobenzene involves introducing five additional carbon atoms and two additional hydrogen atoms into the calculation which would increase the computational time considerably. The compromise that was reached in the Cl...O=C study (Lommerse *et. al.*, 1996) was to use chloroacetylene as the model Cl 'donor'. However, preliminary IMPT calculations on the nitromethane-haloacetylene dimer indicated that hydrogen bonding interactions between the highly acidic alkynic proton and the nitro oxygen atoms dictated dimer formation. To eliminate this problem 1-halo-2-methylacetylene was substitued for haloacetylene in the model system that was eventually used.

The decision to use nitromethane as the model NO_2 'acceptor' was initially made for reasons of simplicity. However, subsequent analysis of the results of the database searches provided experimental evidence to support the choice. These results show that

$C(sp^3)$-NO_2 'acceptors' are no less effective than $C(sp^2)$-NO_2 or C(aromatic)-NO_2 groups in this context (see Section 7.3.1.).

7.2.2.2 IMPT Calculations

The model monomers, 1-chloro-2-methylacetylene and nitromethane were constructed and geometry optimized using 6-31G* basis sets from the standard CADPAC library* . Interacting dimers were then constructed (***Figure 7.2.3***) and energies were calculated for the Cl...O_2N contacts described below -

- With D_1 fixed at the sum of the van der Waal's radii (3.27Å) and χ fixed at 0°, ϕ was varied from 90° to -90° in 15° increments. The interaction energy was determined at each ϕ angle (IMPTX)
- With ϕ fixed at -135° and χ fixed at 0°, D_1 was varied from 2.80Å to 3.40Å in 0.1Å increments. The interaction energy was determined at each distance D_1 (IMPTY).
- With D_1 fixed at the sum of the van der Waal's radii and ϕ fixed at -135°, χ was varied from 0° to 90° in 15° increments. The interaction energy was determined at each χ angle (IMPTZ).

In all cases the C-X...O(1) angle, α, was fixed at 180° (see Section 7.3.3).

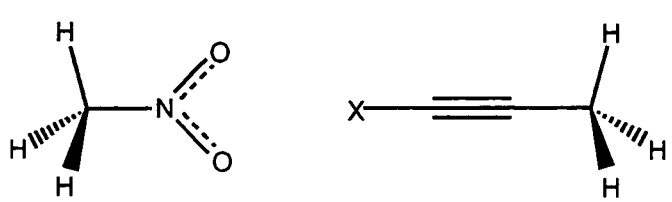

X = Cl or Br

Figure 7.2.3 *- Model system selected for IMPT calculations.*

* Calculations could not be performed for 1-bromo- and 1-iodo-2-methylacetylene model systems because basis sets for Br and I are not available in the standard CADPAC library.

7.3 CRYSTAL STRUCTURE DATA ANALYSIS

7.3.1 Summary Statistics

Table 7.3.1.contains a summary of the results from both the preliminary searches and the searches for X...O_2N contacts satisfying criteria **A** and **B** divided up according to halogen type. A total of 311 database entries containing 531 unique C-X groups were located in the preliminary searches. Of these 256 (48%) participate in X...O_2N contacts which fulfill criteria **A** and 134 (25%) are involved in X...O_2N contacts satisfying criteria **B**. Inspection of ***Table 7.3.1*** also reveals that the proportion of short X...O_2N contacts formed at both the **A** and **B** levels increases in the order Cl < Br <I (**A**: 44% < 52% < 64%, **B**: 23% < 32% < 50%). The mean van der Waal's normalised contact distance, R, decreases correspondingly. This ordering was also observed in a previous database study of short X...O, N and S contacts (Lommerse *et. al.*, 1996) and mirrors the increasing polarisabilities of the halogen atoms.

Table 7.3.1 also contains the search results for the C(aromatic)-NO_2 and C(sp^3)-NO_2 sub-sets. These results show that although the C(aromatic)-NO_2 sub-sets are larger the C(sp^3)-NO_2 groups that do participate in X...O_2N interactions are equally and sometimes more effective in forming short contacts. (The percentages of criteria **A** contacts formed between Cl, Br, I and C(aromatic)-NO_2 or C(sp^3)-NO_2 are 41% cf.63%, 42% cf. 56% and 60% cf. 20% respectively.) This observation justifies the use of nitromethane as the model NO_2 acceptor in the theoretical calculations described later.

The possibility that the conformation of the NO_2 group with respect to the aromatic ring is a factor in determining the X...O_2N contacting forming abilities of C(aromatic)-NO_2 groups was investigated by comparing the primary X...O distance, D_1, with the torsion angle, τ. ***Figure 7.3.1*** shows a scatterplot of D_1 against τ for the 163 C-Cl...O_2N-C(aromatic) interactions located using criteria **A**. In this plot τ is transformed such that it is always in the 0 - 90° quadrant appropriate to the local symmetry. Of

these163 interactions, 101 have $0° < \tau < 20°$. These NO_2 groups are approximately co-planar with the aromatic ring. There are 40 interactions for which $70 < \tau < 90$ and the NO_2 groups are perpendicular to the aromatic ring. Finally, there are 22 interactions which have $20 < \tau < 70$ representing NO_2 groups which have geometries which are intermediate between planar and perpendicular. The percentages of these NO_2 groups which from short (criteria B) Cl...O contacts are 41% (planar), 41% (perpendicular) and 33% (intermediate) indicating that the X...O_2N bond forming abilities of C(aromatic)-NO_2 groups are independent of their conformations with respect to the aromatic ring.

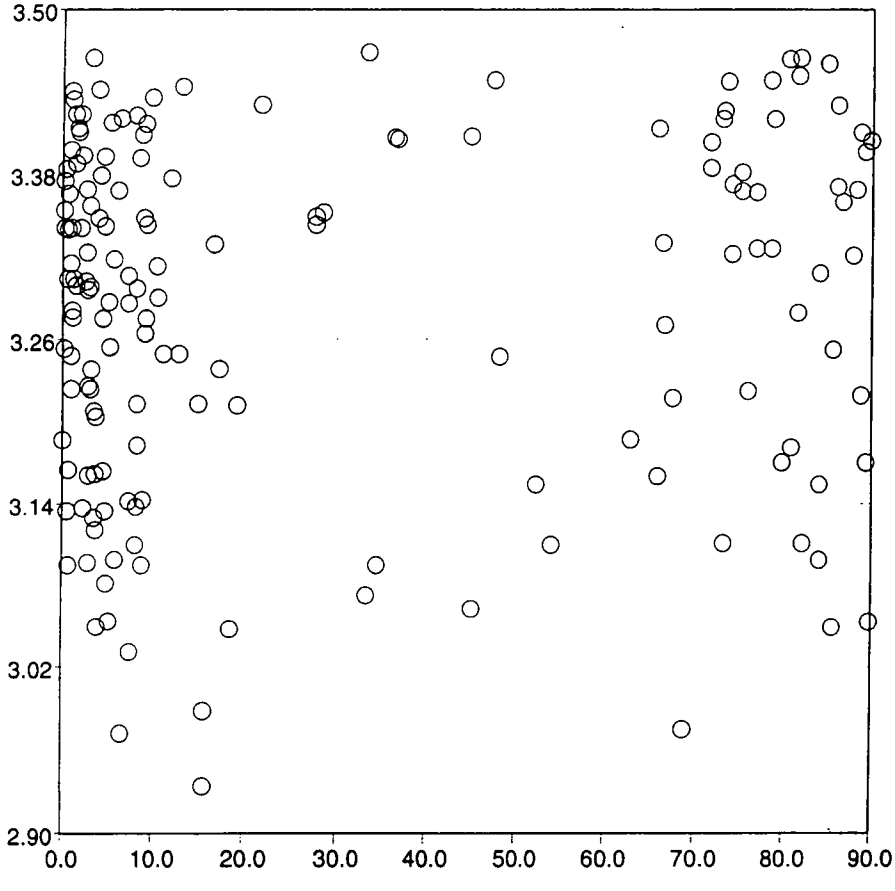

Figure 7.3.1 *- Scatterplot of D_1 versus τ for Cl...O_2N-C(aromatic) contacts.*

Table 7.3.1 - Summary statistics for the preliminary searches (P) and the searches for X...O_2N contacts satisfying criteria A (A) and B (B).

		Cl			Br			I		
Criteria	C_1	N(HITS)	N(Cl)	$N(NO_2)$	N(HITS)	N(Br)	$N(NO_2)$	N(HITS)	N(I)	$N(NO_2)$
P	C*	216	410	357	85	107	133	10	14	15
P	$C(sp^3)$	37	59	75	31	46	51	4	5	4
P	C(aro)	157	317	251	45	50	69	5	5	7
Criteria	C_1	N(HITS)	N(FRAG)	N(Cl) [%]	N(HITS)	N(FRAG)	N(Br) [%]	N(HITS)	N(FRAG)	N(I) [%]
A	C*	119	228	180[44]	46	67	56[52]	6	14	9[64]
A	$C(sp^3)$	26	49	37[63]	18	35	26[56]	1	1	1[20]
A	C(aro)	83	163	130[41]	21	24	21[42]	3	3	3[60]
B	C*	75	96	93[23]	30	34	34[32]	8	8	7[50]
B	$C(sp^3)$	17	23	22[37]	11	14	14[30]	0	0	0[-]
B	C(aro)	51	65	63[20]	12	12	12[24]	2	2	2[40]

7.3.2 The Direction of Approach of X to N-O(1): The Bonding Modes P, Q and R

The indirect parameter Asymm, defined in Section 7.2.1, provides a simple way of distinguishing the three X...O_2N bonding modes **P**, **Q** and **R** (Desiraju *et. al.*, 1993) described in Section 7.1.1. ***Figure 7.3.2*** is a histogram of Asymm for criteria **A** contacts to Cl. The graph shows that the majority of Cl...O_2N bonds in this sub-set are **R** type with $D_2 >> D_1$ giving rise to a sharp maximum at high Asymm. There are also a significant number of slightly asymmetric **P** or **Q** type contacts for whch $D_2 > D_1$ represented by the broad local maximum centred around Asymm = 0.6Å. However, there are relatively few perfectly symmetic **P** type interactions (Asymm = 0.0Å) or highly asymmetric **Q** type interactions (Asymm = 0.9Å to 1.8Å).

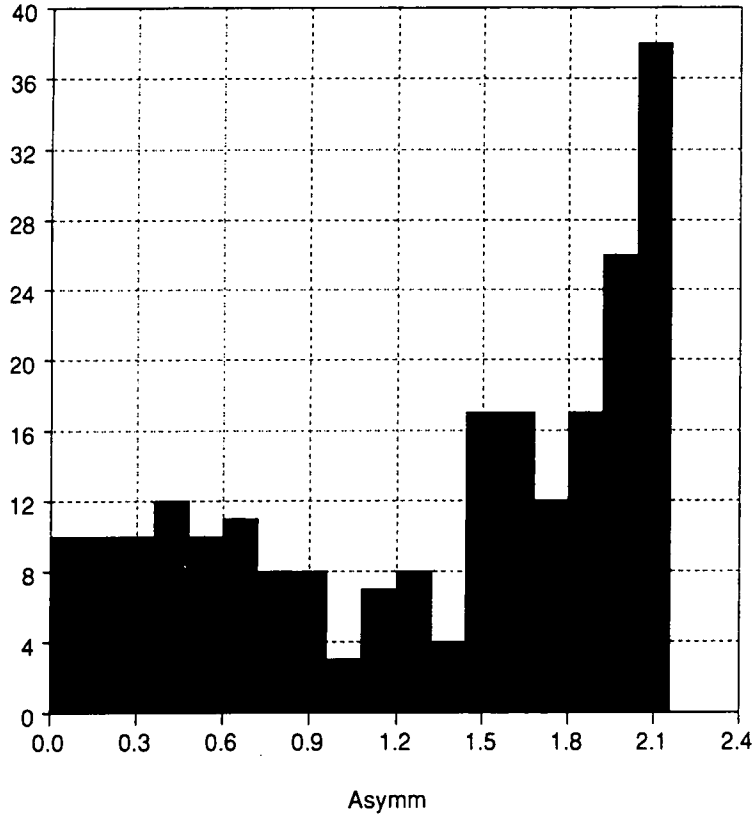

Figure 7.3.2 - *Histogram of Asymm for criteria **A** contacts to Cl.*

A more sophisticated description of the orientation of the halogen with respect to the nitro group can be obtained by analysis of the spherical polar angles, χ and ϕ (***Figure 7.2.2***). These describe the angle of elevation (χ) of [X...O] from the nitro group plane and the angle of rotation (ϕ) of the projection of [X...O] onto nitro group plane about the N-O(1) bond. Since nitro groups are planar the sign of χ is not significant in this study and only absolute values are quoted. However, the sign of ϕ is important since the two 'sides' of the asymmetrically substituted N-O(1) bond are not equivalent. Taking the N-O(1) bond as the 180° reference, positive ϕ rotation is in the direction of O(2) and negative ϕ rotation is in the direction of C. Using this sign convention, the notional sp^2 hybridized lone pairs on O(1) are at $\phi = +120°$ on the 'oxygen side' and $\phi = -120°$ on the 'carbon side' (***Figure 7.3.3***).

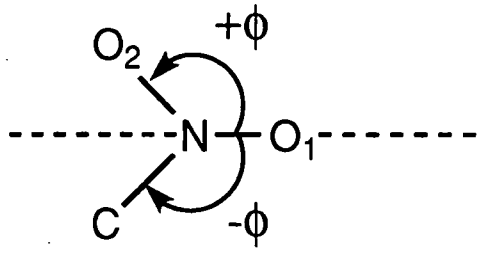

Figure 7.3.3 *- Sign convention used to distinguish the two 'sides' of the C-NO_2 fragment.*

Circular scatterplots of D_2 versus ϕ for criteria **B** X...O_2N contacts to a) Cl, b) Br and c) I are shown in ***Figure 7.3.4***. These plots are visual representations of the directionality of the in-plane approach of X to O(1). They show that shorter values of D_2 ($\approx D_1$) occur for positive ϕ of +110 to +130° (motif **P**) and that D_2 increases to a maximum at ϕ angles of -130 to -150° (motif **R**).

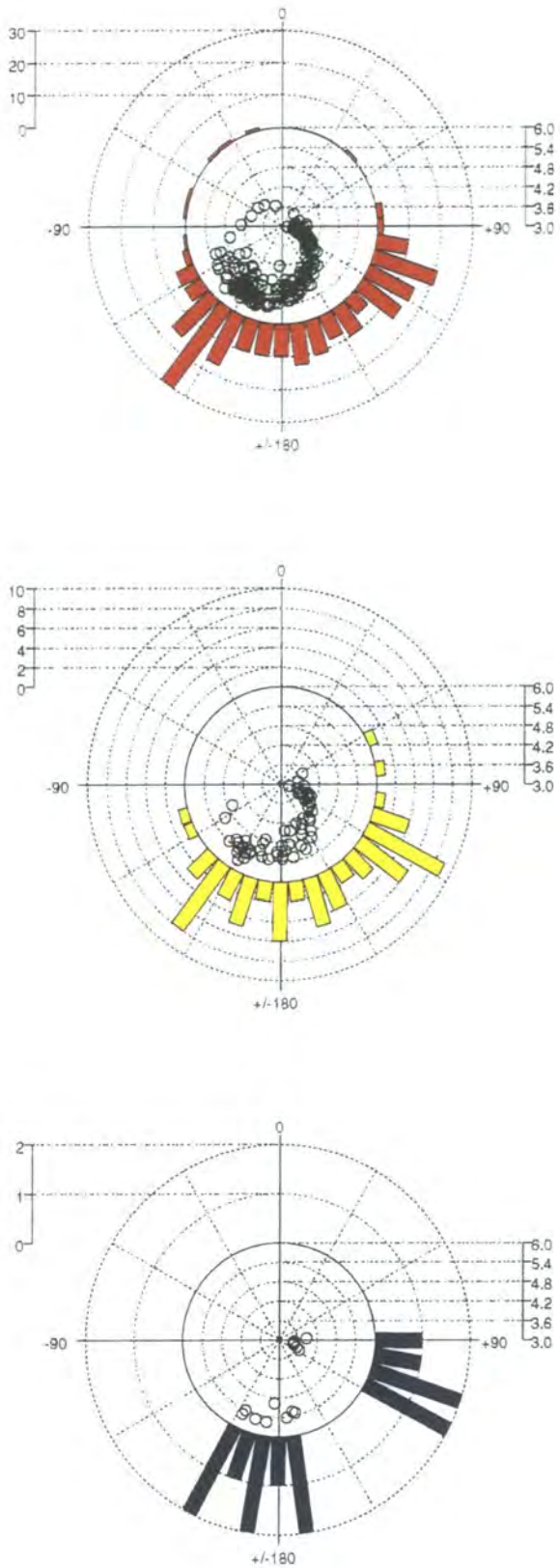

Figure 7.3.4 *- Circular scatterplots of D_2 versus ϕ for a) Cl...O_2N, b) Br...O_2N and c) I...O_2N contacts located using criteria* ***A****.*

Figure 7.3.4a shows a clear preference for Cl to coordinate to only one nitro oxygen atom (motif **R**). There is a smaller peak at $\phi = +120°$ corresponding to symmetrical **P** type interactions. However, there is no peak at ϕ angles of around +150 to +160° which would indicate that asymmetric bifurcated **Q** type interactions were present in the dataset. These results are very similar to those obtained by analysis of ***Figure 7.3.2*** above.

The situation is somewhat different for Br (***Figure 7.3.4b***) where the symmetric motif **P** is preferred. The peak at negative ϕ corresponding to **R** type interactions is much less clearly defined and there are some **Q** type interactions present. The situation is similar for I (***Figure 7.3.4c***) which also forms mostly **P** type contacts.

Since it is difficult to determine at what point **P** type interactions become **Q** type interactions it is simpler to coalesce motifs **P** and **Q** and denote them collectively as bifurcated contacts characterized by ϕ angles in the range +90 to +150°. Similarly, ϕ angles of between -120° and -180° will be regarded as characteristic of mono-coordinate **R** type contacts. Within these definitions, the percentage of mono-coordinate contacts formed by each halogen falls from 46% for Cl through 35% for Br to 25% for I. The percentage of bifurcated contacts formed by each halogen rises correspondingly from 35% for Cl through 44% for Br to 63% for I, mirroring the increasing polarisabilities of the halogen atoms. The remaining contacts are either intermediate spices or obvious outliers. These results suggest that the softer the halogen the more likely it is to interact with both nitro oxygen atoms.

Histograms of the angle of elevation χ for criteria **B** contacts involving Cl, Br and I are shown in ***Figure 7.3.5***. The graphs show that although a significant number of χ values exceed 30°, especially for Cl, there is an increasing tendency for the halogen to approach O(1) at, or close to, the nitro plane as X changes from Cl to Br to I. This tendency is demonstrated quantitatively by the decreasing mean χ values (Cl: 27(2)°, Br: 23(3)° and I: 14(7)°) and increasing percentages of contacts with χ angles of less than 30° (Cl: 58%, Br: 71% and I: 88%).

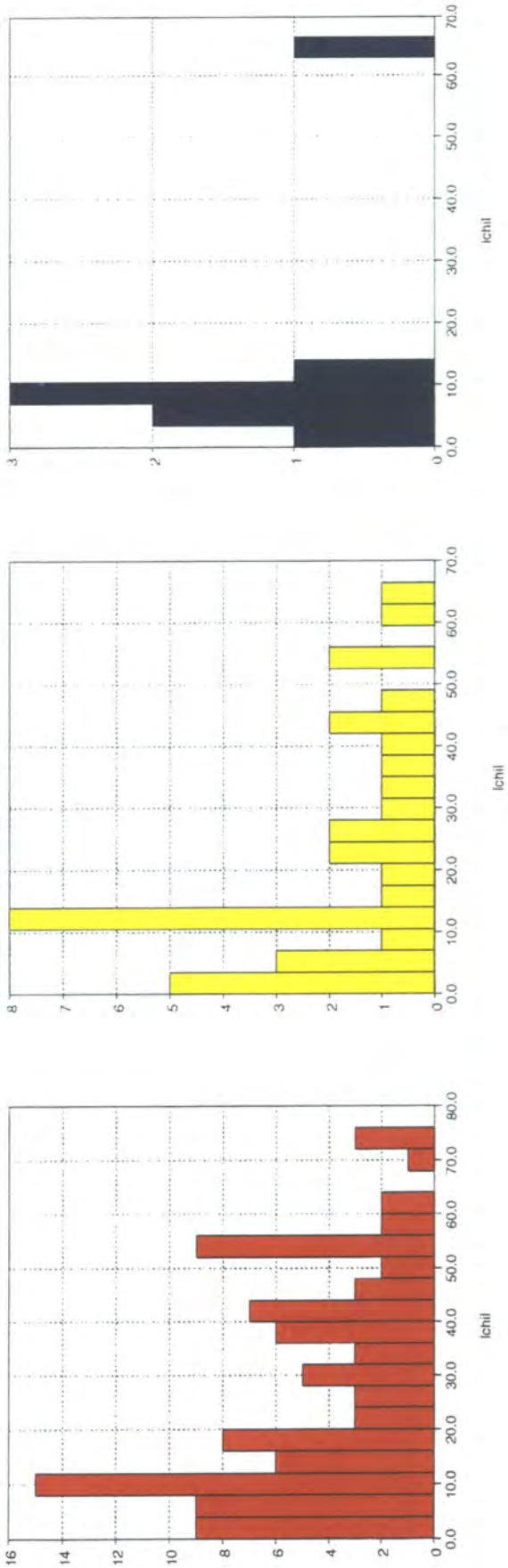

Figure 7.3.5 *- Histograms of χ for criteria* ***B*** *contacts involving a) Cl, b) Br and c) I.*

The results presented in ***Figures 7.3.3*** and ***7.3.4*** might have been expected to suggest an element of lone pair directionality in X...O_2N contacts. However, the ϕ peaks in ***Figures 7.3.4*** occur consistently at +100 to +115° on the 'oxygen side' of O(1) and at around -150° on the 'carbon side' of O(1), somewhat displaced from the lone pair directions of ±120°.

Simple geometric calculations, based on an N-O bond length of 1.2Å, an O-N-O angle of 120° and an X....O(1) contact distance equal to the sums of the van der Waal's radii of X and O, show that ϕ angles of between +101° and +104° result when X approaches NO_2 directly between the two terminal nitro oxygen atoms to form a symmetrical **P** type interaction. This suggests that the position of the peak at positive ϕ is governed by the geometry of motif **P** and not the positions of the lone pairs on O(1). This geometry does, however, bring the incoming halogen into close proximity of the notional lone pairs on both O(1) and O(2).

Similarly, there is 30° difference between the position of the ϕ peak and the lone pair direction on the 'carbon side' of O(1). This is probably due to steric effects. In the majority of cases C is part of an aromatic or other bulky group which prevents the approach of the halogen along the lone pair direction. Since the O(1) lone pair on the 'carbon side' is sterically inaccessible to the halogen it approaches O(1) in a direction more closely aligned with N-O(1) when forming mono-coordinate contacts to NO_2.

It should also be noted that a previous study (Lommerse *et. al.*, 1996) of Cl...O=C interactions found only limited experimental and computational eveidence for lone pair directionality at O, despite the steric accessibilty of both lone pairs in this case. The issue of possible lone pair directionality at O(1) in X...O_2N interactions is discussed further in Section 7.4.1.

7.3.3 The Direction of Approach of C-X to O(1)

Figure 7.3.6 are histograms of the C-Cl...O(1) angle, α, for criteria **A** (***Figure 7.3.6a***) and crieteria **B** (***Figure 7.3.6b***) contacts to C-NO_2. Comparison of these two histograms shows that the majority of contacts with $\alpha < 120°$ only occur in dataset **A** (***Figure 7.3.6a***) and therefore have contact distances D_1 which exceed the sum of the van der Waal's radii (see Section 7.2.1). Similar results are obtained for both the Br and I datasets. These results indicate that, in common with hydrogen bonds and other essentially electrostatic intermolecular interactions, the shortest C-X...O_2N contacts tend to have the most linear C-X...O(1) geometries.

In order to investigate the issue of C-X...O(1) bond linearity further, the van der Waal's normalised X...O(1) contact distance, R, and the C-X...O(1) angle, α, were transformed into $x = R^3$ and $y = 1 - \cos\theta$ (where $\theta = 180 - \alpha$) and plotted against one another (***Figures 7.3.7***). This transformation into a spherical polar coordinate system was first described by Lommerse *et. al.* (1996) and can be rationalised as follows. In spherical polar coordinates (R, θ and ϕ) a volume element is given by $R^2 \sin\theta \, dR \, d\theta \, d\phi$. An element of area $dR \, d\theta$ in a plot of R against θ therefore corresponds to a volume (integrating over ϕ) of $2\pi R^2 \sin\theta \, dR \, d\theta$. By replacing R with $x = R^3$ and θ with $y = 1 - \cos\theta$, the element of area dx dy becomes $3R^2 \, dR \sin\theta \, d\theta$ which is proportional to the volume element $2\pi R^2 \sin\theta \, dR \, d\theta$ and consequently equal areas in the x,y plot correspond to equal volumes in space. As a result uniform distributions of points in space transfrom into unifrom distributions of points in the scattergrams shown in ***Figures 7.3.7***. Additionally, since the van der Waal's normalised contact distance R was used in the transformation, all the points for which $x = R^3$ is less than 1 in ***Figures 7.3.7*** correspond to contacts in which D_1 is less than the sum of the van der Waals' radii of O and X.

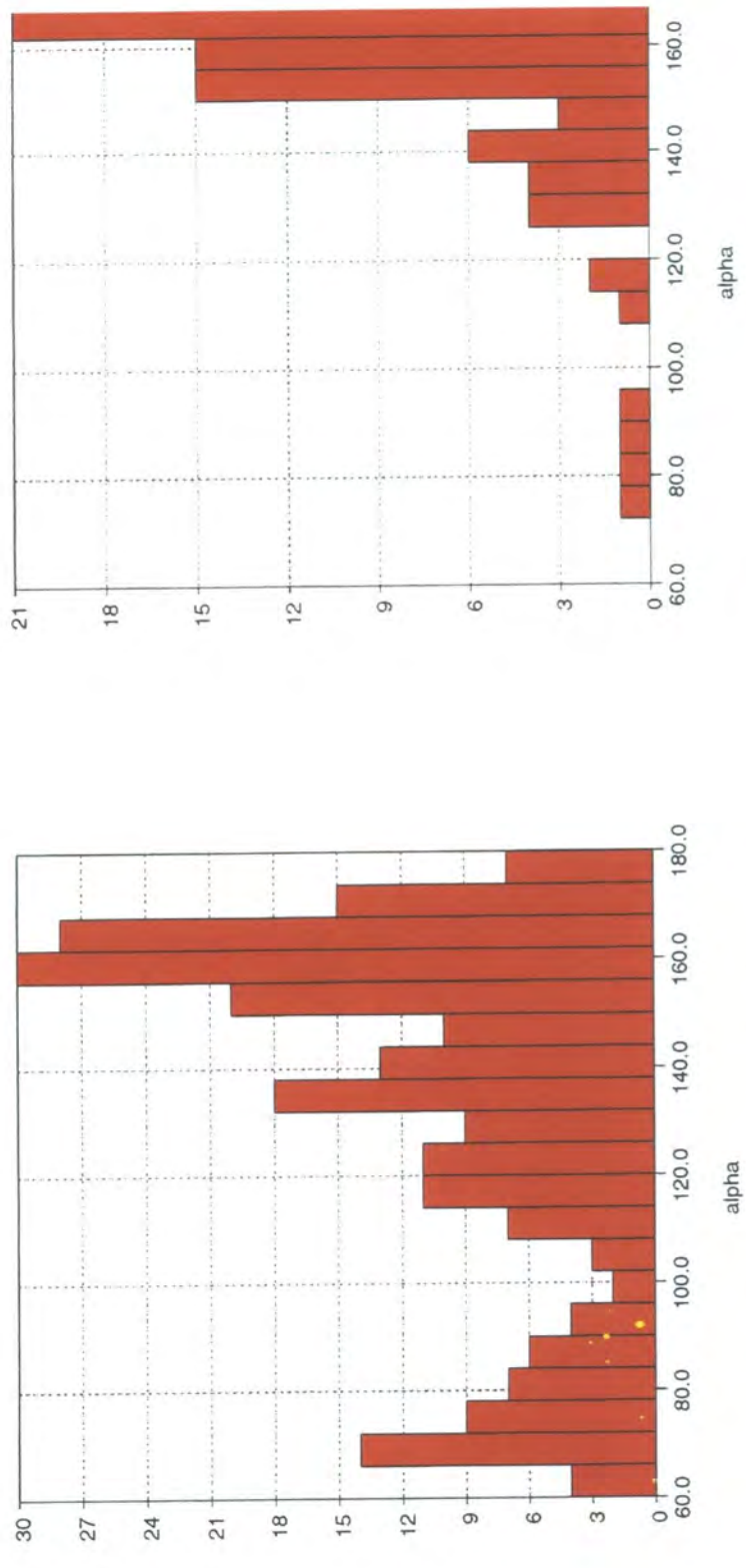

Figure 7.3.6 *- Histograms of α for Cl...O_2N contacts satisfying a) criteria* ***A*** *and b) criteria* ***B****.*

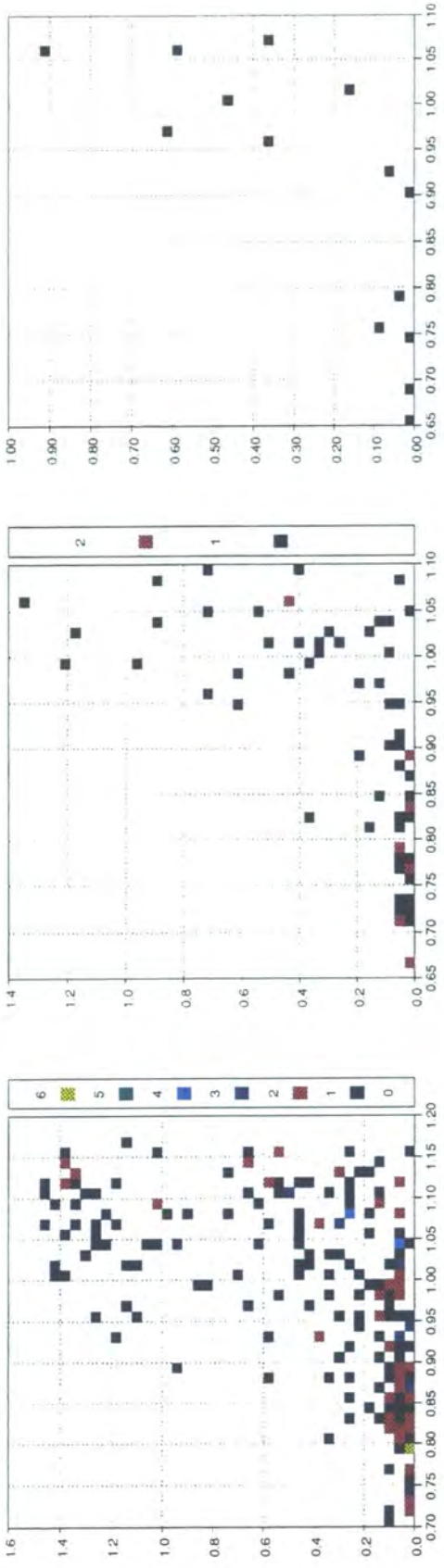

Figure 7.3.7 *- Scatterplots of x versus y for criteria* ***A*** *contacts involving a) Cl, b) Br and c) I.*

Inspection of ***Figures 7.3.7*** reveals that, for contacts between Cl, Br, I and C-NO_2, above the van der Waal's limit ($R^3 > 1$), the direction of approach of C-X to O(1) is random. However, as the X...O(1) separation, D_1, decreases below this limit (decreasing $R^3 < 1$) C-X approaches preferentially in the head-on direction ($1 - \cos\theta = 0°$, $\alpha = 180°$). Further, the percentages of criteria **B** contacts to Cl, Br and I which have $R^3 \leq 1$ and $1 - \cos\theta < 0.18$ ($\alpha > 145°$) are 81%, 88% and 88% respectively, indicating that the tendencey of C-X to approach O(1) more linearly when X...O(1) is short is unaffected by the nature of the halogen.

In the case of the symmetical X...O_2N bonding mode, **P**, it is clearly impossible for C-X to approach both nitro oxygen atoms in the preferred head-on direction. Simple geometric calculations, based on an N-O bond length of 1.2Å, an O-N-O angle of 120° and an X....O contact distances equal to the sums of the van der Waal's radii of X and O, show that in perfectly symmetrical **P** type X...O_2N interactions, C-X...O angles of 161.5°, 162° and 162.7° will be obtained for Cl, Br and I respectively. The experimentally determined values of the C-I...O angles for the symmetrical I...O_2N interactions in compounds **IV** and **V** (see Section 7.1.1) are 161.3° and 163.8° respectively. These values are close to the estimated value of 162.7°, suggesting that the estimates are valid and that the preferred linear C-X...O geometry is only slightly distorted in symmetrical **P** type X...O_2N interactions.

7.4 THEORETICAL RESULTS

7.4.1 Variation of Energy with ϕ

Table 7.4.1 shows the results of the series of calculations, IMPTX described in Section 7.2.2.2, for the Cl model system. These results are displayed graphically in ***Figure 7.4.1***.

Inspection of ***Table 7.4.1*** and ***Figure 7.4.1*** reveals that total interaction energy, Etot, decreases steadily as ϕ increases from 105° and reaches a minimum at -135°. Above this ϕ angle the interaction energy rises sharply. The dominant energy term is the exchange-repulsion, E_{er}, which falls steadily as ϕ increases from 105° to 180° reflecting a decrease in repulsive Cl...O(2) contacts as the chlorine moves away from the second nitro oxygen atom. Above 180° E_{er} begins to increase as the approaching halogen moves closer to the methyl carbon atom. However, between ϕ = 180° and ϕ = -135° this increase is more than off-set by the electrostatic and dispersion energy terms, E_{es} and E_{disp}, which decrease throughout the ϕ rotation. Above -135° E_{er} rises sharply and despite a similarly sharp rise in E_{es}, both interactions become destablizing at ϕ angles above -105°.

The absence of any discrete minimum in either E_{es} or E_{tot} at $\phi = \pm 120°$ rules out any involvment by the oxygen lone pairs in the Cl...O_2N interaction. This correlates well with the the crystallographic data which produced no evidence of lone pair directionality in **P**, **Q** or **R** type interactions (see Section 7.3.2).

Table 7.4.1 *- Variation in interaction energy with ϕ for Cl...O_2N in the model system (IMPTX).*

ϕ / Cl	E_{es}	E_{er}	E_{pol}	E_{ct}	E_{disp}	E_{tot}
105°	-2.104	3.562	-0.728	-0.438	-3.256	-2.965
120°	-2.436	2.325	-0.633	-0.327	-2.725	-3.796
135°	-2.350	2.039	-0.578	-0.271	-2.598	-3.937
150°	-2.390	1.826	-0.518	-0.227	-2.594	-3.903
165°	-2.247	1.663	-0.459	-0.188	-2.626	-3.858
180°	-2.286	1.600	-0.412	-0.173	-2.667	-3.938
-165°	-2.957	1.664	-0.377	-0.178	-2.720	-4.209
-150°	-3.155	1.852	-0.351	-0.204	-2.823	-4.681
-135°	-3.861	2.222	-0.329	-0.246	-3.084	-5.297
-120°	-4.796	3.803	-0.329	-0.350	-3.529	-5.201
-105°	-8.83	17.155	-0.453	-1.017	-5.800	2.055

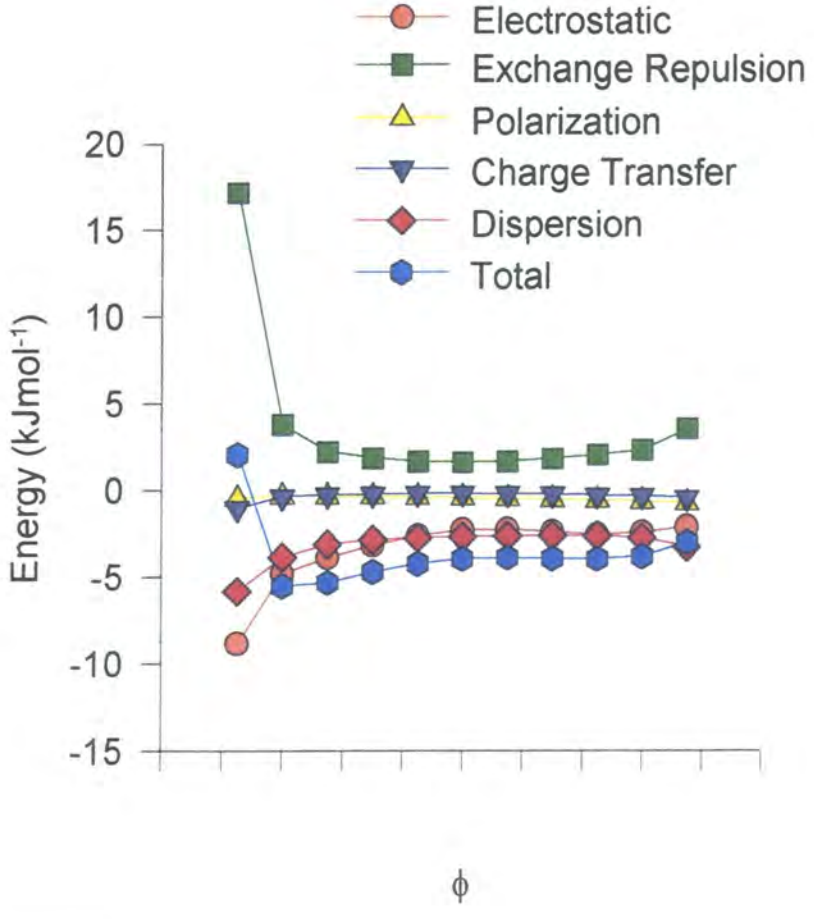

Figure 7.4.1 *- Variation of interaction energy with ϕ for Cl...O_2N.*

The position of the global minimum, at ϕ = -135°, indicates that the mono-coordinate bonding mode **R** is favoured by Cl. The crystallographic data broadly support this, showing that **R** type contacts predominate (see Section 7.3.2). Although, the position of the minimum in ***Figure 7.4.1*** is somewhat closer to the carbon atom than the maximum in Figure ***7.3.4a***, which occurs at ϕ = -150°. This anomaly is probably due to deficiencies in the model system used for the calculations. The large majority of the crystallographic observations of Cl...O_2N involve C(aromatic)-NO_2 or C(sp^3)-NO_2 in which the sp^3 carbon atom is further substituted. Whereas, the model system has nitromethane as the NO_2 'acceptor'. Clearly, all but a few of the crystallographic examples have considerably more sterically bulky carbon centres than CH_3-NO_2. Consequently, the preferred ϕ angle is shifted towards 180° in the experimental data by the increased exchange-repulsion between the incoming Cl and the larger substituents on the carbon atom.

Since the results of the calculations IMPTX indicate that $\phi \approx$ -135° is the preferred direction of approach for Cl, ϕ was fixed at this value in all subsequent calculations.

7.4.2 Variation of Energy with D_1

Table 7.4.2 shows the results of the series of calculations, IMPTY described in section 7.2.2.2, for the Cl model system. These results are displayed graphically in ***Figure 7.4.2***.

The results shown in ***Table 7.4.2*** and ***Figure 7.4.2*** indicate that there is a very small dip ($\approx$ 0.5 kJ mol^{-1}) in the total energy, E_{tot}, of the Cl...O_2N interaction as the chlorine atom penetrates the oxygen atom sphere. The energy minimum occurs at 3.1Å, some 0.17Å shorter than the sum of the van der Waal's radii of Cl and O (3.27Å: Bondi, 1967). Below 3.1Å, the repulsive exchange repulsion energy term, E_{er}, increases significantly and becomes dominant, despite appreciable decreases in both the electrostatic and dispersive energy terms, E_{es} and E_{disp}.

Table 7.4.2 *- Variation in interaction energy with D_1 for Cl...O_2N in the model system (IMPTY).*

D_1 Cl	E_{es}	E_{er}	E_{pol}	E_{ct}	E_{disp}	E_{tot}
2.8	-10.809	15.797	-0.981	-1.378	-6.77	-4.148
2.9	-8.367	10.478	-0.763	-0.948	-5.649	-5.249
3.0	-6.615	6.924	-0.600	-0.655	-4.751	-5.697
3.1	-5.337	4.559	-0.476	-0.454	-4.027	-5.736
3.2	-4.386	2.991	-0.382	-0.316	-3.435	-5.528
3.3	-3.663	1.955	-0.308	-0.221	-2.947	-5.184
3.4	-3.101	1.274	-0.251	-0.155	-2.541	-4.775

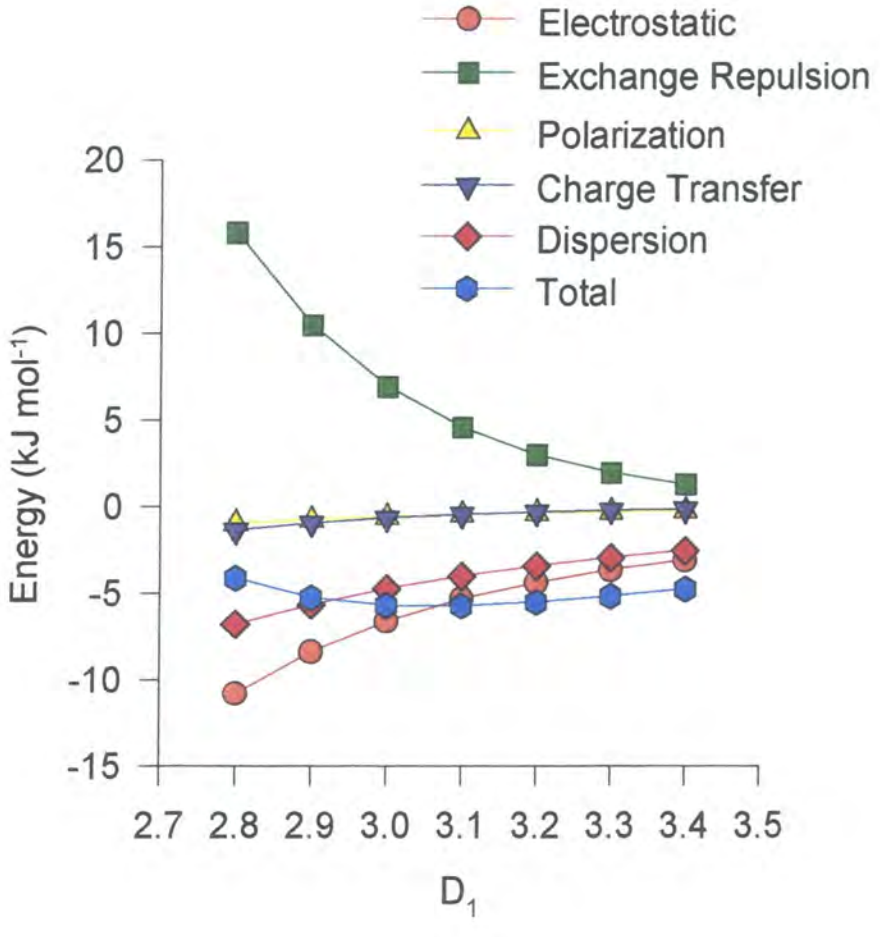

Figure 7.4.2 *- Variation of interaction energy with D_1 for Cl...O_2N.*

These results compare favourably with the crystallographic data. Of the 96 Cl...O_2N contacts satisfying criteria **B** that were located in the CSDS (***Table 7.3.1***), only 8 have $D_1 \leq 3.0$Å and $32 \leq 3.1$Å. The majority of the contacts have values of D_1 which are distibuted evenly in the range 3.1 - 3.27Å.

7.4.3 Variation of Energy with χ

The results of the database survey (***Figure 7.3.5a***) show that the angle of approach of Cl to the C-NO_2 plane, χ, has a broad distribution. 74 of the 96 Cl...O_2N fragments located using criteria **B** have χ angles in the range 0 - 45° and some fragments have χ angles of 70° or more. The results of the series of calculations IMPTZ (***Table 7.4.3*** and ***Figure 7.4.3***) explain why such a broad distribution is obtained The total energy of the Cl...O_2N interaction, E_{tot}, increases by only 0.4 kJ mol^{-1} over the range $0° < \chi < 45°$. Above $\chi = 45°$, the total energy begins to increase more rapidly but does not rise sharply until χ reaches an angle of 75°. The absence of a sharp minimum in E_{es} at $\chi = 0°$ appears to confirm that there is minimal oxygen atom lone pair involvment in the Cl...O_2N interaction.

Table 7.4.3 *- Variation in interaction energy with χ for Cl...O_2N in the model system (IMPTZ).*

χ / Cl	E_{es}	E_{er}	E_{pol}	E_{ct}	E_{disp}	E_{tot}
0°	-3.861	2.222	-0.329	-0.246	-3.084	-5.297
15°	-3.831	2.254	-0.323	-0.252	-3.109	-5.261
30°	-3.735	2.355	-0.309	-0.270	-3.183	-5.143
45°	-3.552	2.531	-0.292	-0.298	-3.299	-4.910
60°	-3.230	2.766	-0.276	-0.321	-3.449	-4.509
75°	-2.694	3.055	-0.264	-0.336	-3.654	-3.892
90°	-1.874	3.598	-0.263	-0.342	-4.037	-2.917

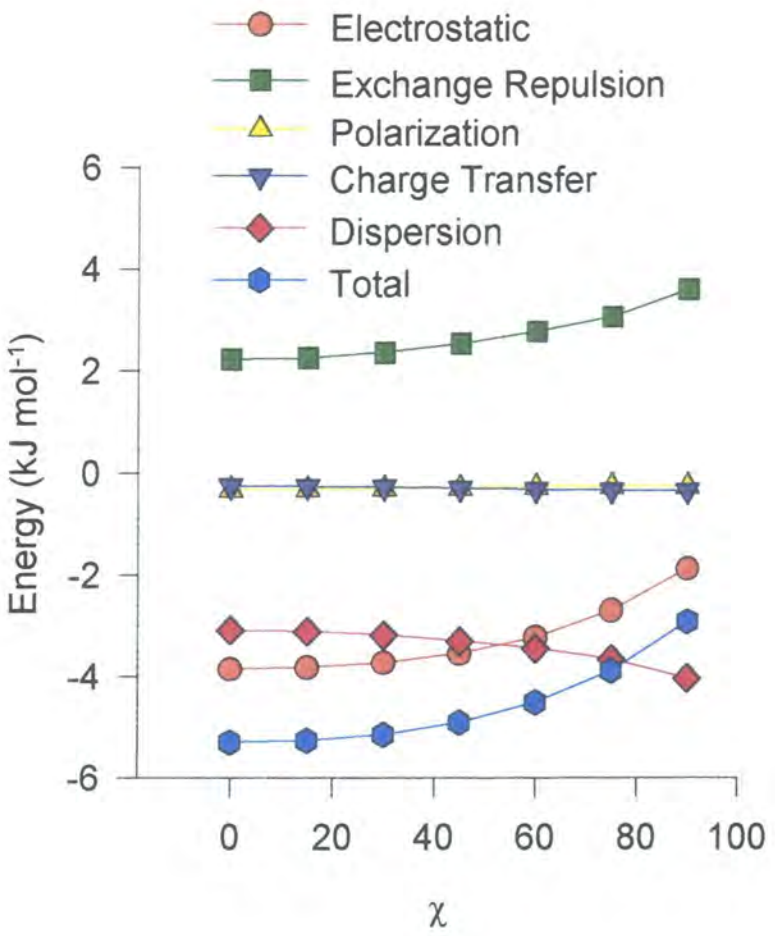

Figure 7.4.3 *- Variation of interaction energy with χ for Cl...O_2N.*

7.5 CONCLUSIONS

The crystallographic evidence presented in this chapter shows that X...O_2N interactions occur frequently in suitable systems and that the propensity of the halogens to form such contacts increases in the order Cl < Br < I. Further, the results show that Cl prefers to form asymmetrical mono-coordinate contacts, **R**, with C-NO_2. Whereas, Br and I tend to form symmetrical bifurcated contacts, **P**. In all cases, statistically corrected distributions of the nitro oxygen atoms about the carbon bound halogens indicate that linear C-X...O(1) geometries are preferred and that this geometry is only slightly distorted in symmetrical **P** type contacts. There is no evidence of any lone pair directionality in any of the contacts, although the halogens do tend to approach the nitro oxygen atoms in or close to the plane of the nitro group. The geometries of the X...O_2N interactions appear to be governed by symmetry and steric factors.

The theoretical calculations on a model Cl...O_2N system show that the interaction is attractive ($\approx$ 5.7 kJ mol^{-1}) at an optimum Cl...O distance of 3.1Å, some 0.17Å shorter than the sum of the van der Waal's radii. Variations in interaction energy with the in-plane angle of approach of Cl to N-O(1), ϕ, suggest that ϕ angles in the region of -135° (corresponding to mono-coordinate **R** contacts) are preferred by Cl. Variations in the out-of-plane approach of Cl to C-NO_2, χ, indicate that χ angles of less than 45° are favoured. However, interactions with χ values of up to 75° are not strongly energetically disfavoured. Once again, there is no evidence of oxygen atom lone pair participation in the Cl...O_2N interaction.

Although it was not possible to perform similar IMPT calculations on model Br and I systems, the crystallographic data presented here and similar results described by others (Lommerse *et. al.*, 1996) indicate the the X...O_2N interaction increases in strength in the order Cl < Br < I. The experimental data also suggest that the tendency for the halogen atom to approach the nitro group between the two nitro oxygen atoms (motifs **P** and **Q**)

increases significantly in the same order. Both effects mirror the increasing polarisability of the halogen atoms.

The results of this study indicate that I...O_2N interaction energies may approach -8.0 kJ mol^{-1} or even 9.0 kJ mol^{-1}, making them at least as strong as more commonly observed C-H...O bonds (Rovria *et. al.*, 1995). This may explain the stucture determining role of the I...O_2N interactions observed recently in some crystal stuctures (Allen *et. al.*, 1994); Thalladi *et. al.*, 1996) and lends support to notion (Desiraju, 1995) that these interactions are valuable supramolecular synthons.

7.6 REFERENCES

Allen, F. H., Goud, B. S., Hoy, V. J., Howard, J. A. K. and Desiraju, G. R. (1994) J. Chem. Soc., Chem. Commun., 2729 - 2730.

Amos, R. D. (1994) CADPAC 4.2; *The Cambridge Analytical Package*, Issue 4.2, a suite of quantum chemistry programs, University of Cambridge.

Desiraju, G. R. (1995) Angew. Chem. (Int. Ed. Engl.), **34**, 2311 - 2327.

Desiraju, G. R. and Pedireddi, V. R. (1989) J. Chem. Soc., Chem. Commun., 1112.

Desiraju, G. R., Pedireddi, V. R., Sarma, J. A. R. P. and Zacharias, D. E. (1993) Acta Chim. Hung., **130** (3-4), 451 - 465.

Hayes, I. C. and Stone, A. J. (1984) J. Mol. Phys., **53**, 83 - 105.

Jeffrey, G. A. and Saenger, W. (1991) *Hydrogen Bonding in Biological Structures*, Springer-Verlag, Berlin.

Lommerse, J. P. M., Stone, A. J., Taylor, R. and Allen, F. H. (1996) J. Am. Chem. Soc, **118**, 3108 - 3116.

Pedireddi, V. R., Sarma, J. A. R. P.and Desiraju, G. R. (1992) J . Chem. Soc., Perkin Trans. 2, 311.

Rovira, M. C., Novoa, J. J., Whangbo, M-H. and Williams, J. M. (1995) Chem. Phys., **200**, 319 - 335.

Stone, A. J. (1993) J. Chem. Phys. Lett., **211**, 101 - 109.

Thalladi, V. R., Goud, B. S., Hoy, V. J., Allen, F. H., Howard, J. A. K. and Desiraju, G. R. (1996) J. Chem. Soc, Chem. Commun., 401 - 402.

CHAPTER 8

Database Studies of the Hydrogen Bonding Properties of Three Membered Rings

8.1 INTRODUCTION

8.1.1 C-H as a Hydrogen Bond Donor

After many years of speculation, based largely on spectroscopic data, the first unambiguous crystallographic evidence for the existence of C-H...X hydrogen bonds appeared in 1982 with the publication of a statistical survey of neutron structures contained in the CSDS (Taylor and Kennard, 1982). This study yielded three significant results. Firstly, that C-H groups tend to form short intermolecular contacts to oxygen, nitrogen, sulphur and chlorine atoms rather than to carbon or hydrogen atoms. Secondly that in C-H...O bonds, the C-H group approaches the oxygen atom in a direction within 30° of the lone pair plane and finally, that the hydrogen bonding ability of C-H groups is enhanced by the presence of electron withdrawing groups adjacent to C-H. In view of this evidence the authors concluded that C-H...X interactions are attractive, the attractive force being derived from electrostatic stabilisation of the X...H close contact and therefore it is reasonable to describe C-H...X interactions as hydrogen bonds.

Research on this new type of hydrogen bond has increased in recent years as workers have tried to assess the hydrogen bonding ability of C-H in various environments and with various acceptor atoms. Principal among these workers is Desiraju who has studied the effect of carbon acidity on C-H...X bond formation. His aim was to confirm that C-H...O and related interactions are essentially electrostatic in nature by demonstrating that there was a correlation between the δ positivity of the donor proton and the length of the C-H...O bond it forms. Such a correlation was already known to exist for strong electrostatic interactions such as O-H...O and N-H...O (see for example Kennard, Taylor and Versichel, 1984).

Desiraju performed his early studies on chloroalkyl compounds (Desiraju, 1989). Using a primitive version of the CSDS's non-bonded contact search facility, he located molecules of the type $Cl_{(3-n)}C_nCH$ ($0 \leq n \leq 3$) which also contained a C-H...O contact

satisfying certain geometrical criteria. Molecules containing other electron withdrawing substituents adjacent to the chlorinated centre were excluded to avoid bias in the data. Comparision of the data from each of the four fragment types (Cl_3CH, Cl_2CCH, ClC_2CH and C_3CH) clearly showed that the mean C...O separations increase steadily as the extent of chlorination increases and hence the carbon acidity of the adjacent C-H group decreases (3.32Å for Cl_3CH cf. 3.59Å for C_3CH). Encouraged by this convincing evidence of a link between carbon acidity and C-H...O bonding ability Desiraju went on to investigate C-H...O hydrogen bonding in molecules containing terminal alkynes.

Terminal alkynes possess among the most acidic C-H protons known (pKa ≈ 25: Streitwieser and Heathcock, 1981) and as a consequence were predicted by Desiraju and others (Green, 1974) to form exceptionally short and linear C-H...X bonds. In his alkyne study (Desiraju, 1990), Desiraju compared the geometries of C-H...O hydrogen bonds found in 69 terminal alkynes with those found in some 131 alkenes. Perhaps unsurprisingly, he found that the C-H...O bonds formed by the alkynic C-H groups were shorter than those in the alkenes (mean C...O of 3.46Å cf. 3.64Å). However, he also noted that large numbers of C-H...O bonds were formed in *both* cases and that *all* the C-H...O bonds observed tended to be linear within around 30°.

Desiraju completed his analysis of the C-H...O bonding abilities of C-H groups of varying acidities by correlating mean C-H....O separations with pK_a values for a larger range of organic compounds (Desiraju and Pedireddi, 1992). The results were so convincing that he turned the whole concept on its head by proposing that mean C-H...O separations could be used as a scale of carbon acidity.

The results described here support Taylor and Kennard's view that C-H...X bonds are essentially electrostatic interactions in which strength is highly sensitive to the δ positivity of the participating proton and decreases gradually with increasing H...X separation. So, clearly, in order to observe C-H...X hydrogen bonding we must study

acidic carbon atoms and use generous distance criteria when selecting the contacts which may be significant.

8.1.2 Cyclopropanes and Cyclopropenes as Analogues of Alkenes and Alkynes

It has been known for some time that cyclopropane has chemical properties more akin to those of alkenes than of alkanes (Charton, 1970). Furthermore, theoretical calculations (Hoffman, 1970; Hoffman and Stohrer, 1971) and analysis of crystallographic data (Allen, 1980 and 1981) have shown that cyclopropane uses approximately $sp^{2.2}$ hybridized orbitals to form the exocyclic bonds to its hydrogen atoms. This hybridization state is intermediate between the sp^3 hybrids used by straight chain alkanes and the sp^2 hybrids used for bonds to hydrogen atoms in alkenes and suggests that cyclopropane has a carbon acidity closer to that of ethylene than of propane. The effect is known to be enhanced by the presence of electronegative heteroatoms (Allen, 1982a), with the proportion of s character in the orbitals of the exocyclic bonds increasing from around 31% in cyclopropane to nearly 33% in aziridine. Further, if cyclopropane is alkene-like then cyclopropene is alkyne-like. Crystallographic data indicate that the bonds from the unsaturated carbon atom to the exocylic hydrogen atoms of cyclopropene are made from approximately $sp^{1.2}$ hybrid orbitals (Allen, 1982b), comparable with those of acetylene

In order to compare, more quantitatively, the natures of alkanic, alkenic and alkynic C-H groups with those of cyclopropane, cyclopropene and their derivatives a series of *ab initio* molecular orbital calculations were carried out (Allen *et. al.*, 1996a). The residual atomic point charges on the carbon, nitrogen, oxygen and hydrogen atoms of cyclopropane, oxirane, aziridine and cyclopropene as well as those of the straight chain analogues propane, dimethyl ether and dimethylamine were calculated. Similar calculations for ethylene and acetylene were also performed. The GAMESS-UK package (Guest *et. al.*, 1993) was used to perform closed shell self consistent field (restricted Hartree-Fock) calculations using a 6-31G** basis set with full geometry

optimization. Partial charges were obtained using a Mullikan population analysis. The results of these calculations are shown in ***Table 8.1.1***.

Table 8.1.1 *- Residual atomic point charges for various three membered ring systems and their straight chain analogues.*

Molecule	Atom	Charge (eV)	Charge on equivalent atom in open chain analogue
cyclopropane	C_1	-0.261	-0.220
	H_1	+0.131	+0.110
	C_2	symm equiv to C_1	-0.340
	H_2	symm equiv to H_1	+0.110
aziridine	N_1	-0.568	-0.621
	H_1	+0.276	+0.265
	C_2	-0.116	-0.139
	H_2*syn*	+0.123	+0.080 - +0.120
	H_2*anti*	+0.139	+0.080 - +0.120
oxirane	O_1	-0.553	-0.690
	C_2	+0.015	-0.006
	H_2	+0.131	+0.090 - +0.120
cyclopropene	C_1	-0.242	-
	H_1	+0.104	-
	C_2	-0.141	-
	H_2	+0.158	-
ethylene	C_1	-0.254	-
	H_1	+0.127	-
acetylene	C_1	-0.233	-
	H_1	+0.233	-

The partial charges on the hydrogen atoms attached to the rings cyclopropane and oxirane are the same (+0.131eV). The two symmetry independent protons attatched to carbon in aziridine vary slightly from this value (+0.123eV *syn* and +0.139eV *anti*) but the differences are small. As predicted, the partial charges on the ring protons are very similar to the partial charge on the proton in ethylene (+0.127eV) and greater than those on the alkanic protons in the open chain analogues of each ring (+0.080eV - +0.120eV).

The residual charge on the alkenic proton in cyclopropene (+0.158eV) is larger than those on both the alkanic ring protons and the proton on ethylene but smaller than the partial charge on the acetylenic proton (+0.233eV).

These results match perfectly the predictions made earlier on the basis of hybridization arguments and indicate that cyclopropanes and cyclopropenes have acidities which are comparable to those of alkenes and alkynes. If the electrostatic model of the C-H...X interaction is correct, these results also suggest that three membered ring systems should make excellent C-H hydrogen bond donors.

8.1.3 π Systems as Hydrogen Bond Acceptors.

The body of spectroscopic evidence for the existence of O-H...π and N-H...π bonds to aromatic, alkenic and alkynic acceptors is large (see for example Gleiter, Joris and Schleyer, 1968 and references cited therein) and crystallographers have been describing, for many years the O-H...π interactions which are clearly present in some organic crystal structures (see for example Hardy and MacNicol, 1976; Nakatsu *et. al.*, 1978; Ueji *et. al.*, 1982; Rzepa *et. al.*, 1991; Al-Juaid *et. al.*, 1992). However, only recently has a systematic analysis of the crystallographic data relating to the occurence of hydrogen bonds to π systems been presented (Viswamitra *et. al.*, 1993). The authors of the study concluded that although hydrogen bonds to π systems are rare and rather weak, they can be structurally significant interactions when they do occur. These findings were confirmed by Steiner (1995a and b) who has published structural data, database analyses and quantum mechanical calculations on C≡C-H...π bonds in alkynic and aromatic systems. His survey of the CSDS located 19 C≡C-H...π bonds with H...π distances in the range 2.5Å to 2.9Å and the theoretical calculations they performed indicate that C≡C-H...π bonds have energies in the region of 5 - 10 kJ mol^{-1}.

Although most of the recent research on hydrogen bonds to π systems has focused on alkynic and aromatic acceptors, there is evidence to suggest that even weak π bases,

such as pseudo aromatic cyclopropane, can act as π acceptors. Joris, Schleyer and Gleiter (1968), who used infra red spectroscopy to investigate the intramolecular hydrogen bond acceptor ability of cyclopropane, concluded that there was strong evidence to support the notion of O-H...cyclopropane interactions. They proposed two bonding modes for this type of interaction, an edge-on mode and a face-on mode (***Figures 8.1.1***), of which the former was considered more favourable for stereochemical reasons. Recent charge density studies on three membered rings tend to support this theory but for a rather different reason. It has now been proved experimentally the ring bonds in these highly strained systems are bent, leading to local maxima in the electron density in the ring plane which are outside the three interatomic vectors (Nijveldt and Vos, 1988a, b and c). Clearly, such concentrations of electron density will attract potential hydrogen bond donors.

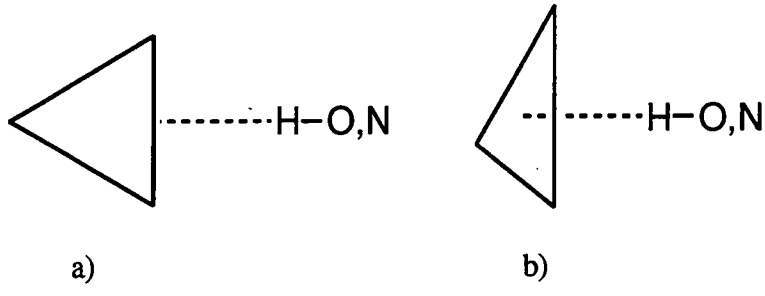

Figure 8.1.1 *- Cyclopropane as a π donor is an a) edge-on and b) face-on manner.*

8.1.4 Aims

It is clear from the evidence presented here that three membered rings have the potential to act as both C-H hydrogen bond donors and π acceptors. However, so far little attention has been paid to these systems in either context. A comprehensive database survey of ring C-H...X contacts in structures containing cyclopropane (I), oxirane (II), aziridine (III) and cyclopropene (IV) and a range of acceptor atoms was therefore carried out . This analysis was completed by comparing the results with results obtained for secondary alkanic (V), terminal alkenic (VI) and alkynic (VII) C-H

groups. The study also attempts to confirm the proposals of Joris and co-workers by obtaining crystallographic evidence for N-H..cyclopropane and O-H...cyclopropane bonds of both the edge-on and face-on types in both intramolecular and intermolecular environments.

8.2 METHODOLOGY

Versions 5.08 and 5.09 of the CSDS (October 1994 and April 1995 containing 126,353 and 140,236 entries resepectively) were used for this study and the general search procedure outlined in Chapter 6 was followed unless otherwise stated.

8.2.1 Three Membered Rings as C-H Donors: Database Searches

Preliminary searches were conducted to locate molecules containing the fragment depicted in ***Figure 8.2.1***. No constraint was placed on the non-bonded contact distance d(HO/N) at this stage and the compounds located formed the database sub-set upon which all subsequent searches were performed.

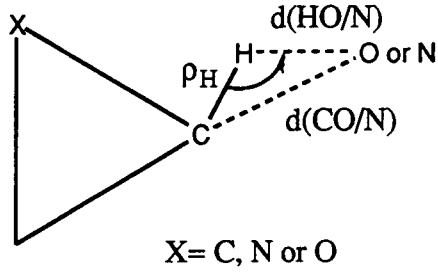

Figure 8.2.1 *- Search fragment used to locate potential C(ring)-H...X interacions.*

Having obtained the basic dataset, searches were conducted for interactions between ring protons in one of the systems cyclopropane, aziridine or oxirane and one of a range of nitrogen and oxygen acceptor groups (***Table 8.2.1***). The parameters shown in ***Figure 8.2.1*** were determined for each interaction located and additionally in the case of the oxgen acceptors, the values of the spherical polar angles χ and ϕ, which describe the elevation (χ) and rotation (ϕ) of the interaction vector, [H...O], with respect to the oxygen lone pair planes, were calculated (***Figure 8.2.2.***) Two sets of geometrical criteria were used to define C-H...X (where X = N or O) interactions. The first set of criteria, referred to as **A**, are those described and used previously by Desiraju in his studies on C-H...X hydrogen bonding (Desiraju, 1991). During the course of our

investigation we refined these geometrical constraints slightly to generate criteria **B** (***Table 8.2.2***)

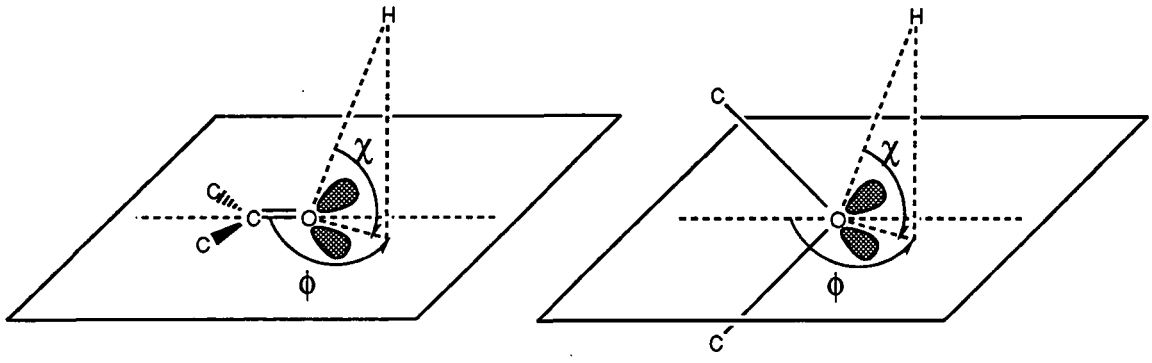

a) b)

Figure 8.2.2 *- Definitions of the spherical polar angles* χ *and* ϕ *for a)* $O(sp^2)$ *and b)* $O(sp^3)$.

Table 8.2.1 *- Numbers of interactions of types* ***A*** *and* ***(B)*** *located for each ring/acceptor combination.*

Acceptor	Cyclopropane	Aziridine	Oxirane
C=O	410 (327)	79 (63)	235 (181)
H_2O	9 (7)	0 (0)	5 (3)
C-OH	34 (15)	10 (8)	66 (58)
C-O-C	29 (24)	8 (6)	292 (214)
$C\text{-}NH_2$	2 (2)	0 (0)	0 (0)
C-NH-C	0 (0)	7 (4)	1 (1)
C-NC-C	4 (3)	4 (2)	2 (2)
C=N-C	11 (10)	9 (7)	1 (1)

Table 8.2.1 shows the number of C-H...X interactions of types **A** and **B** located for each ring/acceptor combination. The number of interactions involving nitrogen acceptors is clearly very small and therefore it was decided to restrict subsequent effort to the analysis of interactions involving oxygen acceptor groups only.

Table 8.2.2 *- Geometrical constraints used to define C-H...X contacts of types* ***A*** *and* ***B****.*

Parameter	Criteria **A**	Criteria **B**
d(HO) or d(HN) max	3.0Å	2.9Å
d(CO) or d(CN) max	4.0Å	3.9Å
ρH	110 - 180°	120 - 180°
|φ|	any	60 - 180°

8.2.2 Three Membered Rings as π Acceptors: Database Searches

Since the number of structures relevant to this portion of the study was thought to be small no preliminary screening of the database was conducted. Instead we searched for the fragment depicted in ***Figure 8.2.3*** directly. The distances X_1...H and Y...H were constrained to be less than 3.0Å and greater than 2.4Å respectively and the angle HX_1Y was required to be within the range 45° - 180°. These geometrical constraints were applied in order to locate interactions of both the edge-on and face-on types described in Section 8.1.3 but to exclude interactions of the type X-H...Y (where Y = N or O).

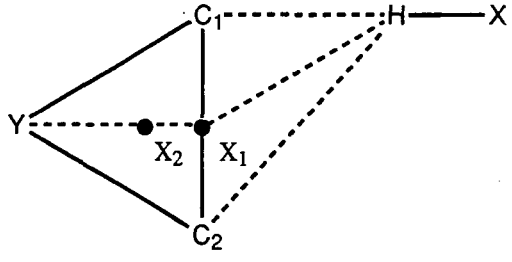

Figure 8.2.3 *- Search fragment used to locate X-H...π bonds to three membered rings.*

8.3 THREE MEMBERED RINGS AS HYDROGEN BOND DONORS

8.3.1 Summary Statistics

Table 8.3.1 gives details of the numbers of donor C-H groups (n_1) and acceptor oxygen atoms (n_2) present in data sets containing all CSDS entries with at least one example of the relevent donor I, II, III, IV, V, VI or VII and one of the appropriate oxygen acceptor groups. The totals reported are irrespective of whether or not the donor and acceptor atom are in contact. The numbers of C-H...O contacts of types **A** (n_4) and **B** (n_5) located within each donor/acceptor group are also shown.

Although the number of donors relative to acceptors (n_3) varies tremendously from group to group, the numbers of contacts formed by each type of donor as percentages of the total number of potential donors in each group (n_4/n_1 and n_5/n_1) are surprisingly consistent. For instance, consider the number of contacts formed by the three membered rings I, II and III to carbonyl acceptors. The percentages for **A** and **B** criteria contacts are 32.7% and 26.1% for I, 33.6% and 26.8% for II and 34.1% and 26.7% for III. The similarities, particularly for criteria **B** contacts, are clear. The equivalent percentages for terminal alkenes are somewhat lower at 21.2% and 15.8%, possibly because the alkenic donors are less accessible than their three membered ring counterparts. However, both of these donors form more contacts than secondary alkanes (17.5% and 12.5%) and far fewer than alkynic C-H (47.5% and 34.4%) as predicted on the basis of the *ab initio* results described in Section 8.1.2.

Table 8.3.1 also contains data for contacts between C-H and C=O in compounds which lack any O-H or N-H donor groups. The percentages of contacts formed to this acceptor (denoted by C=O*) are marginally higher than those for C=O in every donor group, suggesting that the absence of stronger hydrogen bond donors increases slightly the chance of C-H...X bond formation. However, the presence of other donor groups appears to be much less important than the nature of the acceptor group in dictating

how many C-H...X contacts will form. Consider the percentages of contacts formed by one donor, cyclopropane, to all of the acceptor groups listed in ***Table 8.3.1***. The percentages for **A** and **B** criteria contacts are 32.7% and 26.1% for carbonyl, 10.0% and 4.4% for alcohol and 11.2% and 9.3% for ether (comparable results are obtained for other donors). Clearly, carbonyl oxygen atoms are much more potent acceptors of C-H...X bonds than either hydroxyl or ether oxygen atoms. This fact is already well documented for the stronger O-H...O and N-H...O bonds (Jeffrey and Saenger, 1991).

Table 8.3.1 *- Summary statistics for C-H...O contacts formed by donors I, II, III, V, VI, VII and oxygen atom acceptor groups. The figures in the first row of each entry are the numbers of C-H donors (n_1) and O acceptors (n_2) located in each sub-set, the second row shows the ratio of these ($n_3 = n_1/n_2$), in the third row are numbers of C-H...O contacts found in each sub-set which satisfy criteria **A** (n_4, with the percentage contacts formed relative to the number of avialable donors in brackets), the fourth row contains the same information for criteria **B** contacts (n_5).*

			Donor			
Acceptor	I	II	III	V	VI	VII
C=O	1253/785	235/178	679/745	5910/2092	1586/1324	61/75
	1.596	1.320	0.911	2.825	1.198	0.813
	410(32.7)	79(33.6)	235(34.6)	1034(17.5)	336(21.2)	29(47.5)
	327(26.1)	63(26.8)	181(26.7)	740(12.5)	250(15.8)	21(34.4)
C=O*	711/472	71/57	391/428	2750/859	720/582	22/27
	1.506	1.246	0.914	3.201	1.237	0.815
	248(34.9)	41(57.7)	153(39.1)	534(19.4)	167(23.2)	16(72.7)
	195(27.4)	35(49.3)	116(29.7)	384(14.0)	132(18.3)	15(68.2)
C-O-H	340/144	39/19	384/315	7052/1319	842/597	63/75
	2.361	2.05	1.219	5.347	1.410	0.840
	34(10.0)	10(25.6)	66(17.2)	522(7.4)	81(9.6)	26(41.3)
	15(4.4)	8(20.5)	58(15.1)	360(5.1)	56(6.7)	24(38.1)
C-O-C	258/132	41/25	1044/926	6944/2000	544/415	25/34
	1.954	1.640	1.127	3.472	1.311	0.735
	29(11.2)	8(19.5)	292(27.9)	344(4.9)	54(9.9)	12(48.0)
	24(9.3)	6(14.6)	214(20.5)	344(4.9)	44(8.1)	11(44.0)

8.3.2 C-H...O Bond Geometry

Table 8.3.2 lists the mean values of the geometrical parameters depicted in ***Figure 8.2.1*** and described in Section 8.2.1 for C-H...O interactions between the ring systems I, II and III and the acceptors C=O, C-O-H and C-O-C.

Table 8.3.2 - *Geometrical parameters for contacts between three membered ring donors I, II, III and various oxygen atom acceptor groups.*

Ring	Criteria	Nobs	d(HO)	d(CO)	ρH	|χ|	|φ|
C=O							
I	**A**	410	2.65(1)	3.54(1)	142(1)	36(1)	139(2)
	B	327	2.60(1)	3.52(1)	145(1)	25(1)	136(2)
II	**A**	79	2.61(2)	3.46(2)	138(2)	35(2)	135(3)
	B	63	2.56(2)	3.46(2)	143(2)	3293)	139(3)
III	**A**	235	2.63(1)	3.50(1)	140(1)	35(2)	139(2)
	B	181	2.58(1)	3.49(1)	144(1)	32(2)	141(2)
C-O-H							
I	**A**	34	2.80(3)	3.62(3)	134(3)	29(3)	130(7)
	B	15	2.68(4)	3.62(4)	147(3)	28(5)	133(9)
II	**A**	10	2.71(5)	3.62(6)	144(5)	30(7)	134(10)
	B	8	2.66(5)	3.59(6)	146(5)	33(8)	130(11)
III	**A**	66	2.64(2)	3.52(2)	141(2)	22(2)	131(4)
	B	58	2.61(2)	3.51(2)	142(2)	21(2)	134(4)
C-O-C							
I	**A**	29	2.66(4)	3.55(4)	142(3)	14(2)	143(4)
	B	24	2.60(4)	3.52(4)	144(3)	12(2)	140(5)
II	**A**	8	2.60(5)	3.38(6)	129(3)	17(3)	152(6)
	B	6	2.58(7)	3.41(8)	134(30	15(4)	159(4)
III	**A**	292	2.65(1)	3.49(1)	138(2)	26(1)	140(1)
	B	214	2.58(1)	3.49(1)	143(1)	24(1)	140(2)

In all of the acceptor sub-sets which contain more than about 50 contacts the overall picture is similar. The mean H...O separations, d(HO), in all of these sub-sets fall within the ranges 2.60Å - 2.65Å for criteria **A** contacts and 2.58Å - 2.61Å for criteria **B** contacts. These values are satisfyingly close to the sum of the van der Waal's radii of oxygen and hydrogen, which are 1.52Å (Bondi, 1964) and 1.10Å (Rowland and Taylor, 1996) respectively. Mean C-H...O angles, ρH, are equally consistent and fall within the ranges 138° - 142° for criteria **A** contacts and 141° - 145° for criteria **B** contacts.

The similarity between the geometries of the contacts formed by the three rings I, II and III is, perhaps, surprising since the intrinsic electronegativities of the different heteroatoms present increase considerably in the order C < N < O and might be expected to increase the δ positivity of the protons on adjacent carbon atoms in the same order. This would result in decreasing donor ability in the sequence I > II > III. However, no such trend is observed in the mean d(HO) or mean d(CO) distances given above. Neither is it seen in the partial charges derived by *ab initio* methods and described in Section 8.1.2 or in the statistical data presented in Section 8.3.1. Thus, heteroatom effects are, if they are present at all, very small and therefore the donors I, II and III have approximately equivalent C-H...X bond forming abilities. For this reason we have grouped the three types of rings together under the common heading C(r)-H donors in all subsequent analyses.

Table 8.3.3 compares the geometries of C-H...O contacts fulfilling criteria **B** between C(r)-H donors and both C=O and C-O-C/H acceptors with those of the equivalent contacts formed by $C(sp^3)$-H, $C(sp^2)$-H and C(sp)-H donors. The most obvious feature of ***Table 8.3.3*** is the gradual decrease in the mean contact distances, d(HO) and d(CO), as the formal hybridization state of the donor carbon changes from sp^3 to sp^2 to sp. ***Figure 8.3.1*** illustrates this relationship graphically for contacts to C=O acceptors. It is also clear from ***Table 8.3.3*** that the ring donors, C(r)-H, form contacts with geometries which are more typical of alkenic, $C(sp^2)$-H, donors than of the formally analogous alkanic, $C(sp^3)$-H, donors (mean d(HO) of 2.59(1)Å c.f. 2.62(1)Å for sp^2 and 2.67(1)Å

for sp^3). These results confirm that cyclopropanes have alkenic properties and support the theory, descibed in Section 8.1.2, that these ring systems use orbitals that are approximately $sp^{2.2}$ hybridized to form the exocyclic bonds to hydrogen atoms.

Table 8.3.3 *- Comparsion of the geometries of contacts formed by C(r)-H, C(sp^3)-H, C(sp^2)-H and C(sp)-H donors to C=O and C-O-C/H acceptors.*

Donor	Nobs	d(OH)	d(CO)	ρH	|χ|	|φ|	n(vdW)	r
				C=O				
C(r)-H	577	2.59(1)	3.50(1)	145(1)	33(1)	141(1)	56.5	-0.385
C(sp^3)-H	740	2.67(1)	3.57(1)	143(1)	36(1)	140(1)	36.6	-0.320
C(sp^2)-H	296	2.62(1)	3.56(1)	147(1)	33(1)	136(2)	48.0	-0.365
C(sp)-H	29	2.30(4)	3.31(3)	157(3)	23(3)	139(4)	89.7	-0.646
				COC/H				
C(r)-H	540	2.61(1)	3.52(1)	144(1)	21(1)	138(1)	51.5	-0.300
C(sp^3)-H	704	2.68(1)	3.60(1)	145(1)	23(1)	138(1)	30.0	-0.292
C(sp^2)-H	208	2.65(1)	3.58(1)	146(1)	23(1)	135(2)	40.9	-0.243
C(sp)-H	40	2.43(4)	3.39(3)	151(2)	20(2)	142(4)	75.0	-0.613

The geometrical data in ***Table 8.3.3*** are also in good agreement with the values for residual partial charges on the various protons given in ***Table 8.1.1***. ***Figure 8.3.2*** is a plot of the mean contact distance, d(HO), against the partial charge on the proton for contacts to C=O acceptors. The linear relationship between the two is clear and in particular we note that the large jump in the δ positivity which is observed on going from an alkenic to an alkynic system (+0.127eV cf. +0.233eV) is mirrored by an equally dramatic shortening of the mean H...O distance, d(HO), from 2.62Å for C(sp^2)-H to 2.30Å for C(sp)-H.

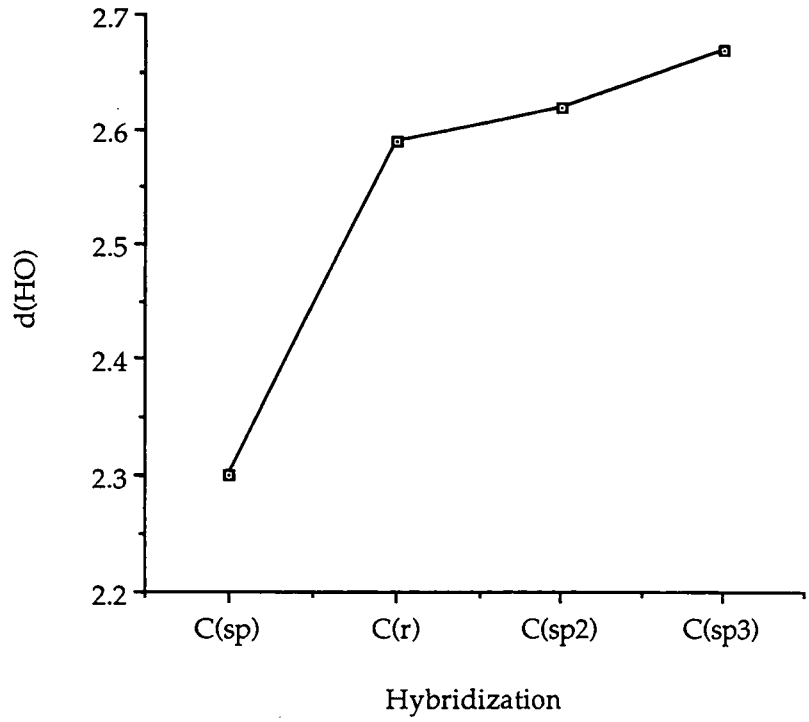

Figure 8.3.1 *- Plot of d(HO) for C(sp), C(sp^2) and C(sp^3) donors bonded to C=O.*

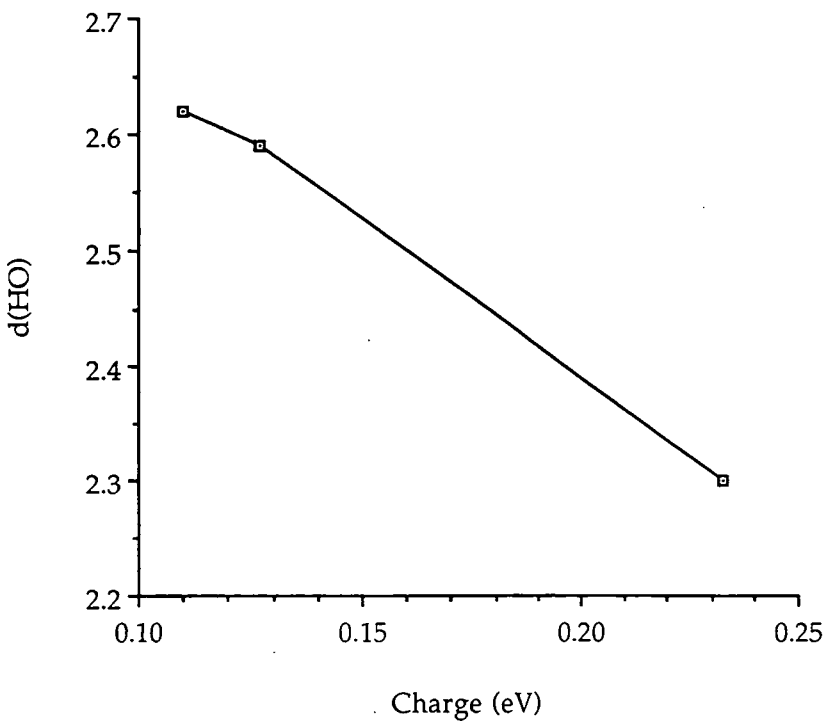

Figure 8.3.2 *- Plot of d(HO) versus partial charge for various types of C-H bonded to C=O.*

The increasing ability of the systems $C(sp^3)$-H, $C(sp^2)$-H, C(r)-H and C(sp)-H to donate protons to C-H...O hydrogen bonds is also reflected in the percentage of contacts formed by each type of donor which are less than the sum of the van der Waal's radii of oxygen and hydrogen. This value, n(vdW) in ***Table 8.3.3***, increases steadily and then dramatically in the order $C(sp^3) < C(sp^2) < C(r) << C(sp)$ matching exactly the behaviour of the residual partial charges and mean contact distances described above.

The mean C-H...O contact angles, ρH, are also shown in ***Table 8.3.3***. The values of ρH for $C(sp^3)$-H, $C(sp^2)$-H and C(r)-H donors are all very similar and in the region of 145°. However, the mean angle increases considerably for C(sp)-H donors, which form C-H...O contacts with angles of more than 150°. The tendancy for short contacts to be more linear is well known for a variety of electrostatic interactions and was described in Section 8.1.1. ***Figure 8.3.3*** shows, graphically, the relationship between contact distance, d(HO), and contact angle, ρH, for a) C(r)-H donors and b) C(sp)-H donors. Regression lines are included on both plots and the correlation coefficient, r in ***Table 8.3.3*** is considerably higher for the data shown in ***Figure 8.3.3b***.

An indication of the lone pair directionality of the the C-H...O contacts located in the various groups is given by the mean values of the spherical polar angles, $|\chi|$ and $|\phi|$. $|\chi|$ is the angle of elevation of the [H...O] vector from the conventional lone pair planes of either the sp^3 hybridized oxygen atoms of the C-O-C/H acceptors or the sp^2 hybridized oxygen atom present in the C=O acceptors. Therefore values of $|\chi|$ close to 0° would indicate close alignment of the [H...O] vector with the lone pair direction. $|\phi|$ describes the angle of rotation of the projection of the [H...O] vector onto the conventional lone pair plane with respect to the vector between the C...C/H mid-point and O in the case of sp^3 hybridized oxygen atoms and the C=O bond vector for sp^2 hybridized oxygen atoms (see ***Figure 8.2.2***). This, somewhat complex, definition ensures that for both oxygen hybridization states, values of $|\phi|$ in the region of 120° indicate a close alignment of the [H...O] vector with the notional lone pair direction.

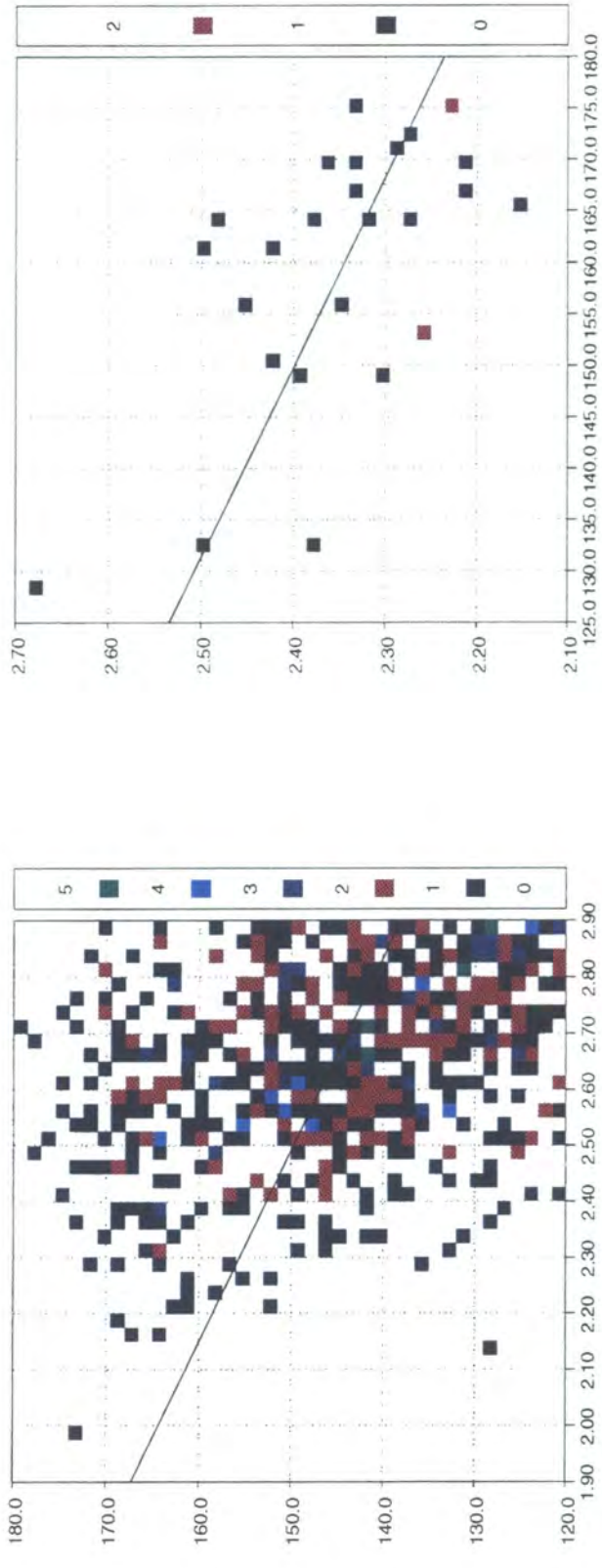

Figure 8.3.3 *- Plots of d(HO) versus ρ_H for a) C(r)-H and b) C(sp)-H donors.*

The values of $|\chi|$ for both the carbonyl and ether/alcohol acceptor groups (***Table 8.3.3***) are somewhat higher, in the range 20 - 36°, than might be expected for strong electrostatic interactions. However, contacts to ether/alcohol acceptors are clearly more planar than those to carbonyl acceptors, where $|\chi|$ only falls below 30° for the strongest C(sp)-H donors. By contrast, the values of $|\phi|$ (***Table 8.3.3***) are comparable for all of the donor/acceptor groups. The mean value of 138.6° is considerably higher than the expectation value of 120° but is consistent with similar data for O-H...O=C and N-H...O=C systems (Kennard, Taylor and Versichel, 1984; Allen, Bird and Rowland, 1996).

8.3.3 Cyclopropene as a C-H Donor

Version 5.09 of the CSDS contains only 46 examples of cyclopropene rings in 43 entries which also pass the secondary search criteria described in Chapter 6. Of these, 10 are benzocyclopropenes which have no C_1-H donors and do not contain any potential hydrogen bond acceptor groups. The remaining 36 rings contain between them a total of 6 potential C_1-H donors and 4 potential C_2-H donors. The geometries of the type A contacts formed by these donors are given in ***Table 8.3.4***

Only one of the C_1-H donors forms hydrogen bonds (PSMCPR in ***Table 8.3.4***) but both contacts are long and somewhat acute. This is unsurprising given that C_1-H is formally sp^3 hybridized and has a residual partial charge which is lower than that of the protons in propane (+0.104eV cf. +0.110eV). By contrast, all of the C_2-H donors present in the data set form hydrogen bonds. Only two of the contacts, those formed by TANHAR to nitro oxygen atoms, are especially long or acute. The remaining three contacts have good hydrogen bond geometries and mean bond distances that are comparable with the mean values obtained for the equivalent contact formed by alkynic C-H groups (2.31Å and 2.40Å cf. 2.30Å and 2.38Å). Clearly, cyclopropene, although rarely found, is a potent C-H hydrogen bond donor. This fact matches well the prediction, based on

crystallographic (Allen, 1982b) and theoretical evidence, that cyclopropenes have hydrogen bond donor properties more akin to those of alkynes than alkenes.

Table 8.3.4 *- Geometries of contacts of type* ***A*** *formed by cyclopropene donors. ([a]Beckhaus et. a.l., 1979; [b]Baird, Clegg and Hussein, 1988 ;[c]Dyrbusch et. al., 1988; [d]Carroll, Dailey and O'Bannon, 1991; [e]Frei et. al., 1979)*

Refcode	R	Acceptor	d(HX)	d(CX)	ρH
			C_1-H		
PSMCPR[a]	0.078	O(S=O)	2.75	3.00	92
PSMCPR[a]	0.078	O(S=O)	2.68	3.17	107
			C_2-H		
GATXEE[b]	0.054	O(C=O)	2.31	3.28	148
GIDHUW[c]	0.052	N(-N-)	2.38	3.36	151
TANHAR[d]	0.046	O(NO2)	2.66	3.42	126
TANHAR[d]	0.046	O(NO2)	2.83	3.17	98
TMSOCO[e]	0.037	O(C=O)	2.40	3.42	158

8.4 THREE MEMBERED RINGS AS π HYDROGEN BOND ACCEPTORS

8.4.1.1 Edge-on versus Face-on Contacts

Version 5.09 of the CSDS contains 41 fragments like the one depicted in ***Figure 8.2.3*** in 32 entries which also pass the secondary search criteria described in Chapter 6. Of these, 21 involve intramolecular contacts and 20 are intermolecular. Cyclopropane is the most common π acceptor with 30 contacts, followed by oxirane with 7 and aziridine with 4. The most common donor is O-H which participates in 31 contacts, the remaining 10 contacts involve N-H donors.

Figure 8.4.1 is a scatterplot of the distance from the approaching hydrogen atom, H, to the atom, Y, at the apex of the three membered ring; d(HY), versus the angle between the approaching hydrogen atom, H, the C-C bond midpoint, X_1, and the ring apex atom, Y; a(HX_1Y), for all 41 contacts. The plot is linear (correlation coefficient 0.945) and has three discrete clusters of points. The largest cluster, containing 25 points, occurs at approximately a(HX_1Y) = 180°and d(HY) > 4.0Å. A second smaller cluster, containing 13 points, occurs at around a(HX_1Y) = 60° and d(HY) < 2.8Å. Finally, there is a very small cluster of around 5 points which have intermediate values of a(HX_1Y) and d(HY).

Figure 8.4.1 is, in essence, a map of the interconversion pathway between the edge-on and face-on geometries described in Section 8.1.3. The large cluster of points at a(HX_1Y) angles close to 180° are the edge-on contacts depicted in ***Figure 8.1.1a.*** While the somewhat smaller cluster of points at a(HX_1Y) angles in the region of 60° to 90° are the face-on contacts shown in ***Figure 8.1.1b.*** The points at intermediate values can be thought of as distorted edge-on contacts, in which the donor atom has moved out of the ring plane but is still much closer to two of the ring carbon atoms than it is to the third. The edge-on contact is clearly the more common of the two bonding modes, confirming the predictions made in Section 8.1.3.

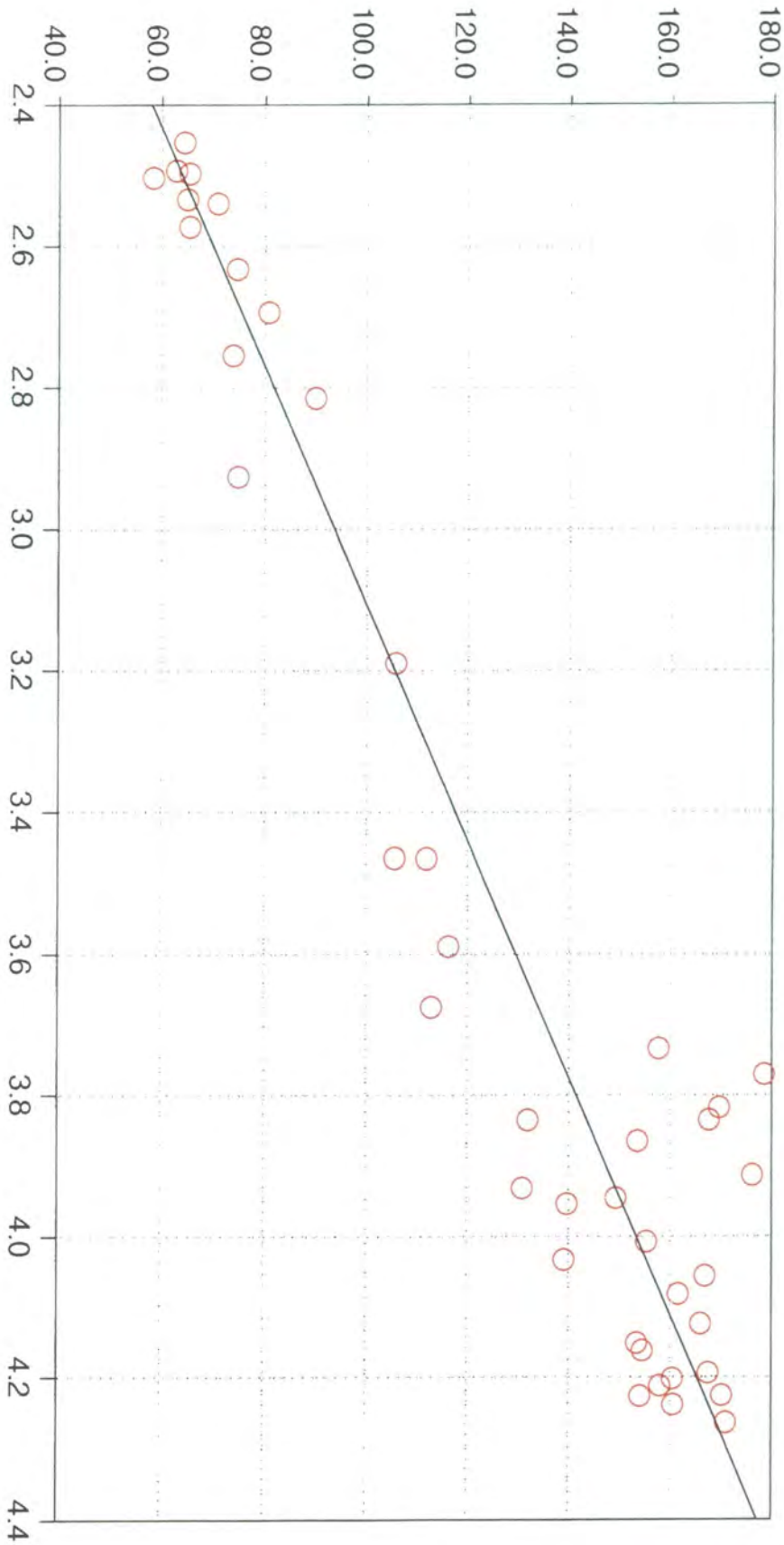

Figure 8.4.1 *- Scatterplot of d(HY) versus a(HX$_1$Y) for short X-H...π contacts.*

8.4.2 X-H...π Bond Geometries

Mean geometrical parameters for contacts in the two major clusters and for the minor cluster are shown in ***Table 8.4.1***. The mean contact distances, d, are the distance between H and X_1 for the edge-on contacts and the distance from H to X_2 for face-on contacts. These mean values, of 2.81(4)Å and 2.68(4)Å for the edge-on and face-on contacts respectively, are comparable to values cited in the recent literature for other types of X-H...π bond, for example the O-H...π(alkynic) bond in 2-ethynyladamantan-2-ol (2.258Å; Allen *et. al.*, 1996b) and the C-H...π bonds in acetylene and aromatic systems (Steiner, 1995a and b).

Table 8.4.1 - *Mean geometries of edge-on, intermediate and face-on X-H...π contacts.*

Parameter	Edge-on	Intermediate	Face-on
Nobs	23	5	13
d	2.81(4)	2.82(5)	2.68(4)
θ_1	158(3)	114(3)	111(3)
θ_2	102(2)	102(5)	84(1)
θ_3	78(2)	78(5)	76(2)

The X-H...π bond angles θ_1, θ_2 and θ_3 deviate somewhat from their expectation values of 180° for edge-on contacts and 90° for face-on contacts. Presumably, this is the result of asymmetry in the rings and some consequent distortion of the hydrogen bonds away from ideal geometry. However, despite these deviations, it is clear from an examination of contact distances alone that three membered rings can act as π hydrogen bond acceptors in both an edge-on and a face-on manner. This crystallographic evidence confirms speculation made, almost thirty years ago, on the basis of spectroscopic evidence (Gleiter, Joris and Schleyer, 1968).

8.5 CONCLUSIONS

This study provides clear evidence for the existence of C-H...O (and particularly C-H...O=C) hydrogen bonds in which the donor proton is attached to a saturated three membered carbocyclic or heterocyclic (N, O) ring. The relative frequencies of hydrogen bond formation and a comparison of the geometries of the contacts formed indicate that hydrogen bond strength increases in the order $C(sp^3)$-H...O < $C(sp^2)$-H...O ≈ C(r)-H...O << C(sp)-H...O. This result agrees well those obtained by others which have suggested that three membered rings have alkenic properties. It also matches the ordering expected on the basis of the partial charges on protons in each of the relavent systems derived using *ab initio* methods.

Although the number of relevant examples is small, there is evidence to suggest that cyclopropene is a potent C-H hydrogen bond donor, forming bonds which have strengths that approach those formed by alkynic C-H groups. Again, this result agrees with the previously observed alkynic properties of cyclopropenes.

Finally, the study confirms *crystallographically* that three membered rings can and do act as π hydrogen bond acceptors to both O-H and N-H groups. Geometrical data indicate that both the edge-on and face-on bonding modes proposed previously are observed. More edge-on contacts are located than face-on contacts consistent with the fact that the bent bonds in the strained three membered rings have local electron density maxima in the ring plane and outside the three interatomic vectors, thus attracting potential hydrogen bond donors to the ring bond mid-points.

8.6 REFERENCES

Al-Juaid, S. S., Al-Nasr, A. K. A., Eaborn, C. and Hitchcock, P. B. (1992) J. Organomet. Chem., **429**, C9.

Allen, F. H. (1980) Acta Crystallogr. B**36**, 81 - 96.

Allen, F. H. (1981) Acta Crystallogr. B**37**, 890 - 900.

Allen, F. H. (1982a) Tetrahedron, **38**, 2843 - 2853

Allen, F. H. (1982b) Tetrahedron, **38**, 645 - 653.

Allen, F. H., Bird, C. M. and Rowland, R. S. (1996) Acta Crystallogr. B, in preparation.

Allen, F. H., Howard, J. A. K., Hoy, V. J., Desiraju, G. R., Reddy, D. S. and Wilson, C. C. (1996b) J. Am. Chem. Soc., **118**, 4081 - 4084.

Allen, F. H., Lommerse, J. P. M., Howard, J. A. K., Hoy, V. J. and Desiraju,. G. R. (1996a) Acta Crystallogr. B**52**, 734 - 745.

Baird, M., Clegg, W. and Hussain, H. (1988) J. Chem. Res., 110 - 111.

Beckhaus, H., Kimura, M., Kojic-Prodic, B., Venier, C. and Watson, W. (1979), Acta Crystallogr. B**35**, 3119 - 3124.

Carroll, P., Dailey, W. and O'Bannon, P. (1991) Struct. Chem., **2**, 133 - 138.

Charlton, M. (1970) in *The Chemistry of Alkenes, Vol II* , ed. Zabicky, J., Interscience, London, pp. 511 - 610.

Chiou, D., Lin, S., Noble, L. and Okaya, Y. (1982) Acta Crystallogr. B**38**, 1669 - 1671.

Desiraju, G. R. (1989) J. Chem. Soc., Chem. Commun., 179 - 180.

Desiraju, G. R. (1990) J. Chem. Soc., Chem. Commun., 454 - 455.

Desiraju, G. R. (1991) Acc. Chem. Res., **24**, 290 - 296.

Desiraju, G. R., and Pedireddi, V. (1992) J. Chem. Soc., Chem. Commun., 988 - 990.

Dyrbush, M., Egert, E., Hupfeld, B., Kuper, S. and Schollkopf, U. (1988) Angew. Chem. (Int. Ed. Engl.), **27**, 433 - 435.

Frei, B., Jeger, O., Schweizer, W. and Wolf, H. (1979) Rec. Trav. Chim. Pays-Bas., **98**, 271 - 276.

Gleiter, R., Joris, L. and Schleyer, P. (1968) J. Am. Chem. Soc., **90**, 327 - 336.

Green, R. (1974) *Hydrogen Bonding by C-H Groups*, Wiley, New York.

Guest, M., Harrision, R., van Lenthe, J., Kendrick, J., Schoeffel, K. and Sherwood, P.(1993) *GAMESS-UK Users Guide and Reference Manual,* Computing for Science Ltd., Daresbury Laboratory, Warrington, U.K.

Hardy, A. D. U.and MacNicol, D. D. (1976) J. Chem. Soc., Perkin Trans. 2, 1140.

Hoffman, R. (1970) Tetrahedron Lett., **1**, 2907 - 2909.

Hoffman, R. and Stohrer, W. (1971) J. Am. Chem. Soc., **93**, 6941 - 6948.

Jeffrey, G. and Saenger, W. (1991) *Hydrogen Bonding in Biological Systems*, Springer-Verlag, Berlin.

Kennard, O., Taylor, R. and Verschiel, W. (1984) Acta Crystallogr. B**40**, 280.

Nakatsu, K., Yoshioka, H., Kunimoto, K., Kinugasa, T. and Ueji, S. (1978) Acta Crystallogr. B**34**, 2357 - 2359.

Nijveldt, D. and Vos, A. (1988a) Acta Crystallogr. B**44**, 281 - 288.

Nijveldt, D. and Vos, A. (1988b) Acta Crystallogr. B**44**, 289 - 295.

Nijveldt, D. and Vos, A. (1988c) Acta Crystallogr. B**44**, 296 - 301.

Rowland, R. S. and Taylor, R. (1996) J. Chem. Phys., **100**, 7384 - 7391.

Rzepa, H. S., Webb, M. L., Slawin, A. M. Z. and Williams, J. (1991), J. Chem. Soc., Chem. Commun., 765.

Steiner, T. (1995a) J. Chem. Soc., Chem. Commun., 95 - 97.

Steiner, T. (1995b) J. Chem. Soc., Perkin Trans. 2, 1321 - 1326.

Streitwieser, A. and Heathcock, C. H. (1981) *Introduction to Organic Chemistry, 2nd Edn.*, Macmillan, NewYork.

Taylor, R. and Kennard, O. (1982) J. Am. Chem. Soc., **104**, 5061 - 5070.

Ueji, S., Nakatsu, K., Yoshioka, H., Kunimoto, K., and Kinoshita, K. (1982) Tetrahedron Lett., **23**, 1173.

Viswamitra, M., Radhakrishnan, R., Bandekar, J. and Desiraju, G. R. (1993) J. Am. Chem. Soc., **115**, 4868 - 4869.

CHAPTER 9

Database Studies of Fluorine...Hydrogen Interactions in Mono-fluorinated Systems

9.1 INTRODUCTION

9.1.1 Fluorine as a Hydroxyl Mimic

In bio-organic chemistry hydrogen atoms and particularly hydroxyl groups are often replaced by fluorine atoms to generate the fluorinated analogues of a variety of naturally occuring and biologically active compounds. Such compounds are of interest because of their potential to act as drugs (see for example Taylor, 1988; Welch and Eswarakrishnan, 1991 and references cited therein) and their usefulness in probing the nature of enzyme substrate binding in certain systems (see for example Withers *et. al.*, 1988 and references cited therein).

Fluorine is often considered to be a suitable substitute for hydroxyl because it is a similar size to oxygen, the van der Waal's radii of F and O are 1.47Å and 1.52Å respectively (Bondi, 1964) and both functionalities have comparable electronegativities (Boyd and Edgecombe, 1988). However, the deoxyfluorinated analogues of substrates will only retain their activity if the fluorine atom can participate in the same enzyme binding interactions as the hydroxyl group.

Clearly, fluorine cannot fulfil the hydrogen bond donor role of hydroxyl since it lacks an acidic proton and in situations where substrate-O-H...X-enzyme interactions play a role in substrate binding, fluorine will not be an effective hydroxyl mimic. However, fluorine is generally thought to be able to act as a hydrogen bond acceptor and there are a number of examples of deoxyfluorinated analogues which do retain, or even enhance, the biological activity of the parent compound.

One such compound is 4-deoxy-4-fluoromuscarine (I) which binds to the muscarinic receptors in guinea pig heart tissue, which control heart rate, with an affinity which is an order or magnitude greater than that of muscarine itself (Bravo *et. al.*, 1992). Two other examples are the nucleotide deoxyfluorosugars UDP-4-deoxy-4-fluoro-α-D-galactose

(**II**) and UDP-4-deoxy-4-fluoro-α-D-glucose (**III**). Both analogues are found to bind to galactose 4-epimerase although they are not substrates for this enzyme because transient oxidation of the 4-hydroxyl group is a vital step in the epimerization mechanism. However, **III** is a substrate for bovine liver UDP-glucose dehydrogenase, to which it binds with a slightly greater affinity than UDP-glucose. Similarly, **II** is found to be a competitive inhibitor for UDP-glucose dehydrogenase as is the unfluorinated analogue, UDP-galactose (Chapeau and Frey, 1994).

All of the deoxyfluoro compounds described here are thought to retain their biological activity because the fluorine substituent mimics the hydrogen bond acceptor role of the hydroxyl group it replaces and forms F...H-X hydrogen bonds, which bind the substrate molecule to the appropriate receptor site on the enzyme.

9.1.2 Previous Database and Theoretical Analyses of F...H Interactions

F...H-X interactions have been studied previously using both database (Murray-Rust *et. al.*, 1983; Shimoni and Glusker, 1994) and theoretical techniques (Dixon and Smart, 1991).

Database evidence for F...H-X bonding is mixed. The results from a survey of intermolecular interactions in crystal structures led Murry-Rust *et. al.* (1983) to conclude that "... the C-F bond is capable of significant interactions with ... proton donors ...". However, in a recent study (Shimoni and Glusker, 1994) investigating F...H-C interactions in fluorinated hydrocarbons (ie. compounds containing only carbon, hydrogen and fluorine) only 18 compounds containing F...H-C contacts of less than 2.8Å were found. The mean F...H separation in these 18 examples is 2.6(1)Å which is close to the sum of the van der Waal's radii of fluorine and hydrogen (2.67Å: Bondi, 1964; 2.57Å: Rowland and Taylor, 1996). The mean F...H-C angle is 136°. When the analysis was extended to include compounds which also contain oxygen and nitrogen, the number of relevant structures present in the CSDS and thus the number of close F...H

contacts increased. However, the mean geometry of the F...H-X interactions in this second group of compounds is similar to that of the first (F...H = 2.5 - 2.6Å, F...H-C = 139 - 146°). Furthermore, of the 287 compounds present in the second group, only 7 contain F...H-X interactions involving acidic H-O or H-N protons. In the overwhelming majority of cases H-O and H-N protons form hydrogen bonds with oxygen and nitrogen acceptors and fluorine forms close contacts with less acidic C-H protons. Clearly, fluorine, despite its high electronegativity, is a poorer hydrogen bond acceptor than either oxygen or nitrogen.

The study by Shimoni and Glusker (1994) indicates that F...H and particularly F...H-O and F...H-N interactions are rare. However, examples of short (< 2.3Å) F...H interactions are found suggesting that they can be energetically favourable in certain systems. Theoretical studies of F...H bonds tend to support this view. *Ab initio* molecular orbtial calculations on the intramolecular F...H-O bonds in 2-fluoroethanol and 2-fluoroacetaldehyde enol (Dixon and Smart, 1991) yield attractive F...H-O bond energies of between 1.9 and 3.5 kcal mol^{-1} at equilibrium F...H seperations of between 2.3 and 2.5Å. These energies are comparable to those calculated for C-H...O bonds in a variety of model systems (1.0 - 3.2 kcal mol^{-1}: Rovira *et. al.*, 1995; van Mourik, 1994) and are around a quarter of the energy of a typical O-H...O bond (10.0 kcal mol^{-1}: Jeffrey and Saenger, 1991).

9.1.3 Aims

The evidence presented here indicates that short F...H contacts are rare and that fluorine is a poor hydrogen bond acceptor. However, theoretical calculations show that such interactions are attractive and the limited success of fluorine as a hydroxyl mimic in bio-organic systems suggests that F...H-X interactions can play a biological role. In order to assess the ability of fluorine to act as a hydrogen bond acceptor in a bio-organic context a comprehensive database survey of short F...H contacts in compounds containing mono-fluorinated carbon atoms and a suitable hydrogen bond donor was conducted. The results

of this survey were used to determine the conditions which favour the formation of short F...H-X contacts.

9.2 METHODOLOGY

Version 5.10 of the CSDS (October 1995 containing 146,272 entries) was used for this study and the general search procedure outlined in Chapter 6 was followed unless otherwise stated.

Preliminary searches were conducted to locate compounds containing the fragments depicted in ***Figure 9.2.1***. CF_2 and CF_3 groups were excluded from the search since interest was focused on determining the hydrogen bond accepting ability of the fluorine atom in mono-fluorinated functional groups where O is replaced by F and it was judged important not to make false comparisons. Hits were divided into two groups ($C(sp^3)$-F and $C(sp^2)$-F) according to the hybridization of the carbon atom to which the fluorine atom is bound. These two groups were further divided according to the nature of the hydrogen bond donor groups (C-H, O-H or N-H) present, generating six sub-sets of compounds; $C(sp^3)$-F...H-C, $C(sp^3)$-F...H-O, $C(sp^3)$-F...H-N, $C(sp^2)$-F...H-C, $C(sp^2)$-F...H-O and $C(sp^2)$-F...H-N. The numbers of compounds, donors and acceptors in the sub-sets are given in ***Table 9.2.1***.

Searches for inter- and intramolecular contacts between fluorine atoms and carbon, oxygen or nitrogen bound hydrogen atoms were conducted on the sub-sets of data obtained during the preliminary searches. The searches were restricted to short interactions of less than 2.35Å. No restriction was placed on the F...H-C/O/N angle. For each short contact located the F...H and F...C/N/O distances, D_1 and D_2, and the F...H-C/N/O angle, α, were determined (***Figure 9.2.2***). The numbers of inter- and intramolecular contacts located in each of the six sub-sets, along with the totals, are given in ***Table 9.2.2***.

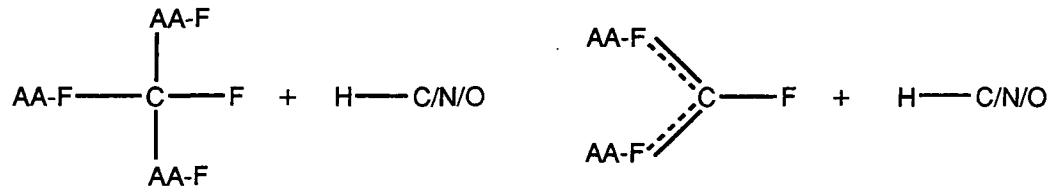

a) b)

Figure 9.2.1 *- Fragments used for preliminary searches of a) C(sp^3)-F and b) C(sp^2)-F containing compounds.*

Table 9.2.1 *- Numbers of compounds and potential F...H hydrogen bond donors and acceptors in each of the sub-sets of the preliminary search.*

C(sp^3)-F	n(COMPOUNDS)	n(C-F)	n(H-C/O/N)
O-H	71	89	132
N-H	69	85	100
C-H	177	237	2851
Total	177	237	-
C(sp^2)-F			
O-H	89	177	170
N-H	113	214	223
C-H	360	929	5080
Total	371	967	-

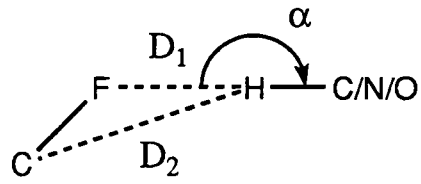

Figure 9.2.2 *- Parameters determined for each inter- and intramolecular F...H-C/N/O contact located.*

Table 9.2.2 *- Numbers of short inter- and intramolecular F...H contacts present in each of the six donor acceptor sub-sets.*

	Inter		Intra	
	n(COMPOUNDS)	n(CONTACTS)	n(COMPOUNDS)	n(CONTACTS)
$C(sp^3)$-F				
O-H	1	1	5	5
N-H	3	3	8	8
C-H	16	18	15	16
Total	20	22	28	29
$C(sp^2)$-F				
O-H	3	3	3	3
N-H	8	8	7	9
C-H	35	39	41	53
Total	45	50	48	65

9.3 FLUORINE AS A HYDROGEN BOND ACCEPTOR

9.3.1 F...H-X Bond Frequencies and Geometries

Comparison of the third and fourth columns of ***Table 9.2.1*** reveals that in all but one of the donor acceptor sub-sets the number of relevant donors exceeds the number of fluorine acceptors. The exception is the C(sp^2)-F...H-O sub-set in which the numbers of donors and acceptors are almost equal (170 cf. 177). In view of this the number of fluorine acceptors in each sub-set, rather than the number of donor groups, is assumed to represent the maximum number of F...H bonds which could occur, in subsequent analyses.

Table 9.2.2 shows that of the 1204 potential F...H contacts present in the dataset only 166 or 13.8% are observed. The majority of these involve carbon bound hydrogen atoms and only 28 contacts involving N-H donors and 12 involving O-H donors are found. These results are in good agreement with those obtained previously by Shimoni and Glusker (1994) and Murry-Rust *et. al.* (1983) and illustrate that O-H and N-H donors favour oxygen and nitrogen over fluorine in systems where both types of acceptor are present.

The numbers of inter- and intramolecular contacts in each of the donor acceptor sub-sets are similar although, in general, there are slightly fewer intermolecular contacts. The geometies of the inter- and intramolecular contacts are compared in ***Figure 9.3.1*** which are scattergrams of F...H contact distance, D_1, against F...H-X angle, α, for the C(sp^3)-F...H-N, C(sp^3)-F...H-O, C(sp^2)-F...H-N and C(sp^2)-F...H-O sub-sets. The intermolecular contacts are represented by red triangles and intramolecular contacts are represented by blue circles in these Figures. The scattergrams show that most of the intramolecular contacts have F...H-X angles which are close to 110° and which vary little with F...H distance. Whereas, the intermolecular contacts have F...H-X angles in the

range 120° to 180° and there is no discernable relationship between F...H-X angle and F...H distance.

The small F...H-X angles observed for the intramolecular contacts are due to conformational constraints. The geometries of the intermolecular F...H-X interactions are more typical of hydrogen bonds. However, the poor correlation between F...H-X bond lengths and inter-bond angles suggests that the interactions are rather weaker than O-H...O, O-H...N and similar hydrogen bonds.

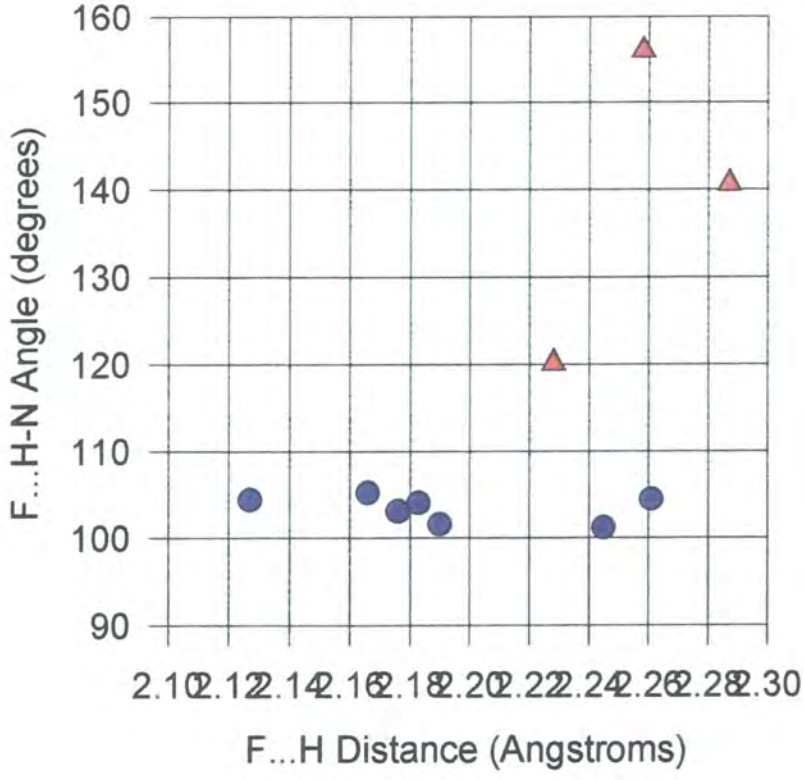
160
150
140
130
120
110
100
90
F...H-N Angle (degrees)
2.10
2.12
2.14
2.16
2.18
2.20
2.22
2.24
2.26
2.28
2.30
F...H Distance (Angstroms)

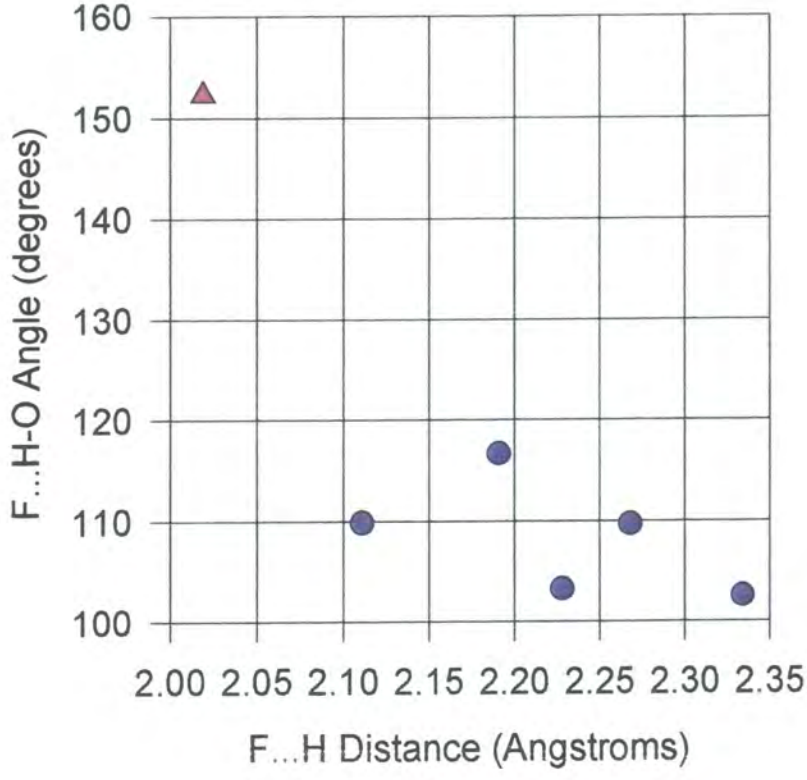
160
150
140
130
120
110
100
F...H-O Angle (degrees)
2.00
2.05
2.10
2.15
2.20
2.25
2.30
2.35
F...H Distance (Angstroms)

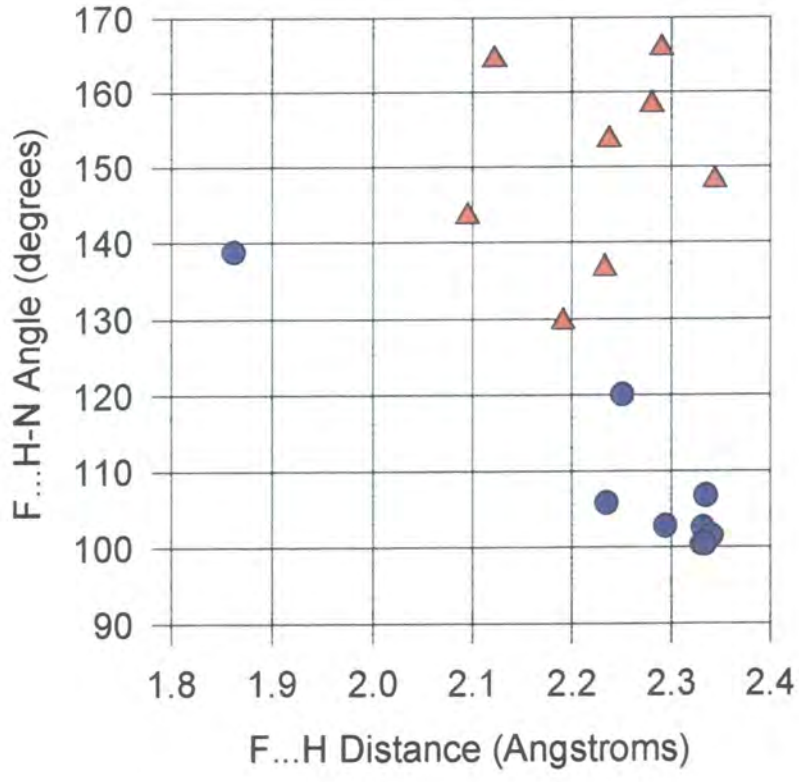

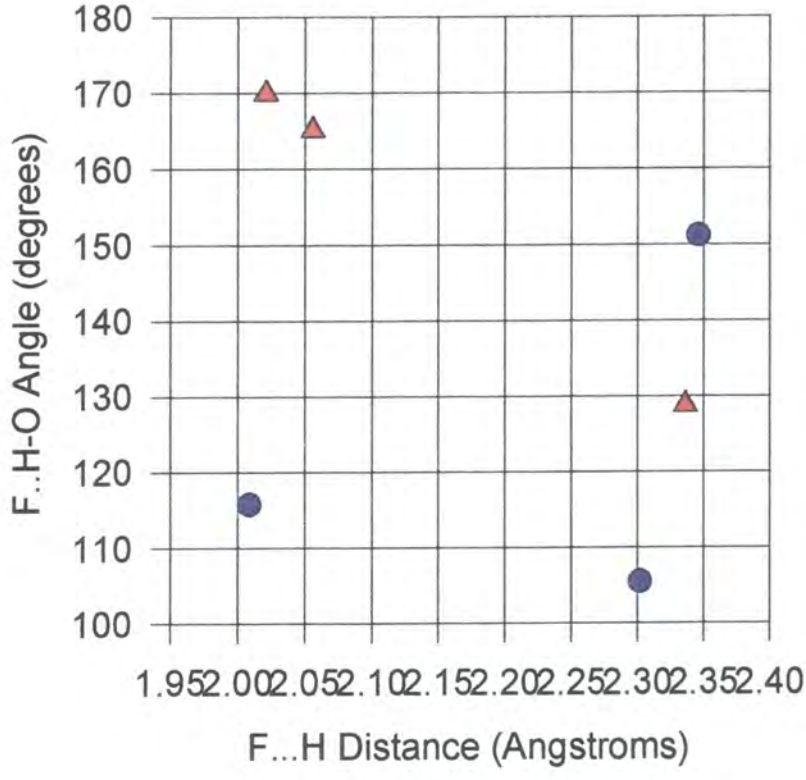

Figure 9.3.1 *- Scattergrams of D_1 versus α for short a) $C(sp^3)$-F...H-N, b) $C(sp^3)$-F...H-O, c) $C(sp^2)$-F...H-N and d) $C(sp^2)$-F...H-O.*

9.3.2 Comparison of the Acceptor Abilities $C(sp^3)$-F and $C(sp^2)$-F

The numbers of F...H-X contacts formed as percentages of the numbers of C-F bonds present in each donor acceptor sub-set are presented in ***Table 9.3.1***.

Table 9.3.1 - *Numbers of F...H-X contacts formed as percentages of the numbers of C-F groups available in each donor acceptor sub-set.*

Donor	$C(sp^3)$-F			$C(sp^2)$-F		
	n(C-F)	n(CONTS)	%	n(C-F)	n(CONTS)	%
O-H	89	6	6.74	177	6	3.39
N-H	85	11	12.94	214	17	7.94
C-H	237	34	14.35	929	92	9.90

Inspection of ***Table 9.3.1*** reveals that, although there are many more F...H-X contacts involving $C(sp^2)$-F acceptors, $C(sp^3)$-F acceptors form up to twice as many F...H-O and F...H-N contacts in real terms. The increase is smaller in the case of the C-H donors. However, $C(sp^3)$-F is clearly a better hydrogen bond acceptor than $C(sp^2)$-F in all three donor sub-sets. This observation is easily rationalised if the effects of conjugation are considered. The lone pairs on fluorine atoms bound to unsaturated carbon atoms, particularly the aromatic carbon atoms of which most of the $C(sp^2)$-F dataset is comprised, will tend to conjugate with the adjacent π system. This will reduce the δ^- charge on fluorine and as a result decrease the electrostatic stabilization of the $F^{\delta-}...H^{\delta+}$-X interaction making $C(sp^2)$-F...H-X less attractive than $C(sp^3)$-F...H-X.

Theoretical calculations on model $C(sp^3)$-F...H-O and $C(sp^2)$-F...H-O systems carried out by G.T. Smith, University of Durham, provide additional evidence to support this theory. *Ab initio* molecular orbital calculations were used to determine the energies of the F...H-O interactions in the fluoromethane...water dimer and the fluoroethene...water dimer (Howard *et. al.*, 1996). Both interactions were found to be stabilizing for F...H separations of between 1.5Å and 2.5Å. However, the F...H-O interaction present in the

fluoromethane system is almost twice the strength of the interaction in the fluoroethene system (2.38 kcal mol^{-1} cf. 1.48 kcal mol^{-1}). The additional stabilization energy in the fluoromethane...water dimer is due entirely to an increase in the electrostatic contribution to the F...H-O interaction energy compared with that of fluoroethene...water dimer.

Similar calculations were performed on the fluoromethane...methane dimer and the fluoroethene...methane dimer in order to compare the strength of F...H-O with that of the more common F...H-C. The F...H-C interactions in both of these dimers were found to have stabilizing energies of around 0.2 kcal mol^{-1} at an equilibrium F...H distance of 2.2Å. Clearly, F...H-C is much weaker than F...H-O indicating that the large numbers of short F...H-C interactions located using the CSDS are present because there are large numbers of C-H donors available and not because the interaction is energetically favoured. Indeed, the F...H-C interaction is so weak that it is best described as a van der Waal's interaction rather than a hydrogen bond.

9.4 CONCLUSIONS

This study shows that mono-fluorinated C-F groups can act as hydrogen bond acceptors in certain organic crystals. However, the majority of the short F...H-X contacts found involve C-H donors. Only a small number of F...H-O and F...H-N interactions are present. Analysis of these F...H-X contacts reveals that $C(sp^3)$-F acceptors form twice as many close contacts to O-H and N-H groups as $C(sp^2)$-F acceptors. This suggests that in a bio-organic context aliphatic fluorine atoms will be better hydroxyl mimics than vinyl and aryl fluorine atoms.

This conclusion is supported by the results of theoretical calculations. These show that both $C(sp^3)$-F...H-O and $C(sp^2)$-F...H-O interactions are stabilizing and have energies which are comparable to those of other weak hydrogen bonds. However, $C(sp^3)$-F...H-O is almost twice the strength of $C(sp^2)$-F...H-O. Similar calculations on F...H-C reveal that they are much weaker than F...H-O and are best described as van der Waal's interactions.

9.5 REFERENCES

Bondi, A. (1964) J. Chem. Phys., **68**, 441 - 451.

Boyd, R. J. and Edgecombe, K. E. (1988) J. Am. Chem. Soc., **110**, 4182.

Bravo, P., Resnati, G., Angeli, P., Frigerio, M., Viani, F, Arnone, A., Marucci, G. and Cantalamessa, F. (1992) J. Med. Chem., **35**, 3102 - 3110.

Chapeau, M-C. and Frey, P. A. (1994) J. Org. Chem., **59**, 6994 - 6998.

Dixon, D. A. and Smart, B. E. (1991) J. Phys. Chem., **95**, 1609 - 1612.

Howard, J. A. K., Hoy, V. J., O'Hagan, D. and Smith, G. T. (1996) Tetrahedron, **52**, 12613 - 12622.

Jeffrey, G. A. and Saenger, W. (1991) *Hydrogen Bonding in Biological Structures*, Springer-Verlag, Berlin.

Murry-Rust, P, Stallings, W. C., Monti, C. T., Preston, R. K. and Glusker, J. P. (1983) J. Am. Chem. Soc., **105**, 3206.

Rovira, M. C., Novoa, J. J., Whangbo, M-H. and Williams, J. M. (1995) Chem. Phys., **200**, 319 - 335.

Rowland, R. S. and Taylor, R. (1996) J. Chem. Phys., **100**, 7384 - 7391.

Shimoni, L. and Glusker, J. P. (1994) Struct. Chem., **5**, 383 - 397.

Taylor, N. F. (1988) *Fluorinated Carbohydrates, Chemical and Biochemical Aspects*, ACS Symposium Series 374, American Chemical Society, Washington D.C.

van Mourik, T. (1994) *Correlated ab initio Calculations on Weakly Bonded Systems*, Ph.D. thesis, University of Utrecht, pp. 93 - 114.

Welch, J. T. and Eswarakrishnan, S. (1991) *Fluorine in Bioorganic Chemistry*, J. Wiley and Sons, New York.

Withers, S.G., Street, I. P. and Percival, M. D. (1988) *Fluorinated Carbohydrates*, 59 - 77, ACS Symposium Series 374, American Chemical Society, Washington D.C.

APPENDIX A

Atomic Coordinates and Anisotropic Displacement Parameters for the Structures in Chapters 3, 4 and 5

Table A.3.1 *- Atomic coordinates and equivalent isotropic displacement parameters ($Å^2$ x 10^3) for 3,5-dinitrocinnamic acid.*

	x	y	z	U(eq)
C(1)	7561(1)	153(2)	225(1)	8(1)
C(2)	7343(1)	915(2)	966(1)	10(1)
C(3)	7943(1)	958(2)	1649(1)	9(1)
C(4)	8761(1)	283(2)	1649(1)	10(1)
C(5)	8957(1)	-449(2)	904(1)	11(1)
C(6)	8380(1)	-522(2)	186(1)	10(1)
C(7)	6975(1)	120(2)	-549(1)	10(1)
C(8)	6126(1)	354(2)	-592(1)	10(1)
C(9)	5633(1)	381(2)	-1418(1)	11(1)
N(1)	7721(1)	1784(2)	2418(1)	13(1)
N(2)	9810(1)	-1186(2)	860(1)	16(1)
O(1)	4796(2)	351(4)	-1391(2)	21(1)
O(2)	5977(2)	466(3)	-2071(2)	20(1)
O(3)	8219(2)	1668(3)	3043(2)	22(1)
O(4)	7049(2)	2538(4)	2397(2)	27(1)
O(5)	10322(2)	-1055(5)	1469(2)	36(1)
O(6)	9962(2)	-1884(3)	213(2)	16(1)
H(2)	9227(3)	300(6)	2202(3)	30(1)
H(1)	6698(3)	1478(6)	1012(3)	30(1)
H(6)	4509(3)	410(6)	-1964(4)	28(1)
H(3)	8571(3)	-1101(6)	-380(3)	28(1)
H(5)	5771(4)	492(7)	-52(3)	34(1)
H(4)	7268(3)	-98(7)	-1105(4)	34(1)

Table A.3.2 *- Anisotropic displacement parameters ($Å^2 \times 10^3$) for 3,5-dinitrocinnamic acid.*

	U11	U22	U33	U23	U13	U12
C(1)	9(1)	8(1)	7(1)	-1(1)	2(1)	0(1)
C(2)	12(1)	10(1)	8(1)	1(1)	0(1)	-1(1)
C(3)	12(1)	8(1)	8(1)	1(1)	2(1)	0(1)
C(4)	11(1)	9(1)	9(1)	0(1)	-3(1)	0(1)
C(5)	8(1)	11(1)	14(1)	2(1)	-1(1)	1(1)
C(6)	9(1)	12(1)	10(1)	-1(1)	1(1)	1(1)
C(7)	9(1)	13(1)	7(1)	0(1)	0(1)	1(1)
C(8)	10(1)	12(1)	8(1)	2(1)	1(1)	2(1)
C(9)	11(1)	12(1)	11(1)	1(1)	0(1)	0(1)
N(1)	18(1)	13(1)	10(1)	-1(1)	3(1)	-2(1)
N(2)	12(1)	15(1)	21(1)	-1(1)	0(1)	3(1)
O(1)	16(1)	33(1)	15(1)	3(1)	4(1)	0(1)
O(2)	13(1)	30(1)	16(1)	1(1)	0(1)	0(1)
O(3)	28(1)	26(1)	11(1)	0(1)	4(1)	1(1)
O(4)	28(2)	32(1)	20(2)	-8(1)	3(1)	6(1)
O(5)	24(2)	45(2)	36(2)	-6(2)	-6(1)	12(1)
O(6)	15(1)	15(1)	19(1)	-1(1)	2(1)	3(1)
H(2)	29(2)	32(2)	27(3)	-1(2)	-6(2)	2(2)
H(1)	26(2)	32(2)	31(3)	-3(2)	-2(2)	7(2)
H(6)	23(2)	33(2)	27(3)	2(2)	0(2)	-1(2)
H(3)	26(2)	35(2)	25(3)	-7(2)	8(2)	2(2)
H(5)	31(3)	51(3)	22(3)	-3(2)	4(2)	3(2)
H(4)	24(3)	51(3)	27(3)	-1(2)	4(2)	4(2)

Table A.3.3- *Atomic coordinates and equivalent isotropic displacement parameters ($Å^2$ x 10^3) for 2-ethynyladamantan-2-ol.*

	x	y	z	U(eq)
O(1')	977(5)	5929(2)	3385(3)	11(1)
C(2')	1240(4)	6497(1)	2919(2)	7(1)
C(1')	1799(5)	6436(2)	1748(2)	10(1)
C(10')	1983(6)	7053(2)	1250(3)	13(1)
C(5')	-14(6)	7386(2)	1266(3)	16(1)
C(6')	-1643(6)	7030(2)	635(3)	21(1)
C(7')	-1820(5)	6410(2)	1131(3)	15(1)
C(9')	-2363(5)	6477(2)	2285(3)	14(1)
C(3')	-752(5)	6837(2)	2921(3)	10(1)
C(4')	-558(6)	7452(2)	2416(3)	16(1)
C(8')	173(6)	6078(2)	1114(3)	14(1)
C(11')	2812(5)	6820(2)	3563(3)	13(1)
C(12')	4114(6)	7064(2)	4096(3)	22(1)
O(1)	4602(5)	5321(2)	3502(3)	10(1)
C(2)	4318(4)	4690(1)	3364(2)	6(1)
C(1)	3366(4)	4598(2)	2227(2)	8(1)
C(4)	5940(5)	3681(2)	3256(3)	13(1)
C(5)	4995(5)	3596(2)	2127(3)	13(1)
C(6)	6377(5)	3844(2)	1325(3)	15(1)
C(7)	6744(5)	4510(2)	1533(3)	11(1)
C(8)	4757(5)	4845(2)	1423(3)	11(1)
C(3)	6309(4)	4349(2)	3480(2)	9(1)
C(10)	3000(5)	3935(2)	2017(3)	12(1)
C(9)	7703(5)	4592(2)	2664(3)	11(1)
C(11)	2962(5)	4482(2)	4155(2)	9(1)
C(12)	1812(5)	4343(2)	4800(3)	16(1)
H(13')	2223(11)	5719(4)	3461(7)	24(2)
H(1')	3224(11)	6203(4)	1746(7)	25(2)
H(10')	2389(14)	7010(4)	426(6)	32(2)
H(102)	3168(13)	7302(4)	1675(7)	29(2)
H(5')	129(18)	7828(5)	909(10)	48(3)
H(6')	-1279(17)	6989(5)	-198(7)	39(2)

H(62)	-3048(16)	7273(5)	647(9)	43(2)
H(7')	-2948(14)	6143(5)	675(8)	36(2)
H(9')	-2572(14)	6046(4)	2646(8)	30(2)
H(92)	-3785(12)	6722(5)	2312(8)	35(2)
H(3')	-1133(13)	6881(4)	3750(7)	29(2)
H(4')	558(14)	7718(4)	2875(7)	32(2)
H(42)	-1974(14)	7688(5)	2432(8)	39(2)
H(8')	37(14)	5636(4)	1448(7)	32(2)
H(82)	614(16)	6024(5)	308(7)	36(2)
H(12')	5254(20)	7263(7)	4566(9)	56(3)
H(13)	5493(12)	5396(4)	4110(6)	26(2)
H(1)	1943(10)	4840(4)	2165(6)	23(2)
H(4)	7351(14)	3446(4)	3349(8)	33(2)
H(41)	4965(15)	3493(4)	3838(7)	35(2)
H(5)	4747(14)	3125(4)	1990(8)	32(2)
H(6)	7781(13)	3596(4)	1390(7)	32(2)
H(61)	5737(14)	3777(4)	515(7)	30(2)
H(7)	7753(12)	4699(4)	957(7)	28(2)
H(8)	4061(13)	4775(4)	626(6)	29(2)
H(81)	5019(14)	5318(4)	1536(7)	30(2)
H(3)	6990(12)	4407(4)	4290(6)	26(2)
H(10)	2291(14)	3877(4)	1227(7)	32(2)
H(101)	1983(12)	3750(4)	2566(7)	26(2)
H(9)	9098(11)	4346(5)	2773(7)	31(2)
H(91)	8037(12)	5055(4)	2821(7)	29(2)
H(12)	799(13)	4228(5)	5378(7)	33(2)

Table A.3.4 *- Anisotropic displacement parameters ($Å^2 \times 10^3$) for 2-ethynyladamantan-2-ol.*

	U11	U22	U33	U23	U13	U12
O(1')	9(1)	11(2)	12(1)	5(1)	1(1)	-2(1)
C(2')	6(1)	5(1)	9(1)	0(1)	1(1)	0(1)
C(1')	7(1)	12(2)	9(1)	-1(1)	1(1)	1(1)
C(10')	19(2)	10(2)	11(1)	3(1)	2(1)	-4(1)
C(5')	16(2)	12(2)	21(2)	5(1)	-2(1)	1(1)
C(6')	19(2)	23(2)	18(2)	6(1)	-10(1)	0(2)
C(7')	11(1)	19(2)	14(1)	1(1)	-7(1)	-5(1)
C(9')	7(1)	16(2)	19(2)	2(1)	2(1)	-1(1)
C(3')	6(1)	9(2)	13(1)	0(1)	1(1)	3(1)
C(4')	16(2)	10(2)	20(2)	-1(1)	1(1)	4(1)
C(8')	17(2)	12(2)	12(1)	-2(1)	0(1)	-1(1)
C(11')	13(2)	16(2)	9(1)	-1(1)	-1(1)	-1(1)
C(12')	21(2)	26(2)	17(2)	-3(1)	-6(1)	-10(2)
H(13')	19(3)	25(4)	29(4)	1(3)	0(3)	1(3)
H(1')	14(3)	29(4)	33(4)	-6(3)	5(3)	6(3)
H(10')	35(4)	45(6)	17(3)	4(3)	5(3)	-5(4)
H(102)	27(4)	31(4)	30(4)	2(3)	-5(3)	-11(3)
H(5')	50(6)	34(6)	57(7)	24(5)	-15(5)	-4(5)
H(6')	56(6)	36(5)	24(4)	9(3)	-5(4)	-7(5)
H(62)	33(5)	39(6)	56(6)	16(5)	-11(5)	4(4)
H(7')	26(4)	43(6)	36(4)	2(4)	-18(4)	-13(4)
H(9')	27(4)	27(4)	38(4)	2(3)	8(3)	-5(3)
H(92)	16(3)	39(5)	51(6)	-4(4)	6(4)	6(3)
H(3')	27(4)	32(5)	29(4)	-5(3)	11(3)	-1(3)
H(4')	37(5)	25(4)	33(4)	-7(3)	0(4)	-8(4)
H(42)	32(5)	35(5)	49(6)	11(4)	-1(4)	24(4)
H(8')	39(5)	22(4)	34(4)	-2(3)	2(4)	-5(4)
H(82)	46(5)	41(6)	21(4)	-14(4)	9(4)	-4(4)
H(12')	56(7)	72(9)	38(5)	-3(5)	-20(5)	-21(7)
O(1)	10(1)	8(2)	12(1)	-1(1)	1(1)	1(1)
C(2)	4(1)	7(1)	6(1)	0(1)	1(1)	1(1)
C(1)	6(1)	10(1)	8(1)	0(1)	0(1)	1(1)

C(4)	14(1)	11(2)	13(1)	3(1)	2(1)	4(1)
C(5)	15(2)	9(2)	17(1)	-4(1)	5(1)	0(1)
C(6)	13(2)	18(2)	15(1)	-4(1)	4(1)	3(1)
C(7)	8(1)	15(2)	11(1)	0(1)	3(1)	0(1)
C(8)	11(1)	13(2)	9(1)	3(1)	3(1)	0(1)
C(3)	4(1)	13(2)	9(1)	0(1)	-2(1)	2(1)
C(10)	9(1)	14(2)	14(1)	-5(1)	1(1)	-2(1)
C(9)	5(1)	13(2)	16(1)	2(1)	4(1)	0(1)
C(11)	9(1)	12(2)	7(1)	0(1)	2(1)	0(1)
C(12)	13(1)	23(2)	11(1)	1(1)	5(1)	-3(1)
H(13)	25(3)	21(4)	30(4)	-12(3)	-9(3)	-2(3)
H(1)	13(3)	31(4)	24(3)	1(3)	0(2)	9(3)
H(4)	29(4)	28(4)	41(5)	3(4)	-1(4)	15(4)
H(41)	42(5)	32(5)	33(4)	7(4)	11(4)	-4(4)
H(5)	32(4)	20(4)	44(5)	-2(3)	7(4)	-4(3)
H(6)	27(4)	32(5)	38(4)	-4(4)	9(3)	13(3)
H(61)	33(4)	35(5)	23(4)	-10(3)	5(3)	-7(4)
H(7)	25(4)	32(5)	28(4)	3(3)	13(3)	-2(3)
H(8)	32(4)	37(5)	18(3)	3(3)	-3(3)	1(4)
H(81)	33(4)	22(4)	36(4)	5(3)	3(3)	-2(3)
H(3)	26(4)	33(5)	18(3)	-5(3)	-1(3)	1(3)
H(10)	30(4)	38(5)	28(4)	-8(3)	-5(3)	-4(4)
H(101)	24(4)	25(4)	31(4)	0(3)	10(3)	-10(3)
H(9)	13(3)	44(5)	37(4)	1(4)	2(3)	10(3)
H(91)	23(4)	26(4)	37(4)	3(3)	3(3)	-9(3)
H(12)	27(4)	47(6)	25(4)	6(4)	10(3)	-2(4)

Table A.4.1 *- Atomic coordinates and equivalent isotropic displacement parameters ($Å^2 \times 10^3$) for 2-aminophenol.*

	x	y	z	U(eq)
C(2)	1098(1)	9212(2)	7906(1)	7(1)
C(1)	679(1)	10523(2)	7064(1)	7(1)
C(6)	940(1)	11567(2)	5710(2)	11(1)
C(5)	1613(1)	11319(2)	5164(2)	13(1)
C(4)	2032(1)	10030(2)	6000(2)	12(1)
C(3)	1771(1)	8982(2)	7368(2)	10(1)
O(7)	24(1)	10673(2)	7636(2)	10(1)
N(8)	803(1)	8077(1)	9193(1)	9(1)
H(3)	2083(2)	7941(6)	8004(5)	28(1)
H(8B)	497(2)	8791(6)	10025(4)	25(1)
H(7)	-250(2)	11530(5)	6892(4)	21(1)
H(8A)	1159(2)	7352(6)	9880(4)	27(1)
H(6)	612(2)	12539(6)	5057(5)	29(1)
H(4)	2556(2)	9801(7)	5597(5)	31(1)
H(5)	1807(2)	12124(6)	4097(5)	32(1)

Table A.4.2 *- Anisotropic displacement parameters ($Å^2 \times 10^3$) for 2-aminophenol.*

	U11	U22	U33	U23	U13	U12
C(2)	7(1)	7(1)	7(1)	1(1)	-1(1)	0(1)
C(1)	9(1)	6(1)	7(1)	1(1)	0(1)	1(1)
C(6)	11(1)	11(1)	10(1)	4(1)	2(1)	1(1)
C(5)	12(1)	13(1)	13(1)	3(1)	4(1)	0(1)
C(4)	9(1)	13(1)	14(1)	1(1)	2(1)	-1(1)
C(3)	7(1)	12(1)	10(1)	0(1)	-1(1)	1(1)
O(7)	9(1)	12(1)	10(1)	3(1)	2(1)	2(1)
N(8)	11(1)	10(1)	7(1)	2(1)	0(1)	0(1)
H(3)	24(2)	29(2)	29(1)	7(1)	-4(1)	9(1)
H(8B)	26(2)	27(2)	21(1)	0(1)	10(1)	6(1)
H(7)	17(1)	27(2)	19(1)	6(1)	1(1)	9(1)
H(8A)	21(1)	37(2)	24(1)	12(1)	-6(1)	4(1)
H(6)	26(2)	27(2)	34(2)	19(1)	3(1)	9(1)
H(4)	16(1)	41(2)	35(2)	2(2)	9(1)	4(1)
H(5)	30(2)	35(2)	31(2)	19(1)	15(1)	1(1)

Table A.4.3 *- Atomic coordinates and equivalent isotropic displacement parameters ($Å^2 \times 10^3$) for 3-aminophenol.*

	x	y	z	U(eq)
C(2)	-657(2)	3777(3)	947(3)	12(1)
C(1)	188(2)	2701(4)	1927(3)	13(1)
C(3)	-1777(2)	2817(3)	674(3)	12(1)
C(6)	-95(2)	701(4)	2675(3)	15(1)
C(5)	-1209(2)	-264(4)	2370(3)	18(1)
C(4)	-2046(2)	786(4)	1363(3)	16(1)
N(8)	-2659(1)	3987(3)	-211(2)	16(1)
O(7)	1291(2)	3575(4)	2197(4)	16(1)
H(2)	-451(5)	5359(8)	403(6)	28(1)
H(6)	558(5)	-94(11)	3450(8)	36(1)
H(5)	-1430(6)	-1850(9)	2917(8)	37(1)
H(4)	-2913(5)	21(10)	1146(9)	34(1)
H(7)	1565(4)	4503(9)	1259(6)	26(1)
H(8B)	-2291(5)	5025(10)	-1050(7)	31(1)
H(8A)	-3226(5)	2955(11)	-815(7)	34(1)

Table A.4.4 *- Anisotropic displacement parameters ($Å^2 \times 10^3$) for 3-aminophenol.*

	U11	U22	U33	U23	U13	U12
C(2)	10(1)	14(1)	12(1)	2(1)	0(1)	1(1)
C(1)	11(1)	14(1)	14(1)	0(1)	0(1)	0(1)
C(3)	11(1)	13(1)	12(1)	-2(1)	2(1)	-3(1)
C(6)	14(1)	14(1)	16(1)	6(1)	2(1)	3(1)
C(5)	17(1)	15(1)	20(1)	3(1)	5(1)	0(1)
C(4)	14(1)	16(1)	17(1)	-1(1)	3(1)	-4(1)
N(8)	13(1)	22(1)	13(1)	-1(1)	0(1)	0(1)
O(7)	12(1)	19(1)	18(1)	2(1)	-1(1)	-1(1)
H(2)	33(2)	22(2)	30(3)	8(2)	-4(2)	-4(2)
H(6)	26(2)	39(3)	42(3)	14(3)	-6(3)	6(2)
H(5)	39(3)	26(2)	46(3)	15(3)	3(3)	-8(2)
H(4)	24(2)	34(2)	46(3)	3(3)	-1(3)	-11(2)
H(7)	22(2)	31(2)	25(2)	9(2)	-3(2)	-6(2)
H(8B)	23(2)	46(3)	25(2)	8(3)	1(2)	1(2)
H(8A)	29(2)	40(3)	34(2)	-9(3)	-14(3)	-1(2)

Table A.5.1 *- Atomic coordinates and equivalent isotropic displacement parameters ($Å^2 \times 10^3$) for* ***II****.*

	x	y	z	Ueq
I(1)	8417(1)	5000	6774(1)	26(1)
O(1)	8289(3)	3897(4)	1892(3)	37(1)
N(1)	7735(4)	5000	1583(4)	27(1)
C(1)	5682(2)	6233(4)	5367(4)	25(1)
C(2)	6341(5)	5000	5719(5)	21(1)
C(4)	5673(3)	3755(3)	405(3)	25(1)
C(5)	6294(5)	5000	785(5)	22(1)

Table A.5.2 *- Anisotropic displacement parameters ($Å^2 \times 10^3$) for* ***II****.*

	U11	U22	U33	U23	U13	U12
I(1)	19(1)	35(1)	22(1)	0	-2(1)	0
O(1)	30(2)	39(2)	41(1)	1(1)	-1(1)	8(1)
N(1)	26(2)	38(3)	16(2)	0	-4(2)	0
C(1)	25(2)	22(2)	28(1)	-2(1)	-3(1)	1(2)
C(2)	19(2)	26(3)	17(2)	0	2(2)	0
C(4)	27(2)	22(2)	26(1)	1(1)	-2(1)	6(2)
C(5)	19(2)	30(3)	15(2)	0	-4(2)	0

Table A.5.3 *- Atomic coordinates and equivalent isotropic displacement parameters ($Å^2$ x 10^3) for* ***III****.*

	x	y	z	U(eq)
I(1)	2440(1)	1451(1)	-8446(1)	23(1)
O(1)	2188(3)	9352(2)	-3075(3)	34(1)
O(2)	3230(3)	7336(3)	-659(3)	33(1)
C(4)	2453(3)	3555(3)	-6412(3)	18(1)
N(1)	2685(3)	7755(2)	-2414(3)	23(1)
C(1)	2604(3)	6285(2)	-3810(3)	18(1)
C(6)	1844(3)	6794(3)	-5752(3)	23(1)
C(2)	3281(3)	4466(3)	-3119(3)	21(1)
C(3)	3204(3)	3072(3)	-4444(3)	21(1)
C(5)	1771(3)	5396(3)	-7075(3)	22(1)

Table A.5.4 *- Anisotropic displacement parameters ($Å^2$ x 10^3) for* ***III****.*

	U11	U22	U33	U23	U13	U12
I(1)	24(1)	23(1)	22(1)	-7(1)	3(1)	-11(1)
O(1)	45(1)	19(1)	39(1)	-2(1)	-4(1)	-15(1)
O(2)	45(1)	36(1)	23(1)	-5(1)	-2(1)	-22(1)
C(4)	18(1)	18(1)	18(1)	-3(1)	2(1)	-8(1)
N(1)	24(1)	22(1)	24(1)	-4(1)	3(1)	-11(1)
C(1)	18(1)	17(1)	20(1)	-2(1)	1(1)	-9(1)
C(6)	29(1)	18(1)	21(1)	2(1)	-2(1)	-9(1)
C(2)	25(1)	20(1)	17(1)	2(1)	-3(1)	-9(1)
C(3)	26(1)	18(1)	20(1)	1(1)	-2(1)	-9(1)
C(5)	27(1)	20(1)	18(1)	2(1)	-3(1)	-9(1)

Table A.5.5 *- Atomic coordinates and equivalent isotropic displacement parameters ($Å^2 \times 10^3$) for **IV**.*

	x	y	z	U(eq)
I(1)	764(1)	3866(1)	3019(1)	52(1)
N(1)	2330(6)	8434(5)	5688(5)	53(1)
O(3)	9664(4)	8922(4)	1039(4)	55(1)
O(4)	7641(4)	9852(4)	-403(4)	55(1)
C(1)	2711(5)	5044(5)	2495(4)	37(1)
C(6)	2168(6)	5966(5)	1682(5)	45(1)
O(1)	2863(5)	7857(5)	6615(5)	75(1)
C(2)	4551(6)	4909(6)	2976(6)	46(1)
O(2)	697(5)	8373(5)	5023(5)	83(1)
C(11)	3148(6)	10101(5)	4449(5)	48(1)
C(4)	5321(6)	6616(5)	1817(4)	37(1)
C(12)	4456(6)	10860(5)	4114(5)	46(1)
C(10)	3714(6)	9251(5)	5324(5)	40(1)
C(9)	8028(6)	9081(5)	427(5)	42(1)
C(8)	6490(6)	8347(5)	707(5)	45(1)
C(5)	3473(6)	6735(5)	1336(5)	43(1)
C(3)	5834(6)	5703(5)	2638(5)	44(1)
C(7)	6747(6)	7443(5)	1499(5)	42(1)

Table A.5.6 *- Anisotropic displacement parameters ($Å^2 \times 10^3$) for **IV**.*

	U11	U22	U33	U23	U13	U12
I(1)	50(1)	53(1)	65(1)	28(1)	31(1)	4(1)
N(1)	54(3)	45(2)	68(3)	24(2)	30(2)	6(2)
O(3)	39(2)	78(2)	68(2)	50(2)	22(2)	11(2)
O(4)	44(2)	76(2)	68(2)	53(2)	21(2)	14(2)
C(1)	38(2)	36(2)	41(2)	15(2)	20(2)	5(2)
C(6)	35(2)	53(3)	53(3)	27(2)	16(2)	10(2)
O(1)	77(3)	83(3)	93(3)	60(2)	40(2)	11(2)
C(2)	47(3)	49(3)	56(3)	33(2)	22(2)	14(2)
O(2)	45(2)	99(3)	135(4)	73(3)	39(2)	16(2)
C(11)	35(2)	51(3)	58(3)	25(2)	16(2)	10(2)
C(4)	41(2)	35(2)	37(2)	17(2)	15(2)	6(2)
C(12)	45(3)	48(3)	51(3)	30(2)	14(2)	8(2)
C(10)	43(2)	33(2)	45(2)	16(2)	20(2)	4(2)
C(9)	40(2)	46(3)	44(2)	21(2)	18(2)	6(2)
C(8)	36(2)	54(3)	51(3)	28(2)	17(2)	9(2)
C(5)	41(2)	46(3)	51(3)	27(2)	18(2)	11(2)
C(3)	34(2)	54(3)	54(3)	29(2)	20(2)	11(2)
C(7)	36(2)	46(3)	46(3)	21(2)	17(2)	8(2)

Table A.5.7 *- Atomic coordinates and equivalent isotropic displacement parameters ($Å^2$) for* ***V****.*

	x	y	z	Ueq
C(1)	-1.4354(3)	-0.6912(3)	1.2019(3)	0.024(1)
N(1)	-1.5504(3)	-0.7454(3)	1.1589(3)	0.032(1)
C(2)	-1.2981(3)	-0.6287(3)	1.4389(3)	0.023(1)
N(2)	-1.3055(3)	-0.6300(3)	1.5863(3)	0.033(1)
C(3)	-1.2878(3)	-0.6251(3)	1.2524(3)	0.021(1)
C(4)	-1.1454(3)	-0.5631(3)	1.1278(3)	0.020(1)
C(5)	-1.1414(3)	-0.5616(3)	0.9422(3)	0.020(1)
C(6)	-0.9967(3)	-0.4988(3)	1.1792(3)	0.021(1)
I(7)	-0.2210(1)	-0.1304(1)	0.4303(1)	0.028(1)
C(7)	-0.0870(3)	-0.0497(3)	0.1707(3)	0.022(1)
C(8)	-0.1749(3)	-0.0487(3)	0.0279(3)	0.025(1)
C(9)	0.0857(3)	-0.0024(3)	0.1450(3)	0.024(1)

Table A.5.8 *- Anisotropic displacement parameters ($Å^2$) for* ***V****.*

	U11	U22	U33	U12	U13	U23
C(1)	0.0252(12)	0.0248(11)	0.0210(12)	-0.0012(9)	0.0001(10)	-0.0047(10)
N(1)	0.0253(11)	0.0419(12)	0.0323(12)	-0.0064(9)	-0.0050(9)	-0.0104(10)
C(2)	0.0214(12)	0.0224(11)	0.0267(13)	-0.0042(8)	-0.0031(9)	-0.0053(9)
N(2)	0.0367(12)	0.0393(12)	0.0238(12)	-0.0071(9)	-0.0056(9)	-0.0080(9)
C(3)	0.0202(11)	0.0206(10)	0.0224(11)	0.0025(8)	-0.0060(9)	-0.0059(9)
C(4)	0.0214(11)	0.0172(10)	0.0239(12)	0.0017(8)	-0.0063(9)	-0.0063(9)
C(5)	0.0209(11)	0.0195(10)	0.0227(12)	0.0002(8)	-0.0080(9)	-0.0078(9)
C(6)	0.0218(11)	0.0225(10)	0.0190(11)	0.0022(8)	-0.0070(9)	-0.0070(9)
I(7)	0.0345(1)	0.0286(1)	0.0205(1)	-0.0059(1)	0.0012(1)	-0.0052(1)
C(7)	0.0287(12)	0.0201(10)	0.0180(11)	-0.0024(9)	0.0001(9)	-0.0056(9)
C(8)	0.0252(12)	0.0267(12)	0.0265(13)	-0.0040(9)	-0.0044(10)	-0.0084(10)
C(9)	0.0278(12)	0.0259(11)	0.0218(12)	-0.0017(9)	-0.0081(10)	-0.0080(9)

APPENDIX B

Lectures, Meetings, Courses and Conferences Attended

B.1 MEETINGS COURSES AND CONFERENCES

The following meetings, courses and conferences were attended during the period of tution for this thesis -

1993

17/11	BCA CCG Autumn Meeting - *Current Controversies in Chemical Crystallography*, University of Aston, Birmingham.
01/12	4th UK Charge Density Group Meeting, University of Wales, Cardiff.

1994

31/01 - 04/02	A Practical Neutron Training Course, ISIS, Chilton.
26/03 - 28/03	SHELXL-93 Workshop, University of Newcastle, Newcastle.
28/03 - 31/03	BCA Spring Meeting, University of Newcastle, Newcastle. Poster entitled *A Single Crystal Neutron Diffraction Study of 3,5-Dinitrocinnamic Acid* was presented.
18/12	5th UK Charge Density Group Meeting, University of Glasgow, Glasgow.

1995

27/03 - 31/03 BCA Spring Meeting, University of Wales, Cardiff. Poster entitled *The Hydrogen Bonding Properties of Three Membered Rings* presented.

02/04 - 08/04 BCA Intensive Teaching School in X-ray Structure Analysis, University of Aston, Birmingham.

02/06 - 12/06 International School of Crystallography 22nd Course - *Crystallography of Supramolecular Compounds*, Erice, Sicily.

17/11 BCA CCG Autumn Meeting, Siemens House, Manchester.

14/12 - 15/12 6th UK Charge Density Group Meeting, University of Durham, Durham.

1996

01/04 - 04/04 BCA Spring Meeting, University of Cambridge, Cambridge. Lecture entitled *The Experimental Characterization of Weak Non-bonded Interactions* was presented.

07/08 - 17/08 IUCr XVII Congress and General Assembly, Seattle, WA, USA. Poster entitled *Database and Theoretical Studies of Nitro Oxygen...Halogen Interactions* presented.

19/09 - 20/09 UK Neutron and Muon Users Meeting, ISIS, Chilton.

B.2 DEPARTMENTAL SEMINARS

The following is a list of colloquia, lectures and seminars given by invited speakers, in the Department of Chemistry at the University of Durham, during the period of tution for this thesis. Those marked with * were attended by the author.

1993

September 13 — Prof. A.D. Schluter, Frei Universitat Berlin, Germany. *Synthesis and Characterisation of Molecular Rods and Ribbons.*

September 11 — Dr. K.J. Wynne, Office of Naval Research, Washington, USA. *Polymer Surface Design for Minimal Adhesion*

September 14 — Prof. J.M. DeSimone, University of North Carolina, Chapel Hill, USA. *Homogeneous and Heterogeneous Polymensations in Environmentally Responsible Carbon Dioxide.*

September 28 — Prof. H. Ila, North Eastern Hill University, India. *Synthetic Strategies for Cyclopentanoids via Oxoketene Dithioacetals.*

October 4 — Prof. F.J. Feher, University of California, Irvine, USA. *Bridging the Gap between Surfaces and Solution with Sessilquioxanes.*

October 14 — Dr. P. Hubberstey, University of Nottmgham. *Alkali Metals: Alchemist's Nightmare, Biochemist's Puzzle and Technologist's Dream**.

October 20 — Dr. P. Quayle, University of Manchester. *Aspects of Aqueous ROMP Chemistry.*

October 21 Prof. R. Adams, University of South Carolina, USA. *Chemistry of Metal Carbonyl Cluster Complexes: Development of Cluster Based Alkyne Hydrogenation Catalysts.*

October 27 Dr. R.A.L. Jones, Cavendish Laboratory, Cambridge. *Perambulating Polymers.*

November 10 Prof. M.N.R. Ashfold, University of Bristol. *High Resolution Photofragment Translational Spectroscopy: A New Way to Watch Photodissociation.*

November 17 Dr. A. Parker, Rutherford Appleton Laboratory, Didcot. *Applications of Time Resolved Resonance Raman Spectroscopy to Chemical and Biochemical Problems.*

November 24 Dr. P.G. Bruce, University of St. Andrews. *Structure and Properties of Inorganic Solids and Polymers*.*

November 25 Dr. R.P. Wayne, Oxford University. *The Origin and Evolution of the Atmosphere*.*

December 1 Prof. M.A. McKervey, Oueen's University, Belfast. *Synthesis and Applications of Chemically Modified Calixarenes.*

December 8 Prof. O. Meth-Cohn, University of Sunderland. *Friedel's Folly Revisited - A Super Way to Fused Pyridines.*

December 16 Prof. R.F. Hudson, University of Kent. *Close Encounters of the Second Kind*.*

1994

January 26 — Prof. J. Evans, University of Southampton. *Shining Light on Catalysts*.*

February 2 — Dr. A. Masters, University of Manchester. *Modelling Water Without Using Pair Potentials.*

February 9 — Prof. D. Young, University of Sussex. *Chemical and Biological Studies on the Coenzyme Tetrahydrofolic Acid.*

February 16 — Prof. K.H. Theopold, University of Delaware, USA. *Paramagnetic Chromium Alkyls: Synthesis and Reactivity.*

February 23 — Prof. P.M. Maitlis, University of Sheffield. *Across the Border: From Homogeneous to Heterogeneous Catalysis.*

March 2 — Dr. C. Hunter, University of Sheffield. *Noncovalent Interactions between Aromatic Molecules*.*

March 9 — Prof. F. Wilkinson, Loughborough University of Technology. *Nanosecond and Picosecond Laser Flash Photolysis.*

March 10 — Prof. S.V. Ley, University of Cambridge. *New Methods for Organic Synthesis.*

March 25 — Dr. J. Dilworth, University of Essex. *Technetium and Rhenium Compounds with Applications as Imaging Agents.*

April 28 — Prof. R. J. Gillespie, McMaster University, Canada. *The Molecular Structure of some Metal Fluorides and Oxofluorides: Apparent Exceptions to the VSEPR Model*.*

May 12 — Prof. D.A. Humphreys, McMaster University, Canada. *Bringing Knowledge to Life*.*

October 5 — Prof. N.L. Owen, Brigham Young University, Utah, USA. *Determining Molecular Structure - the INADEQUATE NMR way.*

October 19 — Prof. N. Bartlett, University of California. *Some Aspects of Ag(II) and Ag(III) Chemistry*.*

November 2 — Dr. P.G. Edwards, University of Wales, Cardiff. *The Manipulation of Electronic and Structural Diversity in Metal Complexes - New Ligands.*

November 3 — Prof. B.F.G. Johnson, Edinburgh University. *Arene-metal Clusters*.*

November 9 — Dr. G. Hogarth, UCL, London. *New Vistas in Metal-imido Chemistry.*

November 10 — Dr. M. Block, Zeneca Pharmaceuticals, Macclesfield. *Large-scale Manufacture of ZD 1542, a Thromboxane Antagonist Synthase Inhibitor.*

November 16 — Prof. M. Page, University of Huddersfield. *Four-membered Rings and β-Lactamase.*

November 23 Dr. J.M.J. Williams, University of Loughborough. *New Approaches to Asymmetric Catalysis.*

December 7 Prof. D. Briggs, ICI and University of Durham. *Surface Mass Spectrometry.*

1995

January 11 Prof. P. Parsons. University of Reading. *Applications of Tandem Reactions in Organic Synthesis.*

January 18 Dr. G. Rumbles, Imperial College, London. *Real or Imaginary Third Order Non-linear Optical Materials.*

January 25 Dr. D.A. Roberts, Zeneca Pharmaceuticals. *The Design and Synthesis of Inhibitors of the Renin-angiotensin System.*

February 1 Dr. T. Cosgrove, Bristol University. *Polymers do it at Interfaces*.*

February 8 Dr. D. O'Hare, Oxford University. *Synthesis and Solid-state Properties of Poly-, Oligo- and Multidecker Metallocenes.*

February 22 Prof. E. Schaumann, University of Clausthal. *Silicon- and Sulphur-mediated Ring-opening Reactions of Epoxide.*

March 1 Dr. M. Rosseinsky, Oxford University. *Fullerene Intercalation Chemistry*.*

March 22 Dr. M. Taylor, University of Auckland, New Zealand. *Structural Methods in Main-group Chemistry*.*

April 26	Dr. M. Schroder, University of Edinburgh. *Redox-active Macrocyclic Complexes: Rings, Stacks and Liquid Gases* *.
May 4	Prof. A.J. Kresge, University of Toronto. The Ingold Lecture, *Reactive Intermediates: Carboxylic-acid Enols and Other Unstable Species*.
October 11	Prof. P. Luger, Frei Universitat Berlin, Germany. *Low Temperature Crystallography**.
October 13	Prof. R. Schmuitzler, Universitat Braunschwieg, Germany. *Calixarene-Phosphorus Chemistry: A New Dimension in Phosphorus Chemistry*.
October 18	Prof. A. Alexakis, Universite Pierre et Madame Curie, Paris, France. *Synthetic and Analytical Uses of Chiral Diamines*.
October 25	Dr. D.M. Davies, University of Northumbria, Newcastle. *Chemical reactions organised systems*.
November 1	Prof. W. Motherwell, UCL, London. *New Reactions for Organic Synthesis*.
November 3	Dr B. Langlois, University Claude Bernard-Lyon. *Radical Anionic and Psuedo Cationic Trifluoromethylation.*
November 8	Dr. D. Craig, Imperial College, London. *New Stategies for the Assembly of Heterocyclic Systems*.
November 11	Prof. J.P.R. Williams, Oxford University. *Metals in Health and Disease**.

November 15 Dr. A. Andrea, UCL, London. *Chemistry of Lanthanides with Polypyrazoylborate Ligands.*

November 17 Prof. D. Bergbreiter, Texas A&M, USA. *Design of Smart Catalysts, Substrates and Surfaces from Simple Polymers.*

November 22 Prof. I. Soutar, Lancaster University. *A Water of Glass? Luminescence Studies of Water-Soluble Polymers.*

November 29 Prof. D. Tuck, University of Windsor, Ontario, Canada. *New Indium Coordination Chemistry.*

December 8 Prof. M.T. Reetz, Max Planck Institut, Mulheim. *Perkin Regional Meeting.*

1996

Janurary 10 Dr. B. Henderson, Waikato University, New Zealand. *Electrospray Mass spectrometry - a New Sporting Technique.*

Janurary 11 Dr. J.K.M. Sanders, Oxford University. *Enzyme Mimics*.*

Janurary 17 Prof. J.W. Emsley, University of Southhampton. *Liquid Crystals: More than Meets the Eye*.*

Janurary 24 Dr. A. Armstrong, Nottingham University. *Alkene Oxidation and Natural Product Synthesis.*

January 31 Dr. J. Penfold, Rutherford Appleton Laboratory. *Soft Soap and Surfaces*.*

February 7 Dr. R.B. Moody, Exeter University. *Nitrosations, Nitrations and Oxidations with Nitrous Acid.*

February 12 Dr. P. Pringle, University of Bristol. *Catalytic Self-Replication of Phosphines on Platinum(O)*.*

February 14	Dr. J. Rohr, Universitat Göttingen, Germany. *Goals and Aspects of Biosynthetic Studies on Low Molecular Weight Natural Products.*
Feburary 21	Dr. C. Pulham, University of Edinburgh. *Heavy metal Hydrides.*
February 28	Prof. E.W. Randall, Queen Mary and Westfield College. *New Perspectives in NMR Imaging.*
March 6	Dr. R. Whitby, University of Southampton. *New approaches to chiral catalysts: Induction of planar and metal centred asymmetry.*
March 7	Dr. D.S. Wright, University of Cambridge. *Synthetic Applications of Me_2N-p-Block Metal Reagents.*
March 12	Prof. V. Balzani, University of Bologna. RSC Endowed Lecture - *Supramolecular Photochemistry.**
March 13	Prof. Dave Garner, Manchester University. *Mushrooming in Chemistry.*
April 30	Dr. L.D.Pettit, Chairman. *IUPAC Commission of Equilibrium Data pH-metric studies using very small quantities of uncertain purity.*